Development of a Novel Reactor Concept for Minimizing Solid Formation and Enhancing Efficiency in Continuous Supercritical Water Gasification

Zur Erlangung des akademischen Grades eines
DOKTORS DER INGENIEURWISSENSCHAFTEN

von der KIT-Fakultät für Chemieingenieurwesen und Verfahrenstechnik des
Karlsruher Instituts für Technologie (KIT)
genehmigte

DISSERTATION

von
M. Sc. Julian Dutzi
aus Zeutern

Tag der mündlichen Prüfung: 30.10.2026

Erstgutachter: Prof. Dr.-Ing. Jörg Sauer

Zweitgutachter: Prof. Dr.-Ing. Frederik Scheiff

Declaration

I, Julian Dutzi, declare that this thesis represents my own work and that I have written it independently by myself, without the use of other documents or sources beyond those stated in the references.

Acknowledgments

I would like to express my heartfelt thanks to everyone who contributed to the success of my doctoral thesis:

My special thanks go to Prof. Dr.-Ing. Jörg Sauer for the opportunity to carry out my doctoral research at IKFT. I am grateful for the comprehensive supervision of my work, the inspiring scientific discussions, and your valuable advice, which often provided a new perspective. Your support in publishing my results, the opportunity to attend international conferences, and your motivation to continue pushing the topic forward have always driven me. I especially appreciate the trust you placed in me, e.g., when letting me carry out another project in cooperation with the Ministerium für Verkehr Baden-Württemberg at the end of my PhD.

I would to express my gratitude to Prof. Dr.-Ing. Frederik Scheiff for being the second reviewer.

I would also like to thank Dr. Nikolaos Boukis, my direct supervisor, who supported me since my Master's thesis in the group. Thank you for your support from the very beginning, your great ideas, and the insightful scientific discussions. Your advice to abstracts, publications, and posters, as well as your open ear, contributed significantly to the progress of my work.

My thanks also go to TT-Prof. Dr. Moritz Wolf and Dr. Ulrich Arnold who took me into their groups after Dr. Boukis' retirement. Thank you for your support and for seamlessly integrating me into your teams, which allowed me to successfully complete my work.

A special thank you goes to Karl Weiss, whose expertise in the mechanical work on the lab-plant was indispensable. Whether during one of the numerous modifications or the regular maintenance of the system, your work always ensured that each modification represented progress and the system worked flawlessly. A heartfelt thank you to Elena Hauer for your dedicated support in preparing experiments, managing orders and support in carrying out analyses. Thank you, Karl and Elena, for your amazing

support and welcome into the group. In no time, colleagues became friends, and I can't imagine my journey without you.

A big thank you to Dr. Katharina Stoll, who first gave me the opportunity to join IKFT as a working student and later to write my Master's thesis. Your encouragement surely contributed to my decision to pursue a PhD at IKFT.

Many thanks also to Stefan Henecka and Rickie Drexler for your support and valuable advice in the lab and on the lab-plant, especially when Karl was unavailable. Although I didn't experience the time when you were part of the larger “Boukis group”, the connection to it was still evident, and I was always able to rely on your help.

My thanks also go to Volker Meinzer, Dennis Heidenblut and Holger Kahrau for your help with electronic issues, particularly with attaching connectors to the many heating elements I used throughout my time at IKFT. Your support ensured the smooth execution of the experiments. I thank Roland Fritz for reliable IT support and quick assistance with technical issues.

Further thanks go to Veronika Holderied, Armin Lautenbach, Birgit Rolli, Dr. Michael Zimmermann, Jessica Heinrich and Alexandra Böhm for your support, the prompt execution of analyses, and assistance in data interpretation.

I would also like to express my gratitude to the IKFT doctoral students, particularly Moritz Herfet, Philipp Beeskow, Maximilian Wörner, Lukas Perret, Christian Ebel, Marius Drexler, Pia Münzer, Elisabeth Herzinger and Angelina Barthelmeß, for their scientific support as well as the motivation and personal encouragement throughout my dissertation. One PhD student I would like to highlight is Athanasios Vadarlis. Not only did we share an office, but we also shared a research topic. From colleagues to friends in no time – thank you for your valuable input, your willingness to help out at any time, and the great cooperation. The successful collaborations, resulting in several joint publications, are a special milestone in this time. Thank you for everything!

A special thank you goes to Dr. Bruno Lacerda de Oliveira Campos for the excellent collaboration, which resulted in a final publication containing a kinetics model based

on my experimental data. The cooperation not only brought me much joy but also provided a valuable opportunity for learning. Thank you for this enriching experience!

I would also like to thank the members of the CERESiS team for the fruitful discussions and great collaboration throughout the entire project, especially Dr. Dimitrios Katsourinis and Prof. Athanasios Rentizelas for coordinating the H2020 project and Dr. Konstantinos Plakas and Vasilis Sarasidis for outstanding cooperation beyond the CERESiS project.

My deepest thanks go to my parents, who have supported, motivated, and always believed in me throughout my entire academic journey. Without their unconditional support, this path would not have been possible. A special thank you goes to my wife Yasmin and my friends. Your confidence and belief in me have given me strength throughout all phases of this journey. Thank you for always being by my side!

Without the support and collaboration of all these individuals, this work would not have been possible in its current form. Thank you!

Preamble

This thesis is publication-based and therefore most of the content contained in this thesis has been previously published in peer-reviewed articles. Parts of the following work closely align with the published articles, incorporating minor modifications such as adjustments of formatting, citation style, figures, tables, and overall layout.

In Chapter 1, the objectives of the present work are outlined.

In Chapter 2, a comprehensive introduction to the process of supercritical water gasification (SCWG) is provided, to avoid repetition in the beginning of each chapter. The same accounts for Chapter 3, where the materials and methods are presented which were used throughout the experimental work. Additional materials and methods used in the different experimental campaigns are highlighted in Chapters 4 to 7.

Chapters 4 to 7 contain the experimental work conducted within this thesis. The publications which these chapters are based on are named at the beginning of each chapter, including an outline of the contributions of the authors.

Abstract

The growing demand for renewable energy requires the exploration and use of different methods of renewable energy production, including methods for different feedstocks. In this context, it is particularly important to consider waste streams. Wastes streams are often challenging to process, as for example a high water content can hinder their treatment in conventional conversion processes. One promising approach that enables the conversion of a wide range of organic materials and is not affected by high water content is supercritical water gasification (SCWG). With SCWG, valuable syngas can be obtained from biomass, which can be further processed into high-value products such as Fischer-Tropsch fuels or used directly as a fuel gas.

This study investigates the conversion of grasses grown on heavy metal-contaminated soils. These grasses were provided in dry form as part of the H2020 EU project CER-ESiS (Grant-Agreement-No.: 10100671). Primary objective of this work was to assess the suitability of SCWG for processing dry, contaminated biomasses.

In the first part of the work, initial investigations were carried out in a continuous lab-plant. The design of the lab-plant was based on years of experience in the research group. These initial investigations demonstrated the potential of SCWG to process the various biomasses (similar results for multiple biomasses). Additionally, it was demonstrated that the fresh-water usage could be significantly reduced by recycling of the process effluent. However, it was also pointed out that insufficient salt removal is the critical issue hindering long-term operation. A detailed study of the temperature zone for salt precipitation revealed that solid deposits primarily formed in a temperature range of 400 to 440 °C (temperature in reaction medium) while the reactor wall temperature was set to 500 °C. These findings indicated that the solid formation was caused by the heating concept which has been used (electrical heating of the biomass slurry from the outside of the reactor wall).

Therefore, in the second part of this thesis, a novel reactor concept is presented to overcome the problems identified in the initial investigations. Instead of heating the biomass slurry electrically from the outside of the reactor, a heating concept was

implemented, where cold biomass was mixed with supercritical water for heating. This approach improved gasification efficiency, reduced deposition, and demonstrated operational feasibility over 100 hours of testing. A parametric study investigated the effects of biomass type, concentration, temperature, pressure, potassium addition, and residence time on process performance. The results showed that temperature and residence time significantly affected carbon gasification efficiency, reaching 91% at 700 °C and 31 s, while potassium addition and pressure had minimal impact.

Based on the very good results of the new reactor concept, a comparison was made with the thermodynamic equilibrium that can be achieved for the SCWG under the respective conditions. Deviations from equilibrium were evident, which, in most cases, could be explained by the incomplete conversion of methane and water by the steam reforming reaction. Maximizing the hydrogen yield may be possible through the use of an appropriate catalyst. Additionally, experimental observations revealed that the most influential factors have an almost linear impact on gasification (temperature, dry matter content, and residence time). Therefore, a simplified multi-linear model was parametrized and verified through additional experiments. This allows for estimating the amount of gas produced and its composition for the used biomasses (dry grasses) without further experimental effort.

Lastly, the water consumption stemming from the reactions was evaluated using ethanol as a model substance. As process water is commonly treated and reused, the amount of single-pass water demand is relevant for the whole process. Both experimental investigations and thermodynamic equilibrium simulations demonstrated how water usage correlates with biomass concentration. Specifically, as the ethanol concentration increased, water consumption per mole of ethanol decreased significantly, as the product gas composition also shifted. These findings can be transferred to more complex biomasses, enabling the estimation of water consumption in such processes.

The present thesis expands the application of SCWG to new biomasses and presents a long-needed process development in the SCWG process. Through a systematic investigation of the issues that previously hindered long-term operation, not only was the process understanding deepened, but also a new plant configuration was developed, enabling long-term operation with high gasification rates.

Zusammenfassung

Die wachsende Nachfrage nach erneuerbarer Energie erfordert die Erforschung und Nutzung verschiedener Methoden zur Erzeugung erneuerbarer Energie, einschließlich Methoden zur Verwendung verschiedener Rohstoffe. In diesem Zusammenhang ist es besonders wichtig, Abfallströme zu berücksichtigen. Diese sind oft schwierig zu verarbeiten, da z.B. ein hoher Wassergehalt ihre Behandlung in konventionellen Umwandlungsprozessen erschweren kann. Ein vielversprechender Ansatz, der die Umwandlung eines breiten Spektrums organischer Materialien ermöglicht und nicht durch einen hohen Wassergehalt beeinträchtigt wird, ist die Vergasung in überkritischem Wasser (SCWG). Mit SCWG kann aus Biomasse wertvolles Synthesegas gewonnen werden, das zu hochwertigen Produkten wie Fischer-Tropsch-Kraftstoffen weiterverarbeitet oder direkt als Brenngas genutzt werden kann.

In der vorliegenden Arbeit wird die Umwandlung von Gräsern untersucht, die auf schwermetallbelasteten Böden gewachsen sind. Diese Gräser wurden in trockener Form im Rahmen des H2020 EU-Projekts CERESiS (Fördernummer: 10100671) zur Verfügung gestellt. Primäres Ziel dieser Arbeit war es, die Eignung von SCWG für die Verarbeitung trockener, kontaminierter Biomassen zu bewerten.

Die ersten Untersuchungen wurden in der kontinuierlichen SCWG Anlage am KIT durchgeführt, deren Konfiguration auf jahrelanger Erfahrung der Arbeitsgruppe beruhte. Die Ergebnisse zeigten das Potenzial der SCWG für die Verarbeitung der verschiedenen Biomassen (ähnliche Ergebnisse für mehrere Biomassen). Außerdem wurde nachgewiesen, dass der Frischwasserverbrauch durch die Wiederverwendung des Prozessabwassers drastisch reduziert werden kann. Es wurde jedoch auch deutlich, dass eine unzureichende Salzabscheidung das entscheidende Problem ist, das einen Langzeitbetrieb verhindert. Eine detaillierte Untersuchung der Temperaturzone für die Salzausfällung ergab, dass sich feste Ablagerungen hauptsächlich in einem Temperaturbereich von 400 bis 440 °C (Temperatur im Reaktionsmedium) bildeten, während die Wandtemperatur des Reaktors in diesem Bereich auf 500 °C eingestellt war. Diese Ergebnisse deuten darauf hin, dass die Feststoffbildung durch das

verwendete Heizungskonzept (elektrische Beheizung der Biomasse von der Außenseite der Reaktorwand) begünstigt wurde.

Daher wurde im zweiten Teil der vorliegenden Arbeit ein neuartiges Reaktorkonzept entwickelt, um die in den ersten Untersuchungen festgestellten Probleme zu überwinden. Anstatt die Biomasse über die heiße Reaktorwand zu erwärmen, wurde ein Heizkonzept umgesetzt, bei dem kalte Biomasse zur Erwärmung mit überkritischem Wasser gemischt wurde. Dieser Ansatz verbesserte die Vergasungseffizienz, verringerte die Ablagerung und bestätigte die Funktionalität in einem 100-stündigen Test.

In einer parametrischen Studie wurden die Auswirkungen von Biomasseart, Konzentration, Temperatur, Druck, Kaliumzusatz und Verweilzeit auf den Prozess untersucht. Die Ergebnisse zeigten, dass Temperatur und Verweilzeit die Effizienz der Kohlenstoffvergasung erheblich beeinflussten, welche bei 700 °C und 31 s einen Wert von 91% erreichte, während die Kaliumzugabe und der Druck nur minimale Auswirkungen hatten.

Auf der Grundlage der sehr guten Ergebnisse des neuen Reaktorkonzepts wurde ein Vergleich mit dem thermodynamischen Gleichgewicht durchgeführt. Es zeigte sich, dass Abweichungen vom Gleichgewicht vorhanden waren, die in den meisten Fällen durch unzureichend ablaufende Dampfreformierung erklärt werden konnten. Daraus lässt sich ableiten, dass die Wasserstoffausbeute durch den Einsatz eines geeigneten Katalysators maximiert werden könnte. Darüber hinaus machten die experimentellen Beobachtungen deutlich, dass die meisten Einflussfaktoren einen nahezu linearen Einfluss auf die Vergasung haben (Temperatur, Trockenmassegehalt und Verweilzeit bei Werten über 8 s). Daher wurde ein multi-lineares Modell abgeleitet und durch zusätzliche Experimente verifiziert. Dieses erlaubt es nun, die Menge des erzeugten Gases und seine Zusammensetzung für die verwendeten Biomassen (trockene Gräser) ohne weiteren experimentellen Aufwand abzuschätzen.

Abschließend wurde der Wasserverbrauch, der aus den Reaktionen resultiert, unter Verwendung von Ethanol als Modellsubstanz bewertet. Da Prozesswasser üblicherweise aufbereitet und wiederverwendet wird, ist die Menge an Frischwasserbedarf pro Durchlauf für den gesamten Prozess von Bedeutung. Sowohl experimentelle Untersuchungen als auch thermodynamische Gleichgewichtssimulationen zeigten, wie der

Wasserverbrauch mit der Biomassekonzentration zusammenhängt. Insbesondere nahm der Wasserverbrauch pro Mol Ethanol mit steigender Ethanolkonzentration deutlich ab, da sich auch die Zusammensetzung des Produktgases veränderte. Diese Erkenntnisse lassen sich auf komplexere Biomassen übertragen und ermöglichen die Abschätzung des Wasserverbrauchs in solchen Prozessen.

Die vorliegende Arbeit erweitert den Anwendungsbereich von SCWG auf neue Biomassen und stellt eine seit langem benötigte Prozessentwicklung der Vergasung im überkritischen Wasser dar. Durch eine systematische Untersuchung der Probleme, die bisher den Langzeitbetrieb verhinderten, wurde nicht nur das Prozessverständnis vertieft, sondern auch eine neue Anlagenkonfiguration entwickelt, die einen Langzeitbetrieb mit hohen Vergasungsraten ermöglicht.

Table of Content

Declaration ..... **I**

Acknowledgments ..... **II**

Preamble ..... **V**

Abstract ..... **VI**

Zusammenfassung ..... **VIII**

Chapter 1. Objectives of the present work **1**

Chapter 2. Introduction to the supercritical water gasification **3**

2.1 Biomass as energy carrier 4

2.1.1 Hydrothermal processes for biomass conversion 5

2.1.2 Phytoremediation 6

2.2 Supercritical water gasification 7

2.2.1 Supercritical water and its unique properties 8

2.2.2 Influence of process parameters 9

2.2.3 Challenges and knowledge gaps 12

Chapter 3. Materials and methods **14**

3.1 Apparatus 15

3.2 Preparation of educts 15

3.3 Analysis 16

3.4 Data Interpretation 17

Chapter 4. First investigations of dry biomasses in supercritical water gasification **19**

4.1 Introduction 22

4.2 Screening of dry biomasses 24

4.2.1 Materials and methods 24

4.2.2 Results and discussion 30
4.3 First process parameter variations 35
4.3.1 Materials and methods....35
4.3.2 Results and discussion 40
4.4 Process effluent recycling 52
4.4.1 Materials and methods....52
4.4.2 Results and Discussion....54
4.5 Conclusion 67
Chapter 5. Systematic investigation of salt precipitation....70
5.1 Introduction 72
5.2 Materials and methods....73
5.2.1 Preparation of educts....73
5.2.2 Apparatus 74
5.2.3 Experimental....76
5.3 Results and discussion....77
5.3.1 Influence of temperature on solid formation in SCWG 77
5.3.2 Influence of flow direction on the separation of solids....84
5.4 Conclusion 87
Chapter 6. Development and parametrization of novel reactor concept for the supercritical water gasification....88
6.1 Introduction 90
6.2 Materials and methods....91
6.2.1 Setup 91
6.2.2 Description of experiments 93
6.2.3 Thermodynamic equilibrium calculations 95
6.3 Experimental results....96
6.3.1 Proof of concept....96

6.3.2 Parameterization of the newly developed system 99
6.4 Empirical model derived from the experimental data 119
6.5 Comparison of experimental data and equilibrium calculation 122
6.5.1 Pressure 123
6.5.2 Concentration 125
6.5.3 Temperature 126
6.5.4 Summary of gained knowledge from equilibrium calculations 128
6.6 Conclusion 129
Chapter 7. Water consumption of the SCWG process: Investigation with a model compound 132
7.1 Introduction 134
7.2 Materials and method 135
7.2.1 Preparation of educts 135
7.2.2 Apparatus 135
7.2.3 Data interpretation 135
7.3 Results and discussion 137
7.3.1 Investigation of water consumption 137
7.3.2 Comparison of experimental results with thermodynamic equilibrium 143
7.4 Conclusion 145
Chapter 8. Concluding insights and future perspectives 147
8.1 Concluding insights 147
8.2 Future perspectives 152
References 154
Appendix XV
A1 Supporting Information of Chapter 5 XV
A1.1 EDS analysis of salt concentrate solid sample XV
A1.2 Statistical analysis of the empirical model XVII

A1.3 Additional calculations for equilibrium calculations XIX

A2 Supporting Information of Chapter 6 XX

Nomenclature..... XXI

List of Symbols – Latin XXI

List of Symbols – Greek XXII

Subscription XXIII

Abbreviations XXIII

List of Figures..... XXV

List of Tables XXIX

List of Publications XXXI

Chapter 1. Objectives of the present work

Supercritical water gasification (SCWG) is a promising technology for converting biomass into gaseous products. However, the continuous operation of SCWG systems remains challenging due to issues such as salt precipitation, solid deposition (especially when processing high biomass concentrations) and the high water demand of the process.

This dissertation was conducted in the framework of the EU project CERESiS, which aimed at developing sustainable conversion pathways for grassy biomasses. Within this context, the present work focuses on addressing key technical challenges associated with the continuous operation of SCWG systems.

The initial objective of this work was to evaluate the suitability of SCWG for the conversion of dry, mostly grassy biomasses provided within the CERESiS project. This investigation included experiments with different biomasses and process conditions, particularly temperature and residence time. A central aspect of this investigation was the behavior of inorganic species, as salts and heavy metals may precipitate under supercritical conditions. Such precipitation can lead to solid deposition and plugging of reactor components, thereby limiting long-term reactor operation. Consequently, efficient salt separation is a critical requirement for the reliable operation of continuous SCWG systems. The results of these investigations are presented in Chapter 4.

Initial experiments demonstrated that SCWG is generally suitable for processing the investigated biomasses. However, operational challenges remained, most notably insufficient salt separation that resulted in system plugging during extended operation. To address this limitation, a secondary objective of this work was defined: to investigate the mechanisms responsible for insufficient salt separation in the reactor system. Since solid deposit formation appeared to correlate with the reactor temperature profile, a detailed investigation of the temperature zone of salt precipitation was

conducted. This study aimed to identify the conditions under which salts precipitate and accumulate in the system and is presented in Chapter 5.

Based on the insights obtained from the salt precipitation study, the main objective of this thesis was formulated: the development and parameterization of a SCWG reactor system suitable for the continuous processing of grassy biomasses. To achieve this, a novel heating concept was developed and implemented in the experimental setup (see Chapter 6). Following initial successful tests, a comprehensive parametric study was conducted to investigate the influence of key process parameters and to determine suitable operating windows for stable reactor operation. During this investigation, the biomass concentration in the feed was varied, as higher biomass concentrations are generally desirable to improve the economic viability of the process. Based on the experimental data, an empirical model was developed to predict the outcomes of experiments across a wide range of operating conditions. Such a model can significantly reduce the experimental effort required for future investigations.

In addition to the reactor development, another objective of this work was to investigate water consumption in SCWG processes. The large amounts of water required for feed preparation and operation can influence the overall sustainability of the technology. Therefore, strategies to reduce the demand for fresh water are of particular interest. In this context, recycling the process effluent to produce new feed slurry was experimentally evaluated and demonstrated to be a feasible approach to reduce fresh water consumption (see Chapter 4). Furthermore, a fundamental investigation of water consumption in SCWG was conducted to better understand how much water participates in chemical reactions during the process. The results provide fundamental insights into the role of water in SCWG reactions and allow conclusions to be drawn for the processing of complex biomass systems. These findings are presented in Chapter 7.

Chapter 2. Introduction to the supercritical water gasification

Part of the content of this chapter is sourced from the following publications:

- Dutzi, J.; Vadarlis, A.A.; Boukis, N.; Sauer, J. Development and parametrization of novel reactor concept for the supercritical water gasification process. *Ind. Eng. Chem. Res.,* **2025**, 64, 9500-9517. DOI: 10.1021/acs.iecr.4c04267

  Declaration of contributions:
  Julian Dutzi conceptualized the experimental work and analysed the data, evaluated the results, and wrote the manuscript. Julian Dutzi conducted the thermodynamic equilibrium calculations and the comparison with experimental data.
  Athanasios A. Vadarlis conducted the thermodynamic equilibrium calculations and the comparison with experimental data.
  Nikolaos Boukis supervised the work, contributed to the discussion, and reviewed the manuscript.
  Jörg Sauer supervised the work, contributed to the discussion, and reviewed the manuscript.

- Dutzi, J.; Boukis, N.; Sauer, J. Investigating Salt Precipitation in Continuous Supercritical Water Gasification of Biomass. *Processes*, **2024**, 12, 935. DOI: 10.3390/pr12050935

  Declaration of contributions:
  Julian Dutzi conceptualized the experimental work and analysed the data, evaluated the results, and wrote the manuscript.
  Nikolaos Boukis supervised the work, contributed to the discussion, and reviewed the manuscript.
  Jörg Sauer supervised the work, contributed to the discussion, and reviewed the manuscript.

2.1 Biomass as energy carrier

The transition to sustainable energy systems has become a global priority due to the rising demand for energy and the negative environmental impacts of fossil fuels. Biomass, as a renewable and widely available resource, offers significant potential for energy production [1,2]. Biomass refers to all substances of organic origin formed through photosynthesis including their transformation and decomposition products [3,4]. It can be sourced from many different origins such as forestry residues, agricultural waste or algae [1,4].

To utilize the energy in biomass, it is transformed into solid, liquid, or gaseous products through various conversion processes. These are categorized into thermochemical, biochemical and physicochemical methods [3–5]. Biochemical conversion involves the use of microorganisms, such as yeasts or bacteria, or enzymes to transform biomass into energy carriers [6,7]. Fermentation for example uses microorganisms to break down complex organics, especially sugars, into simpler compounds such as ethanol, e.g., for use as biofuel [8,9]. In anaerobic digestion on the other hand, organic matter is digested by bacteria in the absence of oxygen to produce biogas [10,11]. Lignin can for example be converted via enzymes [3], e.g., to release valuable aromatic compounds for the use as bio-based chemicals [12]. Biochemical processes are in general rather simple, but a main disadvantage is that the biochemical processes require a long processing time [13]. Physicochemical methods concern the energetic use of plant oils. The oil first needs to be separated from the solid parts of the biomass e.g. via extraction [3,4]. The oil can be used as a fuel, either directly or after further upgrading, e.g. after esterification to biodiesel [3,5]. Thermochemical methods include processes like direct combustion, gasification, and pyrolysis [3,14,15]. Pyrolysis involves heating biomass in the absence of oxygen, leading to its thermal decomposition into mainly bio-oil and a solid char [10,16]. Gasification aims to convert feedstock primarily into gas at high temperatures (above 700 °C) under sub-stoichiometric air conditions, often using oxygen or steam as gasification agents [3,14,16]. Both direct combustion and gasification can face challenges due to the presence of contaminants like chlorine, sulfur, or alkalis, which may produce harmful emissions or cause equipment corrosion [17–19].

The beforementioned thermochemical conversion methods are particularly suitable for dry biomass (wet biomass would often have to be dried first to tolerable moisture levels) [15,20]. However, since biomass typically contains significant amount of moisture, it often requires energy-intensive drying. Alternatively, a subsection of the thermochemical processes, the so-called hydrothermal processes, provide an efficient solution for handling wet biomass without the need for drying [21–23]. These processes utilize an aqueous environment under elevated temperatures and pressures to convert the biomass [20].

2.1.1 Hydrothermal processes for biomass conversion

Hydrothermal processes facilitate the conversion of moist biomass without the need for prior drying, utilizing an aqueous environment under elevated temperatures and pressures [21–23]. Thus, these processes are especially considered when processing moist biomass, but they are not limited to them. These processes are classified into three main types [24,25]: hydrothermal carbonization (HTC), hydrothermal liquefaction (HTL), and hydrothermal gasification (HTG).

HTC operates at temperatures ranging from 170 to 250 °C [22,26,27], mimicking the natural coalification of biomass [22], a process that typically occurs over millions of years. Under these conditions, liquefaction and gasification are limited, and the primary product is hydrochar [22,26], which exhibits a significantly enhanced calorific value compared to the raw biomass [21,27].

HTL occurs at temperatures between 280 and 370 °C and pressures of 100 to 250 bar [28,29], producing two distinct liquid phases, an aqueous phase rich in dissolved organic compounds and a viscous oil phase known as biocrude, and as byproducts solid char and gaseous emissions [24]. Often the primary objective of HTL is to maximize the conversion of biomass into biocrude, which can be refined into liquid fuels [29–31].

HTG aims to mainly produce a gaseous product containing valuable components such as H_2 and CH_4. There are different hydrothermal gasification processes with varying operating conditions (such as aqueous phase reforming or gasification in the near-critical region or supercritical water gasification) [32]. Supercritical water gasification takes place at high temperatures and pressures exceeding 221 bar. In this regime,

water exists in a supercritical state, enabling efficient conversion of biomass into fuel gases. As this hydrothermal process is of particular interest for the present work, a detailed description follows in section 2.2.

2.1.2 Phytoremediation

Historically, large areas of land have been contaminated with organic substances (e.g., pesticides, petroleum-based compounds) and inorganic substances (e.g., lead, mercury or cadmium) due to industrial activities, mining operations, transportation, and agricultural practices [33–38]. Elevated concentrations of pollutants in soils pose significant risks to human health, ecosystems, and wildlife [33,39]. A promising technique for mitigating soil contamination is phytoremediation, the utilization of plants to remediate the contaminated soil or water [40]. Compared to other remediation methods, such as excavation, chemical treatment or soil washing, phytoremediation is relatively low-cost as it relies on natural plant growth [41–43].

There are different types of phytoremediation [44,45]:

- Phytostabilization: Plants immobilize contaminants in the soil or prevent soil movement itself, e.g., by preventing erosion [46].
- Phytoextraction: Plants extract contaminants and store them in above-ground biomass [45].
- Phytostimulation: Plants can promote the biodegradation of organic contaminants by microbes in their rhizosphere by releasing organic substances that can support the activity of microbes [44,47].
- Phytodegradation: Decomposition of organic contaminants after uptake with the help of enzymes, turning the contaminants into less harmful products [33,40,48].
- Phytovolatilization: Some contaminants can be released from the plant in volatile, less toxic form after extraction from the soil [33,49].

Phytoextraction in particular, leverages the ability of plants to absorb pollutants through their root systems [45]. Multiple steps are involved: contaminant uptake, translocation of contaminants and storage and accumulation in above-ground tissue [40,49,50]. With repeated cycles of plant cultivation and harvesting, the level of contaminants in the soil

can be progressively reduced, ultimately achieving successful remediation (contamination below a tolerable level).

The effectiveness of the extraction depends on soil properties (e.g., the availability of the metal contaminant in the soil, pH) and the plant species (e.g., capacity for metal uptake, growth rate/biomass production) [40,45,51]. Plants capable of accumulating substantial quantities of heavy metals in their above-ground biomass are known as hyperaccumulators [52]. These species can typically absorb heavy metals at concentrations ranging from 0.1 to 1% of their dry mass [44]. For example, the fern *Pteris vittata L*. is recognized for its ability to accumulate arsenic [53], *Tagetes patula L.* presents a hyperaccumulator for cadmium [54], while *Alyssum bertolonii* is effective in absorbing nickel [55].

To prevent secondary environmental contamination, the harvested biomass grown on contaminated soil must be managed through proper disposal or further processing [44,46]. Hydrothermal processing technologies, which are well-suited for handling plant materials with high moisture content, present a viable solution for processing contaminated biomass. This approach has been the focus of numerous experimental studies and offer an efficient way of managing contaminated plant material while minimizing additional environmental impacts [56–61].

In the EU project CERESiS [62] (Grant Agreement No. 101006717) phytoextraction was used to clean up contaminated soils at various sites, e.g. in Brazil, Scotland and Italy. The harvested contaminated biomass was subsequently processed by two conversion technologies: Fast pyrolysis and supercritical water gasification. Fast pyrolysis produced a bio-oil while the product gas of the gasification process was upgraded, e.g. via dry reforming [63], to Fischer-Tropsch fuels.

2.2 Supercritical water gasification

Supercritical Water Gasification (SCWG) utilizes water in its supercritical state as a solvent and reactant. The supercritical state is reached when the critical point of water (T = 374 °C, p = 221 bar) is exceeded. Supercritical water displays unique properties (which are described in detail in section 2.2.1) and acts as a non-polar solvent in which organics can dissolve and thus can be easily hydrolyzed and decomposed to form a

valuable product gas [64], mainly containing H_2, CH_4, CO_2, CO and some C_{2+} hydrocarbons [65–67]. Eq. 2.1 and 2.2 can be defined as global reactions to describe the hydrolysis of the biomass. The gas formed further reacts according to steam reforming (Eq. 2.4) and water gas shift reactions (Eq. 2.3).

$$C_xH_yO_z + (x - z)H_2O \rightarrow xCO + (x - z + 0.5y)H_2 \quad (2.1)$$

$$C_xH_yO_z + (2x - z)H_2O \rightarrow xCO_2 + (2x - z + 0.5y)H_2 \quad (2.2)$$

$$CO + H_2O \leftrightarrow CO_2 + H_2 \quad (2.3)$$

$$C_nH_m + nH_2O \leftrightarrow nCO + (\frac{m}{2} + n)H_2 \quad (2.4)$$

Inorganics are poorly soluble and precipitate in the supercritical water [68,69]. This precipitation can be used to in-situ separate the inorganic components from the organics [70]. Through this separation, valuable nutrients such as phosphorus or potassium can be recovered from the biomass. SCWG also offers the potential to efficiently utilize wet biomass. The use of water as a solvent and reactant eliminates the need for prior drying [71], as is the case with conventional gasification. This allows for the utilization of a wide variety of moist waste biomasses such as sewage sludge [59,72], spent grains [73] or animal manure [74,75]. The composition of the resulting gas and the efficiency of gasification in SCWG heavily depend on process parameters, such as temperature, pressure, and biomass concentration in the feed. The influence of these parameters is described in detail in section 2.2.2.

2.2.1 Supercritical water and its unique properties

The critical point of water, defining the termination of the vapor pressure curve in its phase diagram, is reached at a temperature of 374 °C and a pressure of 221 bar [76,77]. Beyond this point, in the supercritical region, water displays unique properties which stem from the changes in its density, viscosity, diffusivity and dielectric constant.

As the temperature increases, the density of water decreases substantially, with a sharp decline occurring at the critical point [71,78] (see Figure 2.1). Nevertheless, supercritical water retains a higher density compared to steam, enabling high space-time yields in chemical reactions [79]. In the absence of phase boundaries, the density of

supercritical water can be continuously modulated by adjusting temperature or pressure [80,81]. Additionally, water's viscosity decreases with rising temperature, which enhances its diffusivity and supports rapid reactions [78]. In the supercritical state, the viscosity of water approximates the viscosity of a gaseous medium [78,82].

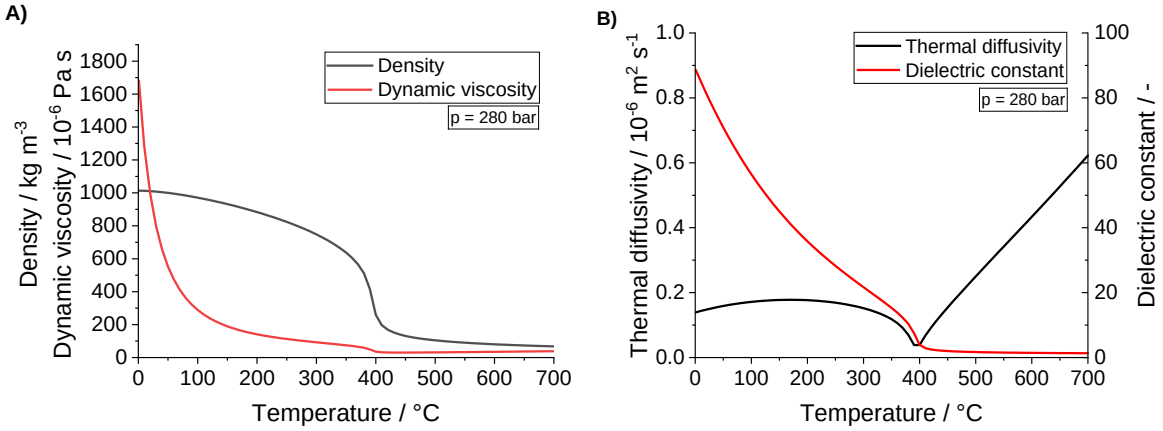


Figure 2.1: Selected properties of water at different temperatures, p = 280 bar (data taken from the IAPWS data base).

The dielectric constant of water, an indicator of its polarity, decreases with increasing temperature [81,83]. While water is a polar solvent under standard conditions, its dielectric constant decreases significantly in the supercritical region, rendering supercritical water a nonpolar solvent capable of efficiently dissolving organic compounds [64,78]. Additionally, gases also exhibit high solubility in supercritical water [81], making it an ideal reaction medium for homogeneous reactions involving organic molecules and gases [82]. However, inorganic salts have limited solubility in supercritical water and typically precipitate [69,84,85].

2.2.2 Influence of process parameters

The gas composition and yield in supercritical water gasification are strongly influenced by several process parameters, which are discussed below.

2.2.2.1 Temperature

In literature, it is well described that increasing the temperature is beneficial for the supercritical water gasification of biomass [66,86], as the decomposition of the

organics is enhanced. This leads to an increase of the amount of gas produced and reduces the organic carbon content of the effluent. Thus, with increasing temperature the gasification efficiency and the organic carbon conversion are expected to rise. An increasing temperature is expected to enhance steam reforming reactions due to their endothermic nature [87]. In literature it is also described that an increasing temperature increases the CO_2 yield due to the promotion of the water gas shift reaction [88].

2.2.2.2 Pressure

Various studies have been conducted in the past on the influence of pressure on the SCWG process in the range of 250 to 450 bar [89–91]. According to the literature, the gasification efficiency is not significantly affected by the system's pressure [92,93]. An increase in pressure generally suppresses methane conversion [94,95]. This would result in a decreased hydrogen yield while the methane yield should increase, when increasing the pressure. Gadhe and Gupta observed this when gasifying methanol in supercritical water [79]. However, other authors didn't see a significant influence of pressure on the gas composition [93,96].

2.2.2.3 Residence time

The residence time at reaction temperature τ is an important process parameter of the process of SCWG. In general, increasing the residence time is beneficial in terms of carbon gasification efficiency (CE), however at a certain residence time a maximum value of CE seems to be reached depending on the gasification conditions and biomasses processed. Guo et al. [97] found an increase of CE from 8% at 5.2 s to 42% at 9.0 s when they gasified 10 wt.% glycerol at 487 °C. At the same time the hydrogen yield increased significantly. However, the slope of the CE increase decreased with increasing residence time, indicating that a limit might be reached. At an elevated temperature of 567 °C they only observed a small increase from 84 to 94% at 4.2 and 7.3 s, respectively. Lu et al. [66] also observed an increase in CE when they increased the residence time during gasification of wood saw dust. The total organic carbon content of the effluent decreased correspondingly. Susanti et al. [67] gasified 15.25 wt.% isooctane at 632 °C. CE increased from 26.6 to 52.5% at residence times of 6.0 and

18.4 s, respectively. However, further increases in residence time up to 33.3 s had no significant beneficial effect. With increasing residence time, they found a decrease of C_{2+} compounds while the H_2 content of the product gas was at maximum at the longest tested residence time. D´Jesus et al. [92] found a linear increase of CE between 0.6 and 1.6 min, when gasifying 5 wt.% corn silage at 700 °C. A further prolonged residence time did not increase CE. This effect was also visible at other temperatures investigated. Chakinala et al. [98] observed similar when gasifying microalgae at 580 °C. CE increased with increasing residence times up to 5 min. Thereafter, a plateau was reached. They assumed that either part of the biomass is resistant to the chosen SCWG conditions or coke/tar formation is occurring, limiting the increase of CE. With increasing residence time, the C_{2+} and CO content of the product gas decrease while H_2 and CH_4 contents increase due to enhanced hydrocarbon reforming and water-gas-shift reaction.

2.2.2.4 Biomass concentration

The dry matter content in the system is a crucial process parameter of SCWG regarding gasification efficiency and also process economics. With increasing dry matter content, the carbon gasification efficiency decreases due to a decreasing water surplus and thus worse splitting of the biomass molecules [89,99,100]. For example, D`Jesus et al. [89] found a reduction of CE from about 82 to 75% when increasing the dry matter content from 2.5 to 10 wt.%. Also, the product gas composition is influenced by the dry matter content in the system. The increasing biomass content influences the water-gas-shift and methanation reactions [99,100]. A decrease in water content favors methanation and reverse water gas shift, thus decreasing the H_2 and CO_2 yield while increasing the CH_4 yield.

Processing high dry matter contents is for one limited by decreasing gasification efficiencies as described above, but also by the pumpability of the feed slurry which depends on the geometry of the SCWG plant and also the biomass [83].

2.2.3 Challenges and knowledge gaps

Supercritical water gasification has been a topic of research since the late 1970s, with M. Modell pioneering the first experiments on glucose conversion [101]. Although, SCWG has been investigated for a few decades there has not yet been a commercial application (to the best of the authors' knowledge). There have been several pilot-scale facilities including one at the Karlsruhe Institute of Technology in Germany [102], which was the first pilot-scale SCWG facility. Another pilot plant is operated by Hiroshima University and Chugoku Electric Power Company in Japan [103]. At the Technical University of Delft, a pilot plant with a biomass throughput of 50 kg h^{-1} has been established, utilizing a fluidized bed reactor [104]. At laboratory scale, studies are often carried out in batch reactors [59,105,106]. Batch reactors are widely used for parameter studies and offer simplicity and controlled conditions. However, they suffer from slow heating rates, limiting their applicability for scaling up SCWG [107]. Tubular reactors on the other hand, enable continuous operation with short residence times, making them more suitable for scaling, but face several challenges in the SCWG process [108].

The commercial viability of SCWG faces several challenges including corrosion, formation of solid deposits consisting of coke and salts and the ability to pump the biomass slurry [83,108]. Only few reactor materials can withstand the harsh conditions of SCWG with temperatures up to 700 °C and pressures above 221 bar. Examples for materials with sufficient mechanical strength are the nickel-based alloys, e.g., alloy 625 (which is used in the present thesis) or alloy 602 [108]. In addition to the high temperatures and pressures, the reactor materials also face corrosion in SCWG. Corrosion presents a major challenge, driven by extreme operating conditions and the presence of corrosive gases and minerals [82]. Precipitating salts, which are poorly soluble in supercritical water [69,84,109,110], enhance corrosion, particularly at temperatures exceeding 500 °C [83,111,112]. Beyond accelerating material degradation, these salts can also obstruct system flow [113,114]. Effective separation of precipitated salts is therefore essential to maintaining long-term reactor performance. While prior studies have examined salt precipitation in salt–water mixtures under supercritical conditions [68,69,85,111], further research is needed to address the complexities introduced by biomass, which contains a diverse range of salts in varying forms in order to design a suitable salt separation.

Compared to conventional gasification methods, SCWG minimizes coke formation due to the dilution effect of supercritical water, which reduces molecular interactions and inhibits tar and coke buildup [64,115]. However, coke formation, even in small amounts, can lower gasification efficiency and cause operational blockages [87]. Coke primarily results from the polymerization of aromatic intermediates, such as furfurals [116,117], and tends to accumulate in heated pipelines where specific temperature conditions promote its formation. Research by Kruse et al. has identified high concentrations of these intermediates at subcritical temperatures [118]. To mitigate coke-related issues, employing rapid heating rates is suggested to be an effective strategy [118–120].

Additionally, a hurdle in SCWG is the difficulty in pumping the biomass slurry, which is directly influenced by the biomass content in the feed. While higher biomass concentrations improve gas production and overall process efficiency [82,121], they also reduce the slurry's pumpability, with the maximum feasible content depending on the specific biomass type [32]. To counteract this limitation, pre-treatment techniques, such as particle size reduction, can enhance slurry flow and improve process stability.

Addressing these technical barriers is crucial for advancing SCWG toward widespread commercial implementation. Continued research and innovation in these areas will be key to optimizing system efficiency and long-term feasibility.

Chapter 3. Materials and methods

Part of the content of this chapter is sourced from the following publication:

- Dutzi, J.; Vadarlis, A.A.; Boukis, N.; Sauer, J. Development and parametrization of novel reactor concept for the supercritical water gasification process. *Ind. Eng. Chem. Res.,* **2025**, 64, 9500-9517. DOI: 10.1021/acs.iecr.4c04267

  Declaration of contributions:

  Julian Dutzi conceptualized the experimental work and analysed the data, evaluated the results, and wrote the manuscript. Julian Dutzi conducted the thermodynamic equilibrium calculations and the comparison with experimental data.

  Athanasios A. Vadarlis conducted the thermodynamic equilibrium calculations and the comparison with experimental data.

  Nikolaos Boukis supervised the work, contributed to the discussion, and reviewed the manuscript.

  Jörg Sauer supervised the work, contributed to the discussion, and reviewed the manuscript.

3.1 Apparatus

The gasification experiments are carried out in a continuous lab-plant for high pressure (p ≤ 300 bar) and high temperature (T ≤ 700 °C) conversion of biomass compounds.



Figure 3.1: Two pictures of the continuous lab-plant.

The development of a suitable reactor concept for the process of SCWG was one of the main objective of the present work. Thus, throughout the present work, the lab-plant has been remodeled several times. Different reactors, preheaters and heating concepts were used. The periphery of the reaction system (feed system, low pressure system downstream of the reactor) stayed the same throughout the present work.

A detailed description of the different configurations can be found in the specific chapters.

3.2 Preparation of educts

The focus of the present work was to gasify biomasses which were mostly dry and grassy. Also, one type of woody biomass and one type of wet biomass were gasified. The biomasses were provided by the CERESiS partners from Scotland, Italy and Brazil. They were delivered in various forms (from powder to large pieces). All of the dry biomasses were milled to a powder (sieve size = 0.2 mm), as a small size was needed to feed the biomass slurry to the system.

To create the slurry, the biomass powder was mixed with distilled water in various ratios. Additionally, xanthan was added as a stabilizing agent. In some experiments, KOH or $KHCO_3$ was added as a homogeneous catalyst. The specific procedure to create the feed slurries varied throughout the work and can be found in the specific chapters.

Additional to the dry biomasses, ethanol, acting as a biomass model compound, was also gasified. For that purpose, ethanol was mixed with distilled water also in various concentrations. The details can be seen in the specific chapters.

3.3 Analysis

Throughout the whole experimental work, the same analytic methods were used. Thus, they are only stated here and not in the individual chapters.

In this work the composition of liquid, solid and gaseous samples was determined. The gaseous products were analyzed regarding the contents of H_2, CO, CH_4, CO_2, C_2H_4, C_2H_6, C_3H_8 and C_3H_6 by gas chromatography (5890 series II plus (Hewlett-Packard GmbH), equipped with a fused silica capillary column (Carboxen 1010 PLOT 30 m, SUPELCO)).

Liquid samples are analyzed regarding the following parameters:

- Total Carbon (TC) by combustion, Total Inorganic Carbon (TIC) by acid extraction and Total Organic Carbon (TOC) by calculation of the difference of TC and TIC in a TOC analyzer (DIMATOC 2100, DIMATEC Analysentechnik GmbH)
- Organic species via HPLC analysis with different columns (Lichrospher 100 RP-18, by Merck; Kinetex 2.6 µl C18 PFP 100A 100x4,6 (OOD-4462-EO), by Phenomenex; Aminex HPX 87H, by Biorad)
- Trace elements (Al, As, Pb, Cd, Ca, Cr, Fe, K, Cu, Mg, Na, Ni, Hg, S, Si, Zn, Co, Li, Mn, P, Sn) by ICP-OES (Inductively Coupled Plasma–Optical Emission Spectrometry) with an Agilent 725 spectrometer (Agilent Technologies).
- Molecular weight by size exclusion chromatography (SEC) with a LaChrom diode array detector DAD L-2455 (Merck), with a Viscotek A2500 column by Malvern Panalytical

The feed slurry is dried in an oven at 105 °C for 24 h to determine its dry matter content. The following parameters of the dry feed are determined:

- Trace elements (Al, As, Pb, Cd, Ca, Cr, Fe, K, Cu, Mg, Na, Ni, Hg, S, Si, Zn, Co, Li, Mn, P, Sn) by ICP-OES (Inductively Coupled Plasma–Optical Emission Spectrometry) with an Agilent 725 spectrometer (Agilent Technologies) after acidic pretreatment.
- CHNS content in the element analyzer vario EL cube (by Elementar Analysensysteme GmbH).

Solid samples, if present (e.g. deposits from the reaction), are analyzed qualitatively via SEM-EDS (Scanning Electron Microscope - Energy Dispersive X-ray Spectroscopy) in a GeminiSEM 500 (Carl Zeiss AG).

3.4 Data Interpretation

Throughout the whole experimental work, the same key figures were calculated. Thus, they are only stated here and not in the individual chapters. For evaluation of the success of the experiments the carbon efficiency (CE) and the total organic carbon (TOC) conversion are determined.

Carbon Efficiency (CE) quantifies the proportion of organic carbon in the feed that is converted to the gas phase during gasification. The calculation for CE is as follows:

$$CE = \frac{C\ in\ Product\ Gas}{TOC\ in\ Feed} = \frac{\sum \beta_i * x_i * \frac{\dot{V}_{Gas} * p}{R*T} * M_c}{\dot{m}_{Feed} * \alpha} \quad (3.1)$$

x_i	Concentration of component ‘i’ in the gas product (vol.%)
α	Organic carbon concentration in the feed (wt.%)
β_i	Number of carbon atoms of component ‘i’ in the gas product
$\dot{m}_{Feed}$	Feed mass flow (g h^{-1})
M_c	Molar mass of carbon (g mol^{-1})
p	Pressure (Pa)
R	Universal constant of gases (J $(mol \times K)^{-1}$)
T	Temperature (K)
$\dot{V}_{Gas}$	Gas flow under ambient conditions (l h^{-1})

CE is an important metric that reflects how effectively the organic components in the feed solution are transformed into gaseous products. The composition of the gaseous

product stream was quantified by gas chromatography. The calibration covered the major gas components, like H_2, CO and CO_2, and light hydrocarbons up to C_4. All chromatographic peaks detected in the experimental analyses could be assigned to calibrated gas components, with no additional unidentified signals observed. Furthermore, the calibrated C_4 hydrocarbons were not detected in the product gas samples. Thus, an extension of the calibration range to higher hydrocarbons was not considered necessary. All detected carbon-containing gas species were included in the calculation of CE. The properties of these gases were approximated using the ideal gas law.

TOC-conversion quantifies the fraction of total organic carbon in the feed slurry that is converted into other forms, such as gases, solubilized inorganic compounds in water, and organic residues like coke, tar, and soot and thus is an indicator of the wastewater's quality. The TOC-conversion is defined as follows:

$$TOC_{conv} = \frac{TOC_{Feed} - TOC_{Effluents}}{TOC_{Feed}} = 1 - \frac{\dot{m}_R * TOC_R + \dot{m}_S * TOC_S}{\dot{m}_{Feed} * \alpha} \quad (3.2)$$

$\dot{m}_R$	Mass flow of reactor effluent (g h^{-1})
$\dot{m}_S$	Mass flow of salt concentrate (g h^{-1})
TOC_R	TOC content of reactor effluent (mg g^{-1})
TOC_S	TOC content of salt concentrate (mg g^{-1})

The residence time (τ) is calculated according to Eq. 3.3. To determine the mass content of the reactor, the density under the existing temperature conditions has to be determined. Therefore, the temperature profile of the reactor is divided into sections of length l, defined by the positioned thermocouples. The average temperature of the two thermocouples is calculated and assumed to be constant over this section. With this information, the density can be determined and thus the mass content of the reactor can be calculated. For simplicity, the density of the mixture is assumed to be the density of water, as water is present in great surplus, and taken from the IAPWS-97 data base (software package by Ruhr University Bochum).

$$\tau = \frac{\pi * \left(\frac{d}{2}\right)^2 * l * \rho_{H_2O}}{\dot{m}_{Feed}} \quad (3.3)$$

d	Inner diameter of the reactor (m)
l	Length of section with constant temperature (m)
ρ_{H_2O}	Water density at given temperature and pressure (kg m^{-3})

In Chapters 3 and 6, further key figures are calculated and specified there.

Chapter 4. First investigations of dry biomasses in supercritical water gasification

The content of this chapter is sourced from the following publications:

- Dutzi, J.; Boukis, N.; Sauer, J. Process Effluent Recycling in the Supercritical Water Gasification of Dry Biomass. *Processes*, **2023**, 11, 797. DOI: 10.3390/pr11030797

  Declaration of contributions:
  Julian Dutzi conceptualized the experimental work and analysed the data, evaluated the results, and wrote the manuscript.
  Nikolaos Boukis supervised the work, contributed to the discussion, and reviewed the manuscript.
  Jörg Sauer supervised the work, contributed to the discussion, and reviewed the manuscript.

- Dutzi, J.; Boukis, N.; Sauer, J. Supercritical water gasification of heavy metal contaminated plants with focus on separation of heavy metal contaminants. *Biomass and Bioenergy,* **2024**, 182, 107059. DOI: 10.1016/j.biombioe.2024.107059

  Declaration of contributions:
  Julian Dutzi conceptualized the experimental work and analysed the data, evaluated the results, and wrote the manuscript.
  Nikolaos Boukis supervised the work, contributed to the discussion, and reviewed the manuscript.
  Jörg Sauer supervised the work, contributed to the discussion, and reviewed the manuscript.

- Dutzi, J.; Stoll, I.K.; Boukis, N.; Sauer, J. Screening of ten different plants in the process of supercritical water gasification. *Sustainable Chemistry for the Environment,* **2024**, 5, 100062. DOI: 10.1016/j.scenv.2024.100062

Declaration of contributions:

Julian Dutzi organized and analysed the data, evaluated the results, and wrote the manuscript.

I. Katharina Stoll conceptualized the experimental work, evaluated the results, contributed to the discussion, and reviewed the manuscript.

Nikolaos Boukis supervised the work, contributed to the discussion, and reviewed the manuscript.

Jörg Sauer supervised the work, contributed to the discussion, and reviewed the manuscript.

Summary of chapter 4

Soil and groundwater contaminated with heavy metals present a serious threat to both human and animal health. Phytoremediation, can effectively reduce soil and groundwater contamination. However, the used plants can accumulate the heavy metals, raising the need for methods to safely process and utilize the contaminated biomass. In principle, supercritical water gasification should allow the generation of a fuel gas from contaminated biomass while simultaneously separating pollutants, particularly heavy metals such as zinc, manganese, and iron, in a continuous laboratory system with process-integrated salt separation. However, there are critical challenges related to gasification efficiency, salt and heavy metal separation, and long-term operability.

In this chapter, various biomasses were investigated for their suitability in SCWG applications, including both moist and dry, woody and grassy types. They revealed minor differences in gasification efficiency and gas composition. A carbon efficiency of 60.3 ± 5.1% was achieved consistently across experiments. However, plugging caused by solid deposits, particularly in the reactor's high-temperature zones, remains a significant obstacle. For the moist biomass Reed Canary Grass, plugging of feed tubing was observed due to inadequate size reduction, highlighting the importance of proper pretreatment.

Process-integrated salt separation (downstream of the preheater) removed up to 35% of heavy metals into the salt concentrate, preventing secondary contamination. Notably, the separation efficiency was dependent on preheating temperatures, improving as temperatures increased from 460 to 550 °C. Despite these advantages, challenges persist with solid deposition, including coke, salts, and corrosion products, which limit experimental durations.

To optimize the economics and the ecological impact of the SCWG process, the influence of process water recycling on dry biomass gasification was explored. Recycling of the effluent from SCWG could reduce costs associated with treating contaminated wastewater but requires effective salt separation to prevent salt buildup, which can cause corrosion and flow blockages in the reactor. Experiments showed that while effluent recycling did not significantly affect product gas composition, it reduced carbon gasification efficiency by approximately 4% and increased the concentrations of

organic carbon and potassium in the reactor effluent. Thus, recycling is possible, but the waste water quality needs to be monitored.

In conclusion, the general suitability of the SCWG technology to process contaminated dry biomasses was demonstrated. However, some major issues such as salt deposition and coke formation, hinder long-term operation and thus require further development.

4.1 Introduction

Due to the careless handling of harmful substances in the past decades, pollutants like heavy metals have been distributed in air, water and soil. The groundwater and soils have been contaminated by mining, industry, transport and agriculture, which poses a threat to humans and animals that feed of the plants growing on contaminated sites [56,122,123]. Phytoremediation is a technology that uses plants to remove contaminants from soil, groundwater, and air [123]. Within the H2020 EU-project “ContaminatEd land Remediation through Energy crops for Soil improvement to liquid fuel Strategies” (CERESiS) the phytoremediation (in form of phytoextraction) of soils that are contaminated with heavy metals (e.g. Pb, Zn, Cr, Mn) and organics is investigated. For phytoextraction it is important to dispose or recycle the plants used appropriately to prevent secondary contamination [56,124,125]. The supercritical water gasification process seems to be suitable for this purpose as many studies have shown [56,58,113,126–128]. In SCWG, organic pollutants can be decomposed and inorganic pollutants like heavy metal salts can be separated in concentrated form. In addition, a hydrogen- and methane-rich product gas is produced [20], which for example can be converted to Fischer-Tropsch fuels after further purification and conversion steps.

In recent studies the fate of heavy metals in the process of SCWG was investigated in batch reactors [56–61]. Chen et al. demonstrated that during the gasification of lignite no heavy metals were transferred into the gas phase and only low concentrations in the liquid phase were detected. Most heavy metals were detected in the solid biochar, that formed in the process [58]. Su et al. postulate in the gasification of the hyperaccumulator *sedum plumbizincicola* that the formed biochar helps to absorb the heavy metals, where they form complexes with inorganic components [56]. In the gasification of

the same plant, Su et al. investigated the influence of alkali catalysts and found that the addition of alkali enhanced the immobilization of heavy metals into the biochar, as these catalysts increase gasification efficiencies and thus reduce the amount of organics in the biochar [57]. Thus, it is easier for heavy metals to form complexes with inorganics in the biochar and to precipitate [60]. Li et al. discovered that during the gasification of oily sludge longer residence times and higher temperatures were beneficial for the transfer of heavy metals from the liquid to the solid phase [61]. During continuous SCWG the formation of char and coke is unwanted since it can lead to blockage of the flow and decreases the gasification efficiency [87,100,115]. Since batch processes are of little interest for an industrial application of the SCWG process the separation of heavy metals in a continuous process needs to be investigated. For this purpose, continuous lab-scale SCWG experiments were conducted with subsequent analysis of the produced samples.

As different biomasses can be grown in different parts of the world depending on climate or soil quality, it is important to investigate whether there are major differences between different biomasses regarding the downstream processing via SCWG. For this purpose, continuous SCWG experiments were conducted with biomasses from different regions of the world (England, Italy and Brazil) in the framework of the current work.

When processing biomass via SCWG, usually wet biomasses were used like sewage sludge, spent grains or animal manure [82,109,129,130]. As SCWG is conducted with water as a reactant the moisture of these biomasses is no issue, as it for example would be in conventional gasification. In contrary dry biomasses are used in the present work as this is the kind of biomass processed in the CERESiS project. When dry biomass is processed a high amount of water with low salt content is necessary to dilute the biomass so that the slurry can be pumped [83] and enough water is available for the reaction. Typically, the dry matter content is 5 to 20 wt.% in the feed slurry [83,131]. The providing of salt-free water and the purification or disposal of the process effluent is cost-intensive and therefore recycling of the process effluent is attractive. This is possible due to low concentrations of salts in the reactor effluent [131]. Salts are poorly soluble in supercritical water [69,84,109] and can block the flow and cause corrosion [32,82]. A salt separation implemented in the process can reduce the amount

of salts in the reactor effluent [73] and therefore enable the recycling of process water [108]. Dry biomass contains little water and thus most of the effluent can be reused. In the past the recycling of process effluent was only investigated for wet biomasses in a small set of experiments at the Karlsruhe Institute of Technology [89], but not for dry biomasses. To optimize the process of SCWG of dry biomasses, the influence of process water recycling has to be investigated. In this chapter, the process water recycling during the supercritical water gasification of dry biomasses is tested and the effects on the SCWG process are described. Two different biomasses, a grass and a biomass with wooden stems and branches, were used for the experiments.

4.2 Screening of dry biomasses

4.2.1 Materials and methods

4.2.1.1 Preparation of educts

Ten different biomasses were used (eight different plant species of which two plants were evaluated from two different growing sites) (see Figure 4.1 and Table 4.1).

Table 4.1: Labeling of biomasses in the current work.

English name	Latin name	Abbreviation in the following text
Switchgrass	*Panicum Virgatum*	PV
Giant Reed	*Arundo donax*	AD
Grapevine	*Vitis vinifera*	GV
Silvergrass	*Miscanthus*	MC (either grown in HH or in ST)
Short rotation coppice	-	SRC (either grown in HH or in ST)
Reed Canary Grass	*Phalaris arundinacea*	RCG
Sugar Cane	*Saccharum officinarum*	SC
Energy Cane	-	EC

They were provided by the CERESiS partners from Scotland, Italy and Brazil in various forms. The biomasses Silvergrass (lat. *Miscanthus*) and Short rotation coppice were grown in two different locations in England, abbreviated with ST and HH. The dry

biomasses (DM > 90 wt.%) had to be milled to a size of 0.25 mm or smaller. Biomasses E, F, G and J (see Figure 4.1) were milled prior to delivery. The size of biomasses A, B, C and D was reduced by a mill with a 0.2 mm sieve (Pulverisette 14, Fritsch GmbH). For biomass I (wooden stems and branches of grapevines) two preliminary size reduction steps were carried out: first in a wood chipper (GE 260, Viking GmbH) to about 2 cm long pieces, then in a mill with 4 mm sieve (Pulverisette 25, Fritsch GmbH).

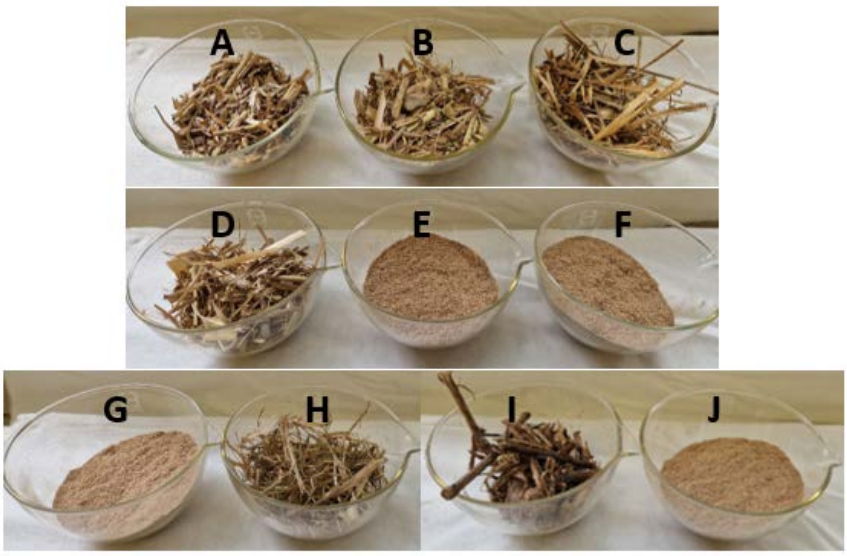


Figure 4.1: Pictures of biomasses as received from project partners (A: PV; B: AD; C: EC; D: SC; E: ST-MC; F: HH-MC; G: ST-SRC; H: RCG; I: GV; J: HH-SRC; for abbreviation see Table 4.1).

Biomass H (RCG) was provided in moist form (DM = 54.2 wt.%). The size was reduced by a meat grinder, as a mill was not sufficient due to the high water content. In different size reduction steps (see Figure 4.2) the size was reduced below 1 mm. A size analysis has not been performed.



Figure 4.2: Inner setup of meat grinder and size reduced Reed Canary Grass (RCG) (Biomass H).

The reduced size biomass H can be seen in Figure 4.2. The biomass is not in the form of powder and displays small fibers. Except for the different size reduction pathways, the further feed preparation was carried out in the same way.

The feed slurry was created by adding distilled water to the biomass powder in such a ratio that a dry matter content of 8 wt.%. was achieved. Xanthan, provided by Carl Roth GmbH, was added as a thickening agent (0.5 wt.%) to prevent phase separation, and KOH (5000 mg K^+/kg feed slurry), provided by Merck KGaA, was added as a homogeneous catalyst. After the addition of the additives the feed was thermally pretreated at T = 70 °C in a mixer for two hours under constant stirring (Thermomix TM31, Vorwerk Deutschland Stiftung & Co. KG).
Before every experiment with the CERESiS biomasses pre-experiments were carried out with ethanol solution (5 wt.% ethanol). The ethanol was supplied by VWR Chemicals. These pre-experiments were conducted to reach a gas-liquid-equilibrium in the system prior to feeding the biomass. With this procedure dead volumes in the lab-plant are filled with a water phase and gases with very similar composition like the later experiment and steady-state operation can be reached more quickly during the main experiment.

4.2.1.2 Apparatus

The SCWG experiments were performed in a continuous lab-plant for high pressure (p ≤ 300 bar) and high temperature (T ≤ 700 °C) conversion of biomass compounds. In the present configuration the lab-plant consists of two main parts: the preheater and the SCWG reactor (see Figure 4.3).

The preheater is made of a 750 mm long SS316 pipe (9/16 inch outer diameter, 8 mm inner diameter). The pipe is heated from the outside by two spiral heaters. Temperatures are monitored by six thermocouples on the outside of the pipe. After the feed is preheated to about 350 °C it enters the gasification reactor which is made of the nickel-base alloy 625 and has a length of 1500 mm (9/16 inch outer diameter, 8 mm inner diameter). Seven spiral heaters and 21 thermocouples are mounted on the outside of the pipe. In the reactor the main reactions between organics and water take place to form mainly gaseous products.

A filter bearing (F01) is installed downstream of the reactor to collect solids and tars that formed in the process. Salts that precipitated in the supercritical state of water (in the gasification reactor) might re-dissolve in the cooled water in the filter bearing. The formed salt concentrate can be retracted from the sump of the filter bearing by a two needle-valves, that open shortly after each other (20 ms) and act as a sluice. They open every 5 min and separate about 3 ml of salt concentrate into a glass container. The product gas and the reactor effluent leave the filter towards the back-pressure regulator (BPR) provided by Tescom. After the BPR follows the phase separation. Gas and liquid samples can be collected and analyzed. The products are quantified using scales and gas meters.

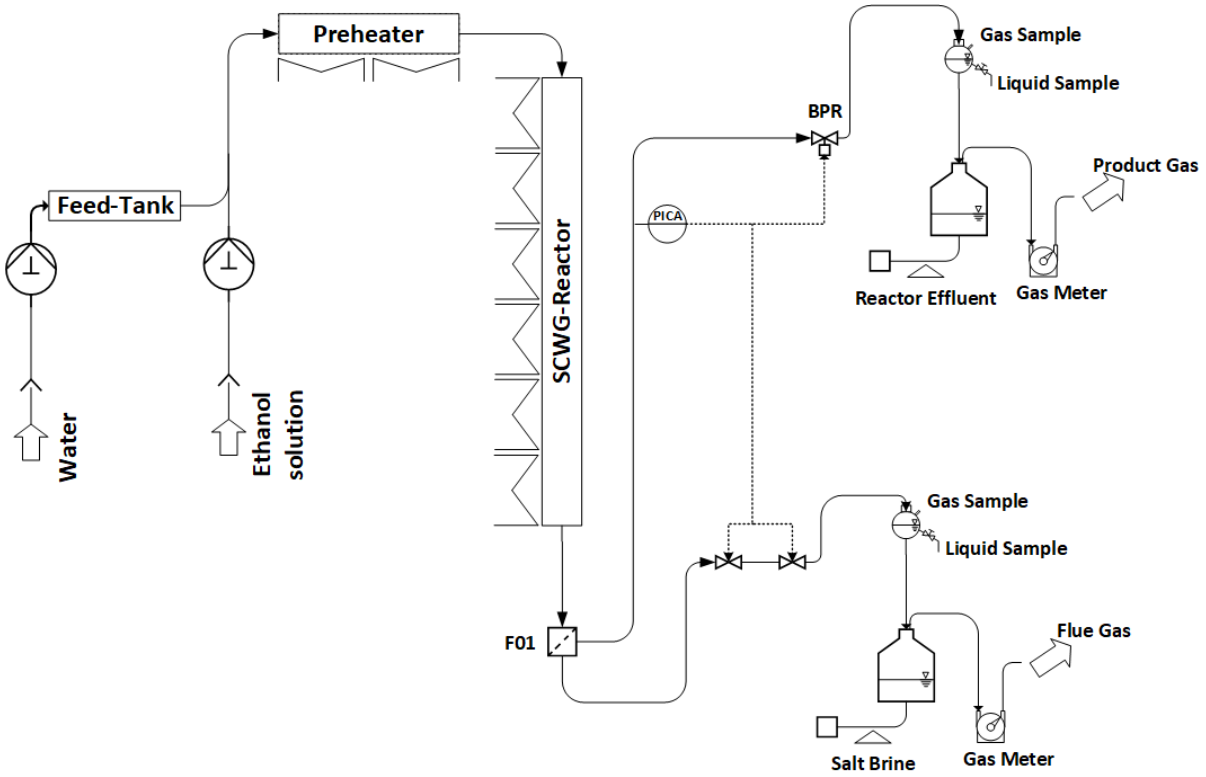


Figure 4.3: Process scheme of the continuous lab-plant in section 4.2.

To start up the experiment the system is pressurized with water using a high-pressure pump by Prominent and subsequently heated. To reach a gas-liquid-equilibrium in the system ethanol solution is gasified prior to feeding the biomass. With this procedure steady-state operation can be reached faster during the main experiment. The ethanol solution is fed into the system by a HPLC pump during the night before the experiment with biomass. For the biomass experiment the feed slurry is stored in a pressurized

tank. A water-driven piston pumps the feed into the system in defined amounts (for details see [113]). Pressure, flow and temperatures are set and monitored in the process control system.

4.2.1.3 Experimental

The SCWG experiments were conducted with a reaction temperature of 650 °C and a pressure of 280 bar. The biomass content in the feed slurry was 8 wt.% and the flow rate was set to 200 g h^{-1}. The set temperature profile can be seen in Figure 4.4.

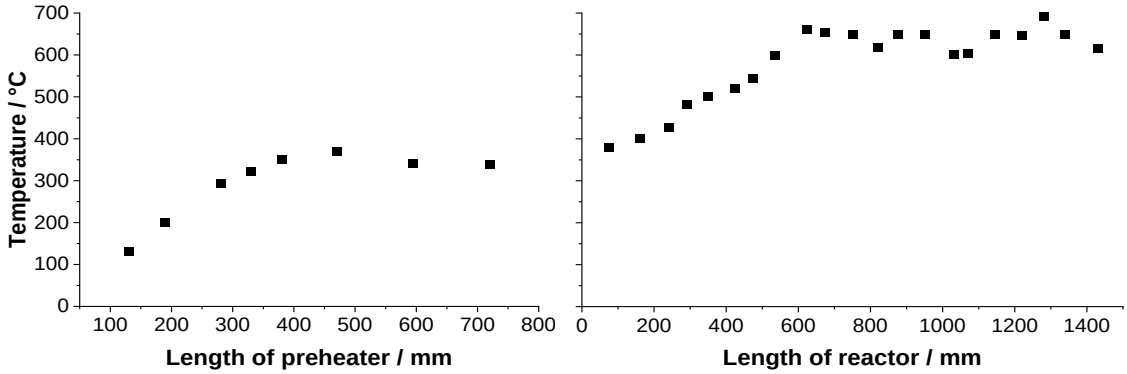


Figure 4.4: Outside temperature profile, representative of the experiments.

The set temperature profile resulted in a 900 mm long zone in which the temperature was greater than 600 °C (relevant for gasification; mean residence time in this zone was 65 s). Ten different biomasses were gasified. Their elemental composition can be seen in Table 4.2.

Table 4.2: Dry Matter (DM) content of biomass, elemental analysis (CHNO) on dry matter basis (wt.%).

Exp. Nr.	Biomass	DM	C	H	N	O
3.2.1	PV	97.7	43.6	6.4	0.4	46.8
3.2.2	SC	92.8	43.2	6.0	0.7	n.d.
3.2.3	AD	95.5	43.1	6.4	0.4	46.2
3.2.4	GV	95.1	47.1	4.5	1.2	47.2
3.2.5	ST-MC	99.4	45.9	6.9	0.8	40.7
3.2.6	ST-SRC	100.0	47.7	7.4	0.5	42.3
3.2.7	HH-MC	99.6	45.2	6.8	0.5	41.3
3.2.8	HH-SRC	100.0	48.2	7.0	0.6	42.1
3.2.9	RCG	54.2	43.7	9.2	1.3	45.8
3.2.10	EC	93.5	42.4	6.1	0.7	n.d.
	Mean μ		45.0	6.7	0.7	44.1
	Standard deviation σ		2.0	1.1	0.3	2.5

*n.d. = not determined

4.2.1.4 Data interpretation

The key figures used to evaluate the process are shown in section 3.4. Additionally, to assess the deviation of the results the mean value μ and the standard deviation σ are calculated according to Eq. 4.1 and 4.2.

$$\mu = \frac{1}{n}\sum_{i=1}^{m} y_i \qquad (4.1)$$

$$\sigma = \sqrt{\frac{\sum_{i=1}^{n}(y_i-\mu)^2}{n}} \qquad (4.2)$$

n	Number of values considered (-)
y_i	Value of sample i (%)

4.2.2 Results and discussion

SCWG is supposed to be able to process a wide variety of biomasses, either moist or dry. In literature it has been reported that kitchen waste, animal manure, sewage sludge, dry plants and many more biomasses have been gasified [82,129,132,133]. For example, D'Jesus et al. found that corn silage and clover grass were equally gasified and produced similar product gases [86]. It is important to understand the influence of the biomass on the process of SCWG. In the case of CERESiS, it must be known if some plants need to be excluded for the phytoremediation because a subsequent processing in SCWG would not be possible. For this purpose, ten different biomasses were evaluated under the same conditions. The feed was prepared according to section 4.2.1.1. The biomasses are listed in Table 4.2. They are very similar in composition, e.g. the carbon content is for example 45.0 ± 2.0 wt.%. The appearance though is very different (as displayed in Figure 4.1). The biomass GV for example is a woody biomass while MC is a grass. Thus, in these experiments a wide range of differently structured plants is covered. The experiments displayed quite similar results. The mean CE is 60.3% with a standard deviation of 5.1% (as can be seen in Table 4.3). The ability to gasify the different plants was thus similar. Regarding the gasification efficiency no differences was detectable between moist biomass like RCG (CE = 59.4%) and the dry biomasses (mean CE of dry biomasses μ = 60.4 ± 5.4%). Thus, the ability to gasify biomasses does not seem to depend on the degree of humidity of the biomass. Seemingly, biomasses with similar elemental composition (see Table 4.2), if moist or not, if woody or grassy, can similarly be gasified. Assuming Gaussian distribution of the CE of similar biomasses, a typical significance interval ($\pm 2\sigma$) can be set (see Figure 4.5). With this tool, future biomasses can be evaluated regarding the ability to gasify them. In case the CE lies inside the significance interval no significant deviation can be detected. If for example, calculating the mean and standard deviation without considering the biomass EC (i.e. prior to the last experiment) it becomes clear that the gasification of EC falls into this interval and thus is not significantly different from the other results.

Table 4.3: Carbon Efficiency (CE) and gas composition of different biomass experiments under same conditions.

Exp. Nr.	**Biomass**	**CE** %	**H_2** vol.%	**CH_4** vol.%	**CO_2** vol.%	**C_2H_6** vol.%
4.2.1	PV	68.0	34.4	17.7	42.3	3.8
4.2.2	SC	55.0	37.3	17.7	39.8	3.7
4.2.3	AD	68.2	33.9	19.6	39.4	4.9
4.2.4	GV	53.2	35.2	16.7	43.4	3.4
4.2.5	ST-MC	60.4	27.9	16.6	48.8	4.5
4.2.6	ST-SRC	65.1	32.3	19.2	42.1	4.3
4.2.7	HH-MC	55.6	31.7	17.3	44.7	4.1
4.2.8	HH-SRC	57.0	30.3	13.2	52.6	2.6
4.2.9	RCG	59.4	39.7	15.0	41.6	2.5
4.2.10	EC	60.7	32.7	16.2	45.6	3.9
	Mean μ	60.3	33.5	16.9	44.0	3.8
	Standard deviation σ	5.1	3.2	1.8	3.9	0.7

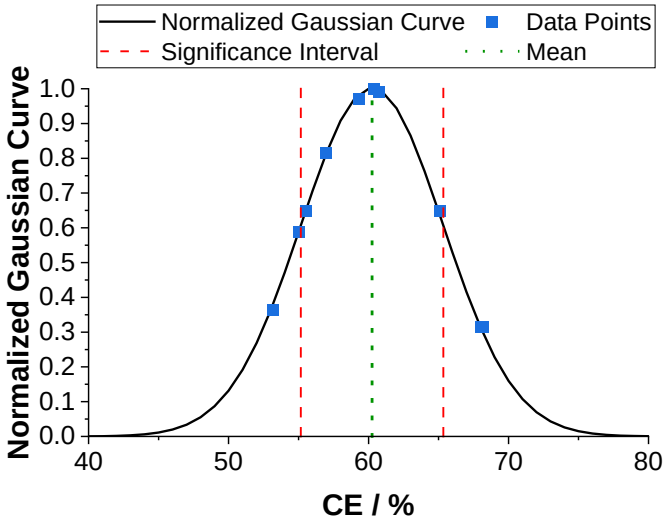


Figure 4.5: Carbon Efficiency (CE) of different biomass experiments in a Gaussian curve ($T_{Reaction}$ = 650 °C, p = 280 bar).

When visualizing the gas compositions (Table 4.3) in box plots (see Figure 4.6) it becomes clear that the gas compositions of the gasification of different biomasses are quite similar.

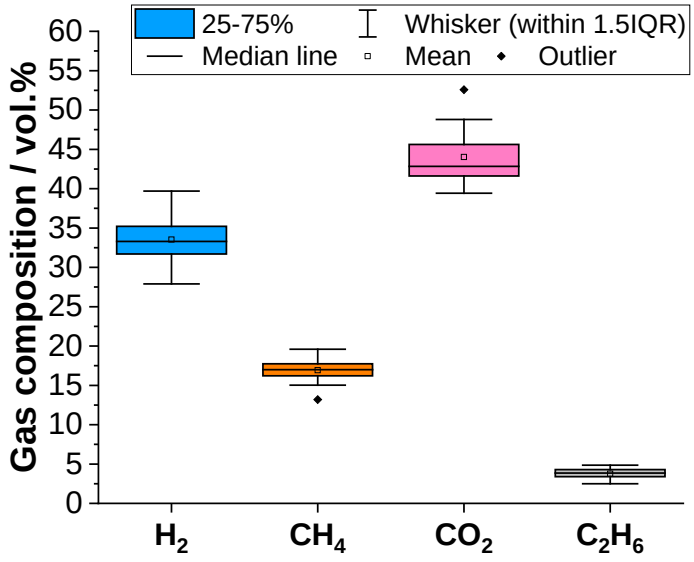


Figure 4.6: Gas compositions of different biomasses ($T_{Reaction}$ = 650 °C, p = 280 bar).

The variance in C_2H_6 content (3.8 ± 0.7 vol.%) and in CH_4 content (16.9 ± 1.8 vol.%) is very low. In H_2 content and CO_2 content more variance is visible. 33.5 ± 3.2 vol.% of H_2 are formed. In case of RCG (moist biomass) most hydrogen formed (39.7 vol.%). This might be due to the fact that RCG shows a higher hydrogen content in the dry biomass (see Table 4.2). Possibly it is also beneficial to feed the biomass that had not been previously dried to generate more H_2. In case of CO_2, 44.0 ± 3.9 vol.% are formed. HH-SRC showed a deviation in the CO_2 content (outlier in Figure 4.6).

One significant difference appeared in the gasification of moist and dry biomass. The experiments with dry biomass all lasted at least 6 hours prior to clogging, except for the biomass GV, but this must have been an outlier as in section 4.4 it is shown that this biomass is equally gasified as grasses with similar elemental composition. With RCG, which was the only biomass processed in moist form, the experiment ended after 3 h but not due to formation of solid deposits in the reaction system but due to blocking of the feed tubing. As described in section 4.2.1.1, RCG was ground up with a meat grinder to a supposed size smaller than 1 mm. As the feed tubing has an inner diameter

of 2.5 mm this size reduction was not sufficient. In future experiments with moist biomasses a different size reduction approach needs to be chosen.

As described above, the gasification efficiency is far from 100%. Some carbon remained in the reactor effluent, but only in small amounts ($TOC_{effluent}$ = 2000 ± 510 ppm). Since the TOC-conversion was 95.3 ± 0.8% in all cases and almost no TIC was detectable most of the carbon that did not form gaseous products deposited in some way. Additionally, tarry material formed that could not be quantified. After all experiments solid deposits were found in the gasification reactor about 50 cm from the top (set temperature on the outside 500 °C). In some cases, these deposits led to blockage of the flow and thus to an early end of the experiment. In section 4.4, this phenomenon is described in detail based on Reed Canary Grass and grapevines. It was found that these deposits consist of coke and salts that precipitate in the process. This can be confirmed by the EDS-analysis of solid deposits that were mechanically removed from the gasification reactor after these experiments (see Table 4.4). The solids in the reactor mainly consisted of carbon and secondly of salt building elements like Si, K and Ca. Not all solids deposited in the gasification reactor, in some cases the solids also dropped into the filter bearing below the reactor. These solids were also collected and analyzed via EDS. The analysis is shown in Table 4.5. It can be seen that also most of these solids are made of carbon in form of coke. In some cases, salt building elements like K (experiments 4.2.3, 4.2.5 and 4.2.7) or Si (experiments 4.2.7 and 4.2.9) are predominant. In experiments 4.2.7 and 4.2.9 the carbon seems to be present in form of carbonate CO_3^-, rather than coke. Some amounts of corrosion products are also in the solids, an extreme case is experiment 4.2.10 with 9.42 wt.% Cr.

It is important to remove salt building elements from the system prior to the gasification reactor. There they precipitate and subsequently can cause blockage of the flow and corrosion (as can be seen in solid sample of experiment 4.2.10). The coke formation has to be reduced as well to ensure high CE and long operation. Possible measures could be the reduction of the dry matter in the feed to increase the water surplus and to reduce the contact rates of biomass molecules and intermediates that could polymerize [89,134,135]. Faster heating rates could as well be beneficial because unwanted side reactions at temperatures below 600 °C could then be reduced

[106,118,119]. Kruse et al. found high concentrations of these aromatic intermediates at subcritical temperature [118].

Table 4.4: EDS-analysis of solids from reactor (in wt.%).

Exp. Nr.	**4.2.2**	**4.2.3**	**4.2.4**	**4.2.5**	**4.2.6**	**4.2.7**	**4.2.8**	**4.2.9**
C	81.15	71.64	89.5	68.87	79.91	74.02	81.55	47.98
O	9.12	15.05	5.91	13.68	11.04	13.87	11.25	27.28
Salt building elements								
Na	0.03	0.03	0.04		0.03	0.05		0.08
Mg	2.27	0.64	0.28	0.57	0.66	0.41	0.66	0.43
Al	0.2	0.04	0.06	0.09	0.09	0.05		0.27
Si	3.79	7.05	1.55	5.11	0.48	6.08	0.55	17.74
P	0.16	0.95	0.09	0.44	0.34	0.43	0.4	0.42
S	0.14	0.12	0.29		0.03	0.04		0.09
K	1.29	0.9	0.15	2.35	0.62	1.38	0.25	1.91
Ca	0.64	3.58	0.66	4.23	6.48	3.47	5.33	3.41
Metals								
Cr	0.22		0.42	2.41				
Fe	0.24		0.18			0.16		0.39
Ni	0.74		0.49	2.14				
Mo			0.37		0.15			
Zn				0.11		0.02		

Based on these insights, it can be concluded that plants with similar elemental composition behave similarly in the process of SCWG. Regarding the framework of CERESiS, this leads to the conclusion that the biomasses can be chosen according to their ability to remediate the grounds without the need to worry about the processing of a wide range of biomasses.

Table 4.5: EDS-analysis of solids from F01 (in wt.%).

Exp. Nr.	**4.2.1**	**4.2.2**	**4.2.3**	**4.2.4**	**4.2.5**	**4.2.6**	**4.2.7**	**4.2.8**	**4.2.9**	**4.2.10**
C	81.38	57.24	41.68	63.27	46.91	92.17	16.29	91.6	26.05	36.45
O	8.64	21.39	24.21	24.78	22.40	4.38	41.16	4.80	37.04	18.13
Salt building elements										
Na	0.04	0.07	0.21	0.32	0.82	0.06	1.02	0.01	0.07	
Mg	0.96	3.82	0.76	0.08	1.81	0.06	0.19	0.17	0.85	2.20
Al	0.09	0.3	0.07	0.17	0.15	0.03	0.07		0.52	0.26
Si	2.19	8.24	7.07	1.02	4.86	0.08	15.78	0.32	27.65	5.13
P	0.20	1.25	0.7	0.08	0.42	0.37	0.16	0.49	0.96	0.48
S	0.20	0.06	0.42	0.59	0.26	0.10	0.13	0.17	0.16	0.34
Cl	0.06		0.53	0.11	0.47		0.35	0.04	0.12	
K	2.51	3.1	11.86	6.37	15.18	1.08	19.02	0.83	1.64	1.29
Ca	0.65	3.03	1.63			1.08	0.35	1.43	3.69	1.62
Metals										
Cr	0.36	0.14	0.86				1.28		0.15	9.42
Fe	0.29	0.35	0.44		0.81		0.18		0.9	1.98
Ni	1.63	0.15	3.19			0.24			0.2	22.7
Mo	0.79	0.69	5.98	3.07	5.89	0.34	4.02			
Zn		0.08						0.15		

4.3 First process parameter variations

4.3.1 Materials and methods

4.3.1.1 Preparation of educts

The grasses Reed Canary Grass (RCG, lat. *Phalaris arundinacea*) and Napier Grass (lat. *Pennisetum purpureum*) and wooden stems and branches of grapevines were used as biomass sources for the gasification experiments (see Table 4.6 and Figure 4.7). The grapevines were delivered in pieces about 10 cm long, which were milled to a powder using a wood chipper (GE 260, Viking), a mill with a 4 mm sieve (Pulverisette 25, Fritsch), and a mill with a 0.2 mm sieve (Pulverisette 14, Fritsch). For the size reduction of Napier Grass the Pulverisette 14 was sufficient. The biomasses were

chosen as they are relevant for the CERESiS project. The CERESiS project strategy is to identify high biomass productivity, low contaminant uptake species suitable for a particular climatic zone, following the results of the BioReGen project [136]. Also, there was a lack of literature on the SCWG of dry biomasses.



Figure 4.7: Gasified biomasses as delivered (left to right: grapevines, Napier Grass, Reed Canary Grass).

Table 4.6: Origin of Biomasses.

Biomass	**Napier Grass**	**Reed Canary Grass**	**Grapevines**
Country of origin	Brazil	England	Italy
Site/main soil issue	Former tannery/Cr	Former landfill/clean soil capping	Vineyard/pesticides
Delivered Form	Straw	Powder (0.25 mm sieve)	About 10 cm long pieces
Dry Matter / %	89.9	97.4	95.1

The elemental composition and the contamination of the biomasses are presented in Table 4.7 and Table 4.8.

Table 4.7: CHNS analysis of biomasses, based on dry weight (in wt.%).

Biomass	**C**	**H**	**N**	**S**
Napier Grass	43.2	6.00	1.0	0.200
Reed Canary Grass	48.9	7.46	<0.3	0.090
Grapevines	47.1	4.47	1.2	0.003

Table 4.8: Heavy metal contamination of biomasses (in ppmw).

Biomass	Pb	Ni	Zn	Cd	Cr	Mn	Fe
Napier Grass	126.18	12.63	49.93	1.05	27.25	70.83	348.10
Reed Canary Grass	0.50	0.60	37.00	<0.10	0.90	490.00	61.00
Grapevines	0.05	0.06	26.61	<0.10	0.15	50.40	42.80

To create a feed slurry, water was added to the biomass powder to adjust the dry mass to about 8 wt.% (up to 20 wt.% of dry matter is possible to gasify [108], but higher dry matter content than 8 wt.% (value from experience) might lead to plugging in feed tubing as the lab-plant is equipped with quarter-inch pipes). Xanthan was added as a thickening agent (0.5 wt.%, based on slurry mass) to prevent phase separation, and KOH (5000 mg K^+/kg feed slurry) was added as a homogeneous catalyst. KOH enhances the water gas shift reaction, increases H_2-yield and weakens the intermolecular bonds of the biopolymers due to its alkaline character (pH = 9.3 in feed), which increases decomposition of the macromolecules [106,137,138]. The components were mixed and thermally pretreated at a temperature of 70 °C for two hours in a mixer (Thermomix TM31, Vorwerk). Low temperature thermal pretreatment is conducted because part of the organics is solubilized after this pretreatment and thus easier to gasify [139,140]. After cooling, samples of the final slurry were taken to analyze dry matter content and elemental composition.

4.3.1.2 Apparatus

A continuous lab-plant for high pressure (p ≤ 300 bar) and high temperature (T ≤ 700 °C) conversion of biomass compounds at the Karlsruhe Institute of Technology was used for laboratory tests. The setup for this investigation included a preheater, a salt separation unit, and a gasification reactor. The dimensions of the preheater and reactor can be seen in Table 4.9.

The set temperatures of the preheater are such that the reaction medium reaches its supercritical state. Salt separation occurs downstream of the preheater using a T-fitting, where inorganic compounds are separated from the biomass slurry due to their low solubility in supercritical water. This salt separation device was installed based on the knowledge gained in section 4.2, that sufficient salt separation is important for long-

term operation and minimization of solid formation. The salts (and heavy metals) are supposed to drop down vertically into the salt concentrate at the T-fitting (separation by gravity) while the organics are transported sideways to the gasification reactor (a schematic drawing can be seen in [113]). A small amount of the salt concentrate is semi-continuously separated in a defined interval by two needle valves that act as a sluice (the valves open 20 ms apart). The salt concentrate is immediately depressurized and collected in a glass container. Since only a small amount of liquid is separated (about 3-5 g per sluice operation) the pressure in the lab-plant is not significantly affected by this.

Table 4.9: Dimensions of preheater and reactor.

	Preheater	**Reactor**
Material	Inconel 625 with SS 316 Liner	Inconel 625
Length / mm	750	1800
Inner Diameter / mm	3.20	8.00
Electric Heating	3 spiral heaters	6 rod heaters

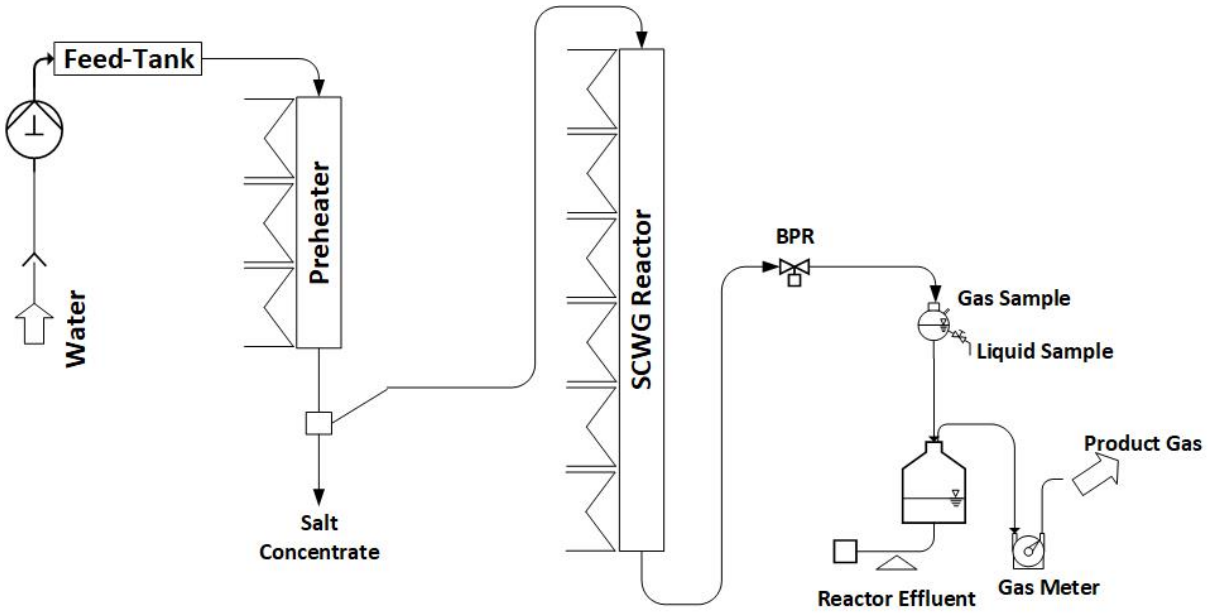


Figure 4.8: Process scheme of the lab-plant in section 4.3.

Gas meters (Ritter GmbH) and scales (Soehnle GmbH) are used to quantify the products of the experiments, positioned in the low-pressure part of the lab-plant. Liquid and gas samples are taken at regular intervals form a glass container in the low-pressure part of the plant during the experiment to ensure a steady-state operating condition. The system is pressurized and heated using a HPLC pump and a process control system. A preliminary test using an ethanol solution is run the day before the main experiment to bring the system into liquid-gas equilibrium (dead volumes of the plant are filled with a gas mixture similar to the gas produced by biomass gasification) and to check for leaks. The feed slurry is stored in a tank and indirectly pumped into the system by a piston using a HPLC pump.

4.3.1.3 Experimental

In total seven experiments were conducted (see Table 4.10). During the experiments the pressure was 280 bar and the temperature of the SCWG reactor was 650 °C. Three different plants were processed. In addition, three different preheating temperatures and three different flow rates were set for the gasification of Reed Canary Grass. The duration of the experiments was limited by the available amount of feed slurry (some experiments were ended prematurely due to blockage of the flow). Each experiment was conducted once due to the limited time and resources and high effort it takes to prepare the experimental setup.

Table 4.10: Process parameters of conducted experiments.

Exp. Nr.	**Feed**	**Duration h**	**$T_{Preheater,max}$ °C**	**Flow rate g h^{-1}**
4.3.1	Napier Grass	4.50	500	700
4.3.2	Grapevines	5.75	500	700
4.3.3	Reed Canary Grass	6.50	500	700
4.3.4	Reed Canary Grass	3.50*	460	700
4.3.5	Reed Canary Grass	3.92*	550	700
4.3.6	Reed Canary Grass	6.25	500	500
4.3.7	Reed Canary Grass	0.25*	500	300

* Premature ending of the experiments due to blockage of the flow.

4.3.2 Results and discussion

4.3.2.1 Influence of biomass type

To investigate the influence of the dry biomass type on the process of SCWG three different dry plants were processed. Two grasses, Napier Grass and Reed Canary Grass, and a plant with wooden stems and branches, grapevines, were gasified (see Table 4.11).

Table 4.11: Results of the gasification experiments.

Exp. Nr.	**Feed**	**CE** %	**TOC-conversion** %	**TOC content in effluent** mg kg^{-1}
4.3.1	Napier Grass	60.45	78.03	3933
4.3.2	Grapevines	55.18	86.20	3027
4.3.3	Reed Canary Grass	59.14	83.83	3204
4.3.4	Reed Canary Grass	67.35	89.69	3765
4.3.5	Reed Canary Grass	63.38	85.66	3310
4.3.6	Reed Canary Grass	61.92	89.13	2821
4.3.7	Reed Canary Grass	-	-	-

The mean steady-state carbon balance was 77% with a standard deviation of 4.3% in all experiments, as not all carbon could be detected either in gas or liquid effluent and solid deposits formed. Obviously, solids remain in the tubing of the plant causing fouling. This leads to premature end of several experiments, mechanical cleaning of the plant had to be performed frequently. The experiments for comparison of the different biomasses (experiments 4.3.1, 4.3.2 and 4.3.3) were finished according to plan.

The feed composition regarding the CHNS content and the content of the main salt building elements can be seen in Table 4.12. There are some differences between the feed compositions, especially the potassium content of the biomass slurry of Napier Grass is higher than the other two kinds of feed. This is due to the high potassium content of the biomass Napier Grass, which has been described in literature [141,142].

Table 4.12: Content of CHNS and main salt building elements in the feed slurry in wt.% (based on dry matter).

Exp. Nr.	Feed	C	H	N	S	K	Ca	Mg	Si	P
4.3.1	Napier Grass	39.3	5.6	0.9	0.2	6.90	0.45	0.03	0.88	0.12
4.3.2	Grapevines	43.6	5.7	0.5	<0.1	4.13	1.53	0.10	0.46	0.13
4.3.3	RCG	39.6	5.5	0.4	0.1	4.68	0.29	0.08	2.27	0.13

Minor differences between the plants regarding carbon efficiency were noticed (experiments 4.3.1, 4.3.2 and 4.3.3) (see Table 4.11). The mean CE for all plants is 58.3% with a maximum deviation of 3.1%. The CE is therefore not influenced by the kind of dry plant that was processed in the present experiments. D'Jesus et al. also noticed only small differences in CE when gasifying clover grass (44.9 wt.% C in biomass) and corn starch (44.4 wt.% C in biomass) in a similar lab-plant [86]. Thus, when biomasses with similar elemental composition are gasified (similar carbon content) the CE does not seem to be significantly influenced by the type of plant. This confirms the knowledge gained in section 4.2, also in a changed experimental setup.

A small difference in the TOC content of the reactor effluent was visible. The TOC-conversion is 78% for Napier Grass, 84% for Reed Canary Grass and 86% for grapevines. Since the TOC conversion compares the amount of TOC that is contained in the effluents with the TOC content of the feed it is an indicator of the effluent purity. During experiment 4.3.1 with Napier Grass a higher TOC content in the effluent of about 20% is visible than in the other two experiments although CE is roughly the same. This can be explained by the formation of solids during the experiments 4.3.2 and 4.3.3 with Reed Canary Grass and grapevines. After each experiment the reactor and the pre-heater are opened and checked for solid deposits. After the experiment with Napier Grass no solid deposits were found in the system. After the other two experiments solid deposits were found at the top of the SCWG reactor (300-500 mm from the top, where a temperature of 500 °C was set). The carbon contained in these solid deposits can not be gasified and is not contained in the reactor effluent and therefore the TOC content of the experiments with Reed Canary Grass and Grapevines was lower than in the

experiment with Napier Grass even though the carbon efficiency and therefore the amount of gas produced was roughly the same.

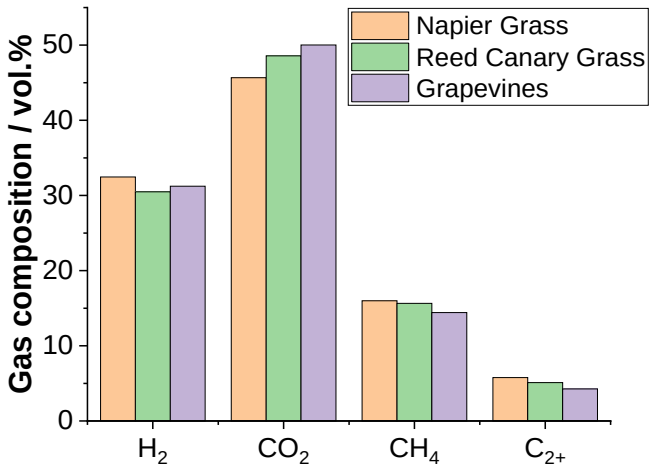


Figure 4.9: Gas composition of the gasification of three different feeds.

The gas composition is also not significantly influenced by the kind of dry plant that is processed (see Figure 4.9). The mean H_2-content of the product gas is 31 vol.% with only little deviation. The most visible difference can be seen when comparing the CO_2 and CH_4-contents of the product gas of Napier Grass and Grapevines. About 4 vol.% more CO_2 and 1.5 vol.% less CH_4 is contained in the product gas of Napier Grass than in the product gas of grapevines. The methanation reactions seem to take place in a slightly greater extend in the case of Napier Grass. Methanation reactions are kinetically limited and therefore longer reaction times result in an increased CH_4-yield [67,143,144]. The flow rate was set at 700 g h^{-1} during all three experiments and thus the residence times were the same initially. As mentioned before, solid deposits occurred during the gasification of grapevines. These solid deposits reduce the free diameter of the reactor and so the residence time decreases over the course of the experiment. This could be a possible reason for the small differences in gas composition.

As the heavy metal contamination (see Table 4.8) of the biomasses is rather low, the gasification process is presumably not influenced by the heavy metals. Thus, the achieved gasification results can be transferred to non-contaminated biomasses of the same species.

4.3.2.2 Influence of the preheating temperature

The temperature settings of the preheater are crucial for the separation of salts in the lab-plant. Salts need to be separated from the reaction medium since salts can cause blockage of the flow due to precipitation [102,111] and enhance corrosion rates at T > 500 °C [83,111,145,146]. Salts are generally poorly soluble in supercritical water [84] and thus can be separated by precipitation. In binary salt-water systems salts are distinguished between type 1 and type 2 salts [68,69,85]. Type 1 salts are soluble in dense supercritical water and only precipitate when the temperature is further increased, while type 2 salts are almost non-soluble in supercritical water. Downstream of the preheater a T-fitting is located where salts are supposed to be separated by precipitation. Since the T-fitting at which salts are supposed to be separated is not externally heated the reaction medium needs to be preheated sufficiently so the temperature is supercritical at the T-fitting. The salt separation is conducted upstream of the gasification reactor to avoid extensive salt deposition in the reactor. To investigate the influence of the preheating temperature on the separation of salts three different maximum preheating temperatures (460 to 550 °C) were set. This resulted in the following temperatures at the T-fitting (measurement on the outside) (see Table 4.13).

Table 4.13: Temperatures of the T-fitting for salt separation.

Exp. Nr.	$T_{Preheater,max}$ **°C**	$T_{T\text{-}Fitting}$ **°C**	Duration of Experiment **h**
4.3.4	460	370	3.5*
4.3.3	500	388	6.5
4.3.5	550	394	3.9*

* Premature ending of the experiments due to blockage of the flow.

To evaluate the quality of salt separation the concentration of relevant salt building elements (Ca, K, Mg, Na, S, Si and P [75,147,148]) is monitored in the effluents of the lab-plant. During the experiment 4.3.4 only a subcritical temperature of 370 °C could be reached at the T-fitting. Thus, the separation of salts based on precipitation does not work. This can be seen when looking at the distribution of the salt building elements (see Figure 4.10).

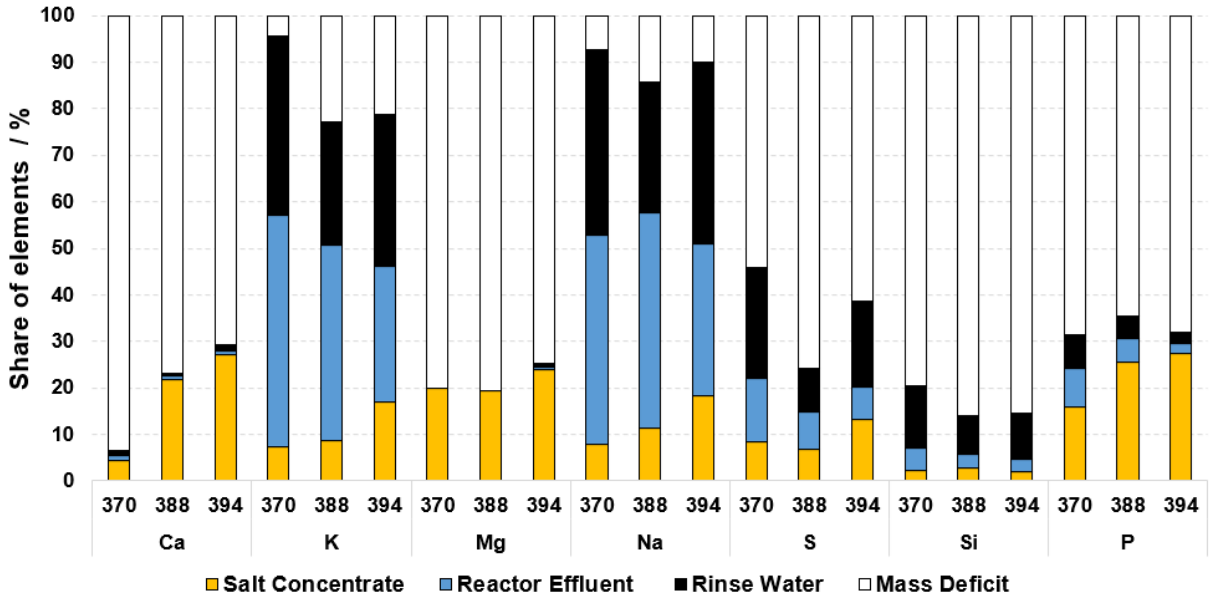


Figure 4.10: Share of elements in the liquid effluents of different experiments with different preheating temperatures (370 - 394 °C) (feed concentration = 100%).

Less than 20%, in most cases even less than 10% of the salt building elements can be detected in the salt concentrate. Potassium and sodium are mostly detected in the reactor effluent and the rinse water (after every experiment the system is flushed with water). For all other salt building elements, a big mass balance deficit can be seen. The balance deficit, as mentioned, can be assumed to consist of solid deposits that mainly stayed in the reaction system (some solids were also contained in the salt concentrate). Solid deposits cannot be quantitively collected and analyzed (due to their inhomogeneities) and therefore cannot be calculated into the mass balance of the elements. After experiment 4.3.4 solid deposits were discovered in the top part of the SCWG reactor where a temperature of 500 °C was set. The formation of solid deposits in the reaction system poses a danger to long-time operation of the process.

The increase of the preheating temperature to 500 °C (experiment 4.3.3) resulted in a slightly supercritical temperature of 388 °C at the T-fitting. The separation of calcium, sodium and phosphorus into the salt separation increased. The separation of the other elements was not influenced by the rise in temperature. As stated earlier, salt separation is influenced by the type of salt. Examples of type 2 salts that could explain the shown behavior of Ca and P could be $CaSO_4$ and Na_3PO_4 [81]. The separation of the other salt building elements was not influenced. These salt building elements might be present in type 1 salt configurations, such as NaCl, K_3PO_4, KCl or K_3SiO_3 [81,111]. The

mass deficit of most elements is very large. Similar to the experiment 4.3.4, after the experiment 4.3.3 solid deposits were discovered in the top part of the reactor where a temperature of 500 °C was set.

The qualitative analysis (EDS-analysis) of the solid deposits of the SCWG reactor (experiment 4.3.3) displays a mixture of carbon and salt building elements (see Figure 4.11). Especially silicon and potassium can be detected. On the right side of the micro photography a big planar structure consisting of nickel can be seen. This can be assumed to be a corrosion product from the reactor. The reactor is made of the nickel-based alloy Inconel 625. Since salts are known to enhance corrosion rates this shows the importance of a functioning salt separation. The functionality of the salt separation was still not given for the selected process conditions.

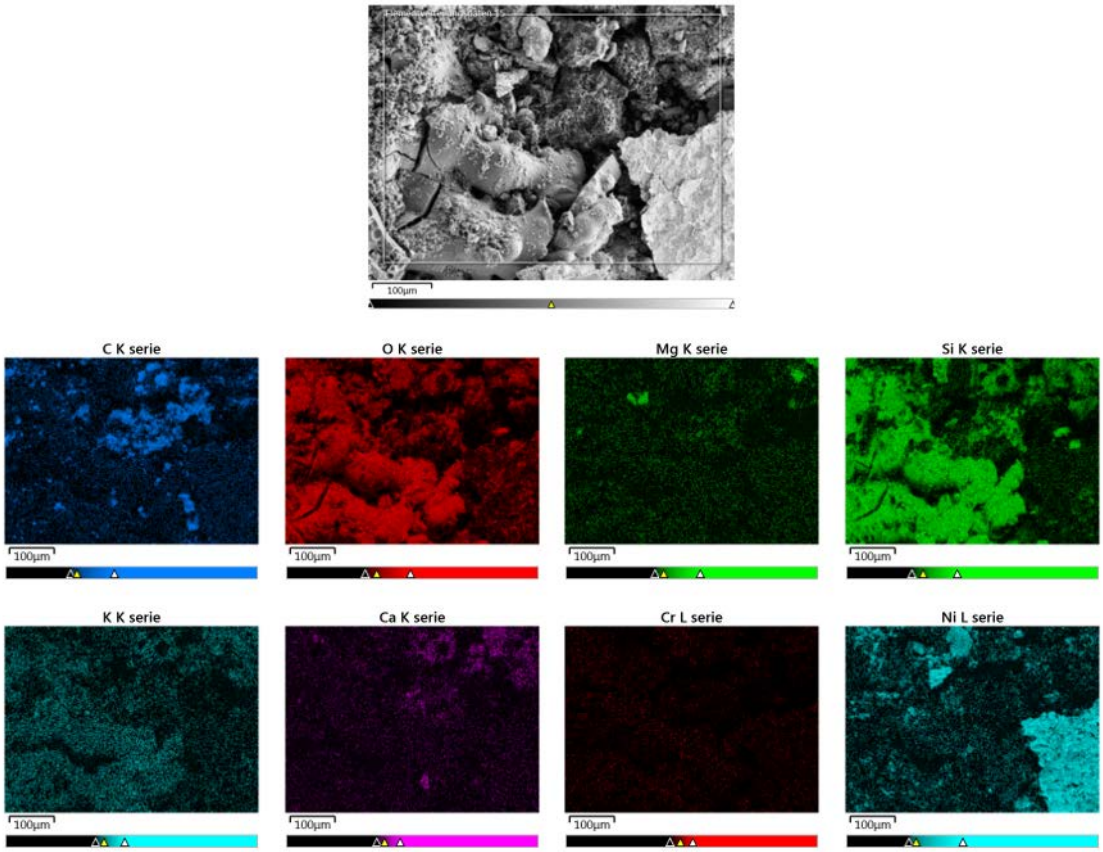


Figure 4.11: SEM-EDS analysis of the solid deposits of experiment 4.3.3.

In both experiments (experiments 4.3.4 and 4.3.3) the solid deposits occurred in the section of the reactor where a temperature of 500 °C was set (on the outside of the pipe). An inner temperature measurement in the reaction medium was not possible.

Therefore, the reaction temperature has to be estimated based on data given in literature. Due to a relatively big inner diameter of 8 mm in the SCWG reactor a low flow speed results. D`Jesus could not detect any temperature gradients between inside the medium and outside of the pipe in a SCWG reactor with 8 mm inner diameter [89]. In the section where the solid deposits occurred the temperature in the reaction medium can therefore be assumed to be above 450 °C (and below 500 °C). This temperature range seems to be critical for the separation of most salts. This has been experimentally confirmed by Schubert et al. [69]. According to Schubert et al., a salt separator set point temperature of 430 °C is necessary to separate more than 90% of K_3PO_4 and 470 °C to separate more than 90% of $Ca(NO_3)_2$ into the salt concentrate [69]. In experiments 4.3.4 and 4.3.3, in which a maximum preheating temperature of 460 and 500 °C was set, these temperatures seem not to be reached in the reaction medium within the preheater and thus the precipitation of salts could not take place at the T-fitting. Due to a small inner diameter of the preheater (3.20 mm) and thus higher flow speed a lower maximum temperature of the reaction medium is reached.

A further increase in the preheating temperature to 550 °C (experiment 4.3.5) resulted in 394 °C at the T-fitting. Even though this temperature is only 6 °C higher than when the preheating temperature was 500 °C, an improved salt separation can be seen for almost all salt building elements. Almost 30% of Ca and P can be separated. The separation of K, Na, Mg and S also improves by about 5%. Solely silicon is not influenced by the increasing temperature. The mass deficit is still very high for most salt building elements (except K and Na). During this experiment solid deposits formed in the preheater, leading to faster plugging even though the salts were separated more efficiently as the inner diameter of the preheater was smaller than that of the reactor. Due to the high maximum preheating temperature of 550 °C the temperature in the reaction medium can be assumed to be higher than 450 °C in the preheater. This resulted in improved salt separation but also in precipitation of salts in the preheater and led to blockage of the flow in the preheater. In Figure 4.12 it can be seen that Ca, Mg, Si and K are part of the solid deposit in the preheater.

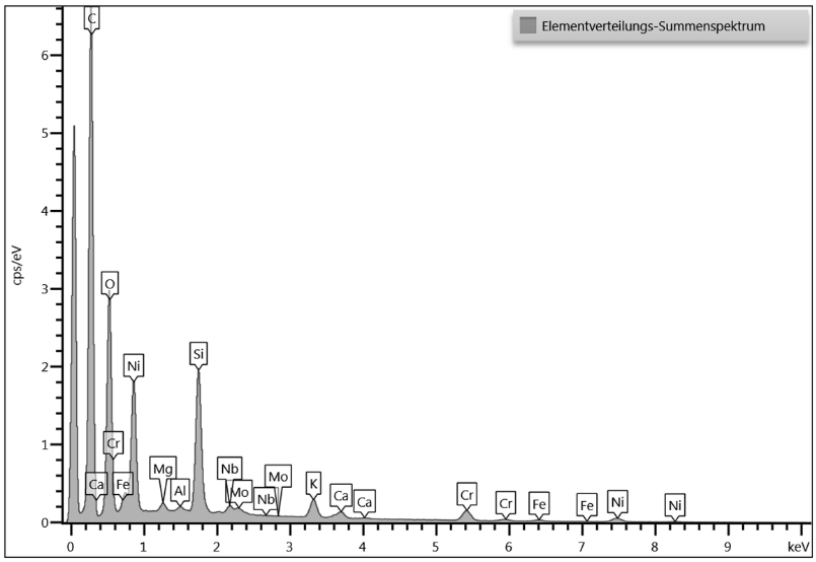


Figure 4.12: Elemental spectrum of a sample of solid deposits in the preheater.

4.3.2.3 Influence of residence time

To investigate the influence of the residence time on CE and the formation of solid deposits during the gasification of Reed Canary Grass three different throughputs were set (see Table 4.14). Experiment 4.3.7 did not reach a steady state and therefore it can not be considered in the evaluation of the trend of CE and TOC. For the other two experiments (4.3.3 and 4.3.6) CE only slightly rises with increasing residence time (17 to 24 s) (see Table 4.14). Generally, it is known that CE rises strongly with increasing residence time [66,143,149]. This cannot be observed in the present experiments. A possible reason for this could be the formation of solid deposits in the SCWG reactor (as stated in section 4.3.2.2). This assumption can be made since the TOC content of the effluent decreases while CE only rises slightly with increasing residence time. Experiment 4.3.6 had to be finished prematurely due to blockage of the flow in the SCWG reactor. After experiment 4.3.3 solid deposits were also detected in the same part of the reactor but they did not lead to blockage of the flow. Therefore, more solid deposits were formed during experiment 4.3.6. A lower flow speed and thus higher residence time in the temperature range of 450 to 500 °C seems to be disadvantageous for the chemistry of SCWG towards gases and favors the formation of solid deposits. Faster heating to the desired temperature of 650 °C should be implemented since tar and char production are significantly influenced by the heating rate [150]. This might avoid

coke formation and additionally enable better salt separation as the salts seem to deposit in a temperature range of 450 to 500 °C, which so far has not been reached at the salt separation T-fitting.

Table 4.14: Residence time and salt separation temperature of different experiments.

Exp. Nr.	**Duration** h	**Flow rate** g h^{-1}	$\tau_{Preheater}$ s	$\tau_{Reactor\ (T>600°C)}$ s	$T_{T\text{-}Fitting}$ °C
4.3.3	6.5	700	4.6	17	388
4.3.6	6.25*	500	7.4	24	400
4.3.7	0.25*	300	12.4	41	420

* Premature ending of the experiments due to blockage of the flow.

The gas composition is not significantly influenced by the increase of the residence time (see Figure 4.13). A slight increase of H_2 can be seen when the residence time is increased from 17 to 24 s. This effect has been reported by other authors [66,135].

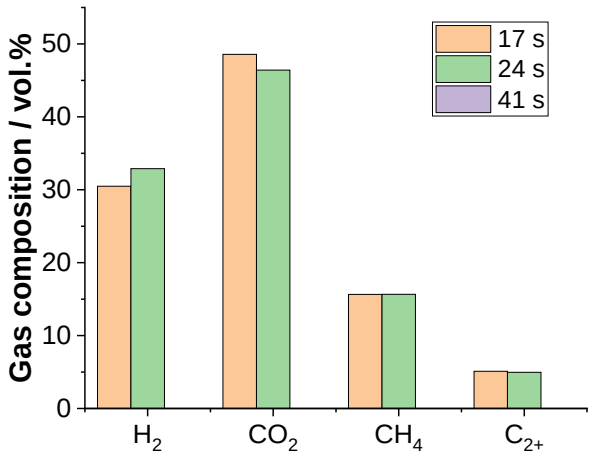


Figure 4.13: Steady state gas composition for three different residence times in the SCWG reactor (T > 600 °C), no steady state reached for the mean residence time of 41 s.

As stated above, experiment 4.3.7 did not reach steady state operation due to blockage of the flow. Solid deposits blocked the flow in the preheater. As described in section 4.3.2.2, a temperature of above 450 °C in the reaction medium seems to be critical

for the formation of solid deposits that consist of coke and salts (see Figure 4.11 and Figure 4.12). In order to achieve higher residence times, the throughput was reduced from 700 to 300 g h^{-1}. This resulted in reduced flow speed in the preheater. Due to the reduced flow speed higher temperatures can be reached in the preheater. An indicator for this is the temperature at the salt separation (T-fitting) downstream of the preheater (see Table 4.14). When a throughput of 700 g h^{-1} was set the temperature was 388 °C but when the throughput was 300 g h^{-1} it was 420 °C at the T-fitting. Therefore, it can be assumed that the critical temperature range of T > 450 °C was reached within the preheater (assuming some thermal losses in the not heated part of the plant) and led to precipitation, combined with a low flow speed. This explains why solid deposits formed in the preheater and blocked the flow after a short time and a further increase in residence time could not be investigated.

To achieve higher residence times a larger reactor should be implemented in future experiments instead of reducing the throughput. In that way consistent temperatures of the reaction medium will be ensured. This will avoid the change of a second parameter – the temperature profile – when the residence time is changed and thus clear correlations between residence time and CE can be determined.

4.3.2.4 Separation of heavy metals

In batch SCWG experiments with contaminated biomasses most heavy metals remain in the forming biochar and only low concentrations are measured in the liquid effluents [56–58]. The suggested separation mechanism by Lin et al. is that the heavy metals compound with inorganic components in the reaction mixture and precipitate due to low solubility in supercritical water [60]. Therefore, the addition of inorganic components in alkali metal catalysts (K, Ca, Na) promotes the precipitation [57].

Since batch experiments are not relevant for an industrial application of SCWG in this work the experiments were conducted in a continuous lab-plant. KOH was added to the feed as a homogeneous catalyst. To evaluate the separation of the heavy metals the liquid effluents were analyzed. For many heavy metals (metals heavier than 5 g cm^{-3} [151]) the content was below the detection limit in the liquid effluents. Ni, Co, As, Pb, Cd, Cu and Sn were not detectable in the effluents. Most experiments (experiments

4.3.3 to 4.3.7) were conducted with the grass Reed Canary Grass. The heavy metal contamination of this plant from highest to lowest is Mn > Fe > Zn > Cr > Ni > Pb > Cd (for exact concentration see Table 4.8). The mean content of detectable heavy metals is displayed in Figure 4.14.

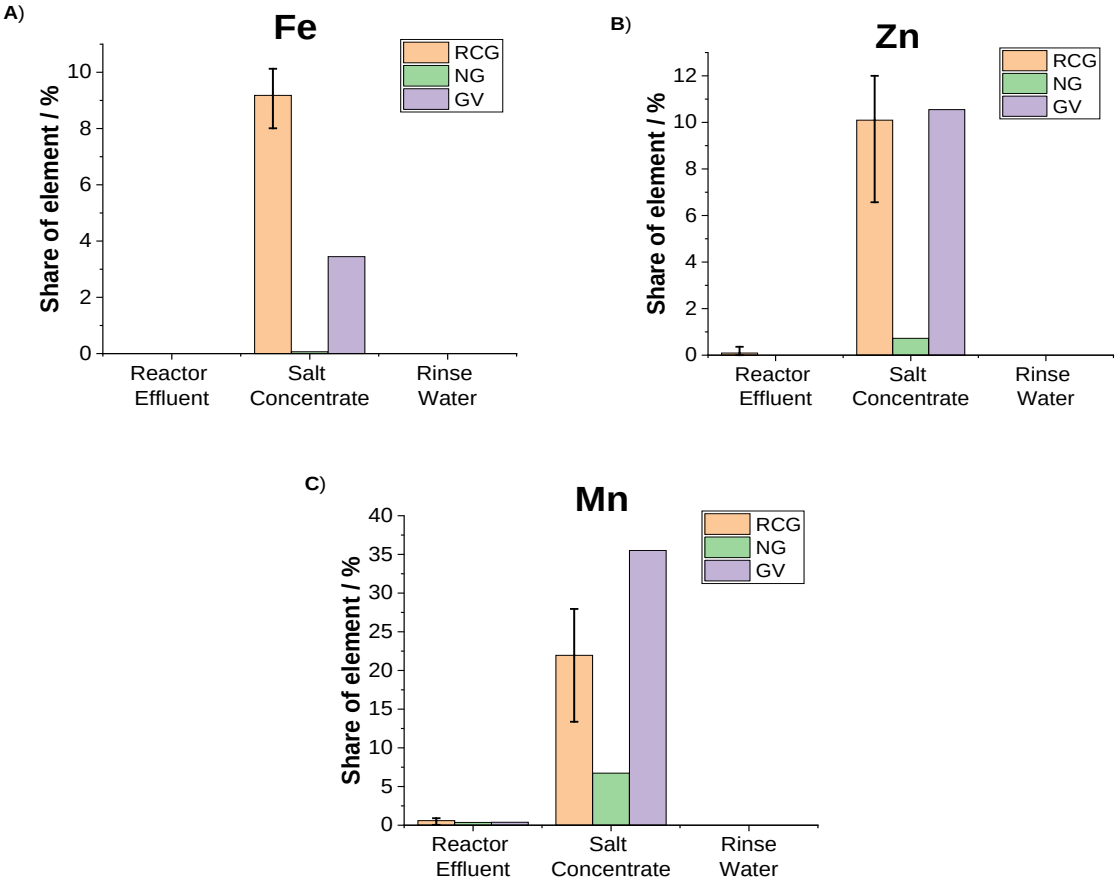


Figure 4.14: Mean content of heavy metals in the effluents of the experiments (100% = feed concentration).

Only three heavy metals are detectable, Mn, Fe and Zn. The content of the other heavy metals was below the detection limit in the feed slurry and therefore also in the effluents. About 21.5 ± 8% of Mn, that was in the feed slurry, can be detected in the salt concentrate. 9.0 ± 1% of Fe and 10.2 ± 3.6% of Zn are detected in the salt concentrate. Less than 0.6% of the heavy metals can be detected in the reactor effluent and none in the rinse water. The separation of contaminants is based on the precipitation in supercritical water due to low solubility. Since heavy metals are (almost) exclusively detected in the salt concentrate it can be assumed that they form heavy metal-salt-compounds as proposed by Lin et al. [60] and precipitate into the salt concentrate.

Most of the amount of the heavy metals that are fed into the system cannot be found in liquid effluents. One reason for this are the detection limits of the analysis method (ICP-OES). The heavy metals might for example be so diluted that they are not detected in the rinse water even though it might contain some. Another reason is the formation of solid deposits in the reaction system which are also insoluble in water under ambient conditions. As described in section 4.3.2.2 solid deposits form in the system, especially in the SCWG reactor. These solid deposits also contain heavy metals as can be seen in Figure 4.15, in this part of the solid deposit Cr, Ni and Fe.

Only one experiment (experiment 4.3.1) was conducted with Napier Grass and one with grapevines (experiment 4.3.2). In grapevines Mn, Fe and Zn make up the biggest part of the heavy metal contaminants. Only 3.5% of the fed Fe can be detected in the effluents (see Figure 4.14). 35% of Mn and 10% of Zn can be detected in the salt concentrate. The heavy metals show a similar behavior as in the gasification of Reed Canary Grass. Fe, Pb, Mn and Zn are the main contaminants of Napier Grass. In the experiment with Napier Grass almost no heavy metals were detected in the effluents (see Figure 4.14) but as seen in the other gasification experiments the only detected heavy metals were found in the salt concentrate. Little to none were found in the reactor effluent or the rinse water. Pb was not detected at all.

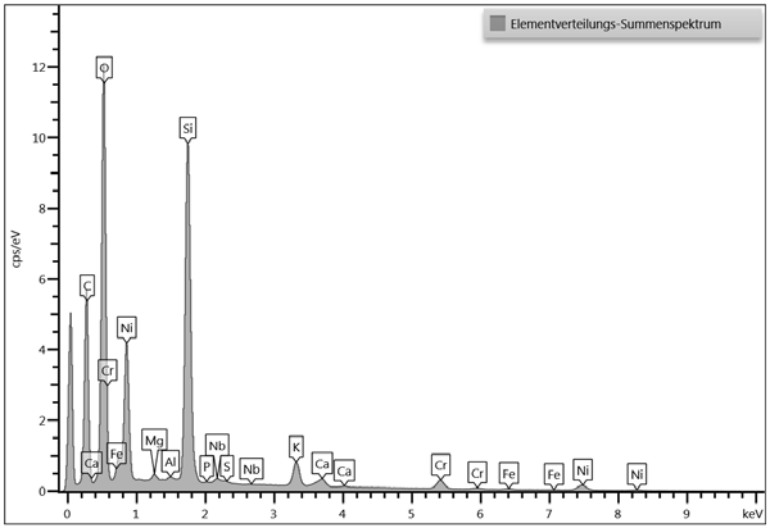


Figure 4.15: Elemental composition of solid deposits in experiment 4.3.1.

In batch experiments it was proposed that the heavy metals formed compounds with inorganics and precipitated. Due to the detection of heavy metals in the salt

concentrate this mechanism seems to be justified. As described in section 4.3.2.2 the salt separation of this lab-plant does not work sufficiently under the selected conditions. In the future an improved salt separation should reduce the formation of solid deposits or transporting the solids towards the salt concentrate and improve the precipitation of salts and thus also of heavy metals into the salt concentrate. Even though, the salt separation was not optimal in the conducted experiments, it is shown that in principle the separation of heavy metals from the reaction mixture is possible during continuous SCWG. It can also be noted that under the chosen conditions the reactor effluent can be considered free of heavy metals (concentration below quantification limit) and therefore can be treated as not contaminated. This is the most important aspect as this effluent would either be discharged or recycled to create new feed in a commercial application. In the framework of the CERESiS project a novel procedure for the separation of the heavy metals from the salt concentrate was developed [152] and thus the separation of heavy metals into the salt concentrate is the desired pathway.

4.4 Process effluent recycling

4.4.1 Materials and methods

4.4.1.1 Preparation of educts

In first experiments Reed Canary Grass (RCG) (lat. *Phalaris arundinacea*) was used as biomass. The grass was cultivated in Warden Law, England [136] and provided as a dry powder by the University of Strathclyde. To compare it to a woody biomass, the stems and branches of grapevines, provided by the University of Tuscia, were processed. Information on the biomasses and the feed preparation is given in section 4.3.1.1.

4.4.1.2 Apparatus

The description of the continuous lab-plant can be seen in section 4.3.1.2.

4.4.1.3 Experimental

In total seven experiments were conducted (see Table 4.15). The pressure of the system was 280 bar and the temperature of the SCWG reactor was set to 650 °C. The flow rate was set to 700 g h^{-1}. The duration of the experiment was limited by the available amount of feed slurry and therefore varies between the experiments. $T_{Preheater,max}$ describes the maximum temperature that was set in the preheater. Except for experiment 4.4.1 the maximum temperature of the preheater was 500 °C. After the preheater salts are separated with the help of a high-pressure valve which opens in certain intervals (see Table 4.15 for the chosen intervals) for a very short time (20 ms). In experiments 4.4.1 and 4.4.3 the interval was extended. Both experiments (4.4.1 and 4.4.3) ended prematurely due to formation of solids in the SCWG reactor. For that reason, the other experiments were conducted with an interval of 120 s.

Table 4.15: Experimental conditions of SCWG process.

Exp. Nr.	**Feed**	**Duration** h	**$T_{Pre-heater,max}$** s	**Salt separation interval** s
4.4.1	Reed Canary Grass (8 wt.%) + distilled water	3.5*	460	180
4.4.2	Reed Canary Grass (8 wt.%) + distilled water	6.5	500	120
4.4.3	Reed Canary Grass (8 wt.%) + distilled water	2.5*	500	240
4.4.4	Reactor effluent of 4.4.2	5.0	500	-
4.4.5	Reed Canary Grass (8 wt.%) + reactor effluent of 4.4.1&4.4.3	4.8	500	120
4.4.6	Grapevines (8 wt.%) + distilled water	5.8	500	120
4.4.7	Grapevines (8 wt.%) + reactor effluent of 4.4.6	4.5	500	120

*Premature end of experiment due to formation of solid deposits in the SCWG reactor.

4.4.2 Results and Discussion

4.4.2.1 Gasification of Reed Canary Grass

To investigate the influence of recycling of the reactor effluent gasification experiments with the grass Reed Canary Grass were conducted (see Table 4.16).

Table 4.16: Results of gasification experiments.

Exp. Nr.	Feed	CE %	TOC-conversion %	TOC content in effluent mg l^{-1}
4.4.1	Reed Canary Grass (8 wt.%) + distilled water	67.35	89.69	3765
4.4.2	Reed Canary Grass (8 wt.%) + distilled water	59.14	83.83	3204
4.4.3	Reed Canary Grass (8 wt.%) + distilled water	57.73	86.85	3230
4.4.4	Reactor effluent of 4.4.2	102.73	59.32	1311
4.4.5	Reed Canary Grass (8 wt.%) + reactor effluent of 4.4.1&4.4.3	55.31	86.11	3902
4.4.6	Grapevines (8 wt.%) + distilled water	55.18	86.20	3027
4.4.7	Grapevines (8 wt.%) + reactor effluent of 4.4.6	51.80	86.51	3805

At first, Reed Canary Grass was mixed with distilled water (as described in section 4.4.1.1) and gasified (experiment 4.4.2). The TOC content in the feed slurry was 36115 mg kg^{-1}. The reactor effluent of experiment 4.4.2 was then gasified under the same conditions (experiment 4.4.4). The reactor effluent had some inhomogeneities (oily substances) on its surface that could not be detected during the TOC-measurement. These oily substances were also recycled and gasified. Due to the inaccuracies in the TOC-measurement, CE and the TOC-conversion might deviate in experiment 4.4.4. Due to the low organic carbon content of the effluent a high gasification efficiency could be reached. As the proportion of organic components decreases, the relative excess of water increases, which results in an increased conversion efficiency [153]. The

mixing of organic components with supercritical water is favored by a small amount of organic matter. This leads to better decomposition of organic components towards gases [134]. Nanda et al. and D'Jesus observed an increase in gasification efficiency with decreasing organic content [89,135]. A lower organic content also results in a higher hydrogen yield [153]. This has been experimentally confirmed by Lu et al. and Nanda et al. [66,135]. The H_2-content in the product gas of the gasified reactor effluent is significantly higher (about 46 vol.%) than in the product gas of gasification experiments with biomass (about 31 vol.%) (see Figure 4.16). The high CE and the high H_2-content indicate that the reactor effluent can be efficiently gasified and could be used for creating new feed slurries.

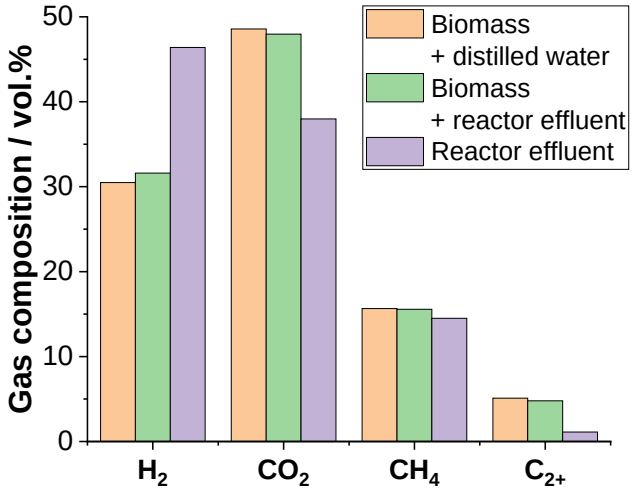


Figure 4.16: Gas composition of experiments with Reed Canary Grass for three different feeds.

Two further experiments (experiment 4.4.1 and 4.4.3) were conducted under similar conditions as experiment 4.4.2 to produce additional reactor effluent. The TOC content of the reactor effluents was similar to experiment 4.4.2 (see Table 4.16). The dry biomass was then mixed with the reactor effluents (instead of distilled water) to create a feed slurry with recycled process water (experiment 4.4.5).

The TOC content of the feed slurry with recycled reactor effluent was 42044 mg kg^{-1}. The experiments show that the recycling of process water does not influence the gas composition of the product gas. In both experiments the content of H_2 is 31 vol.%, CO_2

is 48 vol.% and CH_4 is 16 vol.%. The carbon efficiency decreases slightly by about 4% from 59.1 to 55.3% when the effluent is recycled (as shown in Figure 4.17), which is most probably due to the higher TOC content of the feed.

In general, CE is low under the selected process conditions. Due to high flow rates (700 g h^{-1}) the residence time is short which affects CE negatively. Gasification rates increase with increasing residence time due to further cracking of biomass molecules. This has been demonstrated experimentally in many studies [66,89,154]. In the conducted experiments the residence time is 17 s in the section of the SCWG reactor with temperatures higher than 600 °C. Earlier work at the Karlsruhe Institute of Technology with corn silage (5 wt.%) in a similar lab-plant showed comparable CEs in this range of residence times (τ = 50 s; CE = 60%) [92].

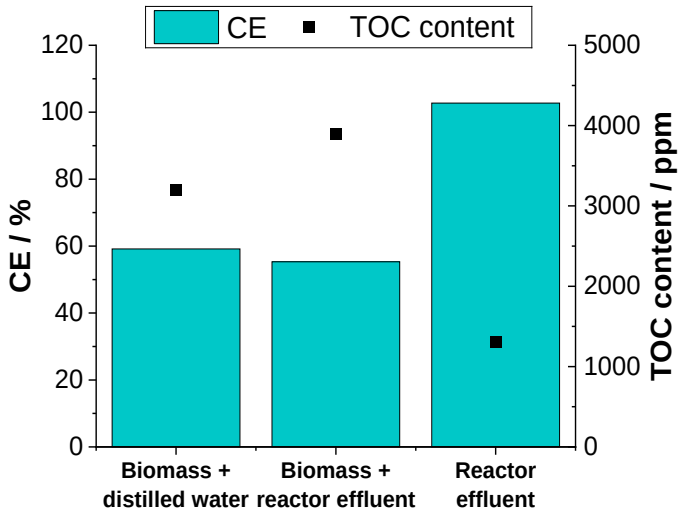


Figure 4.17: Carbon Efficiency and TOC content of reactor effluent of gasification experiments with Reed Canary Grass for three different feeds.

The TOC-conversion is about 0.85 in both experiments but the reactor effluent of the experiment with recycled process water shows a higher TOC content than the reactor effluent of the experiment with distilled water due to the higher TOC content in the feed slurry. As shown in Table 4.17, the content of all detected organic compounds rises when the effluent is recycled, especially the concentration of phenols. Regarding SCWG, phenols are relatively inert [83] and thus might accumulate when recycling the effluent more often. Further investigation on rising TOC content is needed in order to

determine how often the reactor effluent can be recycled without excessive enrichment of TOC in the effluent.

Table 4.17: Organics in reactor effluents of the experiments with RCG (in mg l^{-1}).

Exp. Nr.	Formic Acid	Acetic Acid	Resorcinol	Phenol
4.4.2	640	57	177	361
4.4.5	742	76	187	618

To avoid corrosion and solid deposits the content of other elements, especially salts and metals, has also to be monitored. As shown in Table 4.18, the concentration of calcium, phosphorus, zinc, aluminum and magnesium is approximately the same in the reactor effluent after recycling.

Table 4.18: Elements in reactor effluents of experiments with RCG (in µg ml^{-1}).

Exp. Nr.	Al	Ca	K	Mg	Na	S	Si	Zn	P
4.4.2	<2(0.1)	2.51	2180	<0.8(0.1)	46.1	20.6	75.5	<0.2(0.02)	6.8
4.4.5	<2(0.3)	2.12	3850	<0.8	66.2	43.4	102	n.d.[1]	5.8

[1] n.d. = not detected

The concentrations of sodium, sulfur and silicon rise when the reactor effluent is recycled but remain on a low level. The most significant change can be seen in potassium. The concentration of potassium rises from 2180 to 3850 µg ml^{-1} when the reactor effluent is reused. The implemented salt separation does not separate the salt components efficiently (detailed description in section 4.4.2.3) but limits the accumulation of salt building elements and metals in the reactor effluent.

Most of the experiments were only conducted once due to limited time and resources and due to the high effort, it takes to prepare and conduct the experiments. One experiment was repeated (experiment 4.4.2 and 4.4.3) to produce additional reactor effluent. In these two experiments the carbon efficiency deviated only 1.4%. A possible source of error in TOC measurement and in CE are the inhomogeneities in the reactor effluent which contains a small amount of an oily phase that is too small to be separated (as stated above).

4.4.2.2 Gasification of grapevines

In a second set of experiments grapevines were studied under the same conditions as Reed Canary Grass. At first, the milled grapevines were mixed with distilled water (as described in section 4.4.1.1) to create a feed slurry with about 8% dry mass and then gasified (experiment 4.4.6). The reactor effluent of this experiment was then used to create the feed slurry for the second experiment with recycled process water (experiment 4.4.7). KOH and xanthan were also added. The TOC content of the feed slurry with distilled water was 35120 mg kg^{-1} and with reactor effluent was 41876 mg kg^{-1}. The experiments show that the gas composition is not influenced by the reuse of the process effluent. The yield of the different compounds varies about ± 1% (see Figure 4.18). In both experiments the mean content of H_2 is 32 vol.%, CO_2 is 49 vol.% and CH_4 is 15 vol.%.

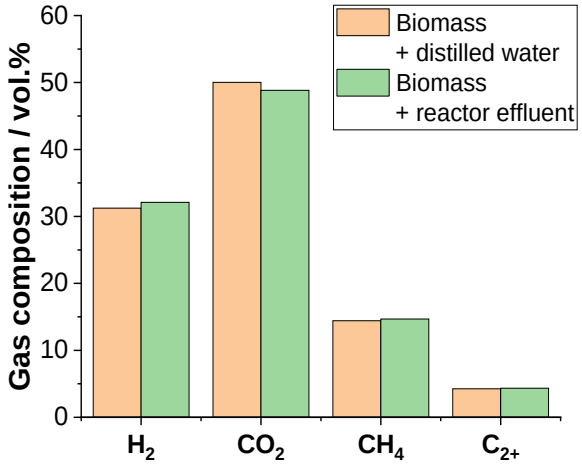


Figure 4.18: Gas composition of gasification experiments with grapevines for two different feeds.

Similar to the findings with Reed Canary Grass, the carbon efficiency decreases from 55.2 to 51.8% when the reactor effluent is recycled (see Figure 4.19). At the same time the TOC content of the reactor effluent rises from 3027 mg l^{-1} to 3805 mg l^{-1}. In Table 4.19 it is shown that similar to the gasification of Reed Canary Grass, the content of all detected organic compounds in the effluent increases when the effluent is recycled. The TOC-conversion does not change (TOC-conversion = 86%).

Table 4.19: Organics in reactor effluent of experiments with grapevines (in mg l^{-1}).

Exp. Nr.	Formic Acid	Acetic Acid	Resorcinol	Phenol
4.4.6	470	32	178	440
4.4.7	808	121	312	760

A maximum TOC content of the reactor effluent needs to be defined to avoid too high TOC contents in the feed when the effluent is reused multiple times. It might also be possible to reduce the biomass content in the feed to lower the TOC content and therefore produce process effluent with constant TOC content. This needs to be investigated in further experiments in the future.

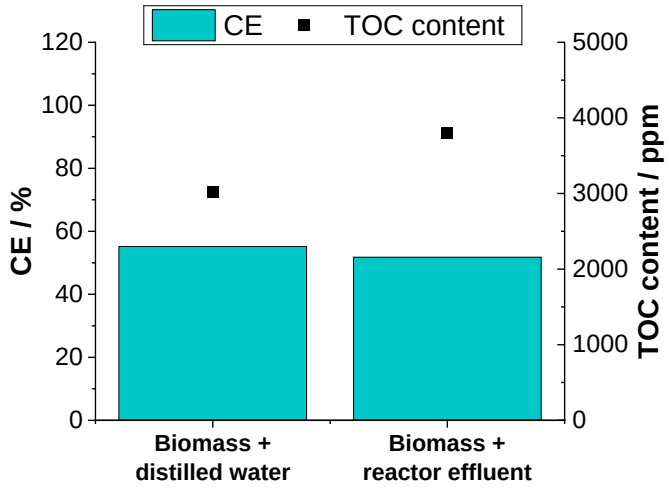


Figure 4.19: Carbon efficiency and TOC content of reactor effluent of gasification experiments with grapevines for two different feeds.

In addition to the TOC content, the concentration of various elements (salt building elements and metal contaminants) in the effluent is monitored. When the effluent is recycled the contents of most contaminants (aluminum, calcium, sodium, sulfur and zinc) are not affected, as can be seen in Table 4.20. These elements either get separated in the salt concentrate or form solid deposits and therefore do not accumulate in the reactor effluent. A rise in the concentration of potassium from 2430 up to 2840 µg ml^{-1} can be seen. This could also be observed in the gasification of Reed Canary Grass (see section 4.4.2.1), although the accumulation is not as significant during the gasification of grapevines.

Table 4.20: Elements in reactor effluents of experiments with grapevines (in µg ml^{-1}).

Exp. Nr.	Al	Ca	K	Mg	Na	S	Si	Zn	P
4.4.6	<2(0.06)	<2(1)	2430	<0.8(0.06)	33.3	4.1	26	n.d.[1]	n.d.
4.4.7	<2(0.3)	6.06	2840	<0.8(0.3)	31.7	6.8	15.9	n.d.	<4(3.2)

[1] n.d. = not detected

The recycling of reactor effluent when gasifying grapevines shows only minor disadvantages regarding CE and the accumulation of TOC in the effluent. In future experiments the accumulation of potassium in the effluent can be avoided by not adding KOH to the feed when K^+ is already contained in the effluent. The same accounts for the gasification of Reed Canary Grass.

4.4.2.3 Separation of salts

Separation of salts is important during the process of SCWG since salts can form solid deposits, cause blockage of the flow [102,111] and also enhance corrosion rates at T > 500 °C [83,111,145,146]. As described in section 4.4.1.2 the salt separation is realized in form of a T-fitting where salts are supposed to drop vertically down into the salt concentrate due to low solubility in supercritical water at T > 374 °C and due to gravity. The organic material and water leave the T-fitting upwards in an angle of 45 ° to the SCWG reactor where the organics are gasified (see Figure 4.20).

The temperature at this T-fitting was T = 388 ± 3 °C during all experiments and thus slightly supercritical (measurement on the outside of the T-fitting). Above its critical point water acts as a nonpolar solvent [78], in which salts generally dissolve poorly. The change in solubility with rising temperature depends on the kind of salt and therefore influences the ability to separate the salts by precipitation [84]. In binary salt-water-systems it is distinguished between type 1 and type 2 salts [68,69,85]. Type 1 salts (e.g. K_2CO_3, NaCl, $CaCl_2$) are soluble in dense supercritical water and only precipitate with further rise in temperature while type 2 salts (e.g. Na_2CO_3, K_2SO_4, Na_2SO_4) are (almost) non-soluble [68,81].

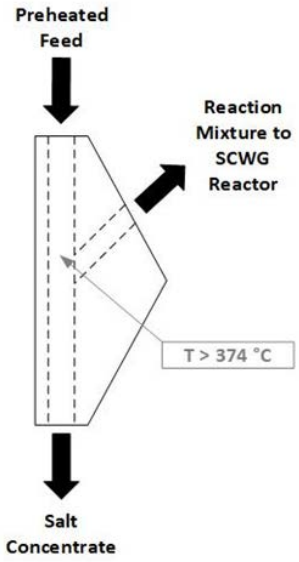


Figure 4.20: Design of salt separation in lab-plant in section 4.4.

Since the temperature of salt separation was at 388 °C, and thus only slightly above the critical point of water, not all salts could be sufficiently removed at the T-fitting. This leads to precipitation of some salts in the SCWG reactor due to further rising in temperatures. The composition of solid deposits that are collected from the SCWG reactor after the experiments cannot be quantitatively detected. The composition of the samples is very heterogeneous (as shown in Figure 4.21) and therefore can only be qualitatively described (see section 4.4.2.4).

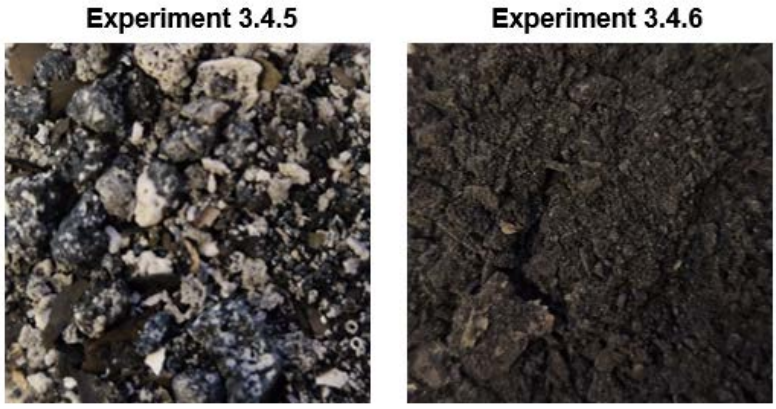


Figure 4.21: Solid sample from SCWG reactor in experiment 4.4.5 and 4.4.6.

Relevant salt forming elements in the SCWG process are K, P, S, Cl, Ca, Mg, Na and Si [75,147,148]. In Figure 4.22 the distribution of relevant salt building elements in the

products of experiment 4.4.2 is displayed (distribution of elements is similar in all experiments).

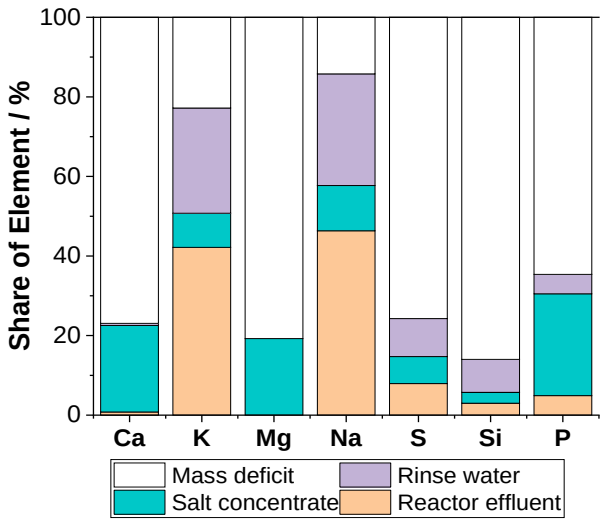


Figure 4.22: Distribution of salt building elements in the products of experiment 4.4.2 (concentration in feed ≙ 100%).

Depending on the element, between 10 and 80% of the feed-content can be detected in the liquid products of the process. Ca, Mg, Na, S and Si can only be detected to 20% or less. 80% of K can be detected, 40% in the reactor effluent and 30% in the rinse water (after the experiments the reactors are flushed with water). Only 10% are separated into the salt concentrate. As described in sections 4.4.2.1 and 4.4.2.2 the accumulation of potassium in the effluent can be reduced by reducing the amount of potassium that is added in the feed slurry when creating the feed slurry with recycled process water. The mass deficit of all elements which is displayed in Figure 4.22 is very high (except for potassium). Most of it can be assumed to be solid deposits in the reaction system, especially in the SCWG reactor, which can only be partially collected. In case of calcium, magnesium and phosphorus most of the feed-content is separated either in the salt concentrate or in form of solid deposits. Thus, these elements do not accumulate in the reactor effluent when it is recycled, as can be seen in Table 4.18.

Due to the high mass deficit and therefore the high amount of salt deposits that are formed in the reactor the salt separation conditions and the hardware installed are insufficient under the selected process conditions. Salt separation needs to be

optimized to ensure that the precipitating salts are removed before a temperature of approximately 450 °C is reached in the SCWG reactor. The geometry of the salt separation T-fitting might show potential for optimization. A sharper redirection of the flow could result in better salt separation. In future experiments an inner temperature measurement should also be completed to accurately determine the temperature of salt precipitation. Also, the flow velocity should be optimized.

4.4.2.4 Formation of solid deposits

Asides from salts that can precipitate and block the flow in continuous SCWG plants, coke and char formation poses an additional process challenge. Due to the dilution of the biomass in supercritical water the contact rate of the biomass molecules with each other decreases, which inhibits the formation of coke [83]. Therefore, the coke and char formation rate is smaller than in conventional gasification [115], but it cannot be completely neglected. Coke and char formation can also cause blockage of the flow and decreases the gasification efficiency [87,100,115]. Two of the conducted experiments had to be stopped prematurely due to blockage of the flow in the SCWG reactor. After the end of these experiments the reactor was opened and solid deposits were removed by a drill. The same procedure was also applied when the experiment was finished according to plan. In all experiments (except for experiment 4.4.4, where only the reactor effluent was gasified) solid deposits were found in the top section of the SCWG reactor (about 300 - 500 mm from the top) in which a temperature of 500 °C was set. An additional indication of the formation of solid deposits is the poor carbon balance of the experiment in the range of 70 to 80%. The collected samples were dried and analyzed via SEM-EDS.

The composition cannot be analyzed quantitively due to heterogeneity of the solids (see Figure 4.21) but can be qualitatively analyzed. Many different structures can be seen by SEM-EDS analysis of the solid sample of experiment 4.4.5 (see Figure 4.23).

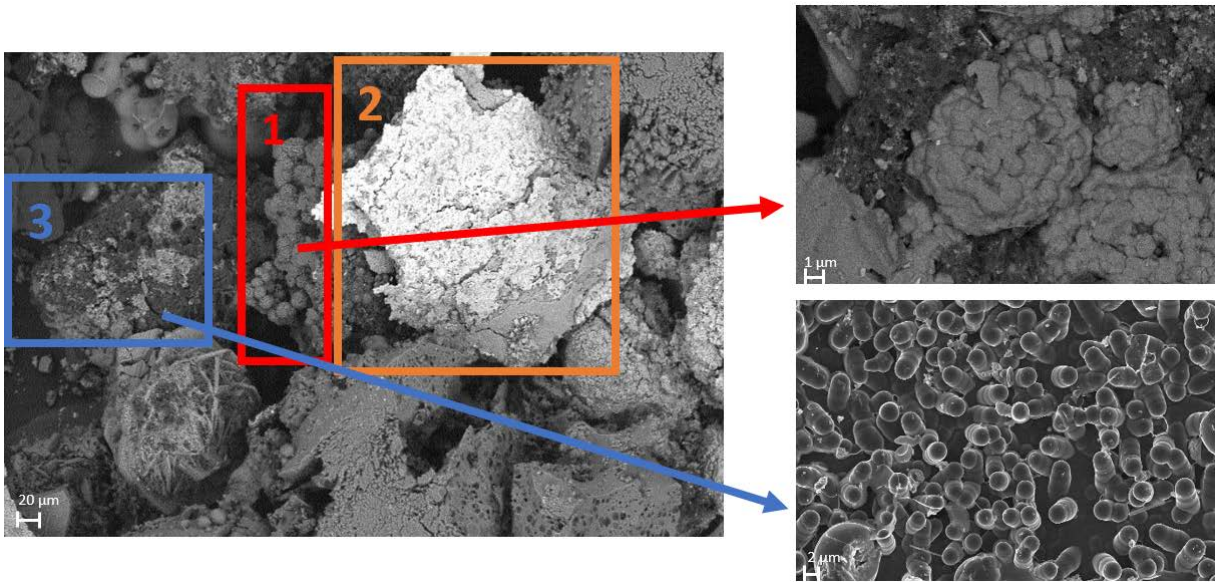


Figure 4.23: SEM recordings of solid deposits of experiment 4.4.5.

Part of the solid deposit is made up mainly by carbon (area 3). This is visible in the EDS-analysis (see Figure 4.24).

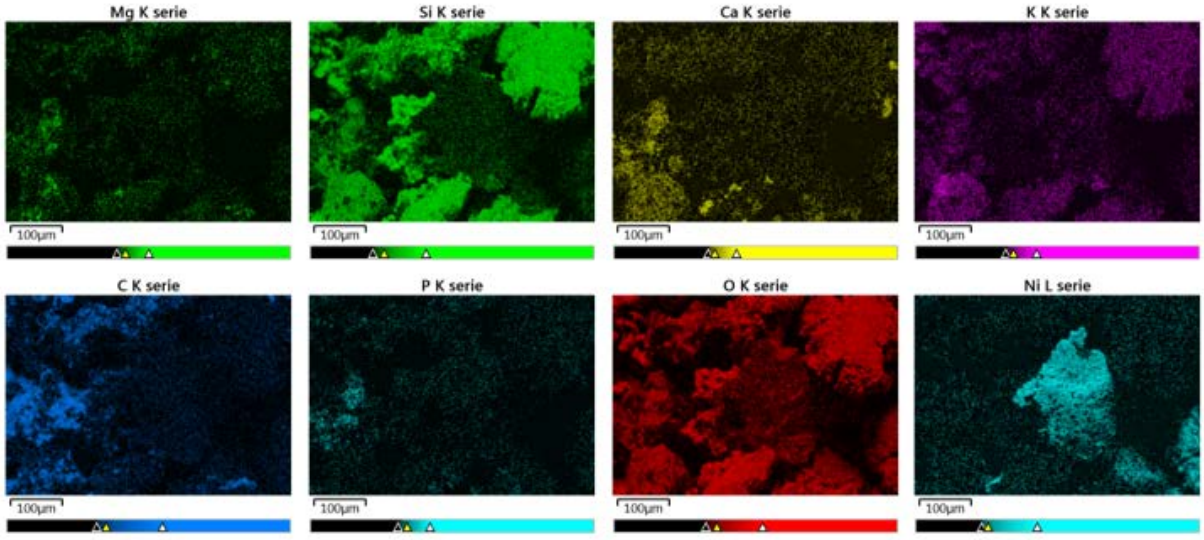


Figure 4.24: EDS analysis of solid deposits from experiment 4.4.5.

Spherical structures can be seen that are fused together in stacks. Spherical carbon structures are known from hydrothermal processes, especially hydrothermal carbonization (HTC) [155–158]. The HTC process is used to synthesize spherical carbon structures. According to Sun et al. and Li et al. the formation of the carbon spheres follows the LaMer model [158,159], which mainly consists of two steps: nucleation and

growth [160]. Sun et al. investigated the HTC of glucose [158]. It is proposed that glucose polymerizes to form aromatic structures and oligosaccharides. Due to further dehydration of these intermediates nuclei are formed. These nuclei grow due to diffusion of further organics to the surface of the nuclei [158]. During long reaction times cross-linking and polymerization of spheres can lead to irregular structures [161]. This effect can also be seen in Figure 4.23. Multiple spheres are fused together and have formed stacks. The sphere formation from glucose was studied in autoclaves at T < 200 °C by many authors [158,159,162,163]. Zheng et al. investigated HTC of starch at temperatures of 500 to 600 °C [164]. They also found spherical structures, with some spheres fused together. As outlined, the formation mechanism and carbon structures are well-described for the process of HTC. In the process of SCWG the formation of solid carbon is supposed to be limited [83]. In this work the solid deposits occurred in the SCWG reactor (T > 500 °C). Since the solid samples can not be collected during the experiment and quenched down to room temperature the point in time these spherical structures formed can not be determined. The solids were collected after the lab-plant cooled down to room temperature. While cooling down the temperature range of HTC (typically 160 to 250 °C [20]) is passed. A possible origin of the spherical structures could be the formation under the temperature conditions of HTC.

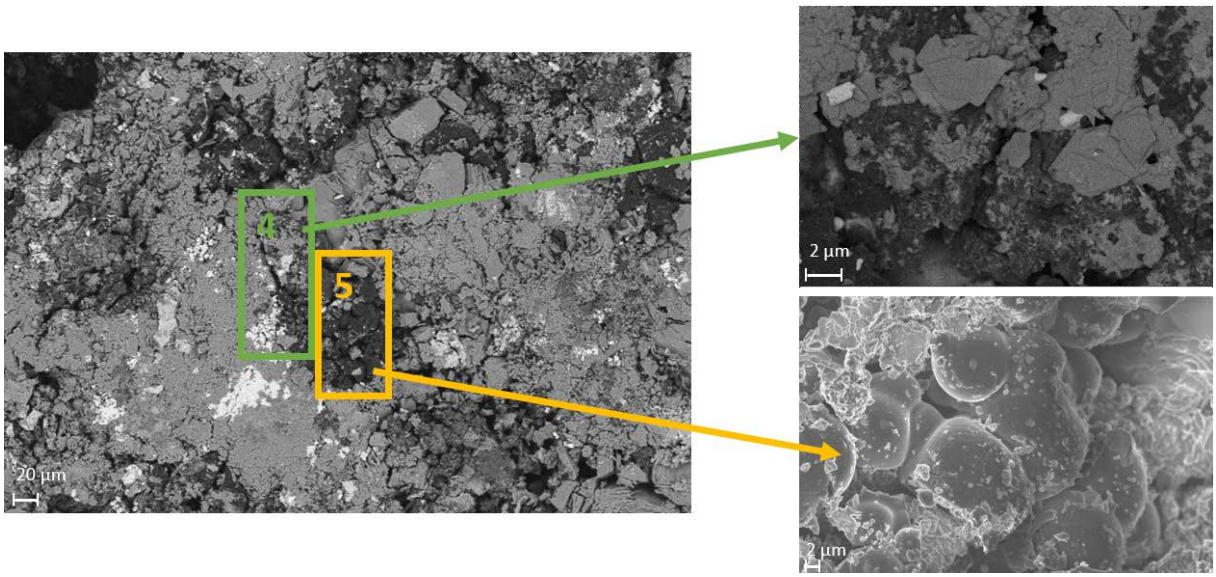


Figure 4.25: SEM recordings of solid deposits of experiment 4.4.6.

Spherical structures that are stuck together can also be seen in the SEM recordings of the solid deposits of experiment 4.4.6 (see Figure 4.25). The spherical structures are

also made up of carbon in this case (see Figure 4.26) but are larger than in the solid sample of experiment 4.4.5.

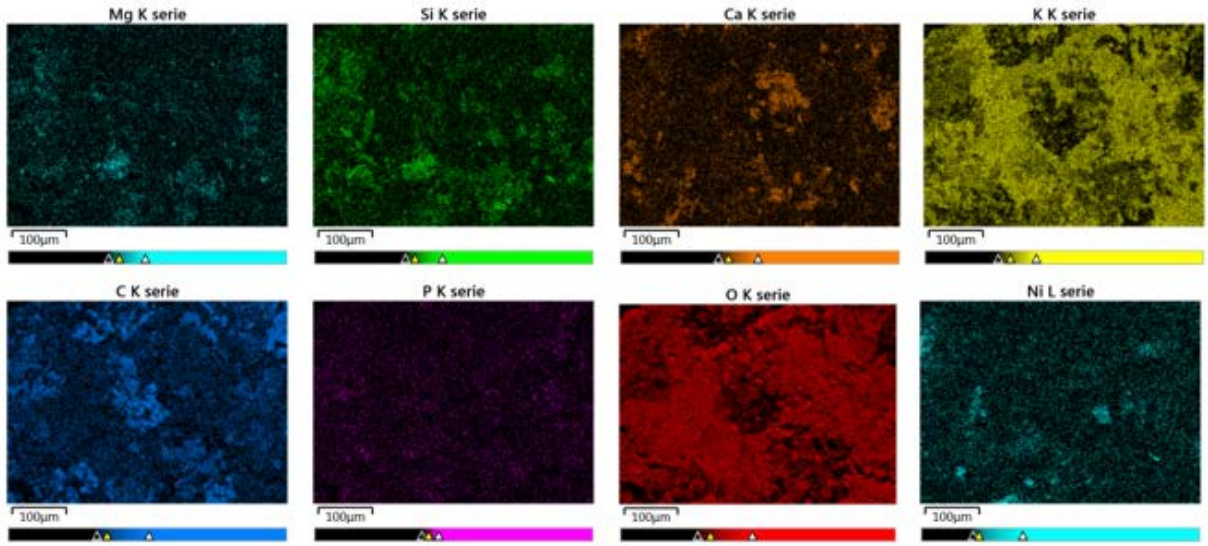


Figure 4.26: EDS analysis of solid deposits from experiment 4.4.6.

In area 1 clusters can be seen. These structures consist mainly of silicon in form of silicon oxide (see Figure 4.24). Under the conditions of supercritical water gasification silicon oxide seems to form clusters. Since the solid deposit is mainly made of silicon, the separation of silicates, like $K_2(SiO_2)_n$ [148], needs to be optimized or a biomass with low silicon content needs to be selected in order to avoid solid deposits and eventually blockage of the flow in the SCWG reactor. Silicon also makes up part of the solid sample of experiment 4.4.6 but potassium is making up the biggest part in form of planar structures (see Figure 4.25 and Figure 4.26). As described in section 4.4.2.3 potassium does not get separated by the salt separation sufficiently. This can result in solid deposits in the SCWG reactor as can be seen in experiment 4.4.6. Thus, no KOH should be added to the feed when K^+ is already contained in the recycled effluent.

Besides the described structures a planar structure can be seen in area 2. The EDS-analysis (see Figure 4.24) shows that this structure mainly consists of nickel. Therefore, this is a corrosion product which originated from the reactor wall. It is known that alkaline salts cause corrosion under the process conditions present [112,146]. The reactor wall thickness needs to be monitored in order to ensure safe operation of the laboratory plant.

Salt building elements (Si, Mg, Ca, P and K) can also be detected throughout both samples (see Figure 4.24 and Figure 4.26). This indicates that various salt deposits have formed and thus shows that the salt separation prior to the SCWG reactor is insufficient (as described in section 4.4.2.3).

The composition of the solid deposits is complex. Corrosion can be minimized by limiting the amount of salts in the SCWG reactor. The solid deposits seem to be mainly made up by salts (especially silicon and potassium compounds). This issue needs to be addressed by optimizing the salt separation.

4.4.2.5 Estimation of water savings through effluent recycling

In the experiments, the feed slurry was pumped with 700 g h^{-1}. In the slurry approximately 640 g h^{-1} is water. On average 570 g h^{-1} of reactor effluent is collected. Due to separation of the salt concentrate after the preheater not the whole amount of water in the feed slurry can be collected in the reactor effluent. In a continuous process the deficit (70 g h^{-1}) needs to be made up with distilled water. This amounts to water savings of 89 % when the complete reactor effluent is recycled (see Eq. 4.3).

$$water\ savings = \frac{\dot{m}_{R,effluent}}{\dot{m}_{water\ in\ feed}} = \frac{570\frac{g}{h}}{640\frac{g}{h}} = 0.89 \qquad (4.3)$$

To create a feed slurry with 8 wt.% biomass, for 1 kg of dry biomass usually about 11 kg of fresh distilled water is necessary. With the recycling of process water only about 1.2 kg of fresh water is needed.

4.5 Conclusion

In the present chapter, first investigations of the SCWG process with contaminated, dry biomasses were conducted. It was demonstrated that the separation of heavy metal contaminants from biomasses was possible with a process integrated salt separation. The heavy metal separation was not influenced by the type of plant that was gasified (Reed Canary Grass, Napier Grass, grapevines). The reactor effluent was heavy metal-free under all conditions tested (concentrations below quantification limit).

An extensive study on the processability of different biomass types was carried out because flexibility regarding the biomass type would be beneficial for an application of SCWG. For ten different biomasses, it was demonstrated that the macroscopic appearance, i.e. woody or grassy biomass, and the level of humidity did not influence the carbon efficiency. Carbon efficiency was 60.3 ± 5.1% for all biomasses. The feed preparation is important in the process of SCWG. Sufficient size reduction is important to avoid plugging of the feed tubing (plugging occurred when size of biomass particles was reduced to about 1 mm with tubing with inner diameter 2.5 mm). It can be concluded that no significant differences could be determined. Thus, when pretreating the biomasses in the same way all of them could be gasified equally well and thus all of them can be considered for preceding phytoremediation.

Solid deposits formed in the reaction system (containing coke, salt building elements and heavy metals), leading to plugging in most cases. Salt and thus heavy metal separation strongly depend on the preheating temperature prior to salt separation. Salt separation temperatures of 394 °C or lower are not sufficient for complete salt separation. This led to formation of solid deposits containing coke, salts and heavy metals in the reaction system. It can be concluded that in principle the process of SCWG can be suitable for processing dry biomasses, however due to the relatively low CE, the formation of solid deposits and the remaining TOC in the effluent, the realization of the SCWG process in this process design is not recommendable and further process development is necessary. To avoid blockage of the flow and enable long-term operation further improving of the salt separation, especially the temperature profile, needs to be investigated. In the following experiments an inner temperature measurement, which is very difficult due to the high pressure and high temperature environment, was completed to accurately determine the temperature of salt precipitation. The set temperature of the preheater should be in such way that the salt separation temperature can then be reached right before the T-fitting. At the same time the flow speed of the preheater needs to be high enough to transport precipitating salts to the salt concentrate and to avoid blockage of the preheater. Additionally, faster heating rates should be applied to reduce solid coke deposit formation.

Lastly, as dry biomasses are used it is important to consider the amount of water that is needed to create a pumpable feed slurry. To reduce the amount of fresh water

needed an investigation on the possibility to recycle the process effluent was conducted. It was demonstrated that the recycling of the SCWG effluent to produce new feed slurry was possible for dry biomasses. The gasification was successful with a grass, Reed Canary Grass, and a wooden biomass, grapevines. About 89% of the needed water to dilute the feed can be saved by reusing the effluent. The gas composition was not influenced by the reuse of the effluent. The carbon efficiency decreased only by 4%, probably due to the higher TOC content of the feed. The TOC content and the content of potassium rise in the reactor effluent when the effluent is recycled.

Chapter 5. Systematic investigation of salt precipitation

The content of this chapter is sourced from the following publication:

- Dutzi, J.; Boukis, N.; Sauer, J. Investigating Salt Precipitation in Continuous Supercritical Water Gasification of Biomass. *Processes*, **2024**, 12, 935. DOI: 10.3390/pr12050935

Declaration of contributions:

Julian Dutzi conceptualized the experimental work and analysed the data, evaluated the results, and wrote the manuscript.

Nikolaos Boukis supervised the work, contributed to the discussion, and reviewed the manuscript.

Jörg Sauer supervised the work, contributed to the discussion, and reviewed the manuscript.

Summary of chapter 5

The formation of solid deposits in the process of supercritical water gasification (SCWG) is one of the main problems hindering the commercial application of the process. Seven experiments were conducted with the grass Reed Canary Grass with different preheating temperatures, but all ended early due to the formation of solid deposits (maximum operation of 3.8 h). The position of solid deposits in the lab plant changed with the variation in the temperature profile. Since the formation of solid deposits consisting of salts, coke, and corrosion products is a severe issue that needs to be resolved in order to enable long-time operation, inner temperature measurements were conducted to determine the temperature range that corresponds with the zone of solid formation. The temperature range was found to be 400 to 440 °C. Wherever this temperature was first reached solid deposits occurred in the system that led to blockage of the flow. Additional to the influence of the temperature, the influence of the flow direction (up-flow or down-flow) on the operation of the continuous SCWG plant was examined. If salts are not separated from the system sufficiently, up-flow reactors should be avoided because they amplify the accumulation of solid deposits leading to a shortened operation time. The heating concept coupled with the salt separation needs to be redesigned in order to separate the salts before entering the gasification reactors. Outside of the determined temperature zone no deposition was visible. Thus, even though the gasification efficiency was low it could be shown that the operation was limited to the deposits forming in the heating section and not by incomplete gasification in the reactor where T > 600 °C.

5.1 Introduction

As described in Chapter 4, the process of supercritical water gasification can be suitable for the processing of contaminated, dry biomasses. Even though, the contamination itself is not a crucial issue influencing the process, salt separation and coke formation are. To further improve the process and with that to enable long-term operation it is important to further understand the phenomena hindering long-term operation.

Common obstacles in the process of SCWG hindering a commercial application include the ability to pump biomass slurry, corrosion, and the formation of coke [83,108].

Corrosion arises from the extreme process conditions and the gases and minerals formed within the process [82]. Especially, precipitating salts enhance corrosion at T > 500 °C [83,111,112]. Salts are generally poorly soluble in supercritical water and thus precipitate [69,84,109,110]. This enhances corrosion rates but can also lead to the blockage of the flow [113,114]. It is thus important to separate salts from the reaction system after they precipitate.

SCWG exhibits lower coke formation compared to conventional gasification methods [64,115]. The dilution of biomass in supercritical water reduces the interaction rate among biomass molecules, thus inhibiting the formation of tar and coke [83]. However, coke formation, even in low quantities, still plays a significant role, leading to decreased gasification efficiency and potential flow blockages [87]. Coke predominantly originates from the polymerization of aromatic intermediates, such as furfurals [116,117]. Coke formation may occur in heated pipelines due to temperature ranges that promote their development. Kruse et al. found high concentrations of these aromatic intermediates at subcritical temperatures [118]. Utilizing high heating rates can help minimize coke formation [118–120].

The following chapter deals with one of the main obstacles described above, the salt precipitation, which also appears to be the major issue causing plugging in the first experiments, as described in Chapter 4. As stated above, precipitating salts can cause corrosion and plugging of the reactors. Thus, salts need to be removed after reaching the supercritical state of water. The behavior of salt–water mixtures under supercritical conditions of water has been studied in the past by other authors [68,69,85,111]. However, it is important to study the precipitation also for biomasses which contain salts in

various forms, in order to design the salt separation properly. Thus, a thorough investigation of the salt precipitation temperature was carried out.

5.2 Materials and methods

5.2.1 Preparation of educts

The grass Reed Canary Grass (RCG) (lat. *Phalaris arundinacea*) was used as biomass source for the gasification experiments. Prior experiments had shown that there are no major differences in the gasification of different plants (see section 4.2), and thus, for the investigation of the present work, only one grass was chosen. The plant was processed in the form of a dry powder with a grain size smaller than 0.25 mm. The elemental analysis of the biomass is displayed in Table 5.1.

Table 5.1: Elemental analysis of RCG (in wt.%).

Biomass	C	H	N	S	K	Ca	Mg	P	Si
Reed Canary Grass	48.9	7.46	<0.3	0.09	0.29	0.17	0.05	0.10	2.3

The feed slurry was created by adding distilled water to the biomass powder in such a ratio that a dry matter content of 8 wt.%. was achieved. Xanthan, supplied by Carl Roth GmbH (Karlsruhe, Germany), was added as a thickening agent (0.5 wt.% based on slurry mass) to prevent phase separation, and $KHCO_3$ (5000 mg K^+/kg feed slurry), supplied by VWR International GmbH (Darmstadt, Germany), was added as a homogeneous catalyst. The homogeneous catalyst was chosen as it is known to enhance gasification efficiencies [165]; however, other homogenous catalysts such as K_2CO_3, KOH, or NaOH would have also been possible [166]. Even though, the homogenous catalysts are known to enhance gasification efficiencies, they might also contribute to plugging if the salt removal in the process is insufficient. A variation in catalyst concentration was not performed in the present work.

5.2.2 Apparatus

The SCWG experiments were performed in a continuous lab-plant for high pressure (p ≤ 300 bar) and high temperature (T ≤ 700 °C) conversion of biomass compounds. In the past, the laboratory plant has been redesigned several times. In the present chapter, the following two configurations are assessed and compared.

5.2.2.1 Configuration 1

The description of Configuration 1 can be found in section 4.3. Compared to Configuration 2, a shorter preheater and only one instead of two reactors were installed. The periphery of the system (low pressure system after the reactor, feed system) is the same as in Configuration 2.

5.2.2.2 Configuration 2

In Configuration 2, the lab-plant consists of a preheater and two gasification reactors (see Figure 5.1.).

The preheater, constructed from the nickel-based alloy Inconel 625, has an inner diameter of 8 mm and a length of 1200 mm. It is equipped with a liner to reduce the inner diameter. Two different liners are used, one made of SS316 with an inner diameter of 3.2 mm and one made of titanium with an inner diameter of 1.5 mm. To heat the preheater, five electric spiral heaters are positioned externally, each with two thermocouples attached to the outer wall of the pipe. In the preheater, the water is heated to its supercritical state. Due to the changes in properties of water, salts are poorly soluble in the supercritical region and thus precipitate. This process is intended to happen at the salt separation, which is realized in the form of a T-fitting at which the flow is redirected sideways. The salts are supposed to drop down vertically into the salt concentrate due to gravity, while the organics are intended to follow the water stream to the SCWG reactor (a schematic drawing can be seen in section 4.4).

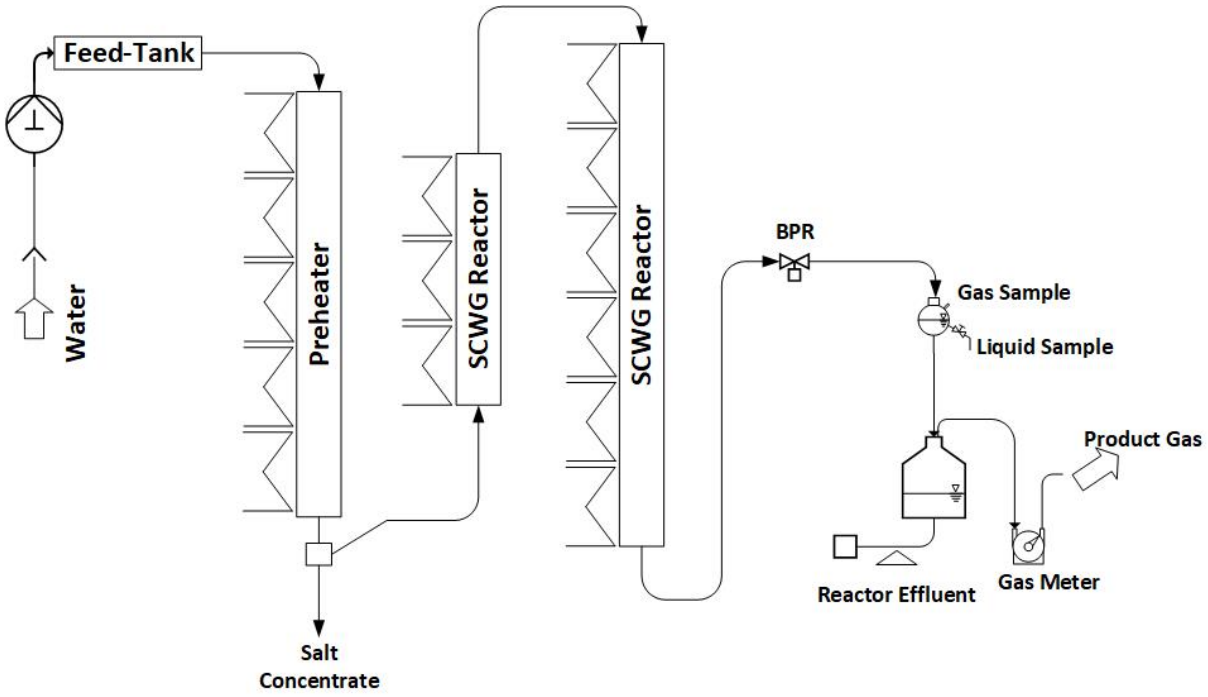


Figure 5.1: Schematic diagram of lab-plant in Configuration 2.

The gasification reactors, also made of Inconel 625, have lengths of 1100 mm and 1800 mm, both with an inner diameter of 8 mm. Reactor 1 is heated externally using an electric spiral heater and three electric rod heaters, while Reactor 2 is heated using one electric spiral heater and six electric rod heaters. Thermocouples are mounted on the outer wall of both reactors to monitor temperature, with seven thermocouples for Reactor 1 and nine for Reactor 2.

The products are quantified using scales (Soehnle Industrial Solutions GmbH, Backnang, Germany) and gas meters (Ritter Apparatebau GmbH & Co. KG, Bochum, Germany). Throughout the experiment, liquid and gas samples are collected at regular intervals. The evaluation is conducted under steady-state operating conditions, ensuring constant gas composition and production.

To pressurize the system, water is pumped using a high-pressure pump (ProMinent GmbH, Heidelberg, Germany) and subsequently heated. The process control system is used for setting the temperatures required for this purpose. The system's pressure is regulated by a TESCOM back-pressure regulator (Emerson Automation Solutions, Selmsdorf, Germany) in the cold part of the lab plant after the reactor.

5.2.3 Experimental

In Table 5.2, the conducted experiments of Configuration 1 are listed in which the biomass and the preheating temperature were varied (data from sections 4.3 and 4.4).

Table 5.2: Conducted experiments in Configuration 1 (data from sections 4.3 and 4.4)

Exp. Nr.	Biomass	Preheating Temperature* °C			Location of Formation of Solid Deposits
		H1	H2	H3	
5.1	Reed Canary Grass	250	350	460	Reactor (30–50 cm from top)
5.2	Napier Grass	350	450	500	Reactor (30–50 cm from top, no plugging)
5.3	Reed Canary Grass	350	450	500	Reactor (30–50 cm from top)
5.4	Reed Canary Grass	350	450	500	Reactor (30–70 cm from top)
5.5	Grapevines	350	450	500	Reactor (30–50 cm from top)
5.6	Reed Canary Grass	390	500	550	Preheater (65–75 cm from top)

* Heater (H) 1 to 3 from top to bottom of preheater.

The SCWG experiments were conducted with a reaction temperature that was set to 650 °C and the pressure of the system was kept at 280 bar. These conditions were chosen out of experience. In general, the pressure does not influence the process significantly according to the literature [89,90]. The gasification efficiency increases with increasing temperature. D'Jesus showed that a temperature of at least 650 °C should be chosen for gasification efficiencies higher than 80% when gasifying 5 wt.% corn silage at different residence times [89]. The biomass content in the feed was 8 wt.% and the flow rate was 700 g h^{-1} in the present study.

In Table 5.3, the seven conducted experiments in Configuration 2 are listed in which the preheating temperature and the inner material of the preheater (SS316 and titanium) were varied. With the variation of materials, a variation in the inner diameter was also realized. The experiments were conducted once. Also, the according inner temperature profiles were measured once.

Table 5.3: Conducted experiments in Configuration 2 (used biomass: RCG).

Exp. Nr.	Liner	Preheating Temperature[+] °C					Location of Formation of Solid Deposits
		H1	H2	H3	H4	H5	
5.7	SS316 (3.2 mm i.D.)	450	500	500	500	500	Preheater (65–75 cm from top)
5.8	SS316 (3.2 mm i.D.)	350	450	500	500	500	Preheater (100–120 cm from top)
5.9	SS316 (3.2 mm i.D.)	-	-	350	450	500	Preheater (95–105 cm from top)
5.10	SS316 (3.2 mm i.D.)	-	-	-	430	570	Preheater (80–105 cm from top)
5.11	SS316 (3.2 mm i.D.)	-	-	250	350	400	Reactor 1 (30–40 cm from bottom)
5.12	Titanium (1.5 mm i.D.)	-	-	350	450	500	Reactor 1 (10–20 cm from bottom)
5.13	Titanium (1.5 mm i.D.)	-	275	375	475	525	Preheater (exact location not detectable due to small diameter of liner)

[+] Heater (H) 1 to 5 from top to bottom of preheater.

5.3 Results and discussion

5.3.1 Influence of temperature on solid formation in SCWG

SCWG experiments conducted with Reed Canary Grass, Napier Grass, and grapevines in Configuration 1 showed that when processing lignocellulosic biomasses, solid deposits can occur in the reaction system that cause a blockage of the flow (see sections 4.3 and 4.4). The solid deposits consist of carbon, precipitating salts, and corrosion products. In previous investigations, it was concluded that the formation of solid deposits can most likely be avoided through sufficient salt separation. The salts were not separated completely (30 wt.% or less of the salt forming elements were removed flow (see sections 4.3 and 4.4)) as the salt separation temperature was only slightly supercritical (at max. 390 °C). The salts that were not removed at the salt separation were transported to the gasification reactor where they precipitated due to the further increase in temperature. An optimization could possibly be conducted in terms of geometry and in terms of salt separation temperature.

These measures were realized in Configuration 2. The optimization of the geometry was realized in the form of a sharper redirection of the flow in the salt separation T-fitting (see Figure 5.2) by extending the liner in the preheater past the outlet in the T-

fitting that leads to the gasification reactors. The flow redirection is more extreme in Configuration 2, in theory resulting in more salts depositing in the salt concentrate due to gravity. At the same time, the preheater was prolonged from 750 mm to 1200 mm in order to achieve higher temperatures at the T-fitting due to a longer heating range without exceeding 500 °C outer temperature, so that excessive local hot-spots at the reactor wall are avoided.

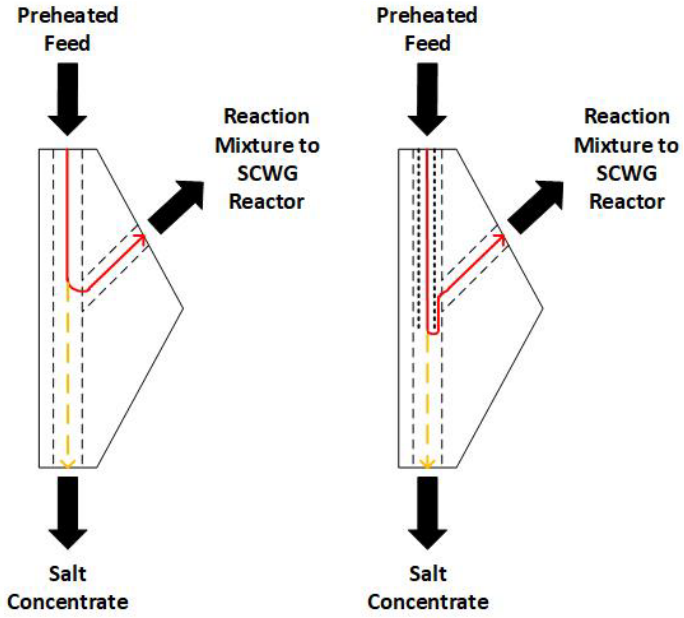


Figure 5.2: Salt separation T-fitting. Red line: flow of reaction mixture. Yellow line: salts separating into salt concentrate. (left): Configuration 1, investigated in sections 4.3 and 4.4. (right): Configuration 2.

Seven experiments were conducted with different preheating temperatures in Configuration 2. All conducted experiments, as listed in Table 5.3, ended early due to the formation of solid deposits. The maximum operation duration with the SS316 liner was 3.8 h. The deposits occurred in the preheater and in Reactor 1 depending on the temperature profile of the preheater. As a first countermeasure, a liner with a smaller inner diameter was installed to increase the flow rate in the preheater to improve the removal of possible precipitating solids. In order to avoid the possibility of the carbon formation on SS316 (through coke formation which can be catalyzed by nickel [167]), this new liner was made out of titanium (experiments 5.12 and 5.13). In these two experiments, solid formation occurred in less than 1.7 h and the location changed again with the preheating temperature profile. In previous work, the authors proposed that salts

mainly precipitate in the reaction system at temperatures of about 450 °C (see sections 4.3 and 4.4). For that reason, at a salt separation temperature of only 390 °C, the salts were not separated sufficiently. In the present experiments, the proposed temperature that leads to solid formation seems to be reached in the preheater when setting the maximum preheating temperature at 500 °C or above when using the SS316 liner. The precipitating salts are not transported to the salt concentrate but rather deposited in the preheater. It is interesting to note that the location of the solid deposits in the preheater varies with the temperature profile. In experiment 5.7, the proposed temperature range seems to be reached far earlier than in the other experiments due to the long heating zone with an outer temperature of 500 °C and thus the solids were found at 65 to 75 cm from the top in the preheater (the middle of the preheater). In the other experiments with the SS316 liner, they occur further down towards the end of the preheater since less heating was applied. When the preheating temperature was below 500 °C (experiment 5.11), the deposits occurred in Reactor 1. In this case, the temperature at the salt separation point was only 365 °C (measured on the outside of the T-fitting) and thus not sufficient to separate salts. The same accounts for the titanium liner where a higher outer temperature and a longer heated zone was necessary in order to reach the proposed temperature range due to the smaller diameter and thus higher flow speed.

Since the formation of solids is the predominant issue hindering long-time operation in both configurations 1 and 2, the temperature zone of solid deposit formation is of great interest. Therefore, an inner temperature measurement was conducted. The inner temperature measurement was conducted by inserting a 1/16-inch capillary (material: SS316) into the preheater and Reactor 1 (over the whole length of the preheater/reactor) as shown in Figure 5.3. The inside of the capillary is open to the environment while the outside is in contact with the reaction medium. A thermocouple (0.5 mm diameter) can be inserted into the capillary and moved along the axis of the preheater/reactor to obtain a temperature profile over the whole length of the preheater/reactor. Due to the small diameter of the capillary, it is assumed that the temperature profile is not changed when inserting the capillary. Additionally, it can be assumed that the measured temperature profile is equal to the temperature profile during experiments since the capillary's walls are so thin that temperature gradients due to heat transfer can be neglected. D'Jesus found that there is no difference in measuring the inner temperature

profile with this method when water is flowing through the system compared to biomass slurry [89]. Thus, for simplicity and to avoid corrosion on the capillary, the temperature measurement is conducted with water. The inner measurement in the preheater could only be conducted with the SS316 liner and not the titanium liner since the inner diameter of the titanium liner (1.5 mm) was too small to insert a capillary.

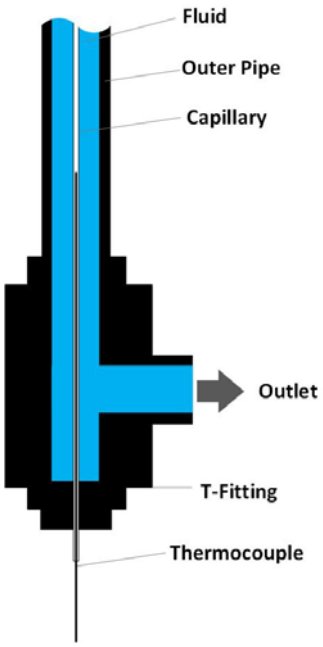


Figure 5.3: Set-up of the inner temperature measurement.

The temperature measurements of the preheater show that the outer pipe temperature profile is (almost) the same during the real experiment and during the temperature measurements with water. They display that the inner temperature is up to 100 °C colder than the set temperature on the outside of the preheater in parts where an outside temperature of 500 °C is reached (see Figure 5.4). Long zones of set outside temperatures of 500 °C are necessary to reach an inner temperature of more than 400 °C. When comparing the measured inner temperature profile and the locations of solid formation for experiments 5.7, 5.8 and 5.9, the temperature range of solid formation lies between 400 and 440 °C in all cases, while the outside temperature is set at 500 °C.

The inside measurements of Reactor 1 reinforce the knowledge gained from the measurements in the preheater (see Figure 5.5). When the maximum preheating temperature was set to 400 °C in the case of the SS316 liner and to 500 °C in case of the

titanium liner, the crucial temperature range of 400 to 440 °C is not reached within the preheater. Subsequently, this temperature range is first reached in Reactor 1 (where the outside temperature is set to 600 °C) as shown by the inside measurement conducted under the set temperatures of experiment 5.11 and 5.12. In this case, the solids also formed in a place where 400 to 430 °C were reached.

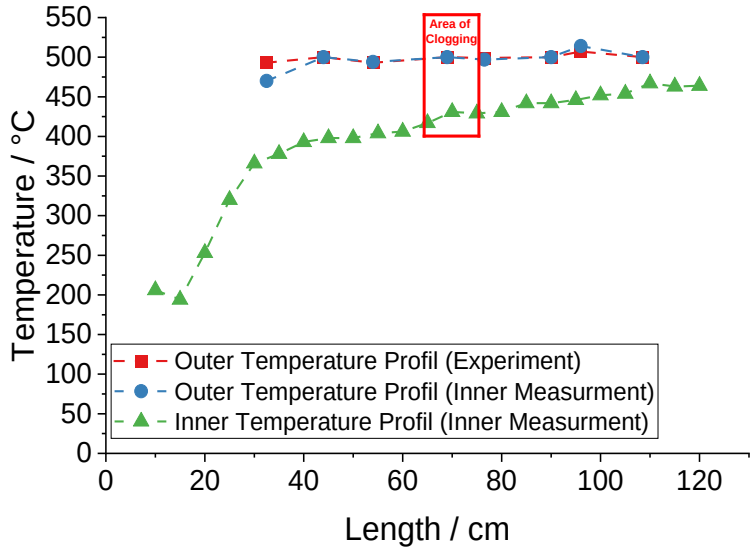


Figure 5.4: Outside and inside temperature profile of experiment 5.7.

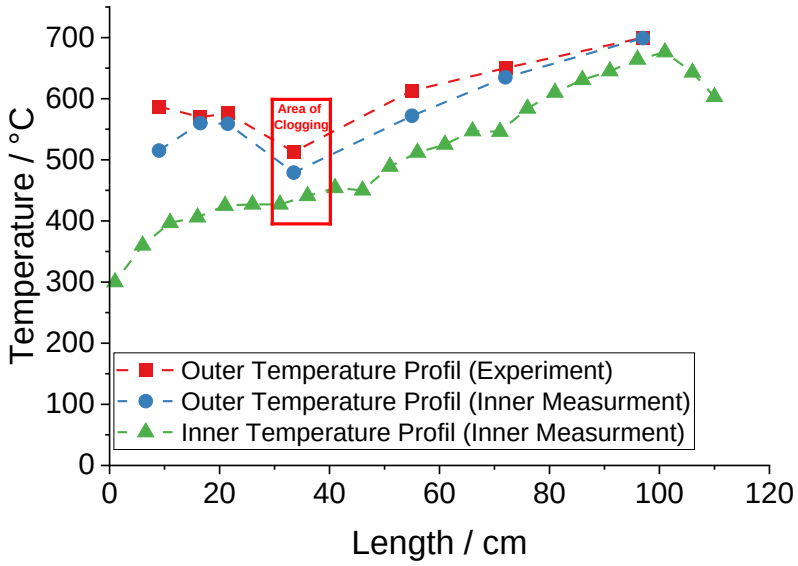


Figure 5.5: Outside and inside temperature profile of experiment 5.11.

In the preheater and as well in Reactor 1, the solid deposits occurred in the same temperature range. In this temperature range, salts precipitate and coke seem to form. It is well known that salts precipitate at temperatures above 374 °C [84,111]. The ability to separate salts by precipitation depends on the kind of salt. In binary salt–water systems, salts are divided into type 1 and type 2 salts [68,69,85]. Type 1 salts dissolve in dense supercritical water and only precipitate when the temperature is further increased (e.g., $KHCO_3$ [68]), while type 2 salts are poorly soluble in supercritical water (e.g., Na_2SO_4 [81]). Thus, in the crucial temperature range of 400 to 440 °C, type 2 salts precipitate but the solubility of type 1 salts also decreases significantly. Due to the addition of $KHCO_3$ as a catalyst in large quantities, this salt is the predominant one present in the system. In a $KHCO_3$–water mixture, Schubert found that a significant amount of potassium can be separated at a salt separation set point of 470 °C, which equals a fluid temperature of about 410 °C in their system [68]. This temperature fits in the interval determined in the present work. In the present case, the precipitation of salts is wanted in the preheater in order to separate them into the salt concentrate. The salts would need to be transported to the salt concentrate by the drag of the water flow, which they are not in the present experiments. Rather, they deposit on the reactor walls. This is also the case when the flow speed is increased through a smaller inner diameter, as shown in experiment 5.13 with the titanium liner. In the titanium liner, the Reynolds (Re) number (calculated based on properties of water taken from IAPWS-IF97 data base) is greater than 3000, and thus, the flow can be assumed to be turbulent, while in the SS316 liner, the flow is either laminar (Re < 2300) or in the transition between laminar and turbulent (2300 < Re < 3000) (see Table 5.4).

Table 5.4: Flow velocities and Re numbers for different temperatures in the preheater.

	SS316 Liner (i.D. = 3.2 mm)		**Titanium Liner (i.D. = 1.5 mm)**	
Temperature / °C	400	440	400	440
Velocity u / cm s^{-1}	9.32	17.22	29.45	54.43
Re / -	2169	2568	3856	4566

The state of the flow thus does not seem to influence the transportation of the solids. A possible reason for this is that the reactor wall is the hottest point in the system as

the reactors are heated from the outside, so there, the solubility of the salts is the lowest and they deposit there. A different heating concept could be implemented in order to avoid this if the present salt separation technique is kept.

In addition to the salt precipitation, coke formation was observed in the present experiments and in the experiments conducted in sections 4.3 and 4.4. A possible explanation for this can be found when looking at the hydrothermal liquefaction (HTL) of biomass. HTL usually is conducted at temperatures lower than 370 °C and elevated pressures of up to 250 bar [28]. The optimal temperature range of HTL for the maximum oil yield depends on the type of biomass, but in general, 275 to 350 °C seems to be optimal [168–171]. At lower temperatures, the biomass is not fully converted, whereas at higher temperatures, the formation of coke is increased due to repolymerization [172]. The optimal residence time also depends on the type of biomass, but in general, too long residence times increase the coke and gas yield due to repolymerization and cracking [172–175]. The residence time in the preheater is about 6 s with the titanium liner and about 29 to 37 s for the SS316 liner in the conducted experiments (depending on the temperature profile). Generally, HTL is conducted in multiple minutes rather than seconds [176–179], but in some cases, residence times as short as 1 or 1.4 min were sufficient to liquefy biomass [180,181]. The residence time in the present experiments under normal operation is too short to explain the coke formation. Assumedly, the coke formation thus might appear after salts precipitate, and thus, obstacles in the flow regime are formed at which biomass particles can get stuck. In this case, the residence time in the preheater is significantly prolonged for these particles. Additionally, once the system is blocked, no flow is possible anymore. Even without active heating, it takes several minutes to hours for the temperature to fall below the HTL temperature range due to the installed insulation leading to increased coke formation. Salt separation thus is the main issue that needs to be resolved.

As there is no sign of deposits outside this temperature window that could cause a blockage of the flow, a SCWG configuration should be developed that applies rapid heating of the biomass slurry to temperatures above the determined 400 to 440 °C, possibly without the pipe being the local hotspot. This might overcome the issue of salt depositions due to slow external heating, as it is the case in the present work.

5.3.2 Influence of flow direction on the separation of solids

In Configuration 1, only one gasification reactor was used (1800 mm long). For Configuration 2, additionally to the redesigned preheater/salt separation, a second reactor was installed to increase the residence time in the temperature range of T > 600 °C. The residence time increased from 17 to 51 s. With this measure, the residence time was increased without changing further parameters. A reduction in the flow rate, for example, would also increase the residence time but also influence temperature profiles and the flow regime.

It is well known from the literature that an increase in residence time increases the gasification efficiency since the splitting of biomass towards gases can further proceed [66,67,143]. Compared to Configuration 1, the gasification efficiency increased by roughly 7%, from 59 to 66% (experiment 5.3 and 5.9) (see Table 5.5).

Table 5.5: CE and TOC conversion of conducted experiments (flow rate = 700 g h^{-1}).

Exp. Nr.	Duration h	CE %	TOC conversion %
	Configuration 1		
5.3	6.5	59.1	83.8
5.4	2.5	57.7	86.9
	Configuration 2		
5.7	0.25	-	-
5.8	0.25	-	-
5.9	3.5	65.8	86.0
5.10	3.8	66.7	85.4
5.11	2.5	63.4	86.0
5.12	1.7	58.1	90.0
5.13	0.8	-	-

Literature shows that this increase in residence time is by far not sufficient to reach a full conversion of the biomass. D'Jesus et al. showed that residence times above 2 min are necessary in order to gasify 5 wt.% corn silage completely at T = 650 °C [92]. When comparing the present results with the results achieved by D'Jesus et al. [92], the

gasification efficiency is in the same magnitude. Thus, in the present case, the residence time needs to increase further to achieve complete gasification, and the issues described in section 5.3.1 need to be resolved. The increase in residence time did not influence the gas composition, as can be seen in Figure 5.6.

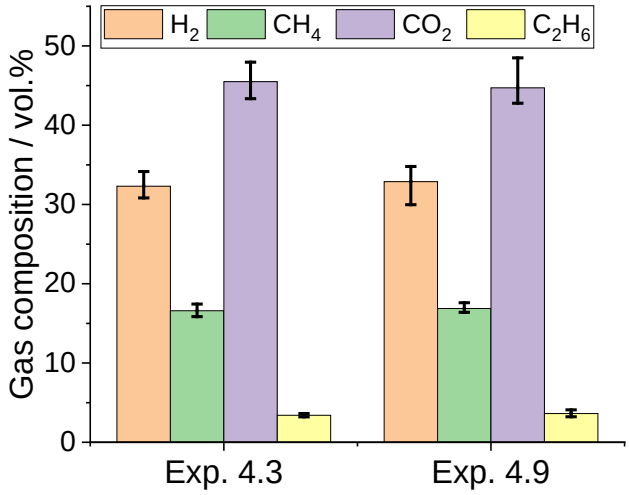


Figure 5.6: Gas composition for configuration 1 and 2.

The implementation of the new reactor (Reactor 1) resulted in new obstacles. When plugging in the gasification reactors occurred, it occurred after less than 2.5 h (experiments 5.11 and 5.12). In Configuration 1, operation of up to 6.5 h could be achieved before the plugging of the reactor. The reason for this seems to be the flow direction in the reactors. In Configuration 1, the reactor is a downflow reactor, and the newly implemented reactor (Reactor 1) in Configuration 2 is an up-flow reactor. The flow direction is important for transporting deposits to the outlet of the system (reactor effluent) to avoid plugging. In the downflow reactor, the gravity and the flow direction result in a force in the same direction, while in the up-flow reactor, they act as opposite forces. Thus, in the up-flow reactor, the deposits (especially the precipitating salts) are not as easily transported with the flow and thus blocking occurs quicker.

An indicator for this is the potassium concentration in the reactor effluent during experiments with only Reactor 2 and with two reactors installed. During operation with only Reactor 2, 1090 to 2180 ppm K^+ is detected in the effluent, and during operation with two reactors, on average, only 465 ppm K^+ is detected (see Table 5.6).

Table 5.6: Potassium concentration in the reactor effluent.

Exp. Nr.	K^+ added to the feed ppm	K^+ in reactor effluent ppm
	Configuration 1	
5.3	5000	2180
5.4	5000	1090
	Configuration 2	
5.9	5000	168
5.10	5000	163
5.11	5000	1260
5.12	5000	270

A reduced number of salts in the effluent is wanted if the salts instead are accumulated in the salt concentrate. But since salt separation was not improved with the newly implemented salt separation system (see Figure 5.7), the difference in potassium stays in the system as solid deposits which can be seen by the increase in potassium in the rinse water.

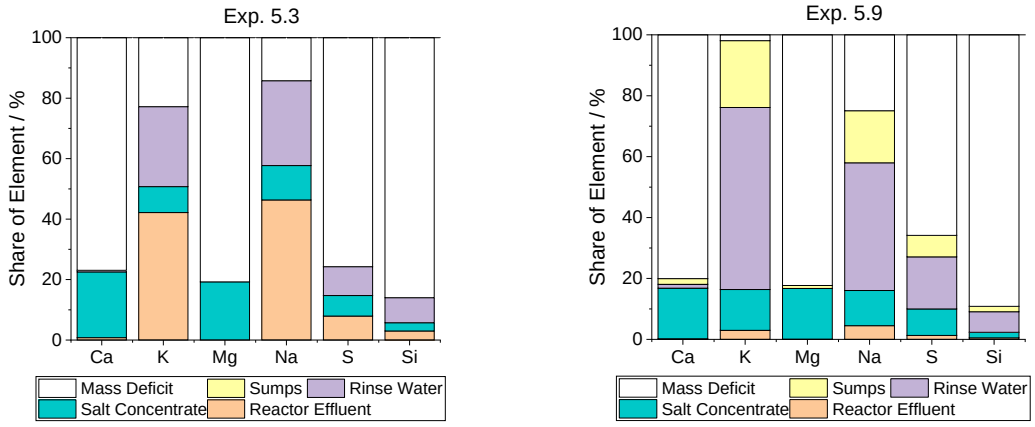


Figure 5.7: Distribution of salt building elements for two configurations.

During cooling of the plant, potassium is soluble again and is washed out of the system. To reach a certain amount of solid deposits, it thus takes less time which leads to quicker plugging. Reactor 1 also needs to be constructed as a downflow reactor to increase the operation time if the salt separation is not sufficient. In the case of

complete salt removal before the gasification reactors, the flow direction in the reactors should not influence the process.

The described issues that result in the short duration of experiments are mainly due to chemical and physical effects (coking and salt precipitation) in the temperature range of 400 to 440 °C. Thus, resolving the heating problem and with that also the issue of salt separation should enable long-term operation. In the current lab plant with the chosen throughput, the residence time is very low (D'Jesus found that residence times well above 2 min are necessary to gasify 5 wt.% corn silage at T = 650 °C completely [92]), but still sufficient for some organics. This becomes clear when gasifying ethanol solutions (up to 72 wt.% ethanol), with no salts in it. Long-time operation with CE = 100% was achieved, as outlined in detail in Chapter 7. RCG obviously requires a higher residence time, as seen in the currently achieved CE.

5.4 Conclusion

The salt precipitation during the supercritical water gasification of biomass was investigated in a continuous SCWG lab plant. By inner temperature measurements in a complex setup, it was discovered that the temperature range in which salts mainly precipitate is 400 to 440 °C. In order to reach the reaction temperature of 650 °C, this temperature window needs to be passed. This could be used to separate the salts from the reaction mixture. However, since the salt separation installed, which is supposed to remove the precipitating salts by gravity, was not able to separate the salts in the current setup, blockage of the flow in the reactors occurred. Additionally, the influence of flow direction in the lab plant on the duration of operation was investigated. The tendency to block the flow by precipitation is strongly influenced by removing the salts by gravity and drag of the flow. It was thus found that the direction of flow is an important factor to consider during salt separation. The importance of the understanding of chemical and physical effects during the heating of biomass slurries in the process of supercritical water gasification was demonstrated. Future optimization of the heating concept coupled with the positioning of the salt separation device is necessary in order to enable long-time operation of SCWG with salt containing biomasses.

Chapter 6. Development and parametrization of novel reactor concept for the supercritical water gasification

The content of this chapter is sourced from the following publication:

- Dutzi, J.; Vadarlis, A.A.; Boukis, N.; Sauer, J. Development and parametrization of novel reactor concept for the supercritical water gasification process. *Ind. Eng. Chem. Res.,* **2025**, 64, 9500-9517. DOI: 10.1021/acs.iecr.4c04267

Declaration of contributions:

Julian Dutzi conceptualized the experimental work and analysed the data, evaluated the results, and wrote the manuscript. Julian Dutzi conducted the thermodynamic equilibrium calculations and the comparison with experimental data.

Athanasios A. Vadarlis conducted the thermodynamic equilibrium calculations and the comparison with experimental data.

Nikolaos Boukis supervised the work, contributed to the discussion, and reviewed the manuscript.

Jörg Sauer supervised the work, contributed to the discussion, and reviewed the manuscript.

Summary of chapter 6

A novel reactor concept for supercritical water gasification was developed, where cold biomass is mixed with supercritical water for heating. This approach enhanced gasification efficiency and reduced solid deposition. Following proof of concept over 100 hours, a parametric study was conducted, varying biomass type, dry matter content (1.3-8.2 wt.%), temperature (550-700 °C), pressure (240-300 bar), potassium addition (0-3750 ppm), and residence time (0-42 s). Results showed that biomass type, pressure, and potassium addition had minimal impact on the process. Higher biomass concentration reduced carbon efficiency (CE) but CE maintained levels around 80%. Increasing residence time at reaction temperature significantly improved CE up to 8 s at 650 °C (τ = 0 s, CE = 27%; τ = 8 s, CE = 72%), beyond which gains plateaued. Temperature strongly influenced CE (T = 550 °C, CE = 58%; T = 700 °C, CE = 91%) and gas composition, with higher temperatures reducing organic carbon and tar formation but increasing methane (T = 550 °C, 9.5 vol.% CH_4; T = 700 °C, 15.9 vol.% CH_4) and C_{2+} (T = 550 °C, 2.3 vol.% C_{2+}; T = 700 °C, 5.1 vol.% C_{2+}) content. Deviations in gas composition from equilibrium calculations, conducted with ASPEN HYSYS, suggested insufficient steam reforming, potentially addressable with a nickel catalyst. An empirical multi-linear regression model was developed, accurately predicting outcomes for the studied biomasses and reducing experimental effort for process optimization. Overall, the study demonstrates the reactor concept's superior performance and provides a strong foundation for further developing and optimizing supercritical water gasification processes that could potentially be applied to other feedstocks.

6.1 Introduction

Although, SCWG offers the possibility of hydrogen- or methane-rich product gas from difficult-to-utilize biomasses such as sewage sludge there has not yet been a commercial application (to the best of the author`s knowledge). This is due to several obstacles in the process [108]. As described in the previous chapter the salt separation appears to be the major bottleneck at lab-scale. It was found that the gradual heating of the biomass slurry to supercritical temperatures by electrically heating the pipes leads to the formation of solids on the reactor walls, since the temperature is locally the hottest at the wall and thus the solubility of the inorganics is the lowest there. Thus, the precipitating salts stick to the wall instead of being separated. A different heating concept needs to be adapted. An alternative heating concept can be derived from pilot-scale results produced in the VERENA plant at KIT [129]**.** When they had implemented heating from the outside of the reactor (as done in this work in Chapter 4) they also observed plugging [182]. Therefore, they developed the so-called “two-stream concept”, in which a pure water stream is heated to supercritical temperatures and then mixed with cold biomass slurry. This process achieves rapid heating of the biomass, without the need for external heating through the reactor walls. In the two-stream concept solid formation was reduced and no plugging occurred in the pilot plant [108]. Due to the configuration of the pilot plant a maximum reaction temperature of only 550 °C was achieved, resulting in a gasification efficiency of less than 60%. A similar setup has been investigated in the past at KIT on lab-scale [183]. However, there was no salt separation. Additionally, it was not possible to ensure that the feed slurry enters the mixing point at T < 100 °C. Thus, further development is required to implement a working two-stream concept at lab-scale.

Once a working SCWG concept has been developed, it is important to investigate the influence of the key process parameters such as biomass concentration, temperature, pressure, catalyst addition and residence time. With such parametric studies, process limitations and the parameter set that generates the maximum amount of product gas with the least input (energy and cost) can be determined.

In this chapter, the two-stream concept has been adapted and further developed on a lab-scale. This newly developed SCWG system is described and tested. After successful proof of concept, a parametric study is performed to fully characterize the new

system, including variation of biomass type and concentration, temperature, pressure, residence time and addition of homogeneous catalysts. Since some process parameters showed a linear influence on the gasification efficiency and gas composition, an empirical model describing the present SCWG system was derived based on multilinear regression and subsequently verified. The model can be used to predict the outcome of new parameter sets for the studied biomasses. The parametric study is accompanied by simulation of equilibrium gas compositions and gas production, carried out in ASPEN HYSYS V14, to determine where further improvement is possible.

6.2 Materials and methods

6.2.1 Setup

The gasification experiments are carried out in the continuous lab-plant for high pressure (p ≤ 300 bar) and high temperature (T ≤ 700 °C) conversion of biomass compounds. In the present configuration, the lab-plant consists of three main parts: the water preheater, the salt separator and the gasification reactor.

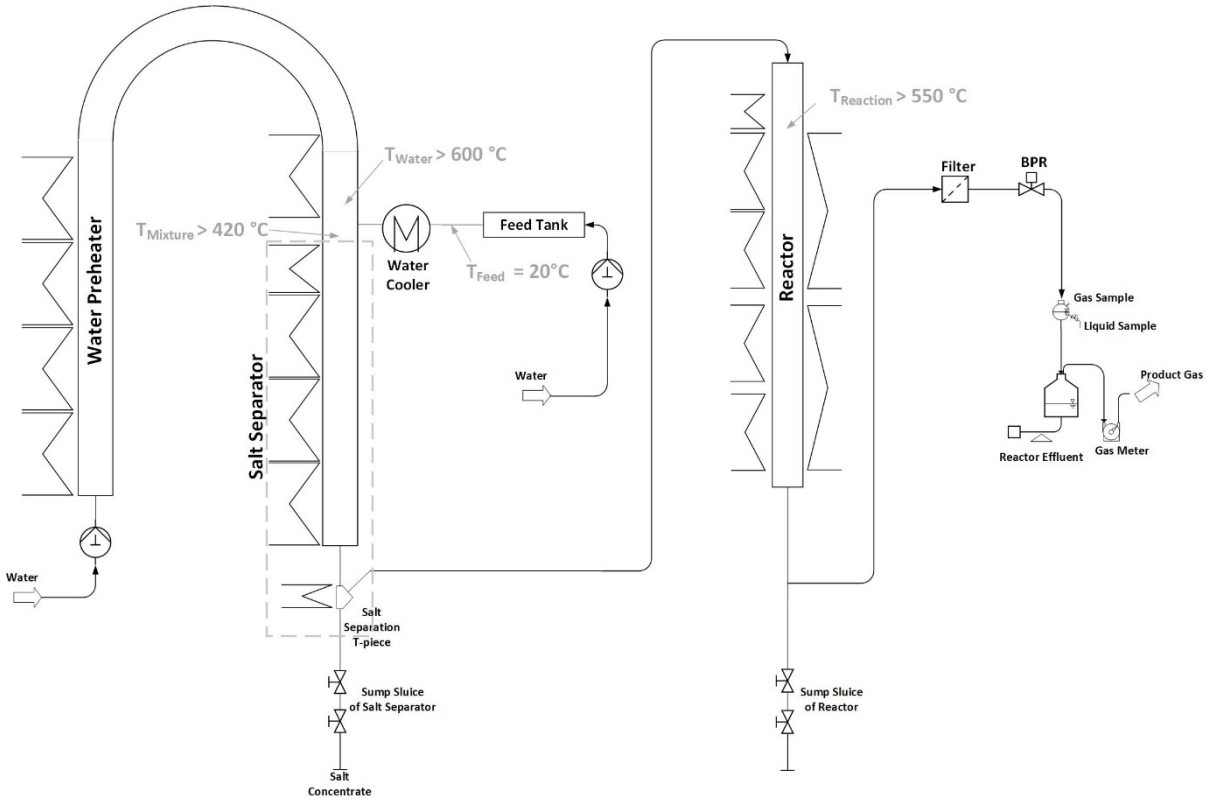


Figure 6.1: Schematic setup of SCWG lab-plant in Chapter 6.

In this configuration, the biomass slurry is rapidly heated by mixing it with supercritical water. This is accomplished by heating distilled water to temperatures up to 650°C through 5 spiral heaters in the water preheater (Inconel 625, 9/16 inch o.D., 8 mm i.D). The water stream (1) is mixed with a cold biomass slurry (2). A thin pipe (1/4-inch pipe) was chosen for the feed stream to ensure a faster flow. To connect the feed stream to the water preheater, a hole was drilled into the side of the water preheater. The feed line was then welded onto this hole. The mixing of the two streams occurs as soon as the feed stream enters the preheated water stream through the drilled opening. From this point onward, the subsequent 9/16-inch pipe is referred to as the salt separator (the water preheater and salt separator are two separate 9/16-inch pipes connected by a screw joint, allowing partial disassembly and cleaning). To ensure that the biomass slurry is not preheated prior to mixing a water cooler is implemented (welded onto the feed piping), with a set temperature of 20 °C (see Figure 6.1). A mixing temperature of over 420 °C is achieved (measured on the outside). The implementation of a cooler is necessary due to low flow rates. At lower flow rates the slurry will be heated to higher temperatures if no cooler is present. At much higher flow rates the implementation of a cooler could be omitted, as realized in the VERENA pilot plant [108].

The mixture enters the salt separator which consists of a tube (Inconel 625, 9/16 inch o.D., 8 mm i.D), with a T-fitting at the bottom. The salt separator is heated from the outside by 5 spiral heaters to ensure that the temperature remains above the critical point of water. The set point for this is T = 450 °C. Inside the tube, the salts in the biomass precipitate due to the properties of the supercritical water. They are separated by gravity at a T-fitting at the bottom of the tube. The precipitated salts fall vertically into the salt concentrate, while the organic-water mixture is transported laterally to the gasification reactor.

In the gasification reactor (Inconel 625, 9/16 inch o.D., 8 mm i.D), heated by 1 spiral and 6 rod heaters, temperatures up to 700 °C (measured on the outside) are used to gasify the organics. Air cooling reduces the temperature to below 30 °C after the reactor. After the reactor a high-pressure filter and a back-pressure regulator by Tescom are located in the cold section of the lab-plant. After pressure reduction to ambient pressure, the gas flow is measured by a gas meter (Ritter Apparatebau GmbH) and the effluent is quantified by a scale (Soehnle GmbH).

At the bottom of both the salt separator and the gasification reactor there are sluices, consisting of two valves, so that the salt concentrate can be drained from the salt separator and possible deposits, like salts and corrosion products, can be drained from the gasification reactor.

The novelty of the current configuration lies in the biomass heating concept. In the past, the laboratory plant consisted of two main components: the preheater and the gasification reactor (see sections 4.3 and 4.4). In the preheater, the biomass slurry was gradually heated by electric heaters on the outside of the reactor wall to reach the supercritical state of water. This gradual heating led to clogging problems due to salt deposits on the wall of the preheater. Therefore, a novel system was developed to overcome this problem.

6.2.2 Description of experiments

6.2.2.1 Preparation of educts

The dry grasses Reed Canary Grass (RCG), Capiacu Grass (CG), Energy Cane (EC) and Napier Grass (NG) were used as biomasses for the present experiments. RCG was provided as a powder with a grain size less than 0.25 mm. The other biomasses were milled in a mill with a 0.2 mm sieve (Pulverisette 14, Fritsch GmbH). The feed slurry was prepared by mixing distilled water with dry biomass to obtain a mixture with the desired dry matter content. Xanthan (Carl Roth GmbH) is added as a thickening agent (0.5 wt% based on slurry mass). $KHCO_3$ (VWR International GmbH) is added as a homogeneous catalyst in various concentrations.

6.2.2.2 Experimental procedure

The experimental procedure is started by feeding water into the lab-plant to pressurize it. Once the desired pressure is reached and no leakage occurs in cold operation, the lab-plant is heated to the desired temperatures. Pressure and temperature are set in the process control system. One day before biomass slurry feeding is started, ethanol solution is pumped into the lab-plant. This procedure fills the dead volumes in the lab plant with water-gas mixtures similar to the product gas during biomass slurry

operation. With this preliminary test, a steady state can be reached faster during the biomass slurry operation.

On the day of the main experiment, the biomass slurry is fed into the system. The biomass slurry is stored in a pressurized tank connected to the system. From this tank, the slurry is fed indirectly into the lab plant by a water driven piston. The lab plant is operated until a steady state is reached, which is required for evaluation. To assess whether steady state has been reached, gas and effluent flows are quantified and gas samples are analyzed at 30-minute intervals. Liquid samples are also collected throughout the experiment. At the end of the experiment, the system is flushed with water to clean it.

During the experiments the following parameters were changed in the following ranges (see Table 6.1). The default values were chosen and only one parameter was varied during each experiment. The default values were chosen and only one parameter was varied during each experiment. As all different biomass types displayed similar behavior (see section 6.3.2.1), the choice of biomass was varied between the four biomasses tested according to their availability. Due to limited time, resources, and the considerable effort involved in preparation and execution, most experiments were performed only a single time. Only a small number of experiments were conducted multiple times, all producing very similar results.

Table 6.1: Investigated parameters.

Parameter	Range	Default value	Unit
Biomass type	4 biomasses		
Dry matter in reaction mixture	1.3 – 8.2	6.6	wt.%
Temperature	550 – 700	650	°C
Pressure	240 – 300	280	bar
Homogeneous catalyst addition	0 – 3750	3750*	mg K^+ / kg mixture
Residence time at T_{Rct}	0 – 42	31	s

*during dry matter variation, K^+ addition was adjusted in such a way that a constant amount of 560 ppm K^+/wt.% dry matter was added.

6.2.3 Thermodynamic equilibrium calculations

Equilibrium calculations with ASPEN HYSYS can serve as a valuable tool for the process evaluation, e.g., investigating the water consumption of the reactions during SCWG of ethanol, as shown in Chapter 7. Additionally, equilibrium calculations allow for the examination of the operational limits of a chemical process, aid in maximizing the production of the target product, minimizing energy consumption, and reducing overall costs [184]. In the present study equilibrium calculations were carried out to determine the deviation of the equilibrium H_2 yield between experiment and equilibrium calculation under different operating conditions. The thermodynamic equilibrium was calculated in Aspen HYSYS V14. Since the real biomass or cellulose as a model compound is not available in the data base of Aspen HYSYS, the monomer of cellulose, glucose $C_6O_6H_{12}$, was chosen instead. A Gibbs reactor was used to model the SCWG of glucose (dextrose), which minimizes the Gibb's free energy of the reaction system [185]. The property package that was applied was the PRSV with the Peng-Robinson equation of state.

To compare the equilibrium data with the experiment, the elemental composition of the dry matter of the feed slurry was first determined. 5 to 12 wt.% of the feed slurry constitute of salt building elements and metals (depending on the addition of homogeneous catalysts), about 1 wt.% and 0.1 to 0.3 wt.% are constituted by N and S, respectively. The C and H contents were analyzed and the O content is calculated by difference. The C/O-ratio in the dry feed mass is 0.91 ± 0.05 (based on mass) and the C/H-ratio is 7.04 ± 0.16 (based on mass). This equals an average molar C/O/H-ratio of 1.00/0.82/1.70, or a theoretical chemical formula of $C_{1.00}O_{0.82}H_{1.70}$. The latter form is similar to cellulose $(C_6O_5H_{10})_n$ ($\widehat{=}$ $C_{1.00}O_{0.83}H_{1.67})_n$. Thus, cellulose use as a model substance for equilibrium calculation is justified, with approximately the same C, H and O content (for details see Supporting Information A1.3). As glucose is gained from cellulose via hydrolyzation [186] and water is present in a great surplus, this should not affect the equilibrium gas composition in a significant way. The concentration of glucose was chosen in such a way that the carbon content in the mixture is equal to the carbon content during the experiments (Supporting Information A1.3). The influence of pressure, temperature, and biomass concentration can be simulated using ASPEN HYSYS. In section 6.5, the gas composition and the gas production of the experiments and of the thermodynamic equilibrium are compared and discussed.

6.3 Experimental results

6.3.1 Proof of concept

The capabilities of the newly developed system were tested by gasifying the grass Reed Canary Grass (RCG). The conditions were chosen so that 100 g h^{-1} cold feed slurry with 8.8 wt.% dry matter content were mixed with 600 g h^{-1} supercritical water. In this way, the dry matter content in the system (after the mixing point) was 1.3 wt.%. The resulting composition of the feed and the reaction mixture is shown in Table 6.2.

Table 6.2: Elemental composition of feed slurry during proof of concept, in wt.%.

	C	K	Ca	Mg	Na	P	Si
Dry feed slurry	39.88	5.45	0.31	0.06	0.05	0.17	2.18
Wet feed slurry (8.8 wt.% dry matter)	3.51	0.48	0.03	0.005	0.004	0.015	0.19
Reaction mixture (1.3 wt.% dry matter)	0.501	0.0685	0.0039	0.0008	0.0006	0.0021	0.027

The water stream was preheated to a temperature of 750 °C (measured on the outside), while the biomass slurry was cooled by water cooler set to a temperature of 20 °C. The outer wall temperature after mixing was 420 °C. By reaching this temperature, the supercritical state of the biomass slurry was immediately reached. Thus, the heating of the salt separator is only used to prevent heat loss of the reaction medium to the environment. The temperature of the salt separator was maintained at 450 °C. Thus, the tube wall is not a local hotspot where the solubility of the salt building elements is the lowest (unlike in the previous configurations [187]). Thus, the precipitation salts should not accumulate on the pipes but should rather be transported to the salt concentrate. The reaction temperature in the gasification reactor was set to 650 °C.

The aim was to achieve the longest possible operation without plugging. More than 100 hours of operation without plugging were achieved with this setup under the chosen conditions. During steady-state operation, the carbon gasification efficiency was 82.0%, while the TOC conversion was 85.3%.

The TOC conversion quantifies the amount of organic carbon that is transferred from the feed to other species, such as gas, inorganics or solids. As CE, which quantifies

the amount of organic carbon transferred from the feed to the gas phase, is approximately the same as the TOC conversion, this indicates that no organic carbon deposition has occurred. This is confirmed by the total carbon balance which is 97.2% and can thus be considered closed within the errors of measurement.

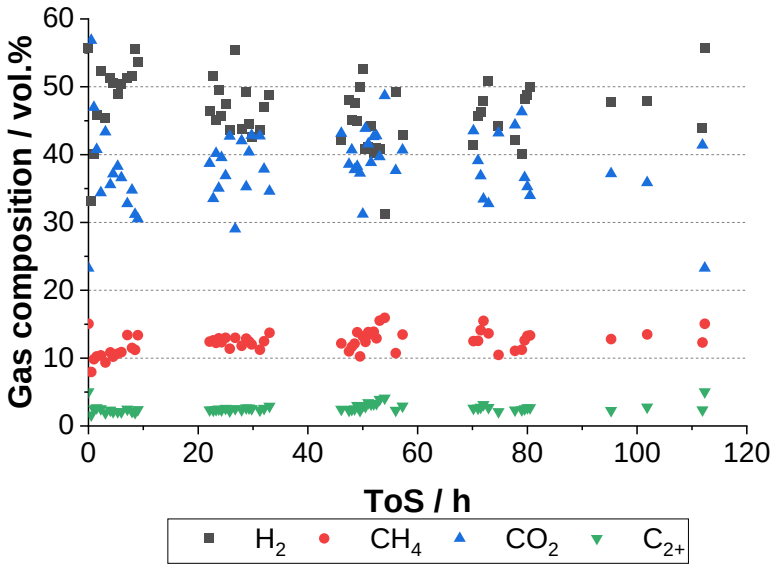


Figure 6.2: Gas composition of product gas during proof of concept (T = 650 °C, p = 280 bar, $DM_{mixture}$ = 1.3 wt.%, $\dot{m}$ = 700 g h^{-1}).

Due to the small amount of biomass present in the system, the gas composition varied greatly between measurements (see Figure 6.2). Within the first few hours steady state is reached. However, on average the gas composition is stable over the entire period of operation. 46.6 vol.% H_2, 12.4 vol.% CH_4, 38.5 vol.% CO_2 and 2.7 vol.% C_{2+} are obtained. CO is present with less than 1 vol.% and thus is not included in Figure 6.2 (this is also the case for the following parameter variation).

After 112.5 h the experiment was stopped and the lab-plant was checked for solid deposits but none were found. This confirms the insight gained from the key figures CE, TOC conversion and carbon balance that no carbon containing deposits formed.

The main factor hindering long-term operation in the past was solid deposits consisting of salts, coke and corrosion products. Regarding the salt balance, poor results were obtained when looking at the liquid effluents (see Figure 6.3). None of the Ca, Mg and P fed to the system can be found in the effluents. This may be due to the high dilution

of the feed slurry resulting in levels of less than 40 ppm in the reaction mixture (see Table 6.2). Although the Na content is in the same range, 58% of the added Na is found in the effluent. Over the course of the experiment, 0.42 g Na was added to the system, resulting in a mass deficit of 0.18 g. The predominant salt-forming elements in the feed slurry are K (added as a homogeneous catalyst) and Si. In both cases, only 28% and 4%, respectively, can be detected in the liquid effluents and only 4% and 3%, respectively, in the reactor effluent. Thus, only small amounts of salt building elements pass through the system.

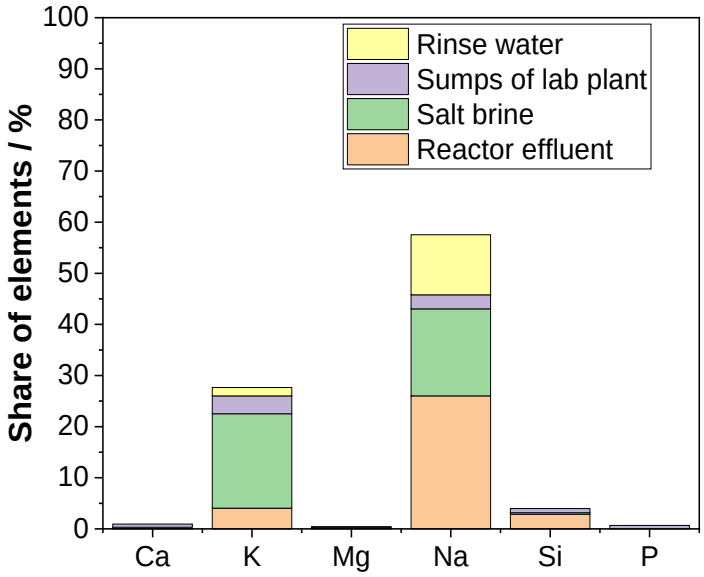


Figure 6.3: Salt balance in liquid effluents (100% = feed content) (T = 650 °C, p = 280 bar, $DM_{mixture}$ = 1.3 wt.%, $\dot{m}$ = 700 g h^{-1}).

In total, 46.7 g of K and 18.6 g of Si were fed to the system, resulting in a mass deficit of 33.8 g of K and 17.9 g of Si. As described above, no deposits could be found in the lab-plant when physically checking after the experiment. Thus, also no solid salts deposited in the lab-plant. However, some solids were found in the salt concentrate. These solids were not analyzed quantitatively and thus not balanced. In Supporting Information A1.1, the EDS-analysis (energy dispersive spectroscopy) of the solid content of a salt concentrate sample is displayed. Some carbon and oxygen are present in the sample, but there are also salt-forming elements, especially Si (10.03 atom%), K (2.99 atom%) and Ca (2.92 atom%), are present, indicating that the salts are also separated in solid form. It can be concluded that the newly developed system can be

successfully operated for long periods of time with high gasification efficiencies. Even though the salt balance in the liquid effluents is not closed, no salt deposition occurred in the system leading to the conclusion that all salt building elements are contained in the salt concentrate (some in the form of solids that were not quantitatively analyzed). Based on the initial successful operation, it can only be assumed that higher dry matter contents are also processable, as high conversion rates were observed and no deposits were detected. However, a further investigation is needed. Additionally, a downside of this first proof of concept is that the low biomass content in the reaction mixture negatively affects the economics of the process. Thus, a further parameter optimization is required.

6.3.2 Parameterization of the newly developed system

The newly developed system was improved in terms of heat losses after a first proof of concept (section 6.3.1). Thus, a maximum water preheating temperature of 650 °C was sufficient to achieve mixing temperatures of more than 420 °C. After this improvement, the parameters that are known to significantly influence the SCWG process, namely the biomass type, temperature, pressure, concentration of biomass, residence time and addition of a homogeneous catalyst, were investigated.

6.3.2.1 Influence of biomass type

In previous studies by the authors different types of dry biomass were gasified. It was observed that there is no significant difference in the gasification of different biomasses with similar composition [188]. This was also observed by D'Jesus et al. who gasified corn starch and glover grass and obtained similar results [86].

In the present work, four different dry biomasses were gasified: Napier Grass, Reed Canary Grass, Energy Cane and Capiacu Grass under the same conditions (T = 650 °C, p = 260-280 bar, $\dot{m}$ = 700 g h^{-1}, 3750 ppm K^+ added to the mixture, dry matter content in mixture 6.6 wt.%). The elemental analysis of these biomasses is given in Table 6.3. The CHN contents are quite similar, with Reed Canary Grass showing a slightly higher carbon content than the other biomasses. A significant difference is

visible in the potassium content. Reed Canary Grass contains almost no potassium while Napier Grass and Capiacu Grass contain about 4 wt.% potassium.

Table 6.3: Elemental analysis of gasified biomasses, based on dry matter in wt.%.

	C	H	N	K	Ca	Mg	P	Si
Napier Grass	43.2	6.00	1.00	4.05	0.75	0.69	0.23	1.71
Reed Canary Grass	48.9	7.46	<0.3	0.29	0.17	0.05	0.10	2.30
Energy Cane	42.4	6.10	0.70	2.59	0.38	0.25	0.14	0.90
Capiacu Grass	41.2	5.80	1.15	3.79	0.40	0.24	0.11	0.87

The product obtained from the gasification of the four biomasses is very similar. There are only small differences. 35.8 ± 1.4 vol.% (standard deviation) of H_2, 45.6 ± 1.5 vol.% of CO_2, 13.5 ± 0.6 vol.% of CH_4 and 4.9 ± 0.6 vol.% of C_{2+} are produced (see Figure 6.4 A).

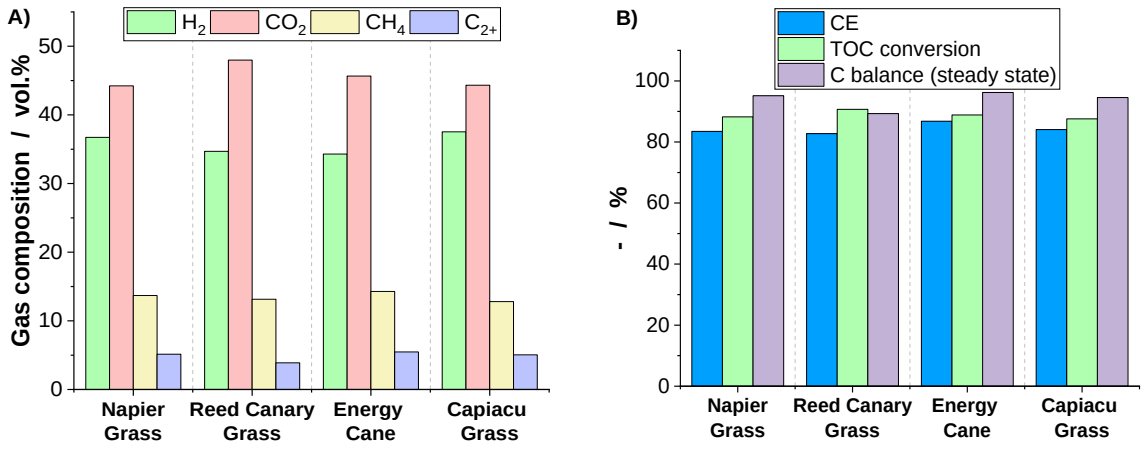


Figure 6.4: Influence of biomass type on A) the product gas composition and on B) CE, TOC conversion and C balance (T = 650 °C, p = 260-280 bar, $DM_{mixture}$ = 6.6 wt.%, $\dot{m}$ = 700 g h^{-1}).

This confirms the knowledge gained from previous results, that similar biomasses produce similar product gases [188]. Thus, the downstream processing of the product gas does not require major adjustments when processing other types of biomasses with similar elemental composition. The flexibility of the feedstock source is an advantage for future commercial application.

The gasification rate was also not affected by the biomass type, as can be seen in Figure 6.4 B (CE = 84.3 ± 1.5% and TOC conversion 88.8 ± 1.2%).

The only difference can be seen in a reduced carbon balance of the experiment with Reed Canary Grass (steady-state carbon balance = 89%). During this experiment a blockage of the flow after the salt separation T-fitting occurred. After the experiment, the solids causing the blockage were removed. Analysis of the solids showed that they consisted almost entirely of SiO_2 (see Table 6.4 and Figure 6.5). Due to the blockage not all of the carbon could be recovered from the system, explaining the reduced carbon balance.

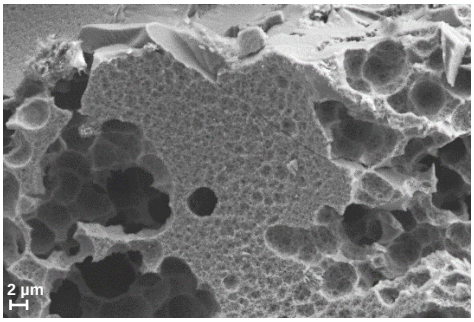


Figure 6.5: SEM picture of solids from experiment with Reed Canary Grass.

Table 6.4: EDS analysis of solids from experiment with Reed Canary Grass.

	wt.%	atom.%
C	3.57	6.05
O	46.60	59.28
Si	45.07	32.66
K	1.83	0.95
Cr	0.91	0.35
Ni	2.02	0.70

Based on the work of Dolejs and Manning, who developed a model to determine the solubility of SiO_2 in supercritical water up to 1100 °C and 20.000 bar [189], the solubility of SiO_2 was estimated for the conditions at the salt separation T-fitting in the present case (see Figure 6.6).

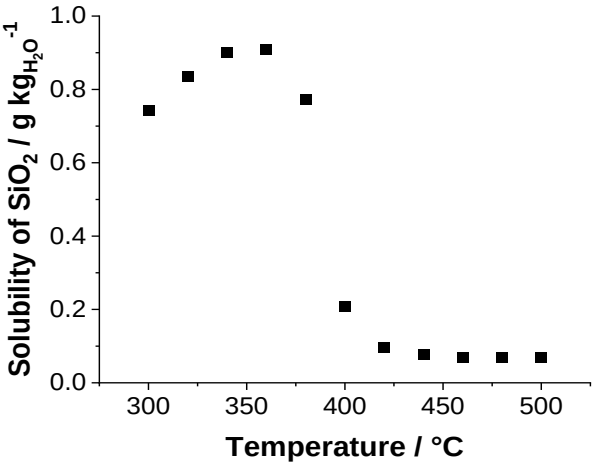


Figure 6.6: Solubility of SiO2 in hot compressed water at different temperatures and p = 280 bar. Data taken from Dolejs and Manning [189].

With increasing temperature, the solubility of SiO_2 initially increases, but around the critical point of water, the solubility of SiO_2 decreases drastically. The SiO_2 that was solubilized with increasing temperature up to the critical point of water, then precipitates again with increasing temperature and can cause plugging. For T = 400 °C and 500 °C at 280 bar, it was calculated to be 0.21 $\frac{\mathrm{g\ SiO_2}}{\mathrm{kg}\ H_2\mathrm{O}}$ and 0.07 $\frac{\mathrm{g\ SiO_2}}{\mathrm{kg}\ H_2\mathrm{O}}$, respectively. This indicates that for all four biomasses most of the Si precipitates in the salt separator, because the Si content in the reaction mixture is higher (see Table 6.5).

Table 6.5: Si content of feed slurry and reaction mixture for different biomasses.

Biomass	Si-Content (wt.%)		
	Dry Feed	Feed Slurry (wet)	Reaction Mixture*
Napier Grass	1.0	0.13	0.066
Reed Canary Grass	2.3	0.29	0.144
Energy Cane	0.7	0.09	0.045
Capiacu Grass	0.9	0.12	0.058

*the wet feed slurry is diluted 1:1 with supercritical water at the mixing point.

As there was no problem with the processing of Energy Cane, Napier Grass or Capiacu Grass there seems to be a crucial silicon content, above which it is not sufficiently removed from the reaction mixture and thus clogs the piping after the salt separator.

As shown in Table 6.5, the Si content of the reaction mixture with Reed Canary Grass is the highest (0.144 wt.%) while all the other feed slurries contain less than 0.1 wt.% of Si. This leads to the conclusion that the salt separation under the current conditions cannot separate precipitating silicon sufficiently, if the content is too high.

It can be concluded that all four biomasses behave similarly with respect to gasification. However, there are differences during salt separation. In the current setup, the silicon content of the biomasses should be monitored to avoid deposition. One way to avoid this is to further dilute the biomass to a silicon content below 0.1 wt.% in the reaction mixture (e.g., in section 6.3.1 where a higher dilution of Reed Canary Grass was present, no deposition was detectable for more than 100 h).

Since the type of biomass (except Reed Canary Grass) does not significantly affect the process, the following experiments were conducted in this study with Napier Grass, Energy Cane and Capiacu Grass.

6.3.2.2 Influence of dry matter content

The dry matter content in the system is a crucial process parameter of SCWG regarding gasification efficiency and also process economics. With increasing dry matter content, the carbon gasification efficiency decreases due to a decreasing water surplus and thus worse splitting of the biomass molecules [89,99,100]. For example, D`Jesus et al. [89] found a reduction of CE from about 82 to 75% when increasing the dry matter content from 2.5 to 10 wt.%. Also, the product gas composition is influenced by the dry matter content in the system. The increasing biomass content influences the water-gas-shift and methanation reactions [99,100]. A decrease in water content favors methanation and reverse water gas shift, thus decreasing the H_2 and CO_2 yield while increasing the CH_4 yield.

Processing high dry matter contents is for one limited by decreasing gasification efficiencies as described above, but also by the pumpability of the feed slurry which depends on the geometry of the SCWG plant and also the biomass [83].

In the present work, the dry matter content in the reaction mixture (after mixing the slurry with supercritical water) was varied from 1.3 to 8.2 wt.%. The dry matter consists of biomass, xanthan and $KHCO_3$ as homogeneous catalyst. To avoid a simultaneous

change of catalyst concentration, the $KHCO_3$ addition was chosen in such a way that the potassium-to-dry matter ratio stayed constant at 560 ppm K^+/wt.% dry matter in the reaction mixture, e.g. at 1.3 wt.% dry matter content 730 ppm K^+ were added to the mixture. The dry matter variation was conducted at T = 650 °C and p = 280 bar.

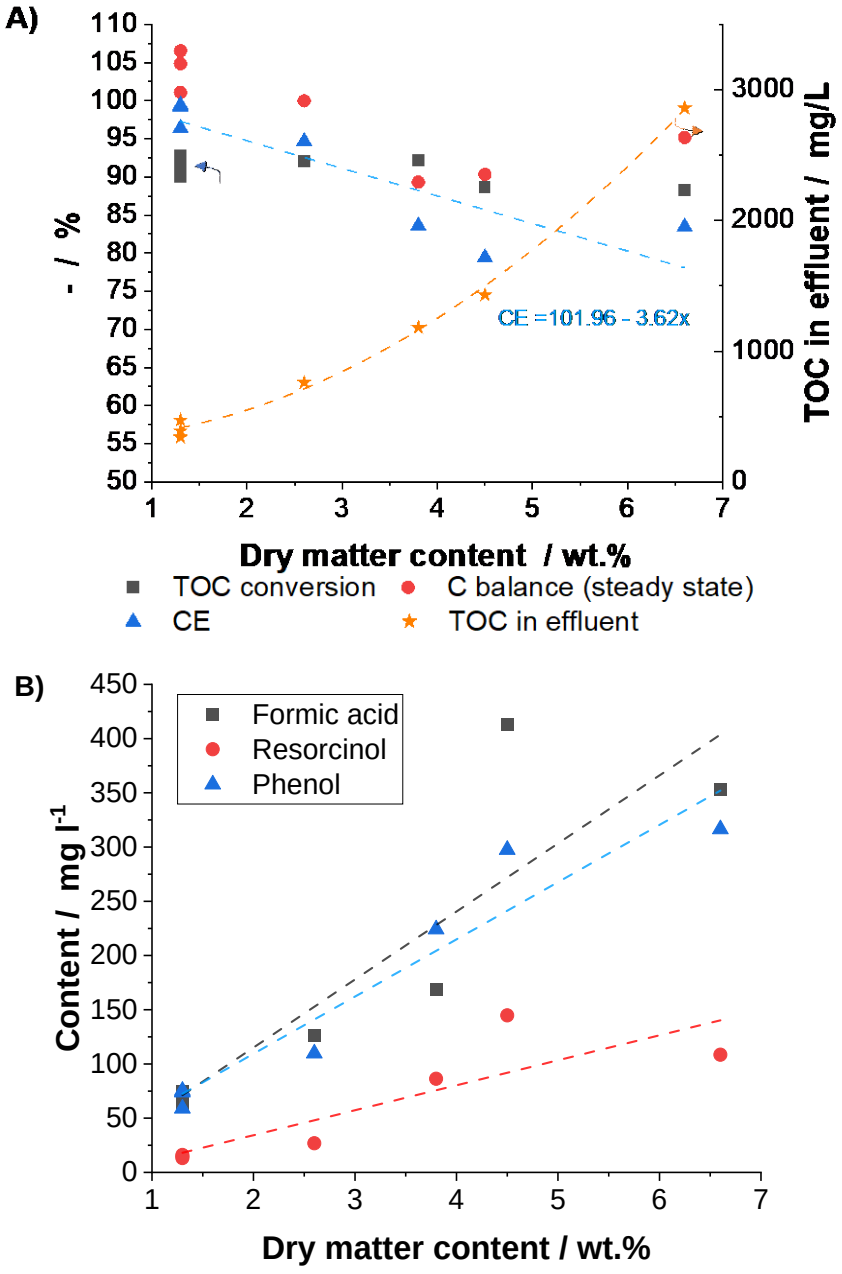


Figure 6.7: Influence of dry matter content in mixture on A) CE, TOC conversion, C balance and TOC content of effluent and B) on the organic species in the effluent (T = 650 °C, p = 280 bar, $\dot{m}$ = 700 g h^{-1}).

As depicted in Figure 6.7 A, the TOC-conversion is almost constant at about 90.7% for all dry matter contents investigated. This means, that 90.7% of the organic carbon in the reaction mixture are converted into other species like gases or inorganic carbon and 9% of the organic carbon of the reaction mixture are still contained in the effluents. This means that with increasing dry matter content in the reaction mixture the TOC content of the effluent also increases (orange line in Figure 6.7 A) from 400 mg l^{-1} at 1.3 wt.% dry matter to 2860 mg l^{-1} at 6.6 wt.% dry matter in the mixture. This is also visible when looking at the main organic species in the reactor effluent, namely phenol, resorcinol and formic acid (see Figure 6.7 B), where also an increase is visible with increasing dry matter content. Formic acid is known as a degradation product of cellulose [83] while phenol and resorcinol are known as decomposition products of lignin [20,117]. Phenols are generally hard to gasify [83], thus a longer residence time or a higher gasification temperature would be beneficial to further decompose these products. As the waste water can be recycled, which has been demonstrated in previous work [113], the TOC in the effluent is not lost to the process.

At dry matter contents of 3.0 wt.% or above, CE, which quantifies how much of the organic carbon was transferred to the gas phase, was approximately 4.8 to 9.2% lower than TOC conversion, which quantifies how much organic carbon was transformed into other species (e.g., gas, solids, TIC) and thus is not present in the effluent in form of TOC. This means that most of the carbon that was transferred from the mixture to other species was transferred to the gas phase. However, a small fraction of TOC was converted into another form. Since no solid deposits were removed from the system (mechanical revision of the lab-plant after the experiments), the missing TOC may have left the system in form of tars or may be present in the reactor sumps as solid particles. The carbon balance is thus also greater than 90% in these cases. Only a slight decrease of CE is occurring with increasing dry matter content. In the interval of 3 to 6.6 wt.% dry matter concentration, even less decrease is detectable. This is not typical for the SCWG process as other authors have described. Nanda et al. found a decrease of CE from 88 to 80% when increasing fructose concentration from 4 to 8 wt.% at T = 700 °C [135]. Guo et al. found a decrease in CE from over 90% to 72% when the feed concentration (sawdust and carboxymethylcellulose) was increased from 4 to 6 wt.% at T = 650 °C [100]. A possible reason for the improved performance of the newly developed system could be the rapid heating of the biomass to supercritical

temperatures. Unfavorable temperature zones that favor the hydrothermal carbonization (typically T = 180 – 350 °C [190]) or the tar formation, which is also favored at lower temperatures than the gasification [119,120], are avoided. Intermediates and by-products such as coke, phenols or other aromatic compounds, which are difficult to gasify and tend to polymerize into solids, are produced in smaller quantities and thus a higher gasification efficiency can be achieved.

This is very promising regarding the economics of the process. Higher dry matter contents thus might also be processable in a similar manner. However, this was not possible in the present work as higher dry matter contents (8.2 wt.% in the reaction mixture was equivalent to 16.4 wt.% dry matter in the feed slurry) caused plugging in the feed tubing (1/4” piping, with 1.5 mm inner diameter). In a commercial plant with larger diameters, this may not be an issue.

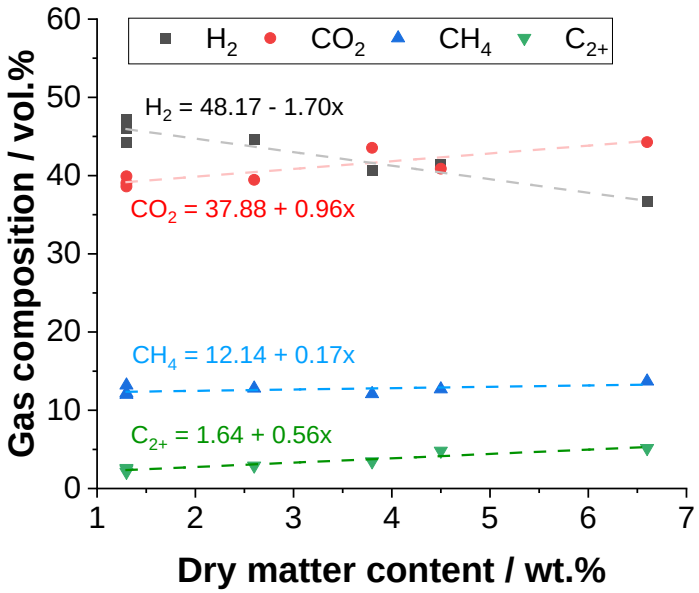


Figure 6.8: Influence of dry matter content on the gas composition (T = 650 °C, p = 280 bar, $\dot{m}$ = 700 g h^{-1}).

The product gas composition is notably influenced by the variation of dry matter content. As the dry matter content increases, the H_2 and CO_2 contents are expected to decrease, while the CH_4 content is expected to increase [99,100]. A decrease in H_2 content can be observed (see Figure 6.8), however the CH_4 content did not increase significantly, but the C_{2+} content (mainly C_2H_6) increased. On the other hand, the CO_2

content increased. This unexpected trend in CO_2 can be explained by the increased formation of C_2H_6. Further progressing of the steam reforming of C_2H_6 (Eq. 6.1) would lead to a relative decrease of CO_2 in the product gas due to the increased amount of H_2, thus achieving the trends expected from the literature.

$$C_2H_6 + 4\,H_2O \rightarrow 2\,CO_2 + 7\,H_2 \qquad (6.1)$$

6.3.2.3 Influence of temperature

It is well known in the literature that increasing the temperature is beneficial for the supercritical water gasification of biomass [66,86], as the decomposition of the organics is enhanced. This leads to an increase of the amount of gas produced and reduces the TOC content of the effluent [191]. Thus, with increasing temperature the gasification efficiency and the TOC conversion are expected to rise. In the present work the temperature was varied between 550 and 700 °C. The maximum temperature of 700 °C was chosen as the limit of the mechanical strength of the reactor material is reached and thus a further increase is not possible, even though it could possibly be beneficial for the gasification.

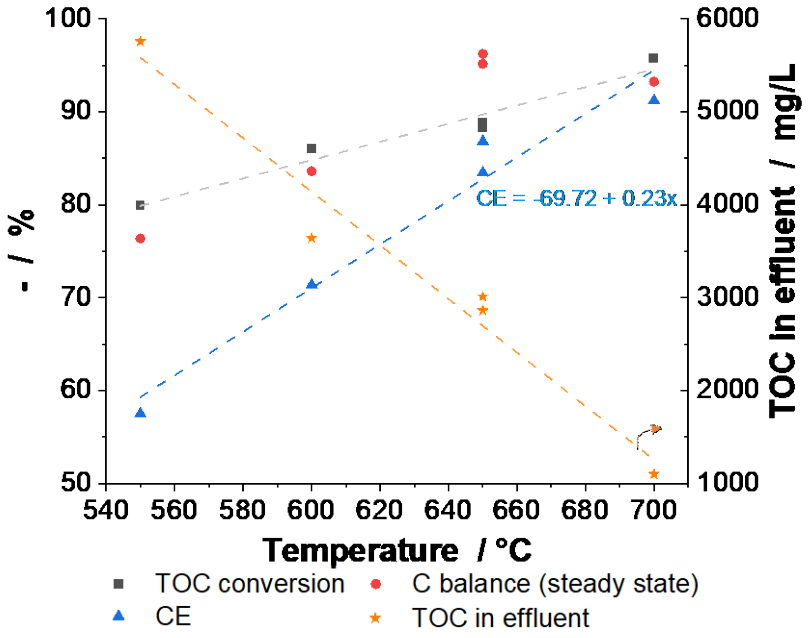


Figure 6.9: Influence of temperature on CE, TOC conversion, C balance and TOC content of effluent (p = 280 bar, $DM_{mixture}$ = 6.6 wt.%, $\dot{m}$ = 700 g h^{-1}).

In Figure 6.9, CE and the TOC conversion are displayed alongside with the TOC content of the effluent. The trends known from literature can be confirmed in the newly developed lab-plant. It is clear that the TOC conversion increases with increasing temperature (80 to 96%). CE also increases significantly from 58 to 91%. The improved gasification with increasing temperature is also evident in the TOC content, which decreases from 5750 to 1100 mg L^{-1} with an increase in temperature from 550 °C to 700 °C.

For T ≥ 650 °C, CE is only slightly smaller than the TOC conversion. This means, that most organic carbon that is transferred from the feed to other species is gasified and thus contained in the product gas. The remaining organic carbon is mostly contained in the effluent, leading to an almost closed steady state carbon balance (C-balance$_{steady\text{-}state}$ ≥ 93%). For T ≤ 550 °C, CE is much lower than the TOC conversion. Thus, not all of the carbon that is transferred from the feed to other species is found in the gas phase. During these experiments, extensive tar formation could be seen in the effluent. The formation of solid residues in the laboratory plant cannot be excluded. Since tars and solids are not quantified in the laboratory plant, the carbon balance for these experiments is reduced (C-balance$_{steady\text{-}state}$ ≤ 84%). It can be concluded that a reaction temperature of T ≥ 650 °C is required to operate the process stably without solid formation.

In literature it is described that an increasing temperature increases the CO_2 yield due to the enhancement of the water gas shift reaction [88]. This is not visible under the investigated conditions (see Figure 6.10 A), as the CO concentration is very low (< 1%) under all conditions due to the catalyst employed which catalyzes the WGS reaction [137,192]. The H_2 content of the product gas decreases while the CH_4 and C_{2+} contents increase with increasing temperature. This is emphasized in Figure 6.10 B. The H_2/CH_4 ratio is decreasing with increasing temperature, while the opposite would be expected based on literature due to the endothermic nature of steam reforming reactions (Eq. 6.2 and 6.3) [87]. This is most likely due to the kinetic limitations of the steam reforming reactions. Usually steam reforming reactions are promoted by nickel catalysts [193,194]. For example, Sepini et al. were able to approach the thermodynamic equilibrium when using a nickel catalyst when processing PET as a model compound for plastic wastes in a batch reactor [195].

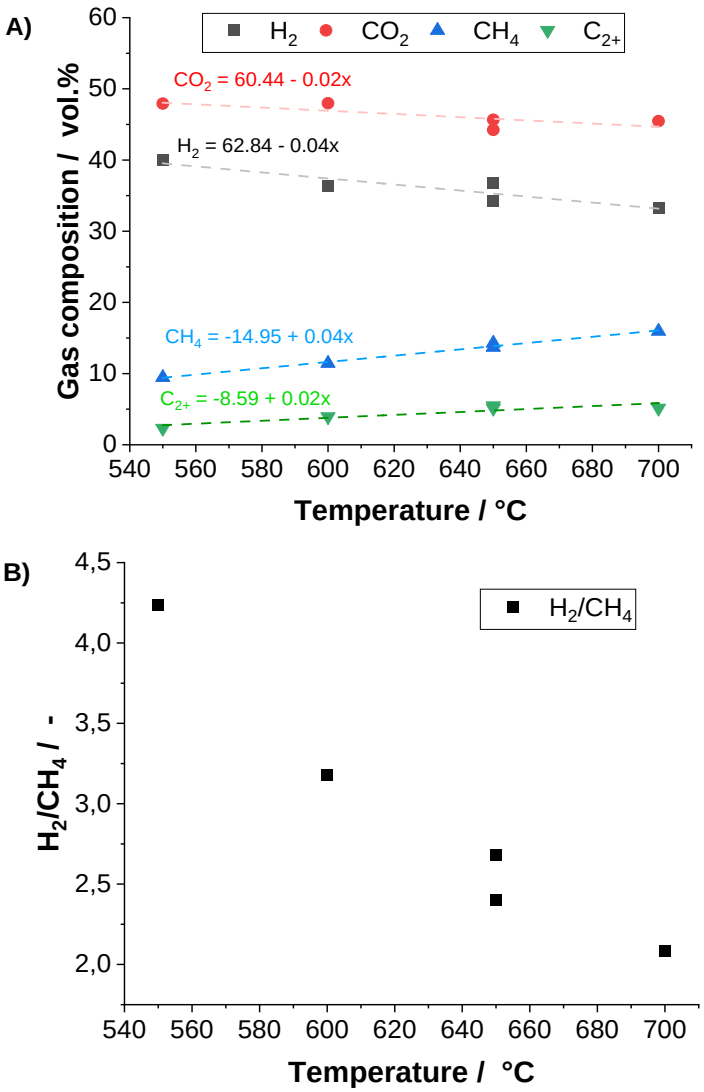


Figure 6.10: Influence of temperature on A) product gas composition and B) on the H_2/CH_4 ratio (p = 280 bar, $DM_{mixture}$ = 6.6 wt.%, $\dot{m}$ = 700 g h^{-1}).

In the present case, the residence time in the reactor without a steam reforming catalyst does not appear to be sufficient to remove the increased number of hydrocarbons in the product gas. A prolonged residence time or the use of heterogeneous catalysts would presumably lead to a decrease of hydrocarbons in the product gas and to an increase of H_2 and CO_2. These measures could be applied depending on the desired product gas composition.

$$CH_4 + 2H_2O \rightarrow 4H_2 + CO_2 \quad (6.2)$$

$$C_xH_y + 2xH_2O \rightarrow (2x + \frac{y}{2})H_2 + xCO_2 \quad (6.3)$$

6.3.2.4 Influence of pressure

Various studies have been conducted in the past on the influence of pressure on the SCWG process in the range of 250 to 450 bar [89–91]. According to the literature, the gasification efficiency is not significantly affected by the system pressure [92,93]. In the present work, the pressure was varied between 240 and 300 bar. Lower pressures than 240 bar were not realized as the supercritical state of water (p > 221 bar) should always be present in the investigations. Higher pressures than 300 bar were not possible to investigate due to the limitations of the lab-plant.

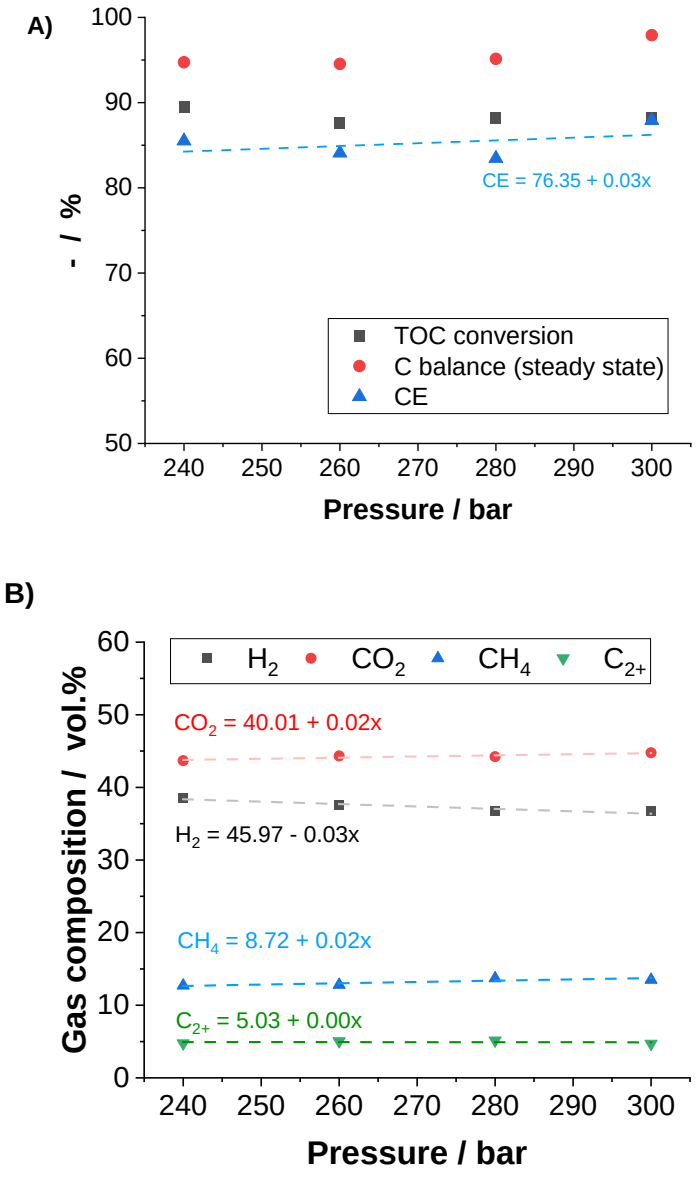


Figure 6.11: Influence of pressure on A) CE, TOC conversion and C balance and B) on gas composition (T = 650 °C, $DM_{mixture}$ = 6.6 wt.%, $\dot{m}$ = 700 g h^{-1}).

As displayed in Figure 6.11 A, CE varies minorly from 85.5% at p = 240 bar to 87.9% at p = 300 bar. This variation lies within the error of measurement. Thus, pressure only has a negligible effect on the TOC conversion and the CE. The steady state carbon balance was greater than 94% in all cases and is thus considered closed. The findings in literature can be confirmed by the present investigation. In order to reduce costs for pumps in a commercial application the lowest possible pressure should be chosen, i.e. p = 240 bar.

An increase in pressure suppresses methane conversion [94,95]. This would result in a decreased hydrogen yield while the methane yield should increase. Gadhe and Gupta observed this when gasifying methanol in supercritical water [79]. However, other authors didn't see a significant influence of pressure on the gas composition [93,96]. In the present work, only a minor influence of the pressure on the gas composition could be observed. The gas composition barely changed with changes in pressure (see Figure 6.11 B). Possibly, as the residence time is low (τ = 31 s), methanation can't occur to a greater extent as is a kinetically limited reaction. Therefore, in order to save energy and also the cost of pressurizing the system, it is recommended to choose the lowest possible pressure (in this case p = 240 bar).

6.3.2.5 Influence of residence time

The residence time at reaction temperature τ is an important process parameter of the process of SCWG. In general, increasing the residence time is beneficial in terms of carbon gasification efficiency (CE), however at a certain residence time a maximum value of CE seems to be reached depending on the gasification conditions and biomasses processed. Guo et al. [97] found an increase of CE from 8% at 5.2 s to 42% at 9.0 s when they gasified 10 wt.% glycerol at 487 °C. At the same time the hydrogen yield increased significantly. However, the slope of the CE increase decreased with increasing residence time, indicating that a limit might be reached. At an elevated temperature of 567 °C they only observed a small increase from 84 to 94% at 4.2 and 7.3 s, respectively. Lu et al. [66] also observed an increase in CE when they increased the residence time during gasification of wood saw dust. The TOC content of the effluent decreased correspondingly. Susanti et al. [67] gasified 15.25 wt.% isooctane at 632 °C. CE increased from 26.6 to 52.5% at residence times of 6.0 and 18.4 s, respectively.

However, further increases in residence time up to 33.3 s had no significant beneficial effect. With increasing residence time, they found a decrease of C_{2+} compounds while the H_2 content of the product gas was at maximum at the longest tested residence time. D´Jesus et al. [92] found a linear increase of CE between 0.6 and 1.6 min, when gasifying 5 wt.% corn silage at 700 °C. A further prolonged residence time did not increase CE. This effect is also visible at other temperatures investigated. Chakinala et al. [98] observed similar when gasifying microalgae at 580 °C. CE increased with increasing residence times up to 5 min. Thereafter, a plateau was reached. They assumed that either part of the biomass is not resistant to the chosen SCWG conditions or coke/tar formation is occurring, limiting the increase of CE. With increasing residence time, the C_{2+} and CO content of the product gas decrease while H_2 and CH_4 contents increase due to enhanced hydrocarbon reforming and water-gas-shift reaction.

In the present work the residence time was varied from 0 to 45 s at 650 °C by varying the flow rate and the inner diameter of the gasification reactor. To reduce the residence time to 6 and 8 s, a liner, made of SS316 with an inner diameter of 4.0 mm, was installed in the gasification reactor. A residence time of 0 s at reaction temperature was achieved by by-passing the gasification reactor and thus leaving the system directly after the salt separator, where a temperature of 450 °C is set. During this experiment, the residence time in the salt separator was 24 s. Thus, the total residence time in the system is not zero, however the residence time at T = 650 °C is.

As the residence time increased, CE increased. A strong increase was observed up to a residence time of 8 s. Further increase of the residence time resulted in only a small increase of the CE, almost as if reaching a plateau. This is also evident when describing the results with a non-linear fit (see Figure 6.12 A). The results are best described by an exponential decay, which approaches a CE of 80.47% with increasing residence time. This behavior is known from literature, as described above. This might be due to organic species (decomposition products of the biomass macromolecules) which are hard to gasify under the chosen conditions, e.g. phenols [83] or tars that formed [115], and that would require higher temperatures to be decomposed (see section 6.3.2.3). However, the residence time to reach this plateau is very low compared to the results reported in literature, e.g. in the work of D`Jesus et al. [92] a residence time greater

than 2 min was required to reach this plateau when gasifying 5 wt.% corn silage at 650 °C. In general, CE is high compared to the work of other authors at such low residence times at similar temperatures, emphasizing the superior performance of the novel system. For comparison, D´Jesus et al. [92] achieved CE of about 60% when gasifying 5 wt.% corn silage at 650 °C at about 45 s. Susanti et al. [67] achieved CE of 52.5% when gasifying 15.25 wt.% isooctane at 632 °C at 33.3 s.

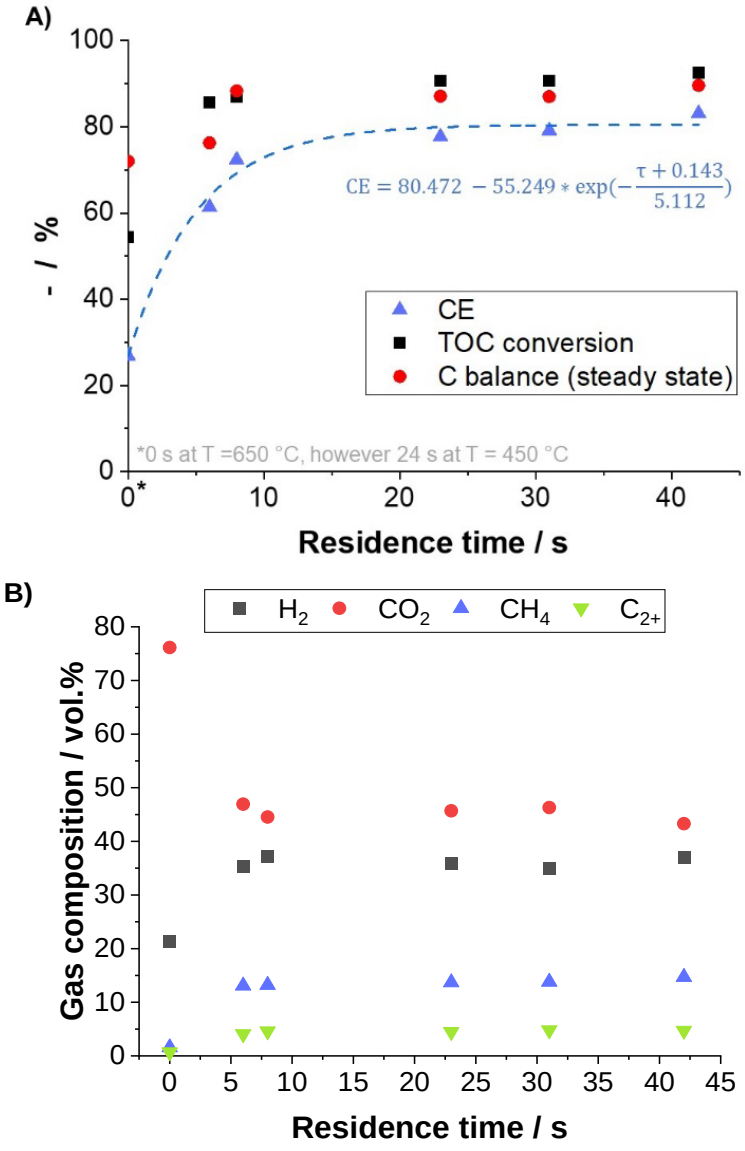


Figure 6.12: Influence of residence time at reaction temperature on A) CE, TOC conversion and C balance (steady state) and B) on gas composition (T = 650 °C, p = 280 bar, DM = 6.6 wt.%).

As the required residence time in the gasification reactor is so low, it is interesting to investigate the influence of the salt separator. Thus, the reaction mixture was retracted from the system by by-passing the reactor (experiment with τ = 0 s). In this experiment, CE was only 26.9%. As the temperature in the salt separator is only 450 °C, a low gasification efficiency is expected. Guo et al. [97] achieved a CE of only 4.3% during gasification of glycerol at T = 445 °C. When gasifying 5 wt.% corn silage, D`Jesus et al. [92] achieved a CE of about 15% and about 35% at T = 400 and T = 500 °C, respectively, indicating similar results as in the present work. During this experiment, the TOC content of the effluent (TOC = 10930 mg l^{-1}) was much higher than for the experiments where the gasification reactor was installed (TOC = 2822 ± 653 mg l^{-1} (standard deviation)). Additionally, an oily substance accumulated in the filter upstream of the back-pressure regulator (see Figure 6.13), which by far exceeds the amount of tar formation when the gasification reactor is installed. As this oily substance is not balanced in the C-balance shown in Figure 6.12, this explains the poor carbon balance for τ = 0 s.



Figure 6.13: Oily substance obtained from the filter before the back-pressure regulator during after the experiment at τ = 0 s.

The oily substance obtained from the experiment at τ = 0 s was analyzed via SEC. The UV signal is plotted versus the retention volume in Figure 6.14. The column was calibrated from 84 to 9740 g mol^{-1}. Most of the recorded volumes are between 84 and 6430 g mol^{-1} (dashed line in Figure 6.14). The maximum peak is at 178 g mol^{-1} (dotted line in Figure 6.14).

The average molar mass, based on mass, $\overline{M_w}$ is 261 g mol^{-1}. The average molar mass, based on numbers, is $\overline{M_n}$ is 165 g mol^{-1}. The macromolecules (cellulose, lignin, hemicellulose) in the fresh biomass are much larger than the molecules in the oily

substance. This indicates that decomposition of the macromolecules has occurred to great extent and only few large molecules are present after the salt separator. As T = 450 °C is close to the typical temperature range of hydrothermal liquefaction (T = 250 – 400 °C) [196], a comparison to HTL oil is useful. During catalytic HTL of lignin, Feng et al. obtained a bio-oil with a $\overline{M_w}$ of 455 to 765 g mol^{-1}, depending on the catalyst used [197]. Haarlemmer and Roubaud [198] obtained a bio-oil with a peak of 431 g mol^{-1} during HTL of biogenic wastes at 300 °C under continuous operation. The low peak in the current work might be due to the elevated temperatures (T = 450 °C) present in the salt separator, which promotes further decomposition of the molecules. The similarity of the oily substance to the HTL oils indicates that in the present configuration the salt separator acts as efficient hydrothermal pretreatment, which could explain the short residence time required in the gasification reactor.

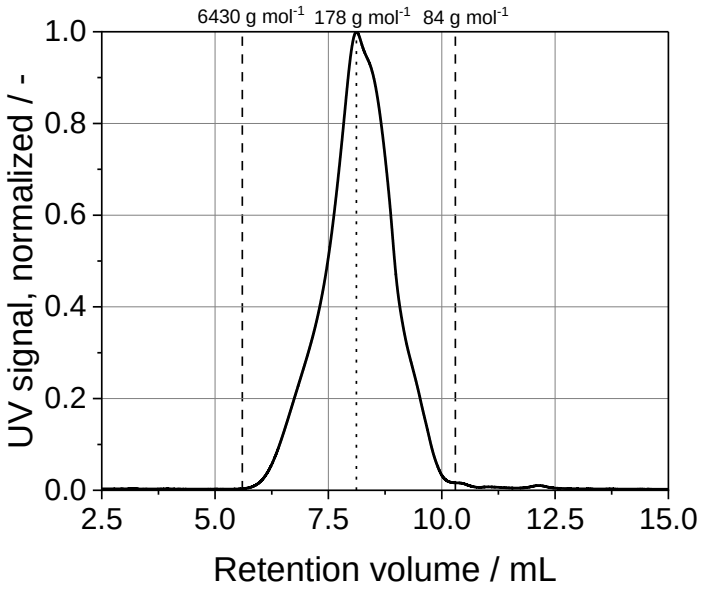


Figure 6.14: SEC analysis the oily substance produced in the experiment with at τ = 0 s.

The gas composition did not change after reaching the previously described plateau at τ > 6 s (see Figure 6.12). This behavior was also reported by D´Jesus et al. [92]. Chakinala et al. [98] and Susanti et al. [67] observed a decrease of C_{2+} compounds, however they observed a much higher C_{2+} content at low residence times than in the present work. Therefore, this effect may not be visible. At τ = 0 s, the product gas

contained much more CO_2 (76.2 vol.%), while almost no CH_4 or C_{2+} were present (1.6 and 0.7 vol.%, respectively). D´Jesus et al. [92] observed similar results when gasifying 5 wt.% corn silage at temperatures of 400 and 500 °C. This suggests a different mechanism of decomposition, as the temperature was only 450 °C, compared to the usual 650 °C in the gasification reactor. Such a high CO_2 content in the product gas is also known from hydrothermal liquefaction [30,199], where decarboxylation reactions are leading to a CO_2 rich gas [172,200]. This again supports the hypothesis that the salt separator acts as a hydrothermal pretreatment step.

6.3.2.6 Influence of potassium as homogeneous catalyst

The use of homogeneous catalysts in the process of SCWG has been studied by many authors [89,166,201]. For homogeneous catalysis alkali metals are typically used as hydroxides and carbonates. Sinag et al. found a significant increase in H_2 yield when using K_2CO_3 compared to operation without catalyst, due to the catalyzed water-gas-shift reaction [137]. On the other hand, these homogeneous catalysts can contribute to solid formation in the system as their solubility is limited in supercritical water [68,202]. The catalysts are costly and can only be partially recovered from the system, which can negatively affect the economics of the process. Therefore, their use should be carefully considered.

In the present work, the addition of potassium in form of $KHCO_3$ was investigated. The potassium addition to the feed slurry was varied from 0 to 7500 mg K^+/kg slurry. As the feed slurry, was diluted by supercritical water in a ratio of 1:1, the potassium addition to the reaction mixture ranged from 0 to 3750 mg K^+/kg reaction mixture.

As displayed in Figure 6.15 A, CE increases slightly with increasing potassium addition from 75.3 to 79.1%, at 0 and 3750 ppm respectively. This marginal increase indicates no significant effect of potassium addition on the gasification process.

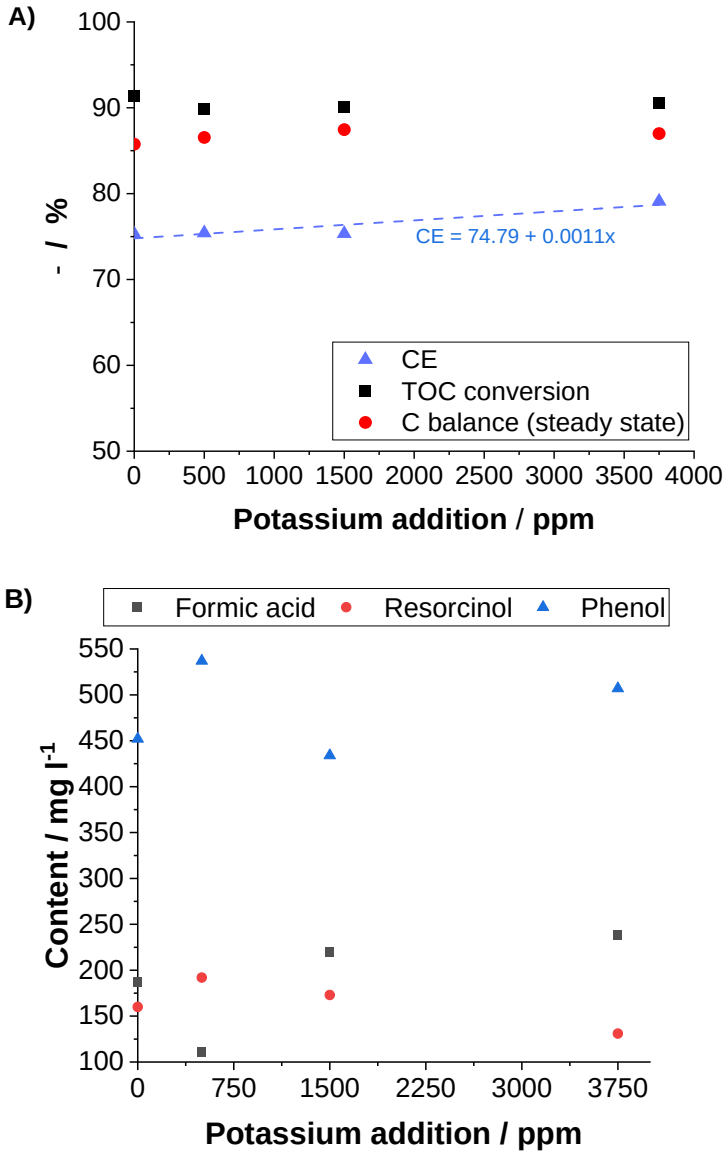


Figure 6.15: Influence of potassium addition to the reaction mixture on A) CE, TOC conversion and C balance (steady state) and B) on organic species in the effluent (T = 650 °C, p = 280 bar, $\dot{m}$ = 700 g h^{-1}).

The TOC conversion averages 90.5% with small variations, showing that in all cases about 90% of the organic carbon is converted and about 10% of the organic carbon remains in the effluent. This is also confirmed by the measurement of the main organic species in the effluent (phenol, resorcinol, formic acid), which appear in the same order of magnitude for all experiments (see Figure 6.15 B). The TOC conversion is about 15% higher than CE, indicating that not all organic carbon is transferred into gaseous form. About 15% of the organic carbon are neither contained in the gas nor in the effluent. A possible explanation is the formation of side products such as tars which

are not quantified. Also, some carbon is contained in the sumps of the lab-plants which is not balanced in steady state operation. As no solid carbon deposits were removed from the reactors, this indicates little to no coke formation in all cases. The steady state carbon balance lies between 85.8 and 87.5% for all experiments. However, as stated above the reactor sumps and the carbon contained in the rinse water (the lab-plant is flushed with water after the experiments) is not balanced in steady state evaluation. When also considering these samples the carbon balance improves. The gasification results are very similar for all potassium concentrations and thus no major influence can be attributed to the addition.

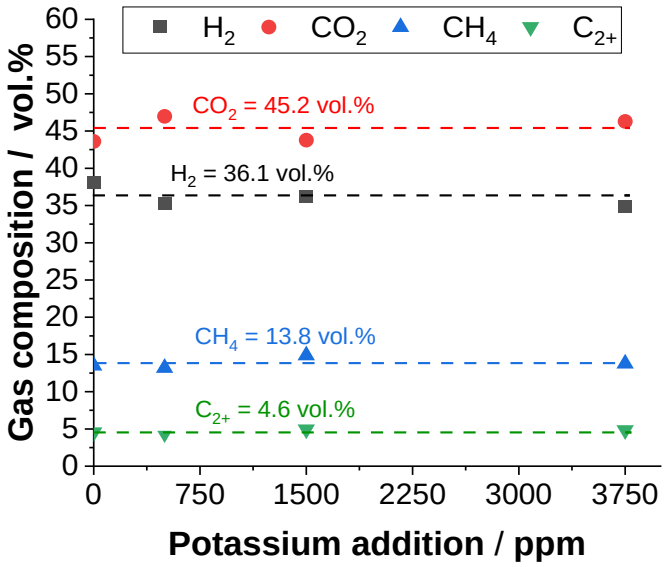


Figure 6.16: Influence of potassium addition to the reaction mixture on gas composition (T = 650 °C, p = 280 bar, $\dot{m}$ = 700 g h^{-1}).

This is also clear when analyzing the gas compositions produced during these experiments. Only little variation in the gas composition can be seen (see Figure 6.16). On average the gas composition is 36.1 vol.% H_2, 45.2 vol.% CO_2, 13.8 vol.% CH_4 and 4.6 vol.% C_{2+}. In all cases, less than 0.3 vol.% CO were present, indicating a catalyzed water-gas-shift reaction. This could be attributed to the added potassium [137], however the reactor material (nickel-base alloy Inconel 625) after corroding can also catalyze this reaction as shown by Boukis et al. [91]. As a reactor that shows corrosion is used in the present experiments this could also explain the negligible effect of

potassium addition on the gas composition (corrosion is visible on the inner surface when the reactor is replaced or checked for deposits; the corrosion rate is not measured).

One possible explanation for the small influence of the potassium addition on the gasification process could be the high level of potassium originating from the biomass itself (see Table 6.6). D'Jesus et al. found that 500 ppm K^+ were sufficient to increase the gasification significantly when processing corn starch [165]. A further increase in K^+ addition had no significant beneficial effect. In all cases, 2400 ppm K^+ or more are present in the reaction mixture in the conducted experiments, this could explain the neglectable effect of the addition of extra K^+. D'Jesus found similar when adding 100 ppm K^+ to fresh biomass which itself contained about 1 wt.% K^+ (based on dry matter) [89].

Table 6.6: Potassium concentration in the reaction mixture.

Addition to reaction mixture	**Biomass used**	**K^+ content of dry feed**	**K^+ content in reaction mixture**	
ppm		wt.%	wt.%	ppm
0	Napier Grass	3.85	0.24	2400
500	Napier Grass	4.77	0.30	3000
1500	Napier Grass	6.26	0.40	4000
3750	Napier Grass	9.22	0.61	6100

6.4 Empirical model derived from the experimental data

As described in the previous sections, pressure, potassium addition and biomass type did not influence the product gas or gasification efficiency in a significant way. Therefore, the most influential process parameters were identified to be temperature, dry matter content and residence time. With increasing temperature, the gasification efficiency CE strongly increases while with increasing dry matter content CE decreases. When the residence time at reaction temperature is increased CE also increases.

As shown in Figure 6.7 to Figure 6.8 and Figure 6.9 to Figure 6.10, for temperature and dry matter content the gasification efficiency and the gas composition follow almost linear trends with changes in temperature (T) and dry matter content (DM). As shown

in Figure 6.12, CE displays a different type of dependencies. Below 8 s, CE strongly increases with increasing residence time (τ) while a further increase than 8 s leads to a flattening of the increase. The further increase can also be approximated by a linear function with great accordance. The region below 8 s shows low gasification rates and is therefore not practically relevant. To keep the model simple and avoid the use of exponential terms, this region is excluded. Thus, as all dependencies display almost linear behavior, a multi-linear regression, using Microsoft Excel, was applied to determine the combined effect of these parameters. Therefore, the parameters a, b, c and d in Eq. 6.4 were fitted to best represent the experimental data. y represents the parameter that is described, e.g. CE or H_2 content in the product gas.

$$y = a * T + b * DM + c * \tau + d \quad (6.4)$$

As a residence time of 8 s or above is required to reach a sufficiently high gasification efficiency, only the residence time interval of 8 to 42 s is considered for the model creation. 15 data points, originating from the variation of T, DM and τ during the experimental work, were used. By a multi-linear parameter fit, the following correlations were found for the gasification efficiency CE, gas production GP and the gaseous components H_2, CH_4, CO_2 and C_{2+} (Eq. 6.5 to 6.10).

$$CE = 0.240 * T - 3.083 * DM + 0.329 * \tau - 65.632 \ [\%] \quad (6.5)$$

$$GP = 0.109 * T + 7.101 * DM + 0.167 * \tau - 69.773 \ [Nl\,h^{-1} kg_{throughput}^{-1}] \quad (6.6)$$

$$H_2 = -0.041 * T - 1.957 * DM - 0.023 * \tau + 75.892 \ [vol.\%] \quad (6.7)$$

$$CH_4 = 0.047 * T + 0.299 * DM + 0.036 * \tau - 19.569 \ [vol.\%] \quad (6.8)$$

$$C_{2+} = 0.021 * T + 0.445 * DM + 0.008 * \tau - 12.053 \ [vol.\%] \quad (6.9)$$

$$CO_2 = -0.026 * T + 1.192 * DM - 0.001 * \tau + 55.012 \ [vol.\%] \quad (6.10)$$

CO is not included as the amount in the product gas is smaller than 1 vol.% in all cases. A measure of certainty $R^2 \geq 0.876$ was reached for all correlations. The gas production GP is related to the throughput, as the throughput changes during the variation of residence time. A changed throughput automatically affects the amount of gas produced. However, if gas production is normalized to the throughput, this unwanted influence is eliminated.

Statistical analysis of the empirical model reveals p-values lower than 0.05 for the parameters T and DM in all cases, indicating the significance of the parameters (see Supporting Information A1.2). The influence of the residence time is in case of the H_2, C_{2+} and CO_2 content not significant as the p-value lies between 0.63 and 0.81. For the influence of the residence time on CE and GP, the p-value however is below 0.05 and thus in these cases the residence time is a significant parameter. As the residence time is significant in some cases it was kept in the model for all the parameters. The regression equations describe the experimental results adequately, as also shown by the parity plots in Supporting Information A1.2. The results all lie within a ± 10% deviation interval (or better), except for the C_{2+} content in the product gas. Here however, the absolute values are low and thus small absolute deviations cause a larger relative error which still remains within a ± 20% deviation interval. Thus, an empirical model (multi-linear fit) with sufficient accuracy was obtained.

During the experiments only one parameter was varied at a time, e.g. the temperature was varied from 550 to 700 °C while the other parameters were unchanged. To verify the general applicability of the empirical model, two new parameter sets were randomly chosen and investigated where several parameters were varied simultaneously compared to the default values (T = 650 °C, DM = 6.6 wt.%, τ = 31 s): Experiment 1) T = 600 °C, DM = 5.1 wt.%, τ = 34 s; Experiment 2) T = 625 °C, DM = 4.2 wt.%, τ = 27 s. The values predicted by the empirical model and the experimental value are displayed in Table 6.7. As shown by the comparison in Table 6.7, the results from the multi-linear regression can be applied also to new parameter combinations with minor errors. The relative deviation is smaller than 10% for all values but C_{2+} and in one instance CH_4. In case of CH_4, the relative error is only slightly above the set 10% threshold and the absolute deviation is only 1.4 vol.% and thus still reasonable accurate. In case of C_{2+} however, the model displays a larger uncertainty to begin with, as the values are very small and close to each other (see Supporting Information A1.2). Thus, the empirical model describes the present SCWG process very well. For the presently investigated biomasses therefore no new experiments need to be conducted to determine the experimental outcome for parameter sets (temperature, dry matter content, potassium addition, residence time, pressure), as long as the SCWG plant is operated at a

residence time above 8 s. At lower values, the residence time will have a significantly different influence, as shown in section 6.3.2.5.

Table 6.7: Comparison of prediction by empirical model and experimental results for a new experiment.

		Experiment 1 T = 600 °C, DM = 5.1 wt.%, τ = 34 s			Experiment 2 T = 625 °C, DM = 4.2 wt.%, τ = 28 s		
		Empirical model	Experimental results	Relative deviation in %	Empirical model	Experimental results	Relative deviation in %
CE	%	74.10	71.98	2.95	80.91	85.33	-5.18
GP	$\mathrm{Nl\,h^{-1}kg_{flow}^{-1}}$	37.37	38.60	-3.19	32.90	36.32	-9.42
H_2	vol.%	40.67	37.67	7.96	41.51	39.09	6.19
CH_4	vol.%	11.14	11.67	-4.54	11.86	13.27	-10.63
C_{2+}	vol.%	3.10	3.59	-13.65	3.19	3.82	-16.49
CO_2	vol.%	44.84	46.83	-4.25	43.17	43.56	-0.90

6.5 Comparison of experimental data and equilibrium calculation

As described in section 6.2.3, equilibrium calculations conducted using ASPEN HYSYS offer a powerful and versatile tool for evaluating and optimizing process performance. It becomes possible to simulate the impact of key variables such as pressure, temperature, and biomass concentration on the overall process. These simulations provide insights into the dynamic behavior of the process under varying conditions, enabling a comprehensive understanding of its operational parameters. In the subsequent analysis, the gas composition and production observed during experiments are systematically compared with the predictions derived from thermodynamic equilibrium calculations. This comparison serves as a foundation for a detailed discussion on the alignment and discrepancies between experimental results and theoretical expectations, shedding light on the underlying mechanisms and potential areas for process improvement.

6.5.1 Pressure

In Figure 6.17, the influence of pressure on the gas composition is displayed. According to the thermodynamic equilibrium, there is a minor promotion of the methanation reaction (Eq. 6.11) with increasing pressure in the investigated pressure range of 240 to 300 bar according to LeChatelier's principle, i.e., the volumetric percentage of H_2 changes from 58.6 to 56.5 vol.%, when the pressure increases from 240 to 300 bar. Likewise, the percentage of CH_4 increases from 5.8 to 7.4 vol.%.

$$4H_2 + CO_2 \rightarrow CH_4 + 2H_2O \qquad (6.11)$$

The experimental results also show a small dependency of the gas composition on pressure. The main difference between experiments and equilibrium is that the CH_4 content is higher than it should be in the case of equilibrium and the H_2 content is lower, e. g., under 280 bar, the equilibrium content of CH_4 and H_2 is 6.8 and 57.2 vol.%, whereas the actual percentages were 13.7 and 36.7 vol.%, respectively. Additionally, the equilibrium calculations don't display any higher hydrocarbons, that make up about 5 vol.% during experiments (not displayed in Figure 6.17). These observations indicate that steam reforming (SR) doesn't proceed to a large enough extent to reach equilibrium concentration (Eq. 6.12). To confirm if limited SR is the cause of this deviation, the hydrocarbon content in the experimental gas was adjusted mathematically according to Eq. 6.12 to match the equilibrium CH_4 (5.5 – 7.6 vol.%) and C_{2+} contents (no C_{2+}).

$$C_xH_y + 2x\ H_2O \rightarrow x\ CO_2 + (\frac{y}{2} + 2x)H_2 \qquad (6.12)$$

The calculated gas composition, is also displayed in Figure 6.17 ("Adjustment"). With this adjustment, the H_2 and CO_2 content are almost in equilibrium concentration with a maximum deviation of 2.2 and 3.0 vol.%, respectively. Thus, the main cause of this deviation of experiment and equilibrium is the unpromoted SR reactions. It can be concluded that the kinetically limited steam reforming reactions hinder reaching equilibrium composition and thus maximum H_2 yield. The implementation of a catalyst suitable to promote the steam reforming would most likely enable reaching the equilibrium [194].

Besides the gas composition, experiment and equilibrium are also compared in terms of gas production. The gas production is displayed relative to the carbon content in the feed (Nl $g_{c\ in\ Feed}^{-1}$). When comparing the gas production in Figure 6.17 d, a significant

deviation between equilibrium and experiment is visible. When adjusting the experimental gas production according to steam reforming reaction, the deviation becomes much smaller, but still remains on average at 0.78 Nl $g_{c\ in\ Feed}^{-1}$. As a last correction factor, the carbon gasification efficiency can be implemented (Eq. 6.13).

$$GP_{SR\ and\ CE} = \frac{GP_{SR}}{CE} \tag{6.13}$$

GP_{SR}: Gas production, corrected by SR (Nl $g_{c\ in\ Feed}^{-1}$)

$GP_{SR\ and\ CE}$: Gas production, corrected by SR and CE (Nl $g_{c\ in\ Feed}^{-1}$)

This correction accounts for incomplete gasification during the experiment. Under thermodynamic equilibrium, all carbon in the feed is gasified and thus a larger quantity of gas is produced. To compensate this, the gas production from the experiments is linearly extrapolated to complete gasification. With this correction, the gas production is close to the predicted amount of gas with a mean relative error of 4%.

Possible origins of the small deviations between the equilibrium data and the adjusted experimental data that remain are that the product gas was only adjusted according to SR reactions but not according to water-gas-shift ($c_{CO,experimental}$ = 0.1 – 0.3 vol.%, $c_{CO,equilibirum}$ = 0.0 – 2.0 vol.% depending on the conditions). Also, incomplete gasification occurs, indicating that some carbon remains in the effluent. The correction of the gas production by assuming complete gasification (CE equals 100%) is only an approximation, since the remaining carbon is not present in the form of glucose, but in different species, which also contain different contents of O and H (as shown in section 6.3.2.2). Lastly, glucose is chosen as a model compound and represents the C, H and O content of the biomass well but does not consider contaminants or a small amount of inorganic carbon in the feed, e.g., originating from carbonates. Thus, in a more complex approach, a real biomass should be chosen for the equilibrium calculations.

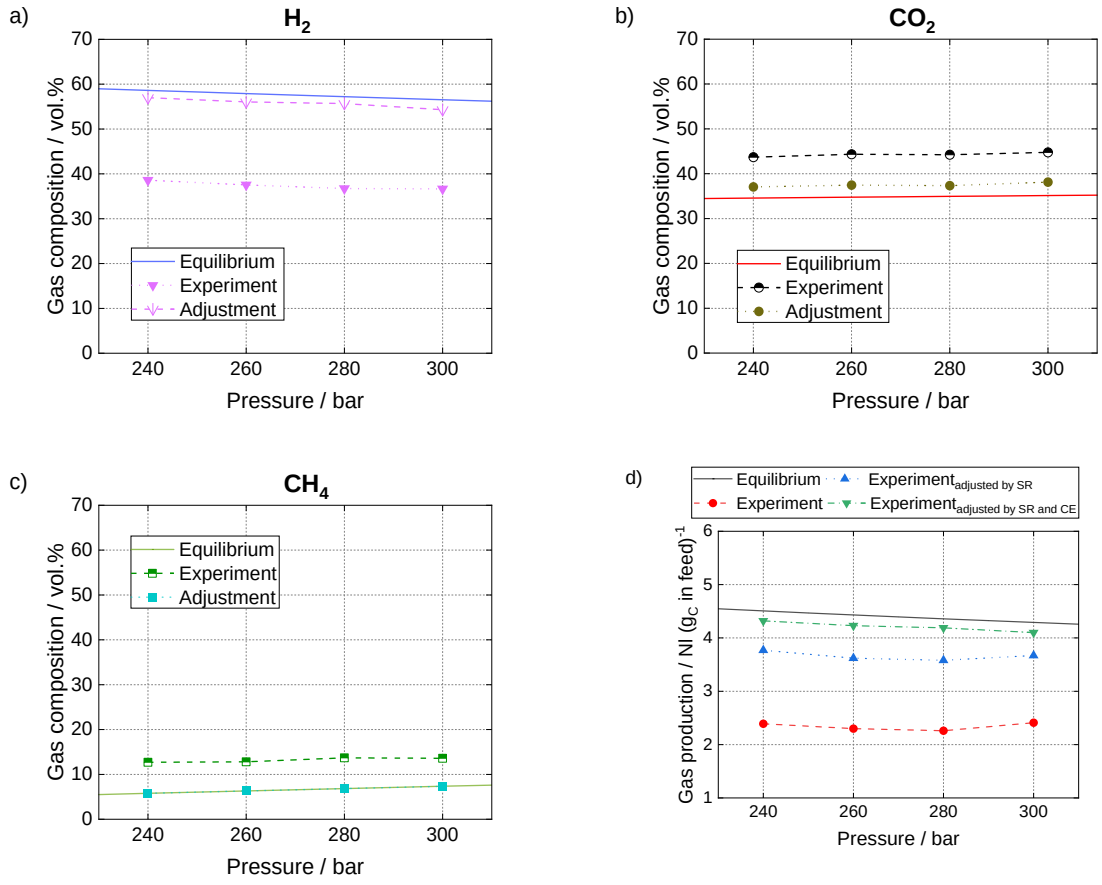


Figure 6.17: Influence of Pressure on a) H_2, b) CO_2, c) CH_4 content in vol.% and d) gas production in Nl $g_{c\ in\ Feed}^{-1}$ at experimental conditions of T = 650 °C, DM content = 6.6 wt.%, $\dot{m}$ = 700 g h^{-1}.

6.5.2 Concentration

As a second parameter, the influence of carbon concentration in the feed (and thus biomass concentration) was assessed. Equilibrium shows that with increasing carbon content, the percentage of H_2 in the product gas drops while that of CH_4 increases (Figure 6.18). This is due to a decrease in water surplus which favors methanation (see section 6.3.2.2). This trend is confirmed by the experimentally measured product gas, however to smaller extent. Again, as described in section 6.5.1, the CH_4 content in the product gas is much higher during experiment than expected from equilibrium. Some C_{2+} compounds (2.1 – 5.1 vol.%) formed during the experiments that were not present in equilibrium. When correcting the gas composition as described in section 6.5.1, the

product gas matches the equilibrium concentrations adequately with a mean deviation in H_2 content of 0.67 vol.% and CO_2 content of 1.01 vol.%.

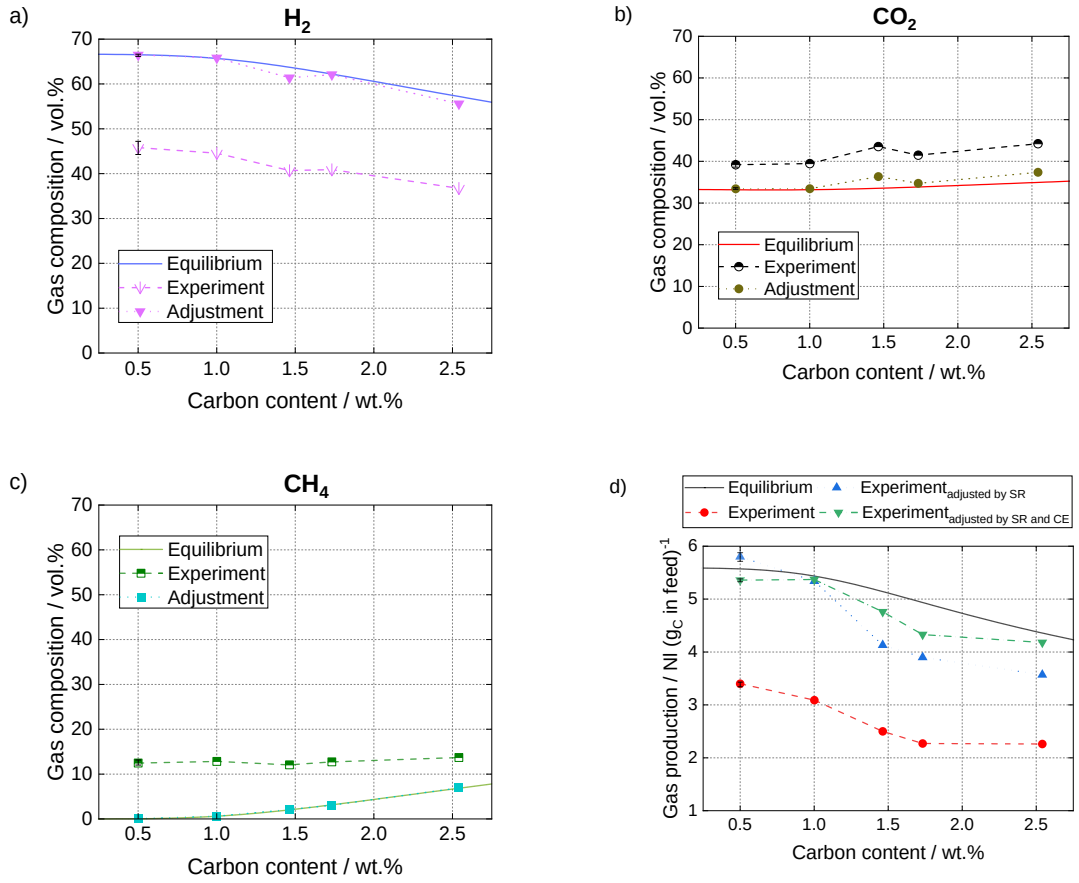


Figure 6.18: Influence of Carbon Content on a) H_2, b) CO_2, c) CH_4 content in vol.% and d) gas production in Nl $g_{c\ in\ Feed}^{-1}$ at experimental conditions of T = 650 °C, p = 280 bar, $\dot{m}$ = 700 g h^{-1}.

The experimental gas production is much lower than expected from equilibrium. This is caused by the insufficient steam reforming and incomplete gasification for carbon contents greater than 1 wt.%. When correcting the gas production by both factors, the deviation becomes much smaller, with a mean relative deviation of 5%.

6.5.3 Temperature

The effect of temperature was also assessed. As described in section 6.3.2.3 (and displayed in Figure 6.19) regarding the experimental results, with increasing temperature the H_2 content decreased and the CH_4 content increased. The opposite is expected from the literature [80,87], and from the present equilibrium calculations, since

a temperature increase should promote hydrocarbons' steam reforming. As steam reforming is kinetically limited in the present case due to the lack of a suitable catalyst (see section 6.5.1), the hydrocarbons are not sufficiently reformed. Due an increase in gasification efficiency from 56 to 93% with an increase in temperature from 550 to 700 °C more carbon is transferred into the gas phase in form of CH_4 and C_{2+}, increasing the share of hydrocarbons in the gas phase.

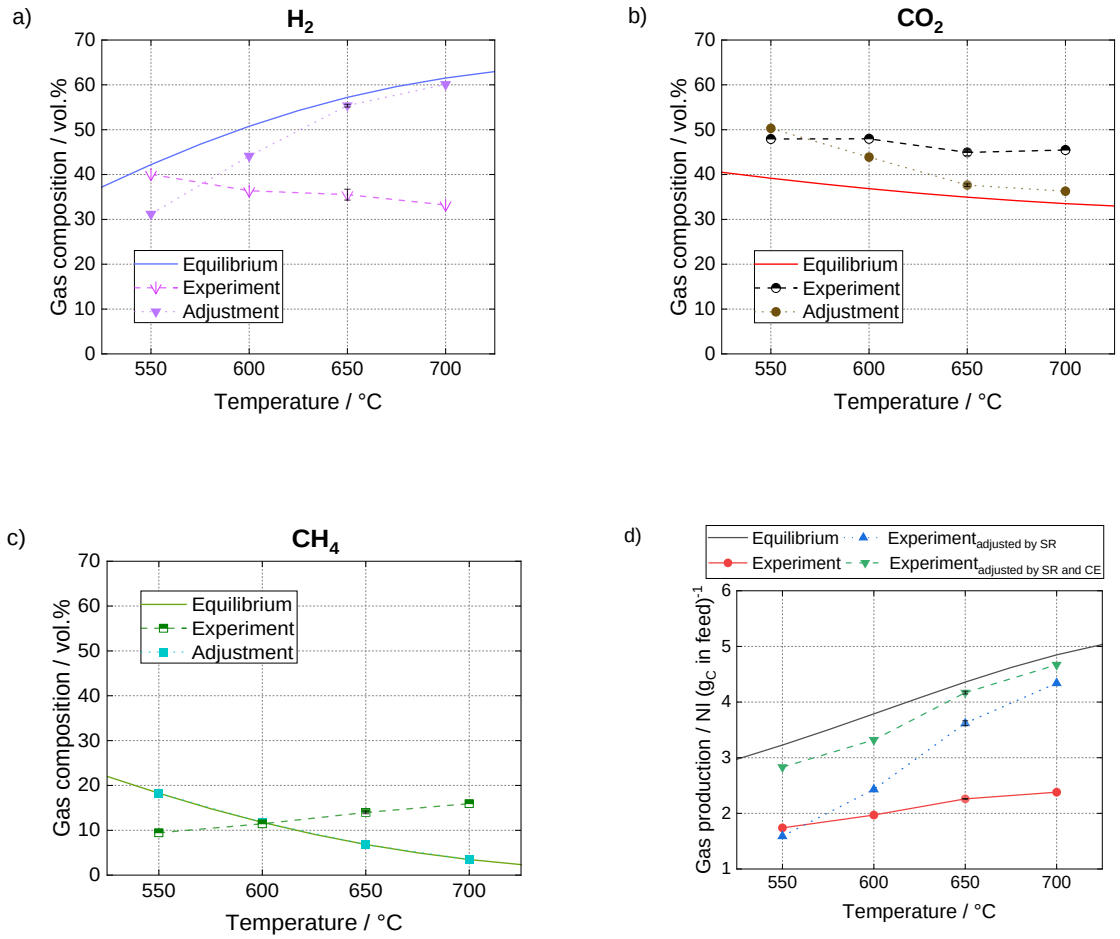


Figure 6.19: Influence of Temperature on a) H_2, b) CO_2, c) CH_4 content in vol.% and d) gas production in Nl $g_{c\ in\ Feed}^{-1}$ at experimental conditions of p = 280 bar, DM content = 6.6 wt.%, $\dot{m}$ = 700 g h^{-1}.

When adjusting the experimental gas composition according to Eq. 6.12, the H_2 and CO_2 concentrations at T ≥ 650 °C agree well with the equilibrium gas composition well with a maximum deviation of 2.2 and 3.0 vol.%, respectively. However, for lower temperatures the deviation increases. At T = 550 °C, the deviation is 11.0 vol.% in H_2 content and 11.1 vol.% in CO_2 content. For T = 550 – 600 °C the correction of the

produced gas by steam reforming reactions is thus not sufficient to reach equilibrium, indicating the influence of other reactions as well. As described in section 6.3.2.3, in these cases the gasification efficiency was low and by-products such as tar and possibly coke were produced. With corrections of the gas production by SR and CE the gas production reaches closer to equilibrium. The mean relative deviation for T ≥ 650 °C is 4.4%, whereas for T < 650 °C it is 12.4%, again emphasizing that at temperatures below 650 °C unwanted reactions take place that hinder gas formation.

6.5.4 Summary of gained knowledge from equilibrium calculations

Even though the equilibrium calculations were only carried out with glucose as model compound and not the real biomass composition, valuable insights could be gained. The comparison of experimental data with equilibrium calculations displayed that thermodynamic equilibrium was not reached during the experiments. It was possible to explain the deviations in gas composition by insufficient steam reforming for T ≥ 650 °C. A suitable catalyst could enable the system to reach equilibrium gas compositions and thus maximum H_2 yields. For T < 650 °C the deviations could not be explained by steam reforming, indicating the influence of other reactions that inhibit the reach of equilibrium. This is confirmed by the experimental observations of tar and coke formation during these experiments.

When choosing reaction conditions that produce little or no unwanted by-products (tar, coke), the equilibrium calculations can be used as a tool to estimate the product gas composition in advance. It can also be used as an indicator of whether further measures need to be taken to achieve maximum hydrogen yield, such as the introduction of a catalyst. In addition, it can be used as a control tool to assess if and to what extent undesirable byproducts may have formed, e.g. T = 550 °C or T = 600 °C as described in section 6.5.3, when deviations in the product gas cannot be explained by gas phase reactions such as steam reforming or water-gas shift. The calculations also provided the amount of gas produced. This can be utilized as an estimate for the amount of product gas for complete gasification and can be adjusted to the gasification efficiency achieved during the experiment.

With the parameters ranges that were experimentally determined to be suitable for sufficient gasification combined with thermodynamic equilibrium calculations, a first prediction of the product gas amount and composition could be made for novel biomasses that have not been gasified before.

6.6 Conclusion

A novel reactor concept for the supercritical water gasification process (SCWG) was developed and a detailed parameter study was performed. The parameter variation included temperature, pressure, biomass type and concentration, potassium addition and residence time.

The novelty of the present SCWG system is the heating concept that uses supercritical water to preheat the biomass instead of electrical heating from the outside of the preheater as was done in the past. In previous setups, low gasification efficiencies and solid deposition hindered long time operation. With this novel reactor concept, more than 100 hours of operation have been achieved without any visible solid formation or plugging. This seems to be due to the rapid heating of the biomass by mixing it with supercritical water.

Pressure had a negligible effect on the process, in terms of gasification efficiency and gas composition. This is most likely due to the fact that the pressure is in all cases very high ($p \geq 240$ bar) and due to technical limitations only pressures up to 300 bar were possible to investigate. Potassium was added as a homogeneous catalyst in form of $KHCO_3$. There was no influence on the gas composition visible and also the gasification efficiency was only minorly affected. This might be due to the fact that the biomass itself contains potassium and thus a further addition does not offer any benefits. A variation of reaction temperature significantly influenced the process. With increasing temperature, the gasification efficiency increased from 58% at T = 550 °C to 91% at T = 700 °C due to an improved splitting of the biomass molecules. At the same time the organic carbon in the effluent decreased. At T < 650 °C increased tar formation and incomplete carbon balance was observed. Thus, for the biomasses tested at least T = 650 °C is required for sufficient gasification without extensive by-product formation. The biomass type did not influence the gasification efficiency or the gas composition.

This is most likely due to the similar macroscopic appearance and elemental composition of the tested biomasses. However, SiO_2 deposition was observed prior to the gasification reactor when the Si content in the reaction mixture was above 0.1 wt.%. This indicates inadequate salt separation at elevated salt levels and underscores the need to further improve the concept being developed. An increase in dry matter content led to a decrease in the gasification efficiency. However, almost no decrease was occurring when the dry matter content was increased from 3.8 to 6.6 wt.%, indicating that also higher dry matter contents should be processible in the future. This was not possible in the present investigation due to plugging of the feed tubing due to its small inner diameter. In larger plants this should not occur. The residence time had a large influence on the gasification efficiency when being increased up to 8 s. A further increase displayed only a minor influence, almost as if a plateau was reached. This behavior is known from other authors. However, 8 s are very low for reaching this plateau, compared to results reported by other authors. This emphasizes the superior behavior of the present reactor concept.

From the parametric study conducted, an optimal set of parameters can be derived in terms of maximizing gas production while reducing processing effort:

- Pressure should be chosen as low as possible to reduce effort for pressurizing the system (p = 240 bar).
- No potassium should be added as catalyst as there was only a minor effect and $KHCO_3$ is expensive to purchase (c_{K^+} = 0 ppm).
- Temperature should be chosen as high as possible, as long as the reactor material can sustain it (T = 700 °C), to reduce by-product formation and to obtain a clean effluent.
- Dry matter content should be chosen as high as possible, in the present case it was limited due to the feed tubing (DM = 6.6 wt.%). The biomass type does not influence the gasification offering flexibility in terms of feedstock type to the process. However, the salt content needs to be monitored.
- The residence time should a chosen to be at 8 s. An increase above 8 s increases the gasification efficiency only minorly, which might not offset the increased invest costs when building a larger reactor.

Based on the experimental results, an empirical model was derived to describe the influence of the different process parameters. As only temperature, dry matter content and residence time displayed a large influence these three parameters were included. They all displayed almost linear influence on the gas composition and gasification efficiency, thus the empirical model is based on multilinear regression. The model was verified for two new parameter sets. The model can thus serve as a valuable tool to reduce the experimental effort. Experimental outcomes can be predicted and thus the parameters can be adjusted in such a way, that e.g. a desire gas composition is obtained.

Besides the experimental work, equilibrium calculations were carried out to determine further optimization potential in terms of maximizing hydrogen yield. From these calculations it was deduced that steam reforming reactions are kinetically limited, preventing the system from reaching equilibrium gas compositions. The utilization of a nickel catalyst, for example, could enhance hydrogen production. It should be noted that equilibrium calculations only provide information about the distribution of gas-phase components in equilibrium. However, since SCWG involves multiphase systems and kinetically controlled reactions, equilibrium calculations cannot reliably predict the actual gasification conversion. Nevertheless, the comparison between experimental results and equilibrium calculations revealed that undesirable side reactions occur at temperatures below 650 °C. Therefore, equilibrium calculations can still serve as a useful tool to evaluate trends in product gas composition and to further guide the optimization of the SCWG process.

Chapter 7. Water consumption of the SCWG process: Investigation with a model compound

The content of this chapter is sourced from the following publication:

- Dutzi, J.; Vadarlis, A.A.; Boukis, N.; Sauer, J. Comparison of Experimental Results with Thermodynamic Equilibrium Simulations of Supercritical Water Gasification of Concentrated Ethanol Solutions with Focus on Water Splitting. *Ind. Eng. Chem. Res.*, **2023**, 62, 12501-12512. DOI: 10.1021/acs.iecr.3c01595

  Declaration of contributions:

  Julian Dutzi conceptualized the experimental work and analysed the data, evaluated the results, and wrote the manuscript. Julian Dutzi conducted the thermodynamic equilibrium calculations and the comparison with experimental data.

  Athanasios A. Vadarlis conducted the thermodynamic equilibrium calculations and the comparison with experimental data.

  Nikolaos Boukis supervised the work, contributed to the discussion, and reviewed the manuscript.

  Jörg Sauer supervised the work, contributed to the discussion, and reviewed the manuscript.

Summary of chapter 7

Supercritical water gasification (SCWG) is a process in which biomass reacts with supercritical water to produce H_2 and CH_4-rich gas. The water-to-biomass ratio is a crucial variable in SCWG that affects the energy efficiency of the process. Despite the clear concept, systematic studies on water consumption during the formation of gaseous products are lacking. As water is a scarce resource and its consumption will gain more attention in the future, a precise understanding is important. This work aims to determine the water consumption in SCWG of organic feedstock. Ethanol was used as an organic model compound since mass balances of complex biomasses like lignocelluloses are often incomplete due to the formation of solid deposits. The ethanol concentration ranged from 1.2 to 72 wt.%, and complete gasification was achieved in all cases. Water consumption decreased with an increase in ethanol concentration due to enhanced methanation reactions with increasing organics. Stoichiometric calculations and ASPEN HYSYS simulations confirmed the experimental results, showing equilibrium gas compositions in the reaction system.

7.1 Introduction

The process of supercritical water gasification revolves around the use of water in its supercritical state as a solvent and reactant [3]. Organic molecules are first hydrolyzed (Eq. 7.1 - 7.2) and then further decomposed into gases, followed by the water gas shift reaction (Eq. 7.3) and methanation reactions (Eq. 7.4 - 7.5) [203–205]. As displayed in Eq. 7.1 to 7.5 water plays an important role as a reactant in the SCWG.

$$C_xH_yO_z + (2x - z)H_2O \rightarrow xCO_2 + (2x - z + 0.5y)H_2 \quad (7.1)$$

$$C_xH_yO_z + (x - z)H_2O \rightarrow xCO + (x - z + 0.5y)H_2 \quad (7.2)$$

$$CO + H_2O \leftrightarrow CO_2 + H_2 \quad (7.3)$$

$$CO + 3H_2 \leftrightarrow CH_4 + H_2O \quad (7.4)$$

$$CO_2 + 4H_2 \leftrightarrow CH_4 + 2H_2O \quad (7.5)$$

Until now the amount of water that reacts to form gaseous products within the process has received little interest and has not been systematically studied. The water-to-biomass ratio in the feed influences the process in terms of gasification efficiency [89,134,135] and is an important factor on the SCWG energy efficiency and economics [206,207]. Fiori et al. simulated the SCWG process of different biomasses and calculated the water consumption of 10 wt.% glycerol solution to be 22.5 kg h^{-1} when processing 1000 kg h^{-1} solution (T = 700 °C, p = 300 bar) [208]. Wang et al. simulated the catalytical SCWG of lignin on molecular scale and calculated the water consumption as a function of total water molecules present in the system [209]. In the following work, the influence of the biomass concentration, conducted with the model component ethanol, on the water consumption of the SCWG is experimentally investigated and theoretically described. Additionally, the experimental data is compared to an ASPEN HYSYS simulation of the thermodynamic equilibrium. The results of these experiments provide valuable insights into the process of supercritical water gasification of ethanol and can be transferred to the conversion of real biomass. The water consumption is an important process factor because if a larger amount of the water is consumed in the reaction, less water remains available for recycling. As a result, additional fresh water must be supplied and heated to supercritical conditions, leading to a decrease in the overall energy efficiency of the process.

7.2 Materials and method

7.2.1 Preparation of educts

Pure ethanol is mixed with distilled water at concentrations of 1.2 to 72 wt.% to create the feed solution. The ethanol is supplied by VWR Chemicals. $KHCO_3$ is added as a catalyst.

7.2.2 Apparatus

The description of the configuration of the continuous lab-plant that was used for this investigation can be seen in section 5.2.2.2 (“Configuration 2”). The only differences compared to section 5.2.2.2 is that in the preheater no liner was installed, thus the inner diameter of the preheater was 8 mm. Additionally, no salt separation was performed as only the model biomass substance ethanol was processed.

For simplicity, a schematic diagram of the lab-plant is shown in Figure 7.1.

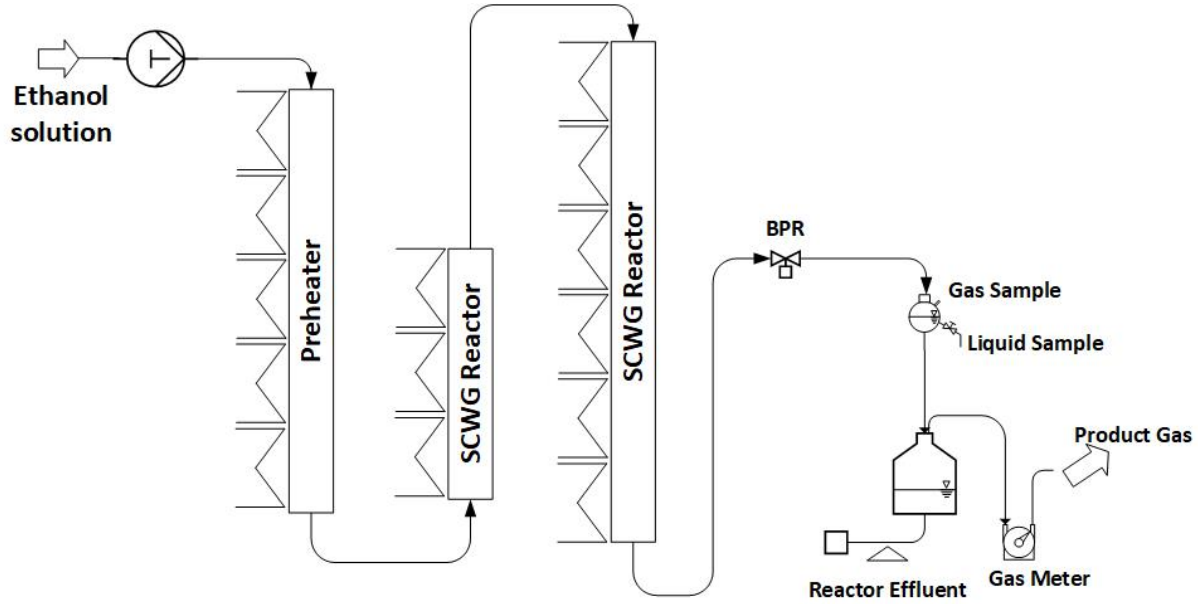


Figure 7.1: Schematic diagram of the lab-plant in Chapter 6.

7.2.3 Data interpretation

Additional to the key figures described in section 3.4, the following key figures are calculated.

For the data interpretation the ethanol mass fraction w_{EtOH} (Eq. 7.6) and the ratio of carbon to water in the feed x_c^* (Eq. 7.7) are used.

$$w_{EtOH} = \frac{\dot{m}_{EtOH}}{\dot{m}_{EtOH}+\dot{m}_{H2O}} \quad (7.6)$$

$\dot{m}_i$ Mass flow of species ´i´ (g/h)

$$x_c^* = \frac{\dot{n}_C}{\dot{n}_{H2O}} = \frac{2\dot{n}_{EtOH}}{\dot{n}_{H2O}} \quad (7.7)$$

$\dot{n}_i$ Molar flow of species ´i´ (mol/h)

The water consumption of the process describes how much water is converted into gaseous products when reacting with the organic compounds. In previous studies it was shown that the reactor effluent of the SCWG process can be recycled [89,113]. The water consumption is thus important for the estimation of how much fresh water needs to be used to make up the difference of water in feed and reactor effluent by distilled water and thus is important for cost estimation of the SCWG process. In order to calculate the generation of H_2 and CH_4 from water, the amount of C, H and O in the gas phase is compared with the amount of C, H and O that originate from the gasified ethanol $\dot{n}_{EtOH,gasified}$.

$$\dot{n}_{EtOH,gasified} = CE * \dot{n}_{EtOH,Feed} \quad (7.8)$$

$\dot{n}_i$ Molar flow of species ´i´ (mol/h)

Any additional H and O ($\Delta H, \Delta O$ (Eq. 7.10 and 7.11)) in the product gas have its origin in water that has reacted with the ethanol since those are the only two components that are fed into the system (except for $KHCO_3$ which is present in neglectable amounts and is assumed to leave the system also in form of $KHCO_3$ and thus does not contribute to gas formation).

$$\Delta C = \dot{n}_{CH_4} + \dot{n}_{CO} + \dot{n}_{CO_2} + 2\dot{n}_{C_2H_4} + 2\dot{n}_{C_2H_6} + 3\dot{n}_{C_3H_6} + 3\dot{n}_{C_3H_8} - 2\dot{n}_{EtOH,gasified} \quad (7.9)$$

$$\Delta O = \dot{n}_{CO} + 2\dot{n}_{CO_2} - \dot{n}_{EtOH,gasified} \quad (7.10)$$

$$\Delta H = 4\dot{n}_{CH_4} + 2\dot{n}_{H_2} + 4\dot{n}_{C_2H_4} + 6\dot{n}_{C_2H_6} + 6\dot{n}_{C_3H_6} + 8\dot{n}_{C_3H_8} - 6\dot{n}_{EtOH,gasified} \quad (7.11)$$

Δj Molar difference of element ´j´ (mol/h)

ΔC is zero since all carbon in the gaseous phase originates from gasified ethanol. Since the differences in H and O in real experiments show little deviations to the elemental composition of water the mean value of these differences ΔO and ΔH is used to calculate the water consumption WC relative to the processed amount of ethanol according to the following equation.

$$WC = \frac{0{,}5\Delta H + \Delta O}{2} * \frac{1}{\dot{n}_{EtOH,gasified}} \frac{mol\ H_2O}{mol\ C_2H_5OH} \tag{7.12}$$

7.3 Results and discussion

7.3.1 Investigation of water consumption

Eight experiments were conducted to investigate the water consumption during the SCWG of different ethanol solutions (100 ppm of K^+ were added) (see Table 7.1). The reaction temperature was 650 °C, and the pressure was 280 bar. The set mass flow was 250 g h^{-1}. In all experiments conducted the TOC conversion was greater than 99%. The carbon efficiency was greater than 95.5% in all cases except for x_c^* = 0.01 (see Table 7.1) and thus the gasification can be considered complete for all concentrations. Since TOC-conversion is complete and no solid carbon was found for x_c^* = 0.01 the relatively low CE is most likely due to uncertainties of the measurement (especially the gas meter) which have greater impact if the gas flow is low.

Table 7.1: Key figures of gasification of different ethanol solutions.

Exp. Nr.	w_{EtOH}	x_c^*	CE	TOC conversion	Mass balance	Carbon balance	Amount of gas
	wt.%	mol/mol	%	%	%	%	$l\ g_{EtOH}^{-1}$
7.1	1.2	0.01	93.6	99.42	99.2	93.6	2.84
7.2	6.0	0.05	97.6	99.94	98.4	96.7	2.26
7.3	11.5	0.10	95.9	99.98	101.8	94.5	1.7
7.4	20.0	0.20	95.6	99.99	98.5	95.6	1.38
7.5	30.0	0.34	98.2	100.00	99.2	98.2	1.24
7.6	39.0	0.50	96.6	100.00	96.9	96.6	1.16
7.7	56.0	1.00	96.2	100.00	96.4	96.3	1.06
7.8	72.0	2.00	96.5	99.95	98.0	96.6	1.01

This is surprising since CE is generally known to decrease with increasing concentration of organics [89,135]. In the present reactor configuration ethanol could be gasified effectively even at high concentrations. The temperatures (T = 650 °C) and residence times (calculation based on the density of water) at T > 600 °C (τ = 3 min) are high for the conversion of ethanol. For high feed concentrations of ethanol, the density of the mixture decreases and thus the residence time will decrease. Since complete gasification is reached in all cases the change in residence time has no impact on the process under the chosen conditions. Byrd et al. 2017 studied the SCWG of ethanol over a Ru(5wt.%)/Al_2O_3 catalyst and demonstrated the significant effect of residence time and of temperature on the yield of products and gasification [96]. More specifically, at 600 °C and low residence time (5 s), they detected high amounts of organic carbon in the liquid effluents and increased ethylene yield. When they increased residence time to 10 s, these products were minimized, while the yields of H_2, CH_4 and CO_2 increased significantly. Voll et al. calculated the thermodynamic equilibrium of ethanol SCWG and compared their results with Byrd et al. [96,210].They argued that a minimum residence time of 4 s results in satisfactory results when it comes to ethanol SCWG. The ethanol decomposition in supercritical water is known to already take place at 500 °C [211]. Since these two factors positively influence the gasification efficiency [66,67,143,149,212–214] the high temperature and residence time could explain why complete gasification could be reached for ethanol concentrations up to 72 wt.%.

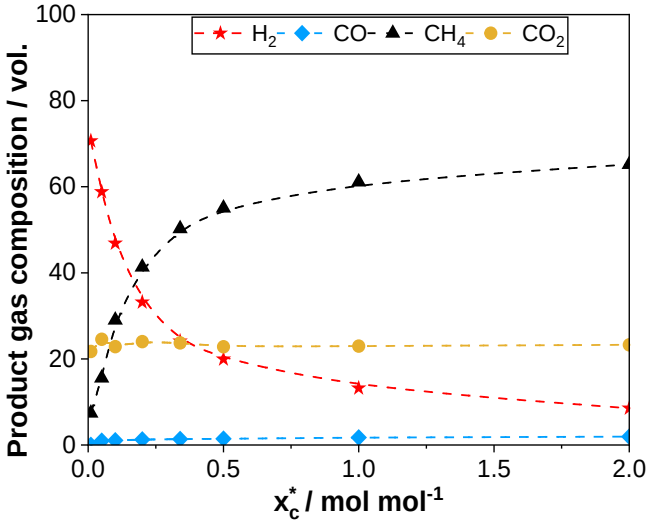


Figure 7.2: Influence of x_c* in the feed solution on the composition of the product gas based on experimental results.

From literature it is well known that the concentration of the organic components significantly influences the composition of the product gas of the SCWG process. With rising organic content the water surplus decreases which reduces the amount of H_2 produced [134,135,153]. The CH_4 was found to increase with rising organic concentration [87,153]. In the case of ethanol the methane could origin from methanation or acetaldehyde decarbonylation. Both of described effects (H_2 decrease and CH_4 increase) could be already seen in the present study (see Figure 7.2).

The H_2 content of the product gas decreased from 70.1 to 8.5 vol.% when increasing the ethanol concentration from 1.2 to 72 wt.% (x_c^* 0.01 to 2 mol/mol). The CO concentration remained below 2 vol.% with little increase. An increase with rising organic concentration is expected due to the reverse water-gas shift reaction [135,215]. When increasing the feed concentration, the CH_4 content of the product gas rose from 7.1 to 65.2 vol.%. The increased methane content correlates with the decrease in the amount of produced gas per gram ethanol gasified (from 2.84 to 1.01 L g_{EtOH}^{-1}) since according to reactions 6.4 and 6.5, four or five gas molecules react to form one molecule of methane and water. Since the gasification of ethanol solutions with 1.2 to 72 wt.% was possible and in all cases complete (CE > 93.6%) it can be assumed that the same reaction mechanism can be applied for all concentrations. Since almost no higher hydrocarbons can be detected the major reaction pathway can be described by dehydrogenation of ethanol, as proposed by Arita et al. [211].

$$C_2H_5OH \rightarrow H_2 + CH_3CHO \quad (7.13)$$

$$CH_3CHO \rightarrow CH_4 + CO \quad (7.14)$$

$$CO + H_2O \rightarrow CO_2 + H_2 \quad (7.15)$$

Subsequently either steam methane reforming or methanation reactions (Eq. 7.4 and 7.5) take place which depend on the amount of water in the system and thus on the ethanol concentration. In case of x_c^* = 0.01 and x_c^* = 0.05 the amount of methane in the product gas is significantly lower than the amount that forms according to Eq. 7.13 and 7.14. In this case steam methane reforming seems to be taking place. For higher x_c^* than 0.05 the amount of methane contained in the product gas can not only be explained by Eq. 7.13 and 7.14 since the amount of methane in the product gas is greater than the amount of ethanol processed on molar base (see Table 7.2).

Table 7.2: Ratio of methane in the product gas to ethanol in feed for different x_c^*.

x_c^* mol/mol	**0.01**	**0.05**	**0.1**	**0.2**	**0.34**	**0.5**	**1**	**2**
n_{CH4} / n_{EtOH} mol/mol	0.44	0.72	1.02	1.17	1.27	1.30	1.34	1.36

The methanation reaction and steam methane reforming thus directly influence the water consumption of the SCWG process since the formed water during methanation reduces the amount of water consumed. This effect can be seen in Figure 7.3 and Table 7.3. The water consumption decreases from 2.38 to 0.06 mol H_2O consumed per mol ethanol when increasing x_c^* from 0.01 to 2.

Table 7.3: Calculation of water consumption from experimental data (according to Eq. 7.9 - 7.12).

x_c^*	**ΔH**	**ΔO**	**Water consumption**		
			Based on ΔH	Based on ΔO	Mean
mol/mol	mol H/mol EtOH	mol O/mol EtOH	mol H_2O/mol EtOH		
0.01	5.64	1.94	2.82	1.94	2.38
0.05	2.74	1.42	1.37	1.42	1.40
0.1	1.91	0.75	0.96	0.75	0.86
0.2	0.95	0.47	0.48	0.47	0.47
0.34	0.61	0.28	0.31	0.28	0.29
0.5	0.55	0.16	0.28	0.16	0.22
1	0.30	0.09	0.15	0.09	0.12
2	0.14	0.05	0.07	0.05	0.06

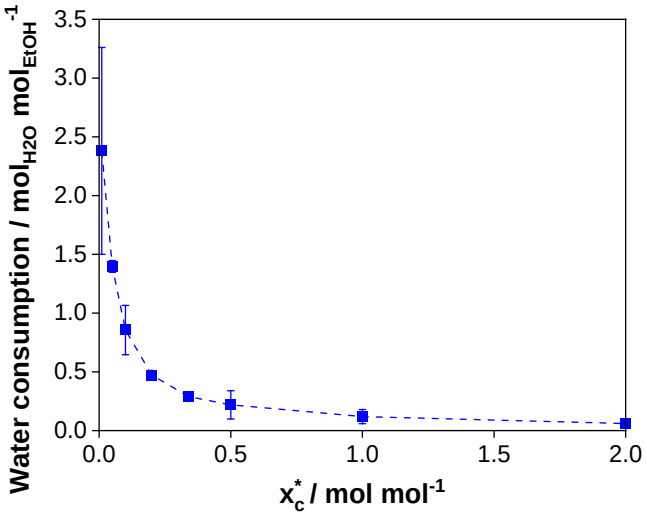


Figure 7.3: Water Consumption of the SCWG process with variation in x_c^* in the feed solution.

At low x_c^* the deviation of the measured water consumption to the water consumption given in equation 7.1 for ethanol (3 mol H_2O per mol ethanol) is the smallest. This deviation can be well explained by the formed methane. When further reducing the feed concentration the water consumption of 3 mol H_2O per mol ethanol would then be the limit. It becomes clear that the higher the methane content of the product gas the lower the water consumption of the process is. To verify the proposed mechanism (Eq. 7.13 to 7.15 and Eq. 7.4 and 7.5) the following theoretical consideration was conducted. The proposed mechanism by Arita et al. [211] can be reduced to Eq. 7.16.

$$C_2H_5OH + H_2O \rightarrow CO_2 + 2H_2 + CH_4 \qquad (7.16)$$

$$CO_2 + 4H_2 \rightarrow CH_4 + 2H_2O \qquad (7.5^*)$$

When also taking the methanation into account (Eq. 7.5, for simplicity again displayed as Eq. 7.5*), the resulting gas composition (CO and higher hydrocarbons are neglected due to the small amount in the product gas) can thus be described by adding these equations. For this, Eq. 7.5* is multiplied by the factor x and Eq. 7.16 with the factor y.

$$yC_2H_5OH + (y-2x)H_2O \rightarrow (y-x)CO_2 + (2y-4x)H_2 + (y+x)CH_4 \qquad (7.17)$$

The water consumption WC can thus be described by the reduced formula (y = $n_{EtOH,gasified}$).

$$WC = \frac{n_{EtOH,gasified} - 2x}{n_{EtOH,gasified}} \frac{mol\ H_2O}{mol\ EtOH} \quad (7.18)$$

The produced amount of gas can be described as displayed in Eq. 7.19 to 7.21.

$$n_{CH4} = y + x = n_{EtOH,gasified} + x \quad (7.19)$$

$$n_{CO2} = y - x = n_{EtOH,gasified} - y \quad (7.20)$$

$$n_{H2} = 2y - 4x = 2n_{EtOH,gasified} - 4x \quad (7.21)$$

The variable ‘x’ can thus be described in various ways.

$$x = n_{CH4} - n_{EtOH,gasified} = \frac{2n_{EtOH,gasified} - n_{H2}}{4} = n_{EtOH,gasified} - n_{CO2} \quad (7.22)$$

With this formula the water consumption can be described as

$$WC = 3 - 2\frac{n_{CH4}}{n_{EtOH,gasified}} = \frac{1}{2}\frac{n_{H2}}{n_{EtOH,gasified}} = 2\frac{n_{CO2}}{n_{EtOH,gasified}} - 1 \quad \frac{mol\ H_2O}{mol\ EtOH} \quad (7.23)$$

To verify this theoretical consideration the experimental data are displayed graphically and approximated with a linear regression (see Figure 7.4). As displayed, the received linear regressions fit the calculations of the theoretical water consumption well with a deviation smaller than 20%. The proposed reaction mechanism is thus justified.

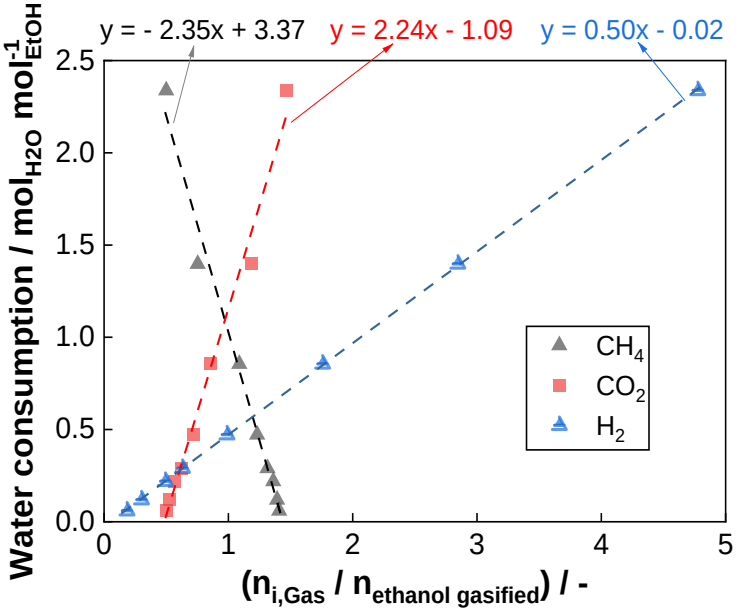


Figure 7.4: Water Consumption as a function of the produced gases.

7.3.2 Comparison of experimental results with thermodynamic equilibrium

The experimental results were additionally compared with the thermodynamic equilibrium calculated with Aspen HYSYS V14. The simulation was carried out with a Gibbs reactor which minimizes the free Gibbs energy of the system. The selected property package was the PR-Twu implementing the Equation of State (EOS) for enthalpy calculations. As stated by Twu et al., their temperature-dependent function for a cubic EOS correctly extrapolates the vapor pressures of pure components to the supercritical region. In addition, they proposed a new mixing rule for predicting the properties of mixtures [216]. Combined with their proposed mixing rule, their cubic EOS can accurately describe the phase equilibria of polar/non-polar systems. The pressure was set to 280 bar and the temperature to 650 °C (as set in the experiments). The feed has a temperature of 20 °C. x_c^* was varied from 0.001 to 8.0 mol/mol (see Figure 7.5). The simulation verified the results from Voll et al., who calculated the thermodynamic equilibrium of the SCWG of ethanol at 800 °C and 221 bar [210]. It was found that the simulation reproduced accurately their results (see Supporting Information A2).

The results indicate that in the present reaction system under the chosen reaction conditions thermodynamic equilibrium is reached for x_c^* greater than 0.05 (see Figure 7.5). According to Aspen HYSYS at x_c^* = 0.08, the gas composition is (almost) exactly the composition described by Eq. 7.16 (24.2 vol.% CO_2, 50.1 vol.% H_2, 24.6 vol.% CH_4), and the water consumption is close to 1 (0.96). At this point, the gas composition can be explained by the ethanol decomposition. For lower x_c^* than 0.08, less methane should be in the product gas than the amount formed according to Eq. 7.16. This means that steam methane reforming needs to take place in order to reach equilibrium. Experimental results show that even though it is true that less methane is in the product gas than the amount that forms according to Eq. 7.16 (see Table 7.2), methane is not completely reformed to reach equilibrium. In the case of x_c^* = 0.05, equilibrium is reached, but for x_c^*= 0.01, the experimental results indicate a higher methane content (7.1 vol.%) than predicted by Aspen HYSYS (0.8 vol.%). More catalytically active sites are needed to reach equilibrium. Steam methane reforming is often promoted on nickel-based catalysts with a high surface area [193]. Thus, the methane content is higher than predicted by the equilibrium. For x_c^* higher than 0.08, the amount of methane in the product gas can be explained by considering methanation. Since

equilibrium is reached in these cases, methanation can be considered to take place completely.

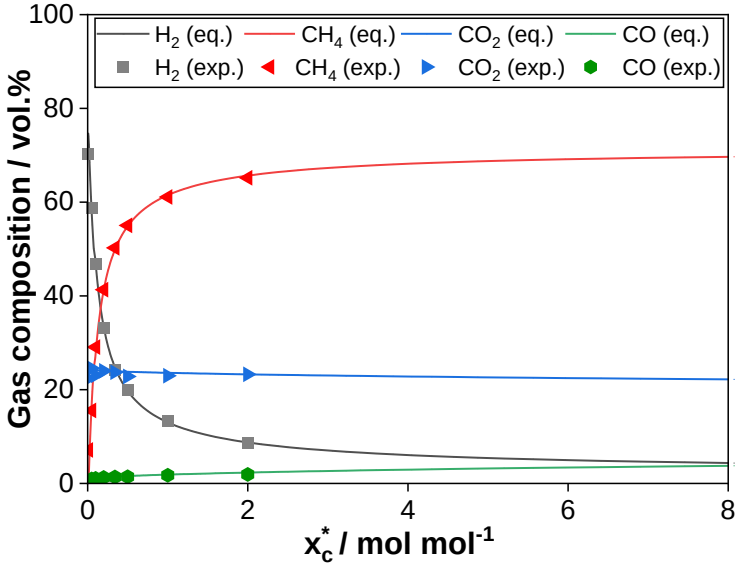


Figure 7.5: Comparison of experimentally measured (exp.) and simulated gas composition (eq.) for different x_c^* in the feed solution.

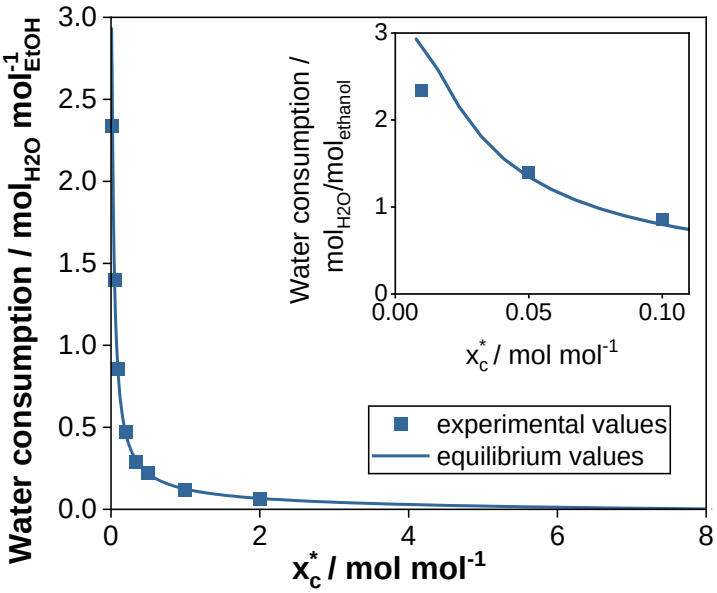


Figure 7.6: Comparison of experimentally measured and simulated water consumption for different x_c^*.

Besides the gas compositions (see Figure 7.5), the water consumption determined by Aspen HYSYS also fits the experimental data well (see Figure 7.6). The deviation is smaller than 0.04 mol/mol for x_c^* greater than 0.05. The deviation is more prominent in

the case of x_c^* = 0.01, but the general trend is still visible. This deviation is due to the deviation in gas compositions as described above. To emphasize the overall accuracy of the simulation with the experiments, the parity plot of the water consumption calculated by Aspen HYSYS and from experimental data is shown (see Figure 7.7).

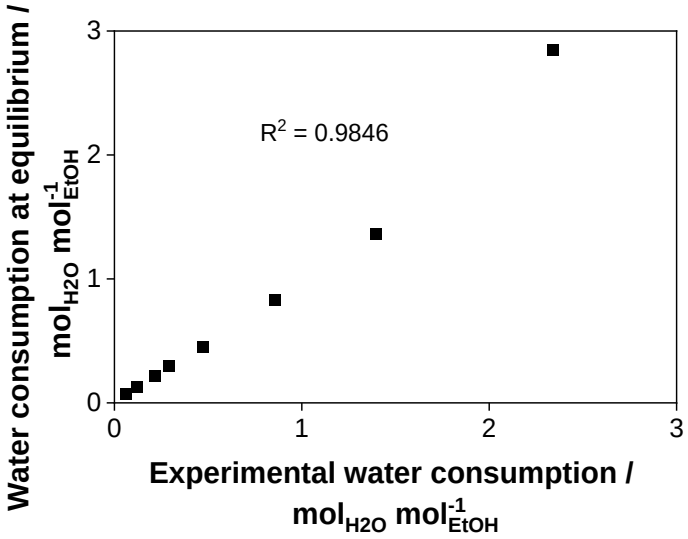


Figure 7.7: Parity plot of water consumption experimentally determined and simulated by ASPEN.

The coefficient of determination R^2 is 0.985 which is very close to 1 (= ideal concordance). This confirms the chosen calculation method for the water consumption based on the experimentally acquired gas compositions.

The simulation of thermodynamic equilibrium with Aspen HYSYS is helpful for determining further reaction parameters that could be investigated. A further extension of residence time would in this case probably not change the outcome of the experiments since under the chosen residence time equilibrium gas composition was reached.

7.4 Conclusion

The water consumption of the supercritical water gasification of ethanol was systematically investigated and described since higher water consumption that results in higher hydrogen generation is an important factor for SCWG. It was demonstrated that the water consumption of the supercritical water gasification of ethanol can be reliably calculated using the composition of the produced gas. The calculation was supported

by thermodynamic equilibrium simulations of the investigated process. The gas composition and the water consumption strongly depend on the ethanol concentration in the feed. With rising ethanol concentration, the water consumption of the process decreases in a logarithmic manner. This is due to increased methanation which produces water as a side product. Simple equations were derived which enable the calculation of the water consumption of the process. In the future, the water consumption should be measured for complex biomasses like lignocellulosic biomasses to extend the knowledge. The influence of other process parameters like reaction temperature or system pressure on this key figure should also be investigated.

Chapter 8. Concluding insights and future perspectives

8.1 Concluding insights

The present work aimed to optimize the SCWG process in such a way that processing dry biomasses (contaminated with heavy metals) becomes possible with high gasification efficiencies in long-term operation.

The initial reaction system, that was based on previous work and experience gained over the last years in our working group, mainly consisted of a preheater, a salt separation and a gasification reactor. Preheater and reactor were electrically heated from the outside (allothermal operation). During these initial experiments technical difficulties arose hindering long-term operation, indicating the need for further investigation and development. However, these initial experiments provided valuable insights that were needed for successful design of the final lab-plant configuration. The most important insights in the initial setup were the following:

Feedstock flexibility

SCWG is supposed to be able to process a wide range of biomasses. In the current work, many different biomasses (grassy and woody) with similar elemental composition were gasified. It was found that neither the carbon gasification efficiency (CE = 60.3 ± 5.1%) nor the gas composition (33.5 ± 3.2 vol.% of H_2 and 44.0 ± 3.9 vol.% of CO_2) was significantly influenced by the variation of biomass. This indicates that biomasses with similar elemental composition behave similarly in SCWG and produce similar product gases. This is especially advantageous as a change in feedstock does not affect the process of SCWG and also not subsequent gas treating/upgrading steps.

Heavy metal and salt separation

The ability of SCWG to separate heavy metals from biomass into the salt concentrate during the process is a significant advantage, as demonstrated by the heavy metal-

free reactor effluent under all tested conditions. This outcome is crucial for processing contaminated biomasses, as a heavy metal-free process water can be reused.

However, a main challenge that arose was insufficient separation of salt building elements into the salt separation device. Insufficient salt separation led to solid deposition in the reaction system, hindering long-term operation. Experiments revealed that salt separation is strongly dependent on the preheating temperatures. An interesting insight was that the location of the deposits changed with changes in the temperature profile.

This insight led to further investigation of the influence of the temperature profile by conducting complex inner-temperature measurements. These measurements revealed that the solid deposits occurred in sections of the lab-plant where temperatures of 400 to 440 °C are first reached inside the medium while an outside temperature was set to 500 °C. From this observation it was concluded that the precipitating salts tend to stick to the wall of the preheater/reactor because the wall is the local hotspot in the section where the salts precipitate and thus the solubility of the salts is the lowest at the wall. Thus, a need for a different heating concept (where the wall is not the local hotspot) was derived.

Water recycling and consumption

SCWG heavily relies on the use of water to create a pumpable feed slurry and to act as a solvent and reactant in the process. As fresh water is a scarce resource it is important to reduce the usage as much as possible. It was successfully demonstrated that the fresh water usage can be reduced by about 89% when the reactor effluent is reused to create new feed slurry.

To quantify how much water reacts in the process and also how much of the produced H_2 stems from the water and not the biomass itself ethanol solutions were gasified with varying ethanol content. It was demonstrated that the water consumption of the supercritical water gasification of ethanol can be reliably calculated using the composition of the produced gas. The calculation was supported by thermodynamic equilibrium simulations of the investigated process. The gas composition and the water consumption strongly depend on the ethanol concentration in the feed. With rising ethanol concentration, the water consumption of the process decreases. This is due to increased

methanation which produces water as a side product. Simple equations were derived which enable the calculation of the water consumption of the process.

Based on the knowledge gained during the first experiments, most importantly the investigation of the salt precipitation, a novel reactor concept was developed. The most important insights from this development and the subsequent testing of the setup are outlined in the following paragraphs.

Process development

During the initial investigation it was found that solid deposition (coke and salts) hinders long-term operation. The salt deposition in the system seems to be caused by the heating concept that was utilized. To avoid salt accumulation on the walls a different heating concept was adapted (“two-stream concept”). Heating of the biomass was achieved by mixing the cold biomass feed with hot supercritical water, allowing rapid heating to supercritical temperatures without the need to directly electrically heat the biomass slurry. This approach helps to reduce salt deposition on the reactor walls and minimize coke formation, as the temperature zone favoring hydrothermal carbonization is avoided. To reach sufficiently high temperatures (up to 700 °C) for efficient gasification, an additional external heating step of the reactor was implemented after salt separation. The novel reactor concept was initially tested by mixing 100 g h^{-1} of biomass slurry (8.8 wt.% DM) with 600 g h^{-1} of supercritical water, resulting in 1.3 wt.% DM in the mixture. More than 100 h of operation was possible with a carbon gasification efficiency of 82.0% at a reaction temperature of 650 °C. An almost closed carbon balance was reached (97.2% could be detected in the products) and no deposits were detected in the lab-plant afterwards. This first promising result encouraged to conduct a further detailed parameter analysis and optimization to maximize the gas production as much as possible.

Process parameters and optimization

After development of the final lab-plant, the parametric study of the reaction system provided valuable insights into how various operational parameters influence the SCWG process. These findings are essential for optimizing process efficiency, reducing by-product formation, and managing costs.

Temperature: Reaction temperature plays the most influential role. Gasification efficiency increased significantly with higher temperatures, peaking at 91% at 700 °C, compared to 58% at 550 °C. At temperatures below 650 °C, tar formation and a poor carbon balance were observed, emphasizing the need for high operating temperatures to ensure stable operation. Even higher temperatures than 700 °C would be desirable to further decompose remaining organics in the effluent. However, temperature levels are limited by the reactor material. Thus, the highest possible reaction temperature should be chosen.

Dry matter content: An increasing dry matter content has the opposite effect on gasification efficiency as temperature. With increasing dry matter content, the gasification efficiency decreased. However, unlike studies by other authors, the system showed minimal decrease of gasification efficiency with increasing dry matter, most likely due to the rapid heating of biomass, avoiding temperature zones that favor hydrothermal carbonization or tar formation, leading to improved gasification efficiency. The effluent TOC content increased with higher dry matter, from 400 mg l^{-1} at 1.3 wt.% dry matter in the reaction mixture to 2860 mg l^{-1} at 6.6 wt.% dry matter, with key organic species (phenol, resorcinol, and formic acid) also increasing. Testing more than 6.6 wt.% in the reaction mixture was not possible because an increased dry matter content led to plugging of the feed tubing. As this plugging should not occur in larger plants and the decrease in gasification efficiency with increasing dry matter content was moderate, an even higher dry matter content should be chosen for operation at large scale to maximize the gas production.

Pressure: Variations in pressure (240 to 300 bar) had negligible effects on gasification efficiency and gas composition. This suggests that operating at the lowest pressure, e.g. 240 bar ($p > 221$ bar, to ensure operation in the supercritical state of water), can minimize pumping efforts and thus costs without compromising performance.

Residence time: With increasing residence time, gasification efficiency improvements were notable up to 8 s of residence time (at 650 °C, 6.6 wt.% dry matter and τ =8 s, CE = 72%), after which gains were marginal (at 650 °C, 6.6 wt.% dry matter and τ =31 s, CE = 79%). This finding highlights the great performance of the developed reaction system. Thus, there is potential for compact reactor designs with short residence times. As the residence time required for sufficiently high gasification efficiency was very low,

the effect of the mixing in the salt separator was investigated by bypassing the gasification reactor after salt separation (which equals an experiment at a residence time of 0 s at reaction temperature). Even though only the salt separator was operated (T = 450 °C) no solid biomass particles were present in the product. A product gas mainly consisting of CO_2 was produced. The effluent's total organic carbon content was much higher (10930 mg l^{-1}) compared to experiments using the gasification reactor (2822 ± 653 mg l^{-1}). Additionally, a large quantity of an oily substance (exceeding typical amount of tars), accumulated in the filter upstream of the back-pressure regulator. Analysis of the oily substance displayed an average molar mass of 261 g mol^{-1}, indicating that the macromolecules of the biomass (cellulose, hemicellulose and lignin) are already greatly decomposed after the salt separator. From these observations, it can be concluded that the salt separator acts as a hydrothermal pretreatment step, similar to hydrothermal liquefaction.

Biomass type: The SCWG process showed consistent performance across different biomass types, with no significant variation in gasification efficiency or gas composition. This confirms the results obtained during the initial testing of the biomasses in the first lab-plant configurations. However, monitoring the salt content, particularly silica, remains crucial, as elevated levels (e.g., >0.1 wt.% SiO_2) led to deposition issues in the lab-plant due to imperfect salt separation.

$KHCO_3$ addition as homogeneous catalyst: Adding potassium as a catalyst showed minimal benefit, most likely due to the inherent potassium content in the biomass. Given the cost of potassium compounds like $KHCO_3$, their use is not recommended.

Empirical model and predictive tools

Based on the parametric investigation of the novel reactor system, an empirical model was derived. The empirical model, which is based on a multi-linear regression, is capable of accurately predicting the outcomes of SCWG experiments for the investigated biomasses in the present reaction system. This model, supported by statistical analysis, shows a high degree of accuracy within ±10% deviation for most parameters. While slightly higher deviations were noted for C_{2+} due to their low absolute values, the model remains robust and reliable for practical application. Additionally, its successful

application to new parameter sets reinforces its generalizability and reduces the need for extensive experimental efforts.

Equilibrium calculations using ASPEN HYSYS further complement the experimental work by providing theoretical insights into the SCWG process. In the present work, large deviations from equilibrium were visible. However, when operation at T ≥ 650 °C, these differences could be explained by insufficient steam reforming. Thus, the equilibrium calculations can serve as a valuable tool to derive further measures to optimize the process (e.g., to maximize the H_2 yield). For T < 650 °C, the deviations between experimental data and equilibrium calculations could not be explained by gas phase reactions, indicating unwanted side reactions. This corresponded well to the experimental observations, especially increased tar formation. Thus, equilibrium calculations can additionally serve as a control tool to check for undesirable side reactions.

This integrated approach of empirical modeling and equilibrium calculations lays a strong base for optimizing SCWG processes. It enables the estimation of gasification outcomes for untested parameters, reducing experimental effort. Future work can focus on extending the empirical model to other feedstocks, incorporating real biomass compositions into equilibrium calculations, and exploring catalytic solutions to bridge the gap between experimental results and theoretical predictions considering maximum H_2 production.

8.2 Future perspectives

Although the general suitability of SCWG was demonstrated for processing the investigated biomasses, several challenges remain for industrial implementation of the process. Key hurdles include the selection of suitable reactor materials, plugging issues in feed piping, particularly with fibrous biomasses or when high dry matter contents are processed, incomplete salt separation that can limit operation, and further development of the reactor concept, e.g. a multi-stage gasification reactor to increase the dry matter content in the reaction mixture to improve process efficiency. Addressing these challenges will be essential to fully exploit the potential of the technology.

Additionally further biomasses (e.g. sewage sludge, animal manure) should be tested as the investigated biomasses represent only a small part of the biomasses that are

processable by SCWG. By treating different biomasses, it will become clear if the novel reactor concept can generally be used or if adaptations need to be made. By this extension to new biomasses, the developed multi-linear model could possibly be refined and generalized to be applicable to many or all biomass inputs, which could have great impact on the future development and application of the process. If a higher salt content limits operation when processing different biomasses, the focus should be on improvement of salt separation. Different concepts have been proposed in literature [69,70,217], which could possibly be adapted in the current setup, e.g., separating the salt concentrate by a cyclone [129].

As long-term operation is now possible in a continuous SCWG plant due to the development in the present work, process integration is becoming possible. For example, in the CERESiS project [62], which accompanied the initial work of the present thesis, a coupling of the SCWG process with gas cleaning units, in particular membrane gas absorption [218], was not meaningful because sufficiently long operation of the SCWG process was not yet possible. Alternatively, the novel reactor concept could be coupled with a steam reforming step to maximize the H_2 yield, as proposed by Vadarlis et al. [219]. They were also limited to processing ethanol as a model compound because no stable operation was possible when operating with complex biomasses. Such process integrations can now be realized to experimentally determine possible obstacles and synergies for operation with complex biomasses that were not visible during theoretical integration.

A future focus should lie on the scale-up on the process. The current plant operates at throughputs of about 1 kg h^{-1}. This scale would not be economically feasible. Thus, for possible implications of the technology it is important to demonstrate the operability of the novel reactor concept at large scale [106]. As limitations in the maximum processable biomass content arose due to the small scale of the feed system, a scale up should also enable processing higher biomass contents, further improving the economics of the process. After scale-up a thorough economic assessment of the system should be conducted and possible use cases should be developed.

References

[1] V.R. Lebaka, Potential bioresources as future sources of biofuels production: An overview, in: Biofuel Technologies: Recent Developments, Springer-Verlag Berlin Heidelberg, 2013: pp. 223–258. https://doi.org/10.1007/978-3-642-34519-7_9.

[2] P. Lauri, P. Havlík, G. Kindermann, N. Forsell, H. Böttcher, M. Obersteiner, Woody biomass energy potential in 2050, Energy Policy 66 (2014) 19–31. https://doi.org/10.1016/j.enpol.2013.11.033.

[3] M. Kaltschmitt, H. Hartmann, H. Hofbauer, Energie aus Biomasse, 2nd ed., Springer Berlin Heidelberg, Heidelberg, Germany, 2009. https://doi.org/10.1007/978-3-540-85095-3.

[4] K. Srirangan, L. Akawi, M. Moo-Young, C.P. Chou, Towards sustainable production of clean energy carriers from biomass resources, Appl. Energy 100 (2012) 172–186. https://doi.org/10.1016/j.apenergy.2012.05.012.

[5] A. Tursi, A review on biomass: Importance, chemistry, classification, and conversion, Biofuel Research Journal 6 (2019) 962–979. https://doi.org/10.18331/BRJ2019.6.2.3.

[6] M.M. Küçük, A. Demirbaş, Biomass conversion processes, Energy Convers. Manag. 38 (1997) 151–165. https://doi.org/10.1016/0196-8904(96)00031-3.

[7] G. Kumar, J. Dharmaraja, S. Arvindnarayan, S. Shoban, P. Bakonyi, G.D. Saratale, N. Nemestóthy, K. Bélafi-Bakó, J.J. Yoon, S.H. Kim, A comprehensive review on thermochemical, biological, biochemical and hybrid conversion methods of bio-derived lignocellulosic molecules into renewable fuels, Fuel 251 (2019) 352–367. https://doi.org/10.1016/j.fuel.2019.04.049.

[8] A.I. Osman, N. Mehta, A.M. Elgarahy, A. Al-Hinai, A.H. Al-Muhtaseb, D.W. Rooney, Conversion of biomass to biofuels and life cycle assessment: a review, Environ. Chem. Lett. 19 (2021) 4075–4118. https://doi.org/10.1007/s10311-021-01273-0.

[9] K. Liu, H.K. Atiyeh, O. Pardo-Planas, T.C. Ezeji, V. Ujor, J.C. Overton, K. Berning, M.R. Wilkins, R.S. Tanner, Butanol production from hydrothermolysis-pretreated switchgrass: Quantification of inhibitors and detoxification of hydrolyzate, Bioresour. Technol. 189 (2015) 292–301. https://doi.org/10.1016/j.biortech.2015.04.018.

[10] F. Wang, D. Ouyang, Z. Zhou, S.J. Page, D. Liu, X. Zhao, Lignocellulosic biomass as sustainable feedstock and materials for power generation and energy storage, Journal of Energy Chemistry 57 (2021) 247–280. https://doi.org/10.1016/j.jechem.2020.08.060.

[11] J. Kainthola, A.S. Kalamdhad, V. V. Goud, A review on enhanced biogas production from anaerobic digestion of lignocellulosic biomass by different enhancement techniques, Process Biochemistry 84 (2019) 81–90. https://doi.org/10.1016/j.procbio.2019.05.023.

[12] C. Weng, X. Peng, Y. Han, Depolymerization and conversion of lignin to value-added bioproducts by microbial and enzymatic catalysis, Biotechnol. Biofuels 14 (2021). https://doi.org/10.1186/s13068-021-01934-w.

[13] H.P. Vu, L.N. Nguyen, M.T. Vu, M.A.H. Johir, R. McLaughlan, L.D. Nghiem, A comprehensive review on the framework to valorise lignocellulosic biomass as biorefinery feedstocks, Science of the Total Environment 743 (2020). https://doi.org/10.1016/j.scitotenv.2020.140630.

[14] S. Guran, Thermochemical Conversion of Biomass, in: Practices and Perspectives in Sustainable Bioenergy, Springer, New Delhi, 2020: pp. 159–194. https://doi.org/10.1007/978-81-322-3965-9_8.

[15] P. Tanger, J.L. Field, C.E. Jahn, M.W. DeFoort, J.E. Leach, Biomass for thermochemical conversion: Targets and challenges, Front. Plant Sci. 4 (2013). https://doi.org/10.3389/fpls.2013.00218.

[16] H.C. Ong, W.H. Chen, Y. Singh, Y.Y. Gan, C.Y. Chen, P.L. Show, A state-of-the-art review on thermochemical conversion of biomass for biofuel production: A TG-FTIR approach, Energy Convers. Manag. 209 (2020). https://doi.org/10.1016/j.enconman.2020.112634.

[17] B.M. Jenkins, L.L. Baxter, T.R. Miles, T.R. Miles, Combustion properties of biomass, Fuel Processing Technology 54 (1998) 17–46. https://doi.org/10.1016/S0378-3820(97)00059-3.

[18] T.R. Miles, T.R. Miles, L.L. Baxter, R.W. Bryers, B.M. Jenkins, L.L. Oden, Boiler deposits from firing biomass fuels, Biomass Bioenergy 10 (1996) 125–138. https://doi.org/10.1016/0961-9534(95)00067-4.

[19] A. Kumar, D.D. Jones, M.A. Hanna, Thermochemical biomass gasification: A review of the current status of the technology, Energies (Basel). 2 (2009) 556–581. https://doi.org/10.3390/en20300556.

[20] A. Kruse, A. Funke, M.M. Titirici, Hydrothermal conversion of biomass to fuels and energetic materials, Curr. Opin. Chem. Biol. 17 (2013) 515–521. https://doi.org/10.1016/j.cbpa.2013.05.004.

[21] S. Carrasco, J. Silva, E. Pino-Cortés, J. Gómez, F. Vallejo, L. Díaz-Robles, V. Campos, F. Cubillos, S. Pelz, S. Paczkowski, F. Cereceda-Balic, A. Vergara-Fernández, M. Lapuerta, A. Pazo, E. Monedero, K. Hoekman, Experimental study on hydrothermal carbonization of lignocellulosic biomass with magnesium chloride for solid fuel production, Processes 8 (2020). https://doi.org/10.3390/PR8040444.

[22] T. Wang, Y. Zhai, Y. Zhu, C. Li, G. Zeng, A review of the hydrothermal carbonization of biomass waste for hydrochar formation: Process conditions, fundamentals, and physicochemical properties, Renewable and Sustainable Energy Reviews 90 (2018) 223–247. https://doi.org/10.1016/j.rser.2018.03.071.

[23] F. Veltri, F. Alessandro, A. Scarcello, A. Beneduci, M.A. Polanco, D.C. Perez, C.V. Gomez, A. Tavolaro, G. Giordano, L.S. Caputi, Porous carbon materials obtained by the hydrothermal carbonization of orange juice, Nanomaterials 10 (2020). https://doi.org/10.3390/nano10040655.

[24] H.A. Ruiz, M. Galbe, G. Garrote, D.M. Ramirez-Gutierrez, E. Ximenes, S.N. Sun, D. Lachos-Perez, R.M. Rodríguez-Jasso, R.C. Sun, B. Yang, M.R. Ladisch, Severity factor kinetic model as a strategic parameter of hydrothermal processing (steam explosion and liquid hot water) for biomass fractionation under biorefinery

concept, Bioresour. Technol. 342 (2021). https://doi.org/10.1016/j.biortech.2021.125961.

[25] W.T. Chen, M.A. Haque, T. Lu, A. Aierzhati, G. Reimonn, A perspective on hydrothermal processing of sewage sludge, Curr. Opin. Environ. Sci. Health 14 (2020) 63–73. https://doi.org/10.1016/j.coesh.2020.02.008.

[26] L. Wang, Y. Chang, A. Li, Hydrothermal carbonization for energy-efficient processing of sewage sludge: A review, Renewable and Sustainable Energy Reviews 108 (2019) 423–440. https://doi.org/10.1016/j.rser.2019.04.011.

[27] N. Stobernack, F. Mayer, C. Malek, R. Bhandari, Evaluation of the energetic and environmental potential of the hydrothermal carbonization of biowaste: Modeling of the entire process chain, Bioresour. Technol. 318 (2020). https://doi.org/10.1016/j.biortech.2020.124038.

[28] S.S. Toor, Modelling and Optimization of Catliq® Liquid Biofuel Process, Dissertation, Aalborg University, 2010.

[29] S. Nagappan, R.R. Bhosale, D.D. Nguyen, N.T.L. Chi, V.K. Ponnusamy, C.S. Woong, G. Kumar, Catalytic hydrothermal liquefaction of biomass into bio-oils and other value-added products – A review, Fuel 285 (2021). https://doi.org/10.1016/j.fuel.2020.119053.

[30] S.S. Toor, L. Rosendahl, A. Rudolf, Hydrothermal liquefaction of biomass: A review of subcritical water technologies, Energy 36 (2011) 2328–2342. https://doi.org/10.1016/j.energy.2011.03.013.

[31] Y.H. Xu, M.F. Li, Hydrothermal liquefaction of lignocellulose for value-added products: Mechanism, parameter and production application, Bioresour. Technol. 342 (2021). https://doi.org/10.1016/j.biortech.2021.126035.

[32] A. Kruse, Hydrothermal biomass gasification, J Supercrit Fluids 47 (2009) 391–399. https://doi.org/10.1016/j.supflu.2008.10.009.

[33] H. Ali, E. Khan, M.A. Sajad, Phytoremediation of heavy metals-Concepts and applications, Chemosphere 91 (2013) 869–881. https://doi.org/10.1016/j.chemosphere.2013.01.075.

[34] S. Khan, Q. Cao, Y.M. Zheng, Y.Z. Huang, Y.G. Zhu, Health risks of heavy metals in contaminated soils and food crops irrigated with wastewater in Beijing, China, Environmental Pollution 152 (2008) 686–692. https://doi.org/10.1016/j.envpol.2007.06.056.

[35] M.K. Zhang, Z.Y. Liu, H. Wang, Use of single extraction methods to predict bioavailability of heavy metals in polluted soils to rice, Commun. Soil Sci. Plant Anal. 41 (2010) 820–831. https://doi.org/10.1080/00103621003592341.

[36] S. Zahermand, M. Vafaeian, M.H. Bazyar, Analysis of the physical and chemical properties of soil contaminated with oil (Petroleum) hydrocarbons, Earth Sciences Research Journal 24 (2020) 161–166. https://doi.org/10.15446/esrj.v24n2.76217.

[37] B.E. Richter, Extraction of hydrocarbon contamination from soils using accelerated solvent extraction, J. Chromatogr. A 874 (2000) 217–224. https://doi.org/10.1016/S0021-9673(00)00073-X.

[38] T. Castelo-Grande, P.A. Augusto, P. Monteiro, A.M. Estevez, D. Barbosa, Remediation of soils contaminated with pesticides: A review, Int. J. Environ. Anal. Chem. 90 (2010) 438–467. https://doi.org/10.1080/03067310903374152.

[39] P. Sharma, S. Pandey, Status of Phytoremediation in World Scenario, Int. J. Environ. Bioremediat. Biodegrad. 2 (2014) 178–191. https://doi.org/10.12691/ijebb-2-4-5.

[40] A. Grzegórska, P. Rybarczyk, A. Rogala, D. Zabrocki, Phytoremediation-from environment cleaning to energy generation-current status and future perspectives, Energies (Basel). 13 (2020). https://doi.org/10.3390/en13112905.

[41] R.L. Chaney, M. Malik, Y.M. Li, S.L. Brown, E.P. Brewer, J.S. Angle, A.J. Baker, Phytoremediation of soil metals, Curr. Opin. Biotechnol. 8 (1997) 279–284. https://doi.org/10.1016/S0958-1669(97)80004-3.

[42] D.E. Salt, M. Blaylock, N.P.B.A. Kumar, V. Dushenkov, B.D. Ensley, I. Chet, I. Raskin, Phytoremediation: A Novel Strategy for the Removal of Toxic Metals from the Environment Using Plants, Nat. Biotechnol. 13 (1995) 468–474. https://doi.org/10.1038/nbt0595-468.

[43] K.E. Gerhardt, X.D. Huang, B.R. Glick, B.M. Greenberg, Phytoremediation and rhizoremediation of organic soil contaminants: Potential and challenges, Plant Science 176 (2009) 20–30. https://doi.org/10.1016/j.plantsci.2008.09.014.

[44] E. Pilon-Smits, Phytoremediation, Annu. Rev. Plant Biol. 56 (2005) 15–39. https://doi.org/10.1146/annurev.arplant.56.032604.144214.

[45] A. Kafle, A. Timilsina, A. Gautam, K. Adhikari, A. Bhattarai, N. Aryal, Phytoremediation: Mechanisms, plant selection and enhancement by natural and synthetic agents, Environmental Advances 8 (2022). https://doi.org/10.1016/j.envadv.2022.100203.

[46] S. Trapp, U. Karlson, Aspects of Phytoremediation of Organic Pollutants, J. Soils & Sediments 1 (2001) 37–43. https://doi.org/https://doi.org/10.1007/BF02986468.

[47] D. Zand, A. Professor, Plant-Aid Remediation of Hydrocarbon-Contaminated Sites, Pollution 2 (2016) 233–246. https://doi.org/10.7508/pj.2016.03.001.

[48] S. Muthusaravanan, N. Sivarajasekar, J.S. Vivek, T. Paramasivan, M. Naushad, J. Prakashmaran, V. Gayathri, O.K. Al-Duaij, Phytoremediation of heavy metals: mechanisms, methods and enhancements, Environ. Chem. Lett. 16 (2018) 1339–1359. https://doi.org/10.1007/s10311-018-0762-3.

[49] A. Yan, Y. Wang, S.N. Tan, M.L. Mohd Yusof, S. Ghosh, Z. Chen, Phytoremediation: A Promising Approach for Revegetation of Heavy Metal-Polluted Land, Front. Plant Sci. 11 (2020). https://doi.org/10.3389/fpls.2020.00359.

[50] J. Pichtel, Oil and gas production wastewater: Soil contamination and pollution prevention, Appl. Environ. Soil Sci. 2016 (2016). https://doi.org/10.1155/2016/2707989.

[51] V. Sheoran, A.S. Sheoran, P. Poonia, Factors Affecting Phytoextraction: A Review, Pedosphere 26 (2016) 148–166. https://doi.org/10.1016/S1002-0160(15)60032-7.

[52] P. Zhuang, Q.W. Yang, H.B. Wang, W.S. Shu, Phytoextraction of heavy metals by eight plant species in the field, Water Air Soil Pollut. 184 (2007) 235–242. https://doi.org/10.1007/s11270-007-9412-2.

[53] C.Y. Poynton, J.W. Huang, M.J. Blaylock, L. V. Kochian, M.P. Elless, Mechanisms of arsenic hyperaccumulation in Pteris species: Root As influx and translocation, Planta 219 (2004) 1080–1088. https://doi.org/10.1007/s00425-004-1304-8.

[54] L. Yuan, X. Zhong, J. Liao, L. Zheng, X. Huang, Efficient phytoremediation of Cd-contaminated soils by Tagetes patula L.: Greenhouse experiment, field study and meta-analysis, Curr. Res. Biotechnol. 7 (2024). https://doi.org/10.1016/j.crbiot.2024.100212.

[55] B.H. Robinson, A. Chiarucci, R.R. Brooks, D. Petit, J.H. Kirkman, P.E.H. Gregg, V. De Dominicis, The nickel hyperaccumulator plant Alyssum bertolonii as a potential agent for phytoremediation and phytomining of nickel, J. Geochem. Explor. 59 (1997) 75–86. https://doi.org/10.1016/S0375-6742(97)00010-1.

[56] W. Su, P. Liu, C. Cai, H. Ma, B. Jiang, Y. Xing, Y. Liang, L. Cai, C. Xia, Q. Van Le, C. Sonne, S.S. Lam, Hydrogen production and heavy metal immobilization using hyperaccumulators in supercritical water gasification, J. Hazard. Mater. 402 (2021) 123541. https://doi.org/10.1016/j.jhazmat.2020.123541.

[57] W. Su, M. Zhao, Y. Xing, H. Ma, P. Liu, X. Li, H. Zhang, Y. Wu, C. Xia, Supercritical water gasification of hyperaccumulators for hydrogen production and heavy metal immobilization with alkali metal catalysts, Environ. Res. 214 (2022) 114093. https://doi.org/10.1016/j.envres.2022.114093.

[58] G. Chen, X. Yang, S. Chen, Y. Dong, L. Cui, Y. Zhang, P. Wang, X. Zhao, C. Ma, Transformation of heavy metals in lignite during supercritical water gasification, Appl. Energy 187 (2017) 272–280. https://doi.org/10.1016/j.apenergy.2016.11.054.

[59] O. Sawai, T. Nunoura, K. Yamamoto, Supercritical water gasification of sewage sludge using bench-scale batch reactor: Advantages and drawbacks, J. Mater. Cycles Waste Manag. 16 (2014) 82–92. https://doi.org/10.1007/s10163-013-0144-7.

[60] J. Lin, S. Sun, C. Cui, R. Ma, L. Fang, P. Zhang, Z. Quan, X. Song, J. Yan, J. Luo, Hydrogen-rich bio-gas generation and optimization in relation to heavy

metals immobilization during Pd-catalyzed supercritical water gasification of sludge, Energy 189 (2019) 116296. https://doi.org/10.1016/j.energy.2019.116296.

[61] L. Li, W. Cao, G. Wang, P. Peng, S. Liu, H. Jin, W. Wei, L. Guo, Experimental and kinetic study of heavy metals transformation in supercritical water gasification of oily sludge, J. Clean. Prod. 373 (2022) 133898. https://doi.org/10.1016/j.jclepro.2022.133898.

[62] CERESiS, CERESiS Website, (2024). https://ceresis.eu/ (accessed March 14, 2024).

[63] C. Bezerra Silva, M. Lugo-Pimentel, C.M. Ceballos, J.M. Lavoie, Effect of the Reactor Material on the Reforming of Primary Syngas, Molecules 29 (2024). https://doi.org/10.3390/molecules29215126.

[64] A. Kruse, E. Dinjus, Hot compressed water as reaction medium and reactant. Properties and synthesis reactions, J Supercrit Fluids 39 (2007) 362–380. https://doi.org/10.1016/j.supflu.2006.03.016.

[65] S. Nanda, S.N. Reddy, D.N. Vo, B.N. Sahoo, J.A. Kozinski, Catalytic gasification of wheat straw in hot compressed (subcritical and supercritical) water for hydrogen production, Energy Sci. Eng. 6 (2018) 448–459. https://doi.org/10.1002/ese3.219.

[66] Y.J. Lu, L.J. Guo, C.M. Ji, X.M. Zhang, X.H. Hao, Q.H. Yan, Hydrogen production by biomass gasification in supercritical water: A parametric study, Int. J. Hydrogen Energy 31 (2006) 822–831. https://doi.org/10.1016/j.ijhydene.2005.08.011.

[67] R.F. Susanti, B. Veriansyah, J.D. Kim, J. Kim, Y.W. Lee, Continuous supercritical water gasification of isooctane: A promising reactor design, Int. J. Hydrogen Energy 35 (2010) 1957–1970. https://doi.org/10.1016/j.ijhydene.2009.12.157.

[68] M. Schubert, Catalytic hydrothermal gasification of biomass salt recovery and continuous gasification of glycerol solutions, Dissertation, ETH Zürich, 2010. https://doi.org/10.3929/ethz-a-006212308.

[69] M. Schubert, J.W. Regler, F. Vogel, Continuous salt precipitation and separation from supercritical water. Part 1: Type 1 salts, J Supercrit Fluids 52 (2010) 99–112. https://doi.org/10.1016/j.supflu.2009.10.002.

[70] N. Boukis, U. Galla, Vorrichtung und Verfahren zur Abscheidung von anorganischen Feststoffen aus einer wässrigen Lösung, DE 10 2005 037 469 B4, 2008.

[71] S. Wang, D. Xu, Y. Guo, X. Tang, Y. Wang, J. Zhang, H. Ma, L. Qian, Y. Li, Supercritical Water Processing Technologies for Environment, Energy and Nanomaterial Applications, Springer Singapore, Singapore, 2020. https://doi.org/10.1007/978-981-13-9326-6.

[72] N.Y. Acelas, D.P. López, D.W.F. (Wim) Brilman, S.R.A. Kersten, A.M.J. Kootstra, Supercritical water gasification of sewage sludge: Gas production and phosphorus recovery, Bioresour. Technol. 174 (2014) 167–175. https://doi.org/10.1016/j.biortech.2014.10.003.

[73] N. Boukis, I.K. Stoll, J. Sauer, J. Fischer, R. Kansy, Separation of salts during the gasification of spent grain in supercritical water, in: 25th European Biomass Conference and Exhibition, Stockholm, Sweden, 2017.

[74] S. Nanda, A.K. Dalai, I. Gökalp, J.A. Kozinski, Valorization of horse manure through catalytic supercritical water gasification, Waste Management 52 (2016) 147–158. https://doi.org/10.1016/j.wasman.2016.03.049.

[75] T. Yanagida, T. Minowa, A. Nakamura, Y. Matsumura, Y. Noda, Behavior of Inorganic Elements in Poultry Manure during Supercritical Water Gasification, Journal of the Japan Institute of Energy 86 (2007) 731–736.

[76] W. Wagner, A. Pruß, The IAPWS formulation 1995 for the thermodynamic properties of ordinary water substance for general and scientific use, J. Phys. Chem. Ref. Data 31 (2002) 387–535. https://doi.org/10.1063/1.1461829.

[77] J.M.H.L. Sengers, J. Straub, K. Watanabe, P.G. Hill, Assessment of Critical Parameter Values for H2O and D2O, J. Phys. Chem. Ref. Data 14 (1985) 193–207. https://doi.org/10.1063/1.555746.

[78] A. Loppinet-Serani, C. Aymonier, F. Cansell, Current and foreseeable applications of supercritical water for energy and the environment, ChemSusChem 1 (2008) 486–503. https://doi.org/10.1002/cssc.200700167.

[79] J.B. Gadhe, R.B. Gupta, Hydrogen production by methanol reforming in supercritical water: Suppression of methane formation, Ind. Eng. Chem. Res. 44 (2005) 4577–4585. https://doi.org/10.1021/ie049268f.

[80] C. Rodriguez Correa, A. Kruse, Supercritical water gasification of biomass for hydrogen production – Review, J. Supercrit. Fluids 133 (2018) 573–590. https://doi.org/10.1016/j.supflu.2017.09.019.

[81] H. Weingärtner, E.U. Franck, Überkritisches Wasser als Lösungsmittel, Angewandte Chemie 117 (2005) 2730–2752. https://doi.org/10.1002/ange.200462468.

[82] O. Yakaboylu, J. Harinck, K.G. Smit, W. de Jong, Supercritical water gasification of biomass: A literature and technology overview, Energies (Basel). 8 (2015) 859–894. https://doi.org/10.3390/en8020859.

[83] A. Kruse, Supercritical water gasification, Biofuels, Bioproducts and Biorefining 2 (2008) 415–437. https://doi.org/10.1002/bbb.93.

[84] F.J. Armellini, Phase equilibria and precipitation phenomena of sodium chloride and sodium, Dissertation, Massachusetts Institute of Technology, 1993.

[85] V.M. Valyashko, Phase behavior in binary and ternary water-salt systems at high temperatures and pressures, Pure and Applied Chemistry 69 (1997) 2271–2280. https://doi.org/10.1351/pac199769112271.

[86] P. D'Jesús, N. Boukis, B. Kraushaar-Czarnetzki, E. Dinjus, Gasification of corn and clover grass in supercritical water, Fuel 85 (2006) 1032–1038. https://doi.org/10.1016/j.fuel.2005.10.022.

[87] S.N. Reddy, S. Nanda, A.K. Dalai, J.A. Kozinski, Supercritical water gasification of biomass for hydrogen production, Int. J. Hydrogen Energy 39 (2014) 6912–6926. https://doi.org/10.1016/j.ijhydene.2014.02.125.

[88] T. Sato, S. Kurosawa, R.L. Smith, T. Adschiri, K. Arai, Water gas shift reaction kinetics under noncatalytic conditions in supercritical water, J. Supercrit. Fluids 29 (2004) 113–119. https://doi.org/10.1016/S0896-8446(03)00049-4.

[89] P. D'Jesús, Die Vergasung von realer Biomasse in überkritischem Wasser, Dissertation, Universität Karlsruhe, 2007.

[90] Y. Zhiyong, T. Xiuyi, Hydrogen generation from oily wastewater via supercritical water gasification (SCWG), Journal of Industrial and Engineering Chemistry 23 (2015) 44–49. https://doi.org/10.1016/j.jiec.2014.07.040.

[91] N. Boukis, V. Diem, W. Habicht, E. Dinjus, Methanol reforming in supercritical water, Ind. Eng. Chem. Res. 42 (2003) 728–735. https://doi.org/10.1021/ie020557i.

[92] P. D'Jesús, N. Boukis, B. Kraushaar-Czarnetzki, E. Dinjus, Influence of process variables on gasification of corn silage in supercritical water, Ind. Eng. Chem. Res. 45 (2006) 1622–1630. https://doi.org/10.1021/ie050367i.

[93] K. Kang, R. Azargohar, A.K. Dalai, H. Wang, Noncatalytic Gasification of Lignin in Supercritical Water Using a Batch Reactor for Hydrogen Production: An Experimental and Modeling Study, Energy & Fuels 29 (2015) 1776–1784. https://doi.org/10.1021/ef5027345.

[94] Z. Liu, Hydrogen production for fuel cells through methane reforming at low temperatures, J. Power Sources 111 (2002) 283–287. https://doi.org/10.1016/S0378-7753(02)00317-8.

[95] J. Gao, Y. Wang, Y. Ping, D. Hu, G. Xu, F. Gu, F. Su, A thermodynamic analysis of methanation reactions of carbon oxides for the production of synthetic natural gas, RSC Adv. 2 (2012) 2358–2368. https://doi.org/10.1039/c2ra00632d.

[96] A.J. Byrd, K.K. Pant, R.B. Gupta, Hydrogen production from ethanol by reforming in supercritical water using Ru/Al2O3 catalyst, Energy and Fuels 21 (2007) 3541–3547. https://doi.org/10.1021/ef700269z.

[97] S. Guo, L. Guo, C. Cao, J. Yin, Y. Lu, X. Zhang, Hydrogen production from glycerol by supercritical water gasification in a continuous flow tubular reactor, Int. J.

Hydrogen Energy 37 (2012) 5559–5568. https://doi.org/10.1016/j.ijhydene.2011.12.135.

[98] A.G. Chakinala, D.W.F. (Wim) Brilman, W.P.M. van Swaaij, S.R.A. Kersten, Catalytic and Non-catalytic Supercritical Water Gasification of Microalgae and Glycerol, Ind. Eng. Chem. Res. 49 (2010) 1113–1122. https://doi.org/10.1021/ie9008293.

[99] O. Yakaboylu, Supercritical Water Gasification of Wet Biomass: Modeling and Experiments, Dissertation, Technische Universiteit Delft, 2016.

[100] L.J. Guo, Y.J. Lu, X.M. Zhang, C.M. Ji, Y. Guan, A.X. Pei, Hydrogen production by biomass gasification in supercritical water: A systematic experimental and analytical study, Catal. Today 129 (2007) 275–286. https://doi.org/10.1016/j.cattod.2007.05.027.

[101] M. Modell, R.C. Reid, S.I. Amin, Gasification Process, 4,113,446, 1978.

[102] N. Boukis, U. Galla, P. D´Jesus, H. Müller, E. Dinjus, Gasification of wet biomass in supercritical water. Results of pilot plant experiments, in: 14th European Biomass Conference, Paris, France, 2005.

[103] Y. Matsumura, S. Inoue, T. Inoue, Y. Kawai, T. Noguchi, H. Tanigawa, Final report on the pilot plant operation for supercritical water gasification of wet biomass, IOP Conf. Ser. Earth Environ. Sci. 460 (2020) 012019. https://doi.org/10.1088/1755-1315/460/1/012019.

[104] O. Yakaboylu, I. Albrecht, J. Harinck, K.G. Smit, G.A. Tsalidis, M. Di Marcello, K. Anastasakis, W. de Jong, Supercritical water gasification of biomass in fluidized bed: First results and experiences obtained from TU Delft/Gensos semi-pilot scale setup, Biomass Bioenergy 111 (2018) 330–342. https://doi.org/10.1016/j.biombioe.2016.12.007.

[105] A. Kruse, T. Henningsen, A. Smag, J. Pfeiffer, Biomass gasification in supercritical water: Influence of the dry matter content and the formation of phenols, Ind. Eng. Chem. Res. 42 (2003) 3711–3717. https://doi.org/10.1021/ie0209430.

[106] A. Sınag, A. Kruse, J. Rathert, Influence of the Heating Rate and the Type of Catalyst on the Formation of Key Intermediates and on the Generation of Gases

During Hydropyrolysis of Glucose in Supercritical Water in a Batch Reactor, Ind. Eng. Chem. Res. (2004). https://doi.org/10.1021/ie030475.

[107] F. Ruiz-Jorge, J.R. Portela, J. Sánchez-Oneto, E.J. Martínez de la Ossa, Synthesis of micro- and nanoparticles in sub- and supercritical water: From the laboratory to larger scales, Applied Sciences 10 (2020) 5508. https://doi.org/10.3390/app10165508.

[108] N. Boukis, I.K. Stoll, Gasification of biomass in supercritical water, challenges for the process design—lessons learned from the operation experience of the first dedicated pilot plant, Processes 9 (2021) 1–17. https://doi.org/10.3390/pr9030455.

[109] D. Castello, Supercritical Water Gasification of Biomass, Dissertation, University of Trento, 2013.

[110] H. Jin, Y. Chen, Z. Ge, S. Liu, C. Ren, L. Guo, Hydrogen production by Zhundong coal gasification in supercritical water, Int. J. Hydrogen Energy 40 (2015) 16096–16103. https://doi.org/10.1016/j.ijhydene.2015.09.003.

[111] M. Hodes, P.A. Marrone, G.T. Hong, K.A. Smith, J.W. Tester, Salt precipitation and scale control in supercritical water oxidation - Part A: Fundamentals and research, Journal of Supercritical Fluids 29 (2004) 265–288. https://doi.org/10.1016/S0896-8446(03)00093-7.

[112] N. Boukis, E. Hauer, W. Habicht, Corrosion Behaviour of Ni-Base Alloys in Supercritical Water Containing Alkali Chlorides., in: EUROCORR 2013, Estoril, Portugal, 2013.

[113] J. Dutzi, N. Boukis, J. Sauer, Process Effluent Recycling in the Supercritical Water Gasification of Dry Biomass, Processes 11 (2023) 797. https://doi.org/10.3390/pr11030797.

[114] J. Dutzi, N. Boukis, J. Sauer, Supercritical water gasification of heavy metal contaminated plants with focus on separation of heavy metal contaminants, Biomass Bioenergy 182 (2024) 107059. https://doi.org/10.1016/j.biombioe.2024.107059.

[115] A. Chuntanapum, Y. Matsumura, Char formation mechanism in supercritical water gasification process: A study of model compounds, Ind. Eng. Chem. Res. 49 (2010) 4055–4062. https://doi.org/10.1021/ie901346h.

[116] T. Karayıldırım, A. Sınağ, A. Kruse, Char and Coke Formation as Unwanted Side Reaction of the Hydrothermal Biomass Gasification, Chem. Eng. Technol. 31 (2008) 1561–1568. https://doi.org/10.1002/ceat.200800278.

[117] T.L.-K. Yong, Y. Matsumura, Reaction Kinetics of the Lignin Conversion in Supercritical Water, Ind. Eng. Chem. Res. 51 (2012) 11975–11988. https://doi.org/10.1021/ie300921d.

[118] A. Kruse, M. Faquir, Hydrothermal Biomass Gasification – Effects of Salts, Backmixing and Their Interaction, Chem. Eng. Technol. 30 (2007) 749–754. https://doi.org/10.1002/ceat.200600409.

[119] Y. Matsumura, M. Harada, K. Nagata, Y. Kikuchi, Effect of heating rate of biomass feedstock on carbon gasification efficiency in supercritical water gasification, Chem. Eng. Commun. 193 (2006) 649–659. https://doi.org/10.1080/00986440500440157.

[120] A. Sinag, A. Kruse, J. Rathert, Influence of the Heating Rate and the Type of Catalyst on the Formation of Key Intermediates and on the Generation of Gases During Hydropyrolysis of Glucose in Supercritical Water in a Batch Reactor, Ind. Eng. Chem. Res. 43 (2004) 502–508. https://doi.org/10.1021/ie030475+.

[121] F.J. Gutiérrez Ortiz, Biofuel production from supercritical water gasification of sustainable biomass, Energy Conversion and Management: X 14 (2022) 100164. https://doi.org/10.1016/j.ecmx.2021.100164.

[122] J.O. Nriagu, Global inventory of natural and anthropogenic emissions of trace metals to the atmosphere, Nature 279 (1979) 409–411. https://doi.org/10.1038/279409a0.

[123] C. Baskar, S. Baskar, S. Dhillion, Biomass Conversion, Springer Berlin Heidelberg, Berlin, Heidelberg, 2012. https://doi.org/10.1007/978-3-642-28418-2.

[124] H. Jiang, R. Yan, C. Cai, X. Chen, F. Zhao, L. Fan, C.C. Xu, W. Yang, Hydrothermal liquefaction of Cd-enriched Amaranthus hypochondriacus L. in ethanol–

water co-solvent: Focus on low-N bio-oil and heavy metal/metal-like distribution, Fuel 303 (2021) 121235. https://doi.org/10.1016/j.fuel.2021.121235.

[125] X. Zhu, F. Qian, C. Zhou, L. Li, Q. Shi, S. Zhang, J. Chen, Inherent Metals of a Phytoremediation Plant Influence Its Recyclability by Hydrothermal Liquefaction, Environ. Sci. Technol. 53 (2019) 6580–6586. https://doi.org/10.1021/acs.est.9b00262.

[126] J. Li, J. Chen, S. Chen, Supercritical water treatment of heavy metal and arsenic metalloid-bioaccumulating-biomass, Ecotoxicol. Environ. Saf. 157 (2018) 102–110. https://doi.org/10.1016/j.ecoenv.2018.03.069.

[127] M. Carrier, A. Loppinet-Serani, C. Absalon, F. Marias, C. Aymonier, M. Mench, Conversion of fern (Pteris vittata L.) biomass from a phytoremediation trial in sub- and supercritical water conditions, Biomass Bioenergy 35 (2011) 872–883. https://doi.org/10.1016/j.biombioe.2010.11.007.

[128] W. Shi, C. Liu, D. Ding, Z. Lei, Y. Yang, C. Feng, Z. Zhang, Immobilization of heavy metals in sewage sludge by using subcritical water technology, Bioresour. Technol. 137 (2013) 18–24. https://doi.org/10.1016/j.biortech.2013.03.106.

[129] N. Boukis, U. Galla, H. Müller, E. Dinjus, Biomass Gasification in Supercritical Water., in: 15th European Biomass Conference & Exhibition, Berlin, Germany, 2007.

[130] P.R. Rout, D.S. Pandey, M. Haynes-Parry, C. Briggs, H.L.C. Manuel, R. Umapathi, S. Mukherjee, S. Panigrahi, M. Goel, Sustainable Valorisation of Animal Manures via Thermochemical Conversion Technologies: An Inclusive Review on Recent Trends, Waste Biomass Valorization 14 (2023) 553–582. https://doi.org/10.1007/s12649-022-01916-5.

[131] N. Boukis, U. Galla, Verfahren zur hydrothermalen Vergasung von Biomasse in überkritischem Wasser, DE 10 2006 044 116 B3, 2008.

[132] D. Castello, A. Kruse, L. Fiori, Supercritical water gasification of glucose/phenol mixtures as model compounds for ligno-cellulosic biomass, Chem. Eng. Trans. 37 (2014) 193–198. https://doi.org/10.3303/CET1437033.

[133] M. Yan, Y. Liu, Y. Song, A. Xu, G. Zhu, J. Jiang, D. Hantoko, Comprehensive experimental study on energy conversion of household kitchen waste via integrated hydrothermal carbonization and supercritical water gasification, Energy 242 (2022) 123054. https://doi.org/10.1016/j.energy.2021.123054.

[134] J.A. Okolie, R. Rana, S. Nanda, A.K. Dalai, J.A. Kozinski, Supercritical water gasification of biomass: A state-of-the-art review of process parameters, reaction mechanisms and catalysis, Sustain. Energy Fuels 3 (2019) 578–598. https://doi.org/10.1039/c8se00565f.

[135] S. Nanda, S.N. Reddy, H.N. Hunter, A.K. Dalai, J.A. Kozinski, Supercritical water gasification of fructose as a model compound for waste fruits and vegetables, J Supercrit Fluids 104 (2015) 112–121. https://doi.org/10.1016/j.supflu.2015.05.009.

[136] R.A. Lord, Reed canary grass (Phalaris arundinacea) outperforms Miscanthus or willow on marginal soils, brownfield and non-agricultural sites for local, sustainable energy crop production, Biomass Bioenergy 78 (2015) 110–125. https://doi.org/10.1016/j.biombioe.2015.04.015.

[137] A. Sinag, A. Kruse, V. Schwarzkopf, Key compounds of the hydropyrolysis of glucose in supercritical water in the presence of K2CO3, Ind. Eng. Chem. Res. 42 (2003) 3516–3521. https://doi.org/10.1021/ie030079r.

[138] Z. Zhu, S.S. Toor, L. Rosendahl, D. Yu, G. Chen, Influence of alkali catalyst on product yield and properties via hydrothermal liquefaction of barley straw, Energy 80 (2015) 284–292. https://doi.org/10.1016/j.energy.2014.11.071.

[139] K. Saritpongteeraka, J. Kaewsung, B. Charnnok, S. Chaiprapat, Comparing low-temperature hydrothermal pretreatments through convective heating versus microwave heating for napier grass digestion, Processes 8 (2020) 1–16. https://doi.org/10.3390/pr8101221.

[140] T. Zheng, K. Zhang, X. Chen, Y. Ma, B. Xiao, J. Liu, Effects of low- and high-temperature thermal-alkaline pretreatments on anaerobic digestion of waste activated sludge, Bioresour. Technol. 337 (2021). https://doi.org/10.1016/j.biortech.2021.125400.

[141] B. Dokbua, N. Waramit, J. Chaugool, C. Thongjoo, Biomass Productivity, Developmental Morphology, and Nutrient Removal Rate of Hybrid Napier Grass (Pennisetum purpureum x Pennisetum americanum) in Response to Potassium and Nitrogen Fertilization in a Multiple-Harvest System, Bioenergy Res. 14 (2021) 1106–1117. https://doi.org/10.1007/s12155-020-10212-w.

[142] I.Y. Mohammed, Y.A. Abakr, F.K. Kazi, S. Yusup, I. Alshareef, S.A. Chin, Comprehensive characterization of Napier grass as a feedstock for thermochemical conversion, Energies (Basel). 8 (2015) 3403–3417. https://doi.org/10.3390/en8053403.

[143] O. Yakaboylu, I. Albrecht, J. Harinck, K.G. Smit, G.-A. Tsalidis, M. Di Marcello, K. Anastasakis, W. de Jong, Supercritical water gasification of biomass in fluidized bed: First results and experiences obtained from TU Delft/Gensos semi-pilot scale setup, Biomass Bioenergy 111 (2018) 330–342. https://doi.org/10.1016/j.biombioe.2016.12.007.

[144] L.J. Sealock, D.C. Elliott, E.G. Baker, R.S. Butner, Chemical processing in high-pressure aqueous environments. 1. Historical perspective and continuing developments, Ind. Eng. Chem. Res. 32 (1993) 1535–1541. https://doi.org/10.1021/ie00020a001.

[145] P. Kritzer, N. Boukis, E. Dinjus, Factors controlling corrosion in high-temperature aqueous solutions: a contribution to the dissociation and solubility data influencing corrosion processes, Journal of Supercritical Fluids 15 (1999) 205–227.

[146] N. Boukis, W. Habicht, E. Hauer, K. Weiss, E. Dinjus, Corrosion behavior of Ni-base alloys and stainless steels in supercritical water containing potassium hydrogen carbonate., in: EUROCORR 2008, Edinburgh, UK, 2008.

[147] U. Ekpo, A.B. Ross, M.A. Camargo-Valero, P.T. Williams, A comparison of product yields and inorganic content in process streams following thermal hydrolysis and hydrothermal processing of microalgae, manure and digestate, Bioresour. Technol. 200 (2016) 951–960. https://doi.org/10.1016/j.biortech.2015.11.018.

[148] L. Zhao, J. Zhang, C.D. Sheng, K. Wang, Q.Z. Ding, Dissolution characteristics of inorganic elements existing in biomass during the supercritical water

gasification process, Energy Sources, Part A: Recovery, Utilization and Environmental Effects 34 (2012) 1893–1900. https://doi.org/10.1080/15567036.2011.592913.

[149] G. Chen, J. Andries, Z. Luo, H. Spliethoff, Biomass pyrolysis/gasification for product gas production: the overall investigation of parametric effects, Energy Convers. Manag. 44 (2003) 1875–1884. https://doi.org/10.1016/S0196-8904(02)00188-7.

[150] M. Tushar, A. Dutta, C. Xu, M. Tushar, A. Dutta, C. Xu, Effects of Reactor Wall Properties, Operating Conditions and Challenges for SCWG of Real Wet Biomass, Biofuels and Biorefineries 2 (2014). https://doi.org/10.1007/978-94-017-8923-3__8.

[151] Egon. Wiberg, Nils. Wiberg, Lehrbuch der anorganischen Chemie, Walter de Gruyter, 2007.

[152] V.C. Sarasidis, J. Dutzi, P.N. Petsi, K. V. Plakas, N. Boukis, J. Sauer, Decontamination of high salinity supercritical water gasification wastewater by an integrated electrocoagulation / electrochemical oxidation process, J. Environ. Chem. Eng. 13 (2025) 118491. https://doi.org/10.1016/j.jece.2025.118491.

[153] S. Nanda, M. Gong, H.N. Hunter, A.K. Dalai, I. Gökalp, J.A. Kozinski, An assessment of pinecone gasification in subcritical, near-critical and supercritical water, Fuel Processing Technology 168 (2017) 84–96. https://doi.org/10.1016/j.fuproc.2017.08.017.

[154] C. Wang, M. Du, H. Feng, H. Jin, Experimental investigation on biomass gasification mechanism in supercritical water for poly-generation of hydrogen-rich gas and biochar, Fuel 319 (2022) 123809. https://doi.org/10.1016/j.fuel.2022.123809.

[155] A.J. Romero-Anaya, M. Ouzzine, M.A. Lillo-Ródenas, A. Linares-Solano, Spherical carbons: Synthesis, characterization and activation processes, Carbon N. Y. 68 (2014) 296–307. https://doi.org/10.1016/j.carbon.2013.11.006.

[156] T. Mwenya, H. Fan, H. Dai, M. Li, The detailed evolution of carbon spheres by hydrothermal method, International Journal of Photoenergy 2016 (2016). https://doi.org/10.1155/2016/9057418.

[157] X. Sun, Y. Li, Hollow carbonaceous capsules from glucose solution, J. Colloid Interface Sci. 291 (2005) 7–12. https://doi.org/10.1016/j.jcis.2005.04.101.

[158] X. Sun, Y. Li, Colloidal Carbon Spheres and Their Core/Shell Structures with Noble-Metal Nanoparticles, Angew. Chem. Int. Ed. 43 (2004) 597–601. https://doi.org/10.1002/anie.200352386.

[159] M. Li, W. Li, S. Liu, Hydrothermal synthesis, characterization, and KOH activation of carbon spheres from glucose, Carbohydr. Res. 346 (2011) 999–1004. https://doi.org/10.1016/j.carres.2011.03.020.

[160] V.K. Lamer, R.H. Dinegar, Theory, Production and Mechanism of Formation of Monodispersed Hydrosols, J. Am. Chem. Soc. 72 (1950) 4847–4854. https://pubs.acs.org/sharingguidelines.

[161] S. Chen, K. Tang, F. Song, Z. Liu, N. Zhang, S. Lan, X. Xie, Z. Wu, Porous hard carbon spheres derived from biomass for high-performance sodium/ potassium-ion batteries, Nanotechnology 33 (2022). https://doi.org/10.1088/1361-6528/ac317d.

[162] X. Qi, Y. Lian, L. Yan, R.L. Smith, One-step preparation of carbonaceous solid acid catalysts by hydrothermal carbonization of glucose for cellulose hydrolysis, Catal. Commun. 57 (2014) 50–54. https://doi.org/10.1016/j.catcom.2014.07.035.

[163] Q. Wang, H. Li, L. Chen, X. Huang, Monodispersed hard carbon spherules with uniform nanopores, Carbon N. Y. 39 (2001) 2211–2214. https://doi.org/10.1016/S0008-6223(01)00040-9.

[164] M. Zheng, Y. Liu, Y. Xiao, Y. Zhu, Q. Guan, D. Yuan, J. Zhang, An Easy Catalyst-Free Hydrothermal Method to Prepare Monodisperse Carbon Microspheres on a Large Scale, The Journal of Physical Chemistry C 113 (2009) 8455–8459. https://doi.org/10.1021/jp811356a.

[165] P. D'Jesús, C. Artiel, N. Boukis, B. Kraushaar-Czarnetzki, E. Dinjus, Influence of Educt Preparation on Gasification of Corn Silage in Supercritical Water, Ind. Eng. Chem. Res. 44 (2005) 9071–9077. https://doi.org/10.1021/ie0508637.

[166] S. Nanda, A.K. Dalai, J.A. Kozinski, Supercritical water gasification of timothy grass as an energy crop in the presence of alkali carbonate and hydroxide catalysts, Biomass Bioenergy 95 (2016) 378–387. https://doi.org/10.1016/j.biombioe.2016.05.023.

[167] J. Rostrup-Nielsen, D.L. Trimm, Mechanisms of carbon formation on nickel-containing catalysts, J. Catal. 48 (1977) 155–165. https://doi.org/10.1016/0021-9517(77)90087-2.

[168] Z. Zhu, L. Rosendahl, S.S. Toor, D. Yu, G. Chen, Hydrothermal liquefaction of barley straw to bio-crude oil: Effects of reaction temperature and aqueous phase recirculation, Appl. Energy 137 (2015) 183–192. https://doi.org/10.1016/j.apenergy.2014.10.005.

[169] T. Minowa, F. Zhen, T. Ogi, Cellulose decomposition in hot-compressed water with alkali or nickel catalyst, J. Supercrit. Fluids 13 (1998) 253–259. https://doi.org/10.1016/S0896-8446(98)00059-X.

[170] K.R. Arturi, M. Strandgaard, R.P. Nielsen, E.G. Søgaard, M. Maschietti, Hydrothermal liquefaction of lignin in near-critical water in a new batch reactor: Influence of phenol and temperature, J. Supercrit. Fluids 123 (2017) 28–39. https://doi.org/10.1016/j.supflu.2016.12.015.

[171] T.D.H. Nguyen, M. Maschietti, L.-E. Åmand, L. Vamling, L. Olausson, S.-I. Andersson, H. Theliander, The effect of temperature on the catalytic conversion of Kraft lignin using near-critical water, Bioresour. Technol. 170 (2014) 196–203. https://doi.org/10.1016/j.biortech.2014.06.051.

[172] A. Mathanker, S. Das, D. Pudasainee, M. Khan, A. Kumar, R. Gupta, A Review of Hydrothermal Liquefaction of Biomass for Biofuels Production with a Special Focus on the Effect of Process Parameters, Co-Solvents, and Extraction Solvents, Energies (Basel). 14 (2021) 4916. https://doi.org/10.3390/en14164916.

[173] T. Ogi, S. Yokoyama, K. Koguchi, Direct liquefaction of wood by catalyst. Part 1. Effects of pressure, temperature, holding time and wood/catalyst/water ratio on oil yield., Journal of The Japan Petroleum Institute 28 (1985) 239–245. https://doi.org/10.1627/jpi1958.28.239.

[174] Y. Qu, X. Wei, C. Zhong, Experimental study on the direct liquefaction of Cunninghamia lanceolata in water, Energy 28 (2003) 597–606. https://doi.org/10.1016/S0360-5442(02)00178-0.

[175] L. Yang, L. Nazari, Z. Yuan, K. Corscadden, C. (Charles) Xu, Q. (Sophia) He, Hydrothermal liquefaction of spent coffee grounds in water medium for bio-oil production, Biomass Bioenergy 86 (2016) 191–198. https://doi.org/10.1016/j.biombioe.2016.02.005.

[176] J. Akhtar, S.K. Kuang, N.S. Amin, Liquefaction of empty palm fruit bunch (EPFB) in alkaline hot compressed water, Renew. Energy 35 (2010) 1220–1227. https://doi.org/10.1016/j.renene.2009.10.003.

[177] K. Alper, K. Tekin, S. Karagöz, Hydrothermal Liquefaction of Lignocellulosic Biomass Using Potassium Fluoride-Doped Alumina, Energy & Fuels 33 (2019) 3248–3256. https://doi.org/10.1021/acs.energyfuels.8b04381.

[178] Q.-V. Bach, M.V. Sillero, K.-Q. Tran, J. Skjermo, Fast hydrothermal liquefaction of a Norwegian macro-alga: Screening tests, Algal Res. 6 (2014) 271–276. https://doi.org/10.1016/j.algal.2014.05.009.

[179] D. Castello, T. Pedersen, L. Rosendahl, Continuous Hydrothermal Liquefaction of Biomass: A Critical Review, Energies (Basel). 11 (2018) 3165. https://doi.org/10.3390/en11113165.

[180] A. Hammerschmidt, N. Boukis, U. Galla, E. Dinjus, B. Hitzmann, Conversion of yeast by hydrothermal treatment under reducing conditions, Fuel 90 (2011) 3424–3432. https://doi.org/10.1016/j.fuel.2011.06.052.

[181] P. Biller, B.K. Sharma, B. Kunwar, A.B. Ross, Hydroprocessing of bio-crude from continuous hydrothermal liquefaction of microalgae, Fuel 159 (2015) 197–205. https://doi.org/10.1016/j.fuel.2015.06.077.

[182] N. Boukis, S. Herbig, E. Hauer, Gasification of Dutch sewage sludge in supercritical water (Final report), Karlsruhe Institute of Technology, 2016. https://doi.org/10.5445/IR/1000051638.

[183] A. Möbius, N. Boukis, U. Galla, E. Dinjus, Gasification of pyroligneous acid in supercritical water, Fuel 94 (2012) 395–400. https://doi.org/10.1016/j.fuel.2011.11.023.

[184] F.J. Gutiérrez Ortiz, A. Kruse, The use of process simulation in supercritical fluids applications, React. Chem. Eng. 5 (2020) 424–451. https://doi.org/10.1039/C9RE00465C.

[185] S.A. Chattanathan, S. Adhikari, M. McVey, O. Fasina, Hydrogen production from biogas reforming and the effect of H2S on CH4 conversion, Int. J. Hydrogen Energy 39 (2014) 19905–19911. https://doi.org/10.1016/j.ijhydene.2014.09.162.

[186] M. Sasaki, Z. Fang, Y. Fukushima, T. Adschiri, K. Arai, Dissolution and Hydrolysis of Cellulose in Subcritical and Supercritical Water, Ind. Eng. Chem. Res. 39 (2000) 2883–2890. https://doi.org/10.1021/ie990690j.

[187] J. Dutzi, N. Boukis, J. Sauer, Investigating Salt Precipitation in Continuous Supercritical Water Gasification of Biomass, Processes 12 (2024) 935. https://doi.org/10.3390/pr12050935.

[188] J. Dutzi, I.K. Stoll, N. Boukis, J. Sauer, Screening of ten different plants in the process of supercritical water gasification, Sustainable Chemistry for the Environment 5 (2024) 100062. https://doi.org/10.1016/j.scenv.2024.100062.

[189] D. Dolejš, C.E. Manning, Thermodynamic model for mineral solubility in aqueous fluids: theory, calibration and application to model fluid-flow systems, Geofluids 10 (2010) 20–40. https://doi.org/10.1111/j.1468-8123.2010.00282.x.

[190] T.A. Khan, A.S. Saud, S.S. Jamari, M.H.A. Rahim, J.-W. Park, H.-J. Kim, Hydrothermal carbonization of lignocellulosic biomass for carbon rich material preparation: A review, Biomass Bioenergy 130 (2019) 105384. https://doi.org/10.1016/j.biombioe.2019.105384.

[191] H. Demey, G. Ratel, B. Lacaze, O. Delattre, G. Haarlemmer, A. Roubaud, Hydrogen Production by Catalytic Supercritical Water Gasification of Black Liquor-Based Wastewater, Energies 16 (2023). https://doi.org/10.3390/en16083343.

[192] C.S. Lee, A. V. Conradie, E. Lester, Review of supercritical water gasification with lignocellulosic real biomass as the feedstocks: Process parameters, biomass composition, catalyst development, reactor design and its challenges, Chemical Engineering Journal 415 (2021) 128837. https://doi.org/10.1016/j.cej.2021.128837.

[193] M. Fowles, M. Carlsson, Steam Reforming of Hydrocarbons for Synthesis Gas Production, Top. Catal. 64 (2021) 856–875. https://doi.org/10.1007/s11244-021-01496-z.

[194] A.A. Vadarlis, S.D. Angeli, A.A. Lemonidou, N. Boukis, J. Sauer, Catalytic Biomass Gasification in Supercritical Water and Product Gas Upgrading, ChemBioEng Reviews 10 (2023) 370–398. https://doi.org/10.1002/cben.202300007.

[195] L. Sepini, R. Mochel, I. Petri, A. Chappaz, H. Demey, Understanding the conversion mechanisms in supercritical water conditions of PET as a model compound of plastic wastes, Chemical Engineering Journal 488 (2024). https://doi.org/10.1016/j.cej.2024.150567.

[196] Y.W. Low, K.F. Yee, A review on lignocellulosic biomass waste into biochar-derived catalyst: Current conversion techniques, sustainable applications and challenges, Biomass Bioenergy 154 (2021) 106245. https://doi.org/10.1016/j.biombioe.2021.106245.

[197] L. Feng, X. Li, Z. Wang, B. Liu, Catalytic hydrothermal liquefaction of lignin for production of aromatic hydrocarbon over metal supported mesoporous catalyst, Bioresour. Technol. 323 (2021) 124569. https://doi.org/10.1016/j.biortech.2020.124569.

[198] G. Haarlemmer, A. Roubaud, Bio-oil production from biogenic wastes, the hydrothermal conversion step, Open Research Europe 2 (2022) 111. https://doi.org/10.12688/openreseurope.14915.1.

[199] A. Mathanker, S. Das, D. Pudasainee, M. Khan, A. Kumar, R. Gupta, A review of hydrothermal liquefaction of biomass for biofuels production with a special focus on the effect of process parameters, co-solvents and extraction solvents, Energies (Basel). 14 (2021). https://doi.org/10.3390/en14164916.

[200] Y. Tian, F. Wang, J.O. Djandja, S.L. Zhang, Y.P. Xu, P.G. Duan, Hydrothermal liquefaction of crop straws: Effect of feedstock composition, Fuel 265 (2020). https://doi.org/10.1016/j.fuel.2019.116946.

[201] B. Lu, Z. Ge, Y. Chen, J. Shi, H. Jin, Study on supercritical water gasification reaction and kinetic of coal model compounds, Fuel Processing Technology 230 (2022) 107210. https://doi.org/10.1016/j.fuproc.2022.107210.

[202] Y. Guo, S.Z. Wang, D.H. Xu, Y.M. Gong, H.H. Ma, X.Y. Tang, Review of catalytic supercritical water gasification for hydrogen production from biomass, Renewable and Sustainable Energy Reviews 14 (2010) 334–343. https://doi.org/10.1016/j.rser.2009.08.012.

[203] Q. Guan, C. Wei, P.E. Savage, Kinetic model for supercritical water gasification of algae, Physical Chemistry Chemical Physics 14 (2012) 3140–3147. https://doi.org/10.1039/c2cp23792j.

[204] F.L.P. Resende, P.E. Savage, Kinetic model for noncatalytic supercritical water gasification of cellulose and lignin, AIChE Journal 56 (2010) 2412–2420. https://doi.org/10.1002/aic.12165.

[205] M.H. Waldner, F. Vogel, Renewable production of methane from woody biomass by catalytic hydrothermal gasification, Ind. Eng. Chem. Res. 44 (2005) 4543–4551. https://doi.org/10.1021/ie050161h.

[206] M. Brandenberger, J. Matzenberger, F. Vogel, C. Ludwig, Producing synthetic natural gas from microalgae via supercritical water gasification: A techno-economic sensitivity analysis, Biomass Bioenergy 51 (2013) 26–34. https://doi.org/10.1016/j.biombioe.2012.12.038.

[207] J. Chen, J. Liang, Z. Xu, J. E, Assessment of supercritical water gasification process for combustible gas production from thermodynamic, environmental and

techno-economic perspectives: A review, Energy Convers. Manag. 226 (2020). https://doi.org/10.1016/j.enconman.2020.113497.

[208] L. Fiori, M. Valbusa, D. Castello, Supercritical water gasification of biomass for H2 production: Process design, Bioresour. Technol. 121 (2012) 139–147. https://doi.org/10.1016/j.biortech.2012.06.116.

[209] T. Wang, X. Liu, H. Liu, M. He, Synergistic effect of supercritical water and nano-catalyst on lignin gasification, Int. J. Hydrogen Energy 46 (2021) 34626–34637. https://doi.org/10.1016/j.ijhydene.2021.08.061.

[210] F.A.P. Voll, C.C.R.S. Rossi, C. Silva, R. Guirardello, R.O.M.A. Souza, V.F. Cabral, L. Cardozo-Filho, Thermodynamic analysis of supercritical water gasification of methanol, ethanol, glycerol, glucose and cellulose, Int. J. Hydrogen Energy 34 (2009) 9737–9744. https://doi.org/10.1016/j.ijhydene.2009.10.017.

[211] T. Arita, K. Nakahara, K. Nagami, O. Kajimoto, Hydrogen generation from ethanol in supercritical water without catalyst, Tetrahedron Lett. 44 (2003) 1083–1086. https://doi.org/10.1016/S0040-4039(02)02704-1.

[212] I.G. Lee, M.S. Kim, S.K. Ihm, Gasification of glucose in supercritical water, Ind. Eng. Chem. Res. 41 (2002) 1182–1188. https://doi.org/10.1021/ie010066i.

[213] A. Demirbaş, Biomass resource facilities and biomass conversion processing for fuels and chemicals, Energy Convers. Manag. 42 (2001) 1357–1378. https://doi.org/10.1016/S0196-8904(00)00137-0.

[214] S. Nanda, R. Rana, H.N. Hunter, Z. Fang, A.K. Dalai, J.A. Kozinski, Hydrothermal catalytic processing of waste cooking oil for hydrogen-rich syngas production, Chem. Eng. Sci. (2019) 935–945. https://doi.org/10.1016/j.ces.2018.10.039.

[215] D. Yu, M. Aihara, M.J. Antal, Hydrogen production by steam reforming glucose in supercritical water, Energy & Fuels 7 (1993) 574–577. https://doi.org/10.1021/ef00041a002.

[216] C.H. Twu, D. Bluck, J.R. Cunningham, J.E. Coon, A cubic equation of state with a new alpha function and a new mixing rule, Fluid Phase Equilib. 69 (1991) 33–50. https://doi.org/10.1016/0378-3812(91)90024-2.

[217] J. Reimer, G. Peng, S. Viereck, E. De Boni, J. Breinl, F. Vogel, A novel salt separator for the supercritical water gasification of biomass, J. Supercrit. Fluids 117 (2016) 113–121. https://doi.org/10.1016/j.supflu.2016.06.009.

[218] D. Koutsonikolas, G. Karagiannakis, K. Plakas, V. Chatzis, G. Skevis, P. Giudicianni, D. Amato, P. Sabia, N. Boukis, K. Stoll, Membrane and Electrochemical Based Technologies for the Decontamination of Exploitable Streams Produced by Thermochemical Processing of Contaminated Biomass, Energies (Basel). 15 (2022). https://doi.org/10.3390/en15072683.

[219] A.A. Vadarlis, B. Lacerda de Oliveira Campos, A.A. Lemonidou, N. Boukis, J. Sauer, Supercritical Water Gasification of Ethanol as Biomass Model Compound in Tandem with Steam Reforming: Kinetic Modeling of the Reforming Step and Techno-Economic Analysis of the Integrated Concept, Ind. Eng. Chem. Res. (2024). https://doi.org/10.1021/acs.iecr.4c01486.

Appendix

A1 Supporting Information of Chapter 5

A1.1 EDS analysis of salt concentrate solid sample.

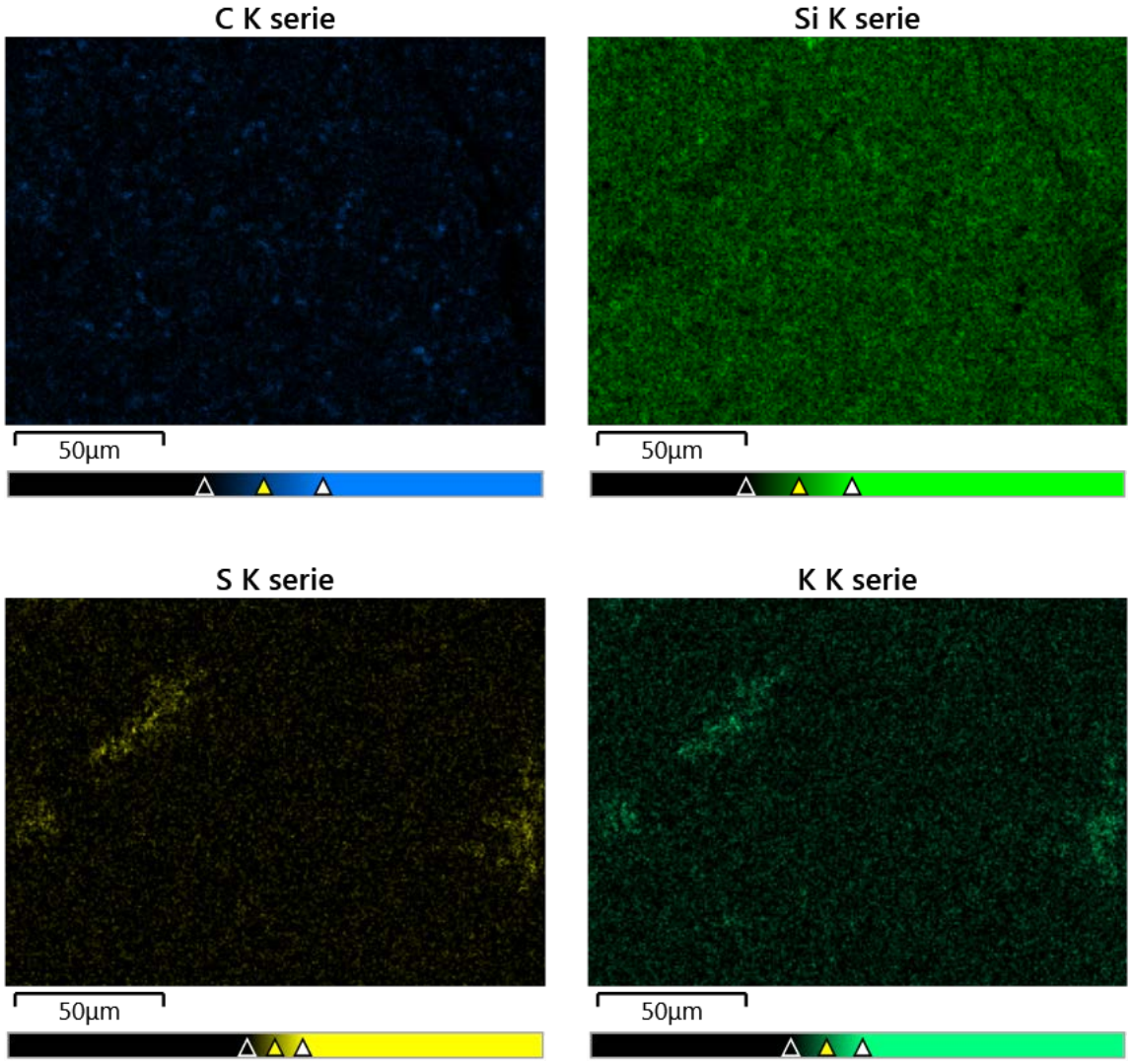


Figure A 1: EDS analysis of salt concentrate solid sample

Table A 1: EDS analysis of salt concentrate solid sample.

Element	**wt.%**	**atom%**
C	26.09	38.94
O	36.09	40.45
Na	0.19	0.15
Mg	1.71	1.26
Al	0.10	0.07
Si	15.71	10.03
P	2.61	1.51
S	0.73	0.41
Cl	0.18	0.09
K	6.51	2.99
Ca	6.53	2.92
Cr	2.25	0.77
Fe	0.67	0.21
Ni	0.64	0.20
Total	**100.00**	**100.00**

A1.2 Statistical analysis of the empirical model

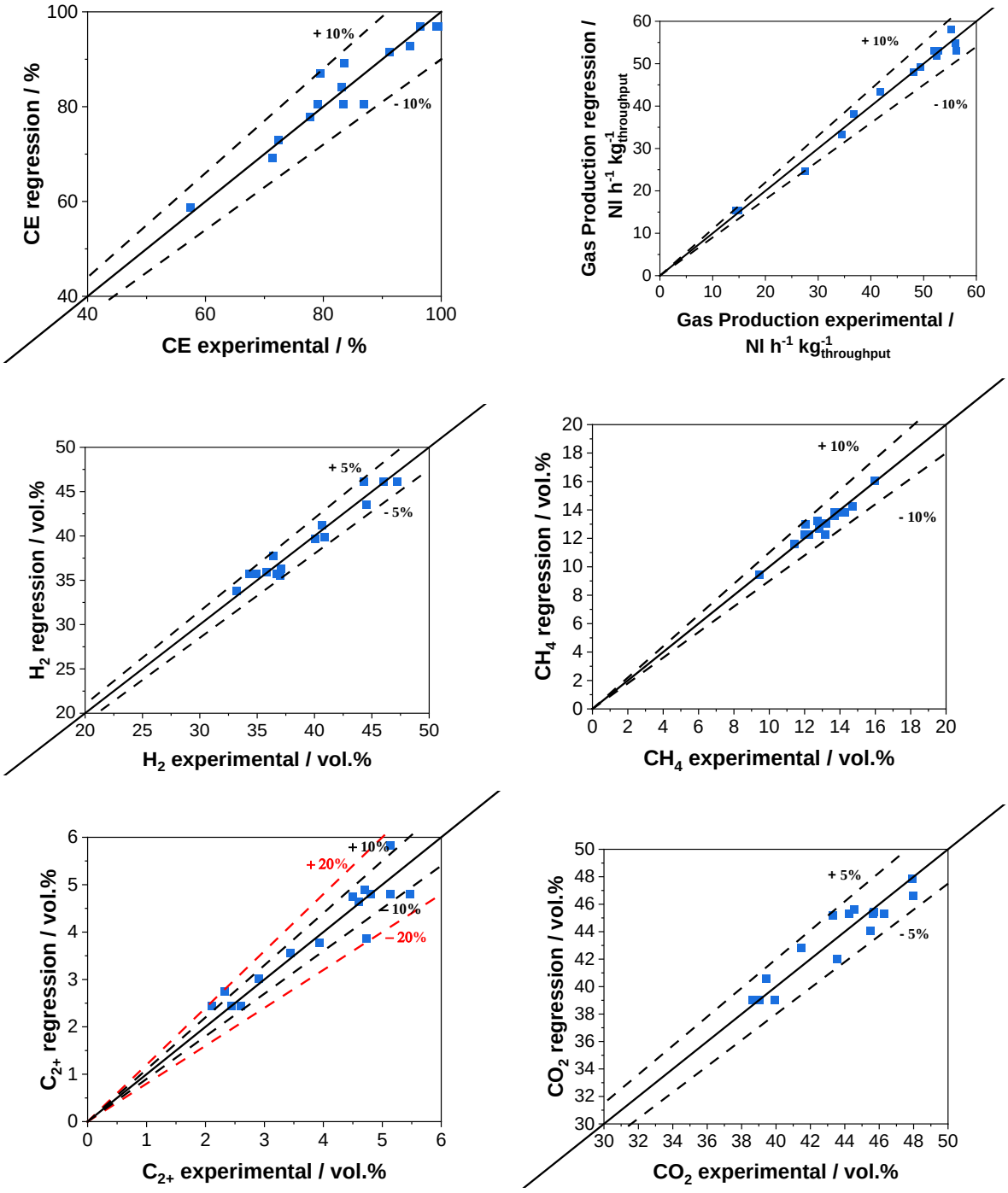


Figure A 2: Parity plots for the developed multi-linear regression.

Table A 2: Statistical information on the determined coefficients in the empirical model.

			CE	GP	H_2	CH_4	C_{2+}	CO_2
		Overall R^2	0.914	0.989	0.944	0.921	0.883	0.876
		Overall Standard Error	3.836	1.826	1.204	0.485	0.453	1.256
Parameter								
Tempera-ture	Determined co-efficient		0.240	0.109	-0.041	0.047	0.021	-0.026
	Interval for 95% confidence	Upper limit	0.316	0.145	-0.017	0.056	0.030	-0.002
		Lower limit	0.164	0.072	-0.065	0.037	0.012	-0.051
	p-value		$2.37x10^{-5}$	$3.69x10^{-5}$	$3.12x10^{-4}$	$3.74x10^{-7}$	$3.08x10^{-4}$	0.039
Dry matter	Determined co-efficient		-3.083	7.101	-1.957	0.299	0.445	1.192
	Interval for 95% confidence	Upper limit	-2.057	7.589	-1.635	0.428	0.566	1.528
		Lower limit	-4.108	6.612	-2.278	0.169	0.324	0.857
	p-value		$3.77x10^{-5}$	$3.28x10^{-12}$	$3.77x10^{-8}$	$3.58x10^{-4}$	$5.81x10^{-6}$	$8.13x10^{-6}$
Residence time	Determined co-efficient		0.329	0.167	0.023	0.036	0.008	-0.001
	Interval for 95% confidence	Upper limit	0.656	0.322	0.079	0.078	0.046	0.095
		Lower limit	0.003	0.012	-0.125	-0.005	-0.031	-0.119
	p-value		0.048	0.038	0.631	0.079	0.673	0.811
Intercept	Determined co-efficient		-65.632	-69.773	75.892	-19.569	-12.053	55.012
	Interval for 95% confidence	Upper limit	-11.262	-43.888	92.960	-12.699	-5.638	72.81
		Lower limit	-120.002	-95.658	58.823	-26.438	-18.468	37.21
	p-value		0.022	$9.83x10^{-5}$	$9.17x10^{-7}$	$6.09x10^{-5}$	0.002	$2.94x10^{-5}$

A1.3 Additional calculations for equilibrium calculations

Explanation of Calculation for Glucose Concentration

In the real dry biomass slurry, the CHO-content was on average 87.40 ± 0.44 wt.% (= salt free dry feed). The remaining 12.6 wt.% consisted of salt building elements, heavy metals and N.

The carbon content in the salt free dry feed was 44.7 wt.%. Cellulose has a carbon content of 44.4 wt.% and thus could be directly utilized with only little deviation. As it is not available in ASPEN HYSYS the monomer glucose was used. As glucose has a different carbon content due to the addition of a water molecule during the splitting of cellulose, the chosen feed concentration needs to be adjusted to keep the carbon content constant. As this hydrolyzation takes place in the real process as well, the adjustment should not affect the outcome of the equilibrium calculation.

Example of calculation for: $\text{Dry matter in Slurry} = 6.56\ wt.\%$

First the salt free dry matter in the slurry (SFDM) is calculated:

$$SFDM = 6.56\ wt.\% * 87.4\% = 5.74\ wt.\%$$

As cellulose shows the same carbon content as the real salt free dry matter, the cellulose concentration for calculation would equal 5.74 wt.%.

$$c_{Cellulose} = SFDM = 5.74\ wt.\%$$

However, when Cellulose is hydrolyzed to form glucose according to the following equation $(C_6H_{10}O_5)_n + nH_2O \rightarrow n\ C_6H_{12}O_6$
the carbon content of the organic molecule changes (carbon content of glucose is 40 wt.%). Thus, in order to keep the carbon content accurate for the calculations the glucose concentration needs to be adjusted:

$$c_{Glucose} = c_{Cellulose} * \frac{C - Content_{Cellulose}}{C - Content_{Glucose}}$$

$$= 5.74\ wt.\% * \frac{44.4\ wt.\%}{40.0\ wt.\%} = 6.37\ wt.\%$$

To compare the results with an experiment that used a dry matter content of 6.56 wt.%, a glucose concentration of 6.37 wt.% needs to be chosen.

A2 Supporting Information of Chapter 6

The used Aspen HYSYS V14 model was compared with the data produced by Voll et al. [210] for ethanol SCWG at 221 bar and 800 °C, in order to depict their close agreement.

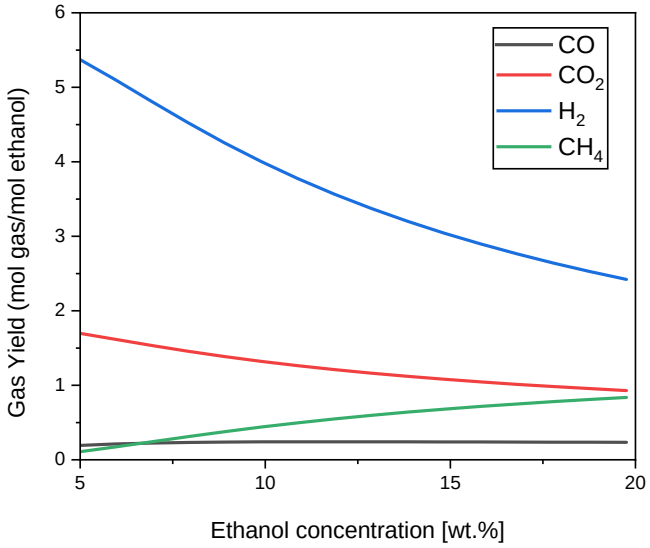


Figure A 3: Gas yields of product gases at thermodynamic equilibrium from SCWG of ethanol at T = 800 °C, p = 221 bar as a function of the ethanol concentration. The data were calculated with Aspen HYSYS V14.

Nomenclature

List of Symbols – Latin

$C - balance$	Carbon balance	%
CE	Carbon gasification efficiency	%
d	Inner diameter of the reactor	m
DM	Dry matter	wt.%
GP	Gas production	$Nl/g_{c\ in\ Feed}$ or $Nl/(h*kg_{throughput})$
GP_{SR}	Gas production corrected by steam reforming	$Nl/g_{c\ in\ Feed}$
$GP_{SR\ and\ CE}$	Gas production corrected by steam reforming and carbon gasification efficiency	$Nl/g_{c\ in\ Feed}$
l	Length of section with constant temperature	m
$\dot{m}$	Mass flow	g/h
$\dot{m}_{EtOH}$	Mass flow of ethanol	g/h
$\dot{m}_{Feed}$	Feed mass flow	g/h
$\dot{m}_{H2O}$	Mass flow of water	g/h
$\dot{m}_i$	Mass flow of species ‘i’	g/h
$\dot{m}_{R,effluent}$	Mass flow of reactor effluent	g/h
$\dot{m}_{S,effluent}$	Mass flow of salt concentrate	g/h
$\dot{m}_{water\ in\ feed}$	Mass flow of water in feed	g/h
M_c	Molar mass of carbon	g/mol
n	Number of values considered	-
$\dot{n}_C$	Molar flow of carbon	mol/h
$\dot{n}_{EtOH}$	Molar flow of ethanol	mol/h
$\dot{n}_{EtOH,gasified}$	Molar flow of gasified ethanol	mol/h
$\dot{n}_{H2O}$	Molar flow of water	mol/h
$\dot{n}_i$	Molar flow of species ‘i’	mol/h
p	Pressure	Pa or bar
R	Universal constant of gases	J/(mol*K)
R^2	Coefficient of determination	-
Re	Reynolds number	-

T	Temperature	K or °C
$T_{Preheater,max}$	Maximum preheating temperature	°C
$T_{T-Fitting}$	Temperature at salt separation T-fitting	°C
T_{Rct}	Reaction temperature	°C
TOC_{Conv}	TOC conversion	%
TOC_R	TOC content of reactor effluent	mg/g
TOC_S	TOC content of salt concentrate	mg/g
$\dot{V}_{Gas}$	Gas flow under ambient conditions	l/h
$Water\ savings$	Amount of water that can be saved by recycling the effluent stream	%
WC	Water consumption	$mol_{H2O}/mol_{ethanol}$
w_{EtOH}	Mass fraction of ethanol	-
x_i	Concentration of component ‘i’ in the gas product	vol.%
y_i	Value of sample ‘i’	%

List of Symbols – Greek

α	Organic carbon concentration in the feed	wt.%
β_i	Number of carbon atoms of component ‘i’ in the gas product	-
ΔC	Molar difference of carbon	mol/h
ΔH	Molar difference of hydrogen	mol/h
Δj	Molar difference of element ´j´	mol/h
ΔO	Molar difference of oxygen	mol/h
μ	Mean value	%
ρ_{H_2O}	Density of water at given temperature and pressure	kg/m³
σ	Standard deviation	%
τ	Residence time	s

Subscription

C	Carbon
$EtOH$	Ethanol
$EtOH, gasified$	Ethanol that was gasified
i	Species or sample ‘i’
$Preheater, max$	Maximum value in preheater
R	Reactor effluent
S	Salt concentrate
SR	Steam reforming
$SR\ and\ CE$	Steam reforming and carbon gasification efficiency

Abbreviations

AD	Arundo donax
BPR	Back pressure regulator
CE	Carbon gasification efficiency
CERESiS	ContaminatEd land Remediation through Energy crops for Soil improvement to liquid fuel Strategies
EC	Energy cane
EDS	Energy Dispersive X-ray Spectroscopy
EOS	Equation of state
EtOH	Ethanol
EU	European union
DM	Dry matter
GP	Gas production
GV	Grapevine
H2020	Horizon 2020
HPLC	High performance liquid chromatography
HTC	Hydrothermal carbonization
HTG	Hydrothermal gasification
HTL	Hydrothermal liquefaction
ICP	Inductively Coupled Plasma
KIT	Karlsruhe Institute of Technology

MC	Miscanthus
OES	Optical Emission Spectrometry
PRSV	Peng-Robinson equation of state modified by Stryjek and Vera
PV	Panicum virgatum
RCG	Reed Canary Grass
SC	Sugar cane
SCWG	Supercritical water gasification
SEC	Size exclusion chromatography
SEM	Scanning Electron Microscope
SR	Steam reforming
SRC	Short rotation coppice
SS316	Stainless steel 316
TC	Total carbon
TIC	Total inorganic carbon
TOC	Total organic carbon
VERENA	German acronym for “Pilot Plant for Energetic Utilization of Agricultural Materials”

List of Figures

Figure 2.1: Selected properties of water at different temperatures, p = 280 bar (data taken from the IAPWS data base). 9
Figure 3.1: Two pictures of the continuous lab-plant. 15
Figure 4.1: Pictures of biomasses as received from project partners (A: PV; B: AD; C: EC; D: SC; E: ST-MC; F: HH-MC; G: ST-SRC; H: RCG; I: GV; J: HH-SRC; for abbreviation see Table 4.1). 25
Figure 4.2: Inner setup of meat grinder and size reduced Reed Canary Grass (RCG) (Biomass H). 25
Figure 4.3: Process scheme of the continuous lab-plant in section 4.2. 27
Figure 4.4: Outside temperature profile, representative of the experiments. 28
Figure 4.5: Carbon Efficiency (CE) of different biomass experiments in a Gaussian curve ($T_{Reaction}$ = 650 °C, p = 280 bar). 31
Figure 4.6: Gas compositions of different biomasses ($T_{Reaction}$ = 650 °C, p = 280 bar). 32
Figure 4.7: Gasified biomasses as delivered (left to right: grapevines, Napier Grass, Reed Canary Grass). 36
Figure 4.8: Process scheme of the lab-plant in section 4.3. 38
Figure 4.9: Gas composition of the gasification of three different feeds. 42
Figure 4.10: Share of elements in the liquid effluents of different experiments with different preheating temperatures (370 - 394 °C) (feed concentration = 100%). 44
Figure 4.11: SEM-EDS analysis of the solid deposits of experiment 4.3.3. 45
Figure 4.12: Elemental spectrum of a sample of solid deposits in the preheater. 47
Figure 4.13: Steady state gas composition for three different residence times in the SCWG reactor (T > 600 °C), no steady state reached for the mean residence time of 41 s. 48
Figure 4.14: Mean content of heavy metals in the effluents of the experiments (100% = feed concentration). 50
Figure 4.15: Elemental composition of solid deposits in experiment 4.3.1. 51
Figure 4.16: Gas composition of experiments with Reed Canary Grass for three different feeds. 55

Figure 4.17: Carbon Efficiency and TOC content of reactor effluent of gasification experiments with Reed Canary Grass for three different feeds. 56
Figure 4.18: Gas composition of gasification experiments with grapevines for two different feeds. 58
Figure 4.19: Carbon efficiency and TOC content of reactor effluent of gasification experiments with grapevines for two different feeds. 59
Figure 4.20: Design of salt separation in lab-plant in section 4.4. 61
Figure 4.21: Solid sample from SCWG reactor in experiment 4.4.5 and 4.4.6. 61
Figure 4.22: Distribution of salt building elements in the products of experiment 4.4.2 (concentration in feed ≙ 100%). 62
Figure 4.23: SEM recordings of solid deposits of experiment 4.4.5. 64
Figure 4.24: EDS analysis of solid deposits from experiment 4.4.5. 64
Figure 4.25: SEM recordings of solid deposits of experiment 4.4.6. 65
Figure 4.26: EDS analysis of solid deposits from experiment 4.4.6. 66
Figure 5.1: Schematic diagram of lab-plant in Configuration 2. 75
Figure 5.2: Salt separation T-fitting. Red line: flow of reaction mixture. Yellow line: salts separating into salt concentrate. (left): Configuration 1, investigated in sections 4.3 and 4.4. (right): Configuration 2. 78
Figure 5.3: Set-up of the inner temperature measurement. 80
Figure 5.4: Outside and inside temperature profile of experiment 5.7. 81
Figure 5.5: Outside and inside temperature profile of experiment 5.11. 81
Figure 5.6: Gas composition for configuration 1 and 2. 85
Figure 5.7: Distribution of salt building elements for two configurations. 86
Figure 6.1: Schematic setup of SCWG lab-plant in Chapter 6. 91
Figure 6.2: Gas composition of product gas during proof of concept (T = 650 °C, p = 280 bar, $DM_{mixture}$ = 1.3 wt.%, $\dot{m}$ = 700 g h^{-1}). 97
Figure 6.3: Salt balance in liquid effluents (100% = feed content) (T = 650 °C, p = 280 bar, $DM_{mixture}$ = 1.3 wt.%, $\dot{m}$ = 700 g h^{-1}). 98
Figure 6.4: Influence of biomass type on A) the product gas composition and on B) CE, TOC conversion and C balance (T = 650 °C, p = 260-280 bar, $DM_{mixture}$ = 6.6 wt.%, $\dot{m}$ = 700 g h^{-1}). 100
Figure 6.5: SEM picture of solids from experiment with Reed Canary Grass. 101

Figure 6.6: Solubility of SiO2 in hot compressed water at different temperatures and p = 280 bar. Data taken from Dolejs and Manning [188]. 102
Figure 6.7: Influence of dry matter content in mixture on A) CE, TOC conversion, C balance and TOC content of effluent and B) on the organic species in the effluent (T = 650 °C, p = 280 bar, $\dot{m}$ = 700 g h^{-1}). 104
Figure 6.8: Influence of dry matter content on the gas composition (T = 650 °C, p = 280 bar, $\dot{m}$ = 700 g h^{-1}). 106
Figure 6.9: Influence of temperature on CE, TOC conversion, C balance and TOC content of effluent (p = 280 bar, $DM_{mixture}$ = 6.6 wt.%, $\dot{m}$ = 700 g h^{-1}). ..107
Figure 6.10: Influence of temperature on A) product gas composition and B) on the H_2/CH_4 ratio (p = 280 bar, $DM_{mixture}$ = 6.6 wt.%, $\dot{m}$ = 700 g h^{-1}). 109
Figure 6.11: Influence of pressure on A) CE, TOC conversion and C balance and B) on gas composition (T = 650 °C, $DM_{mixture}$ = 6.6 wt.%, $\dot{m}$ = 700 g h^{-1}). 110
Figure 6.12: Influence of residence time at reaction temperature on A) CE, TOC conversion and C balance (steady state) and B) on gas composition (T = 650 °C, p = 280 bar, DM = 6.6 wt.%). 113
Figure 6.13: Oily substance obtained from the filter before the back-pressure regulator during after the experiment at τ = 0 s. 114
Figure 6.14: SEC analysis the oily substance produced in the experiment with at τ = 0 s. 115
Figure 6.15: Influence of potassium addition to the reaction mixture on A) CE, TOC conversion and C balance (steady state) and B) on organic species in the effluent (T = 650 °C, p = 280 bar, $\dot{m}$ = 700 g h^{-1}). 117
Figure 6.16: Influence of potassium addition to the reaction mixture on gas composition (T = 650 °C, p = 280 bar, $\dot{m}$ = 700 g h^{-1}). 118
Figure 6.17: Influence of Pressure on a) H_2, b) CO_2, c) CH_4 content in vol.% and d) gas production in Nl $g_{c\ in\ Feed}^{-1}$ at experimental conditions of T = 650 °C, DM content = 6.6 wt.%, $\dot{m}$ = 700 g h^{-1}. 125
Figure 6.18: Influence of Carbon Content on a) H_2, b) CO_2, c) CH_4 content in vol.% and d) gas production in Nl $g_{c\ in\ Feed}^{-1}$ at experimental conditions of T = 650 °C, p = 280 bar, $\dot{m}$ = 700 g h^{-1}. 126

Figure 6.19: Influence of Temperature on a) H_2, b) CO_2, c) CH_4 content in vol.% and d) gas production in Nl $g_{c\ in\ Feed}^{-1}$ at experimental conditions of p = 280 bar, DM content = 6.6 wt.%, $\dot{m}$ = 700 g h^{-1}.....127
Figure 7.1: Schematic diagram of the lab-plant in Chapter 6.....135
Figure 7.2: Influence of x_c* in the feed solution on the composition of the product gas based on experimental results.....138
Figure 7.3: Water Consumption of the SCWG process with variation in x_c* in the feed solution.....141
Figure 7.4: Water Consumption as a function of the produced gases. 142
Figure 7.5: Comparison of experimentally measured (exp.) and simulated gas composition (eq.) for different x_c* in the feed solution. 144
Figure 7.6: Comparison of experimentally measured and simulated water consumption for different x_c*.....144
Figure 7.7: Parity plot of water consumption experimentally determined and simulated by ASPEN.....145
Figure A 1: EDS analysis of salt concentrate solid sample.....XV
Figure A 2: Parity plots for the developed multi-linear regression. XVII
Figure A 3: Gas yields of product gases at thermodynamic equilibrium from SCWG of ethanol at T = 800 °C, p = 221 bar as a function of the ethanol concentration. The data were calculated with Aspen HYSYS V14.....XX

List of Tables

Table 4.1: Labeling of biomasses in the current work. 24
Table 4.2: Dry Matter (DM) content of biomass, elemental analysis (CHNO) on dry matter basis (wt.%). 29
Table 4.3: Carbon Efficiency (CE) and gas composition of different biomass experiments under same conditions.....31
Table 4.4: EDS-analysis of solids from reactor (in wt.%). 34
Table 4.5: EDS-analysis of solids from F01 (in wt.%). 35
Table 4.6: Origin of Biomasses. 36
Table 4.7: CHNS analysis of biomasses, based on dry weight (in wt.%). 36
Table 4.8: Heavy metal contamination of biomasses (in ppmw). 37
Table 4.9: Dimensions of preheater and reactor. 38
Table 4.10: Process parameters of conducted experiments. 39
Table 4.11: Results of the gasification experiments. 40
Table 4.12: Content of CHNS and main salt building elements in the feed slurry in wt.% (based on dry matter). 41
Table 4.13: Temperatures of the T-fitting for salt separation.....43
Table 4.14: Residence time and salt separation temperature of different experiments.....48
Table 4.15: Experimental conditions of SCWG process. 53
Table 4.16: Results of gasification experiments. 54
Table 4.17: Organics in reactor effluents of the experiments with RCG (in mg l^{-1}). 57
Table 4.18: Elements in reactor effluents of experiments with RCG (in µg ml^{-1}). 57
Table 4.19: Organics in reactor effluent of experiments with grapevines (in mg l^{-1}). 59
Table 4.20: Elements in reactor effluents of experiments with grapevines (in µg ml^{-1}). 60
Table 5.1: Elemental analysis of RCG (in wt.%). 73
Table 5.2: Conducted experiments in Configuration 1 (data from sections 4.3 and 4.4) 76
Table 5.3: Conducted experiments in Configuration 2 (used biomass: RCG). 77

Table 5.4: Flow velocities and Re numbers for different temperatures in the preheater. 82
Table 5.5: CE and TOC conversion of conducted experiments (flow rate = 700 g h^{-1}). 84
Table 5.6: Potassium concentration in the reactor effluent. 86
Table 6.1: Investigated parameters. 94
Table 6.2: Elemental composition of feed slurry during proof of concept, in wt.%. ... 96
Table 6.3: Elemental analysis of gasified biomasses, based on dry matter in wt.%. 100
Table 6.4: EDS analysis of solids from experiment with Reed Canary Grass. 101
Table 6.5: Si content of feed slurry and reaction mixture for different biomasses. .. 102
Table 6.6: Potassium concentration in the reaction mixture. 119
Table 6.7: Comparison of prediction by empirical model and experimental results for a new experiment. 122
Table 7.1: Key figures of gasification of different ethanol solutions. 137
Table 7.2: Ratio of methane in the product gas to ethanol in feed for different $xc*$. 140
Table 7.3: Calculation of water consumption from experimental data (according to Eq. 7.9 - 7.12). 140
Table A 1: EDS analysis of salt concentrate solid sample. XVI
Table A 2: Statistical information on the determined coefficients in the empirical model. XVIII

List of Publications

The publications were enlisted in April 2026. An updated list is given in the following links:

- ORCID: Julian Dutzi - ORCID
- Google Scholar: Julian Dutzi - Google Scholar

Peer-reviewed publications

- Dutzi, J.; Boukis, N.; Sauer, J. Process Effluent Recycling in the Supercritical Water Gasification of Dry Biomass. *Processes*, **2023**, 11, 797. DOI: 10.3390/pr11030797.
- Dutzi, J.; Vadarlis, A.A., Boukis, N.; Sauer, J. Comparison of Experimental Results with Thermodynamic Equilibrium Simulations of Supercritical Water Gasification of Concentrated Ethanol Solutions with Focus on Water Splitting. *Ind. Eng. Chem. Res.*, **2023**, 62, 12501-12512. DOI: 10.1021/acs.iecr.3c01595
- Dutzi, J.; Boukis, N.; Sauer, J. Energetic Assessment of SCWG Experiments with Reed Canary Grass and Ethanol Solution on Laboratory and Pilot Scale. *Energies*, **2023**, 16(19), 6848, DOI: 10.3390/en16196848
- Dutzi, J.; Stoll, I.K.; Boukis, N.; Sauer, J. Screening of ten different plants in the process of supercritical water gasification. *Sustainable Chemistry for the Environment,* **2024**, 5, 100062. DOI: 10.1016/j.scenv.2024.100062
- Dutzi, J.; Boukis, N.; Sauer, J. Supercritical water gasification of heavy metal contaminated plants with focus on separation of heavy metal contaminants. *Biomass and Bioenergy,* **2024**, 182, 107059. DOI: 10.1016/j.biombioe.2024.107059
- Dutzi, J.; Boukis, N.; Sauer, J. Investigating Salt Precipitation in Continuous Supercritical Water Gasification of Biomass. *Processes*, **2024**, 12, 935. DOI: 10.3390/pr12050935
- Vadarlis, A.A., Neukum, D., Dutzi, J., Lemonidou, A., Boukis, N., Sauer, J. Supercritical water gasification and subsequent steam reforming of the product gas under elevated temperature and pressure. *Int. J. Hydrogen Energy,* **2025**, 111, 567-580. DOI: 10.1016/j.ijhydene.2025.02.197

- Dutzi, J.; Vadarlis, A.A., Boukis, N.; Sauer, J. Development and parametrization of novel reactor concept for the supercritical water gasification process. *Ind. Eng. Chem. Res.,* **2025**, 64 (19), 9500-9517. DOI: 10.1021/acs.iecr.4c04267
- Sarasidis, V., Dutzi, J., Petsi, P., Plakas, K., Boukis, N., Sauer, J. Decontamination of high salinity supercritical water gasification wastewater by an integrated electro-coagulation / electrochemical oxidation process. *J. Environ. Chem. Eng*., **2025**, 13 (5), 118491. DOI: 10.1016/j.jece.2025.118491
- Lacerda de Oliveira Campos, B., Dutzi, J., Campos Frage, M.M., Vadarlis, A.A., Sauer, Supercritical water gasification of lignocellulosic biomass: Kinetic modeling enhanced by Bayesian optimization. *Chem. Eng. J.,* **2026**, 530, 173614. DOI: 10.1016/j.cej.2026.173614

Conference oral presentations

- Dutzi, J.; Boukis, N.; Sauer, J. Gasification of contaminated biomass under the conditions of supercritical water. *European Biomass Conference and Exhibition 2023*, Bologna, Italy, June 5-8, **2023**
- Dutzi, J.; Boukis, N.; Sauer, J. Development of a novel reactor design for the process of supercritical water gasification to increase gasification efficiency and reduce solid deposition in the reaction system. *DECHEMA Annual Meeting on Reaction Engineering and Electrochemical Processes 2024*, Würzburg, Germany, May 6-8, **2024**
- Dutzi, J.; Boukis, N.; Sauer, J. Development of a two-stream concept to increase the gasification efficiency of the SCWG process. *European Biomass Conference and Exhibition 2024*, Marseille, France, June 24-27, **2024**
- Dutzi, J.; Vadarlis, A.A., Boukis, N.; Sauer, J. Gasification of contaminated biomass to synthesize renewable fuels. *DGMK/ÖGEW/SCI Conference: Energy and Material Flows in Sustainable Petrochemistry – Opportunities and Implications*, Hamburg, Germany, November 27-29, **2024**

Conference poster presentations

- Dutzi, J.; Boukis, N.; Sauer, J. Separation of Heavy Metal Contaminants in the Process of Supercritical Water Gasification. *Promovierenden-Symposium des KIT-Zentrum Energie*, Karlsruhe, Germany, May 10, **2023**
- Dutzi, J.; Boukis, N.; Sauer, J. Hydrogen and methane production from ten biomasses in the process of supercritical water gasification, *Science Week – Scientific Conference "Transforming towards a sustainable society – challenges and solutions*", Karlsruhe, Germany, October 11-13, **2023**
- Dutzi, J.; Boukis, N.; Sauer, J. Supercritical water gasification of contaminated biomasses. *Final Event of H2020 project CERESiS*, GR, Thessaloniki, April 23, **2024**
- Dutzi, J.; Vadarlis, A. A.; Boukis, N.; Sauer, J. Investigation of Water Consumption in Supercritical Water Gasification of Ethanol. *European Biomass Conference and Exhibition 2024,* FR, Marseille, June 24-27, **2024**
- Dutzi, J.; Boukis, N.; Sauer, J. Parametric study of a novel reactor design developed for the process of supercritical water gasification. *KNT-Symposium "Chemical Engineering for a Sustainable World",* Karlsruhe, Germany, September 30 - October 02, **2024**

Verification of the contribution from the co-authors

Title: Process Effluent Recycling in the Supercritical Water Gasification of Dry Biomass

Journal: processes (MDPI)

Authors: Julian Dutzi, Nikolaos Boukis, Jörg Sauer

Position in the dissertation:

The content of this paper has been included in Chapter 4.

Contribution of Julian Dutzi:	Conceptualization, validation, formal analysis, investigation, data curation, writing – original draft preparation, visualization
Contribution of Nikolaos Boukis:	Conceptualization, methodology, validation, resources, writing – review and editing, funding acquisition
Contribution of Jörg Sauer:	Validation, writing – review and editing, supervision

Verification of the contribution from the co-authors

Title: Supercritical water gasification of heavy metal contaminated plants with focus on separation of heavy metal contaminants

Journal: Biomass and Bioenergy (Elsevier)

Authors: Julian Dutzi, Nikolaos Boukis, Jörg Sauer

Position in the dissertation:

The content of this paper has been included in Chapter 4.

Contribution of Julian Dutzi:	Conceptualization, validation, formal analysis, investigation, data curation, writing – original draft preparation, visualization
Contribution of Nikolaos Boukis:	Conceptualization, methodology, validation, resources, writing – review and editing, funding acquisition
Contribution of Jörg Sauer:	Validation, writing – review and editing, supervision

Verification of the contribution from the co-authors

Title: Comparison of Experimental Results with Thermodynamic Equilibrium Simulations of Supercritical Water Gasification of Concentrated Ethanol Solutions with Focus on Water Splitting

Journal: Industrial & Engineering Chemistry Research (ACS)

Authors: Julian Dutzi, Athanasios A. Vadarlis, Nikolaos Boukis, Jörg Sauer

Position in the dissertation:

The content of this paper has been included in Chapter 7.

Contribution of Julian Dutzi:	Conceptualization, validation, formal analysis, investigation, data curation, writing – original draft preparation, visualization
Contribution of Athanasios Vadarlis:	Conceptualization, validation, formal analysis, investigation, data curation, writing – original draft preparation, visualization
Contribution of Nikolaos Boukis:	Conceptualization, methodology, validation, resources, writing – review and editing, funding acquisition
Contribution of Jörg Sauer:	Validation, writing – review and editing, supervision

Verification of the contribution from the co-authors

Title: Screening of ten different plants in the process of supercritical water gasification

Journal: Sustainable Chemistry for the Environment (Elsevier)

Authors: Julian Dutzi, I. Katharina Stoll, Nikolaos Boukis, Jörg Sauer

Position in the dissertation:

The content of this paper has been included in Chapter 4.

Contribution of Julian Dutzi:	Conceptualization, validation, formal analysis, investigation, data curation, writing – original draft preparation, visualization
Contribution of I. Katharina Stoll:	Conceptualization, methodology, data curation, validation, writing – review and editing
Contribution of Nikolaos Boukis:	Conceptualization, methodology, validation, resources, writing – review and editing, funding acquisition
Contribution of Jörg Sauer:	Validation, writing – review and editing, supervision

Verification of the contribution from the co-authors

Title: Investigating Salt Precipitation in Continuous Supercritical Water Gasification of Biomass

Journal: processes (MDPI)

Authors: Julian Dutzi, Nikolaos Boukis, Jörg Sauer

Position in the dissertation:

The content of this paper has been included in Chapters 2 and 5.

Contribution of Julian Dutzi:	Conceptualization, validation, formal analysis, investigation, data curation, writing – original draft preparation, visualization
Contribution of Nikolaos Boukis:	Conceptualization, methodology, validation, resources, writing – review and editing, funding acquisition
Contribution of Jörg Sauer:	Validation, writing – review and editing, supervision

Verification of the contribution from the co-authors

Title: Development and parametrization of a novel reactor concept for the supercritical water gasification process

Journal: Industrial & Engineering Chemistry Research (ACS)

Authors: Julian Dutzi, Athanasios A. Vadarlis, Nikolaos Boukis, Jörg Sauer

Position in the dissertation:

The content of this paper has been included in Chapters 2, 3 and 6.

Contribution of Julian Dutzi:	Conceptualization, validation, formal analysis, investigation, data curation, writing – original draft preparation, visualization
Contribution of Athanasios Vadarlis:	Conceptualization, validation, formal analysis, investigation, data curation, writing – original draft preparation, visualization
Contribution of Nikolaos Boukis:	Conceptualization, methodology, validation, resources, writing – review and editing, funding acquisition
Contribution of Jörg Sauer:	Validation, writing – review and editing, supervision